UNIVERSIDADE FEDERAL DE PERNAMBUCO
DEPARTAMENTO DE FÍSICA – CCEN
PROGRAMA DE PÓS-GRADUAÇÃO EM FÍSICA

WILLIAM OSWALDO SOSA CORREA

HIERARCHICAL MODELS FOR FINANCIAL MARKETS AND TURBULENCE

Recife
2018

WILLIAM OSWALDO SOSA CORREA

HIERARCHICAL MODELS FOR FINANCIAL MARKETS AND TURBULENCE

Doctoral thesis submitted to the Graduate Program in Physics, Department of Physics, Federal University of Pernambuco as a partial requirement for obtaining a doctorate in Physics

Advisor: Prof. Dr. Giovani Lopes Vasconcelos

Recife
2018

Catalogação na fonte
Bibliotecária Elaine Cristina de Freitas CRB4-1790

S715h Sosa Correa, William Oswaldo
Hierarchical models for financial markets and turbulence / William Oswaldo Sosa Correa. – 2018.
183 f., fig.

Orientador: Giovani Lopes Vasconcelos
Tese (doutorado) – Universidade Federal de Pernambuco. CCEN. Física. Recife, 2018.
Inclui referências e apêndices.

1. Mecânica estatística. 2. Dinâmica de Fluidos. 3. Sistemas Complexos Hierárquicos I. Vasconcelos, Giovani Lopes (Orientador) II. Título.

530.13 CDD (22. ed.) UFPE-FQ 2018-32

WILLIAM OSWALDO SOSA CORREA

HIERARCHICAL MODELS FOR FINANCIAL MARKETS AND TURBULENCE

Tese apresentada ao Programa de Pós-Graduação em Física da Universidade Federal de Pernambuco, como requisito parcial para a obtenção do título de Doutor em Física.

Aprovada em: 05/04/2018.

BANCA EXAMINADORA

_____
Prof. Dr. Giovani Lopes Vasconcelos
Orientador
Universidade Federal de Pernambuco

_____
Prof. Dr. Antônio Murilo Santos Macêdo
Examinador Interno
Universidade Federal de Pernambuco

_____
Prof. Dr. Carlos Alberto Batista da Silva Filho
Examinador Interno
Universidade Federal de Pernambuco

_____
Prof. Dr. Dionisio Bazeia Filho
Examinador Externo
Universidade Federal da Paraíba

_____
Prof. Dr. Domingos Sávio Pereira Salazar
Examinador Externo
Universidade Federal Rural de Pernambuco

Acknowledgments

Firstly, I thank my family for their support in all situations during these years in Brazil.

I would also like to express my sincere gratitude to my advisor Prof. Giovani Vasconcelos, for his valuable teaching, advice, motivation and patience. I would also like to thank the colleagues of the ACCA research group for their valuable discussions and contributions in the development of this thesis.

Also, I would like to thank the Department of Physics of the Federal University of Pernambuco for making possible my academic formation during the doctorate.

I also thank the many friends I made during my stay in the department of Physics and the wonderful city of Recife.

Finally, I thank CAPES for the essential financial support for my doctorate.

Abstract

In this thesis we present a study about the modeling of multiscale fluctuation phenomena and its applications to different problems in econophysics and turbulence. The thesis was organized in three parts according to the different problems considered. In the first part, we present an empirical study of the Brazilian option market in light of three option pricing models, namely the Black-Scholes model, the exponential model, and a model based on a power law distribution, the so-called q-Gaussian distribution or Tsallis distribution. It is found that the q-Gaussian performs better than Black-Scholes in about one-third of the option chains analyzed. But among these cases, the exponential model performs better than the q-Gaussian in 75% of the time. The superiority of the exponential model over the q-Gaussian model is particularly impressive for options close to the expiration date. In the second part, we study a general class of hierarchical models for option pricing with stochastic volatility. We adopt the idea of an information cascade from long to short time scales, aiming to implement a hierarchical stochastic volatility model whose dynamics is described by a system of coupled stochastic differential equations. Assuming that the time scales of the different processes in the hierarchy are well separated, the stationary probability distribution for the volatility is obtained analiticaly in terms of a Meijer G-function. The option price is then computed as the average of the Black-Scholes formula over the volatility distribution, resulting in an explicit formula for the price in terms of a bivariate Meijer G-function. We also analyze the behavior of the theoretical price with the parameters of the model and we briefly compare it to empirical data from the Brazilian options market. In the third part, we study a stochastic model for the distribution of velocity increments in turbulent flows. As a basic hypothesis, we assume that the velocity increments distribution conditioned on a given energy transfer rate is a normal distribution whose variance is proportional to the energy transfer rate and whose mean depends linearly on the variance. The dynamics of the energy flux among the different scales of the hierarchy is described by a hierarchical stochastic process similar to that used in the second part of this thesis for the volatility. Therefore, the stationary distribution of the energy transfer rate is also expressed in terms of a Meijer G-function. The marginal probability distribution for the velocity increments is obtained as a statistical composition of the conditional distribution (Gaussian) with the distribution of the energy transfer rate (a G-function), which results in an asymmetric distribution written

in terms of a bivariate Meijer G-function. Our model describes very well the asymmetry observed in empirical velocity increments distributions both from experimental data and numerical simulations of the Navier-Stokes equation.

Keywords: Hierarchical Complex Systems. Econophysics. Options. Stochastic Volatility. Turbulence. Intermittency. Non-Gaussian Distributions.

Resumo

Nesta tese apresentamos um estudo sobre a modelagem de fenômenos de flutuação com múltiplas escalas e suas aplicações a diversos problemas em econofísica e turbulência. A tese foi organizada em três partes de acordo com os diferentes problemas tratados. Na primeira parte, apresentamos um estudo empírico do mercado brasileiro de opções em que comparamos três modelos para precificação de opções, a saber: o modelo padrão de Black-Scholes, o modelo exponencial e o modelo baseado em uma distribuição q-Gaussiana ou distribuição de Tsallis. Encontramos que em aproximadamente 1/3 do total das cadeias de opções analisadas o modelo q-Gaussiano ajusta melhor os dados empíricos que o modelo Black-Scholes. Entretanto, entre esses casos, o modelo exponencial mostra melhores resultados que o modelo q-Gaussiano em 75 % das vezes. A superioridade do modelo exponencial sobre o modelo q-Gaussiano é particularmente notável para opções próximas da data de vencimento. Na segunda parte, estudamos uma classe geral de modelos hierárquicos para precificação de opções com volatilidade estocástica. Adotamos a ideia de uma cascata de informação de escalas longas de tempo para escalas curtas, com o objetivo de implementar um modelo hierárquico para a volatilidade em que a dinâmica da volatilidade é descrita por um sistema de equações diferenciais estocásticas acopladas. Sob a hipótese de que as escalas de tempo dos diferentes processos da hierarquia são bem separadas, a distribuição estacionária de probabilidade para a volatilidade é obtida de forma analítica em termos das funções G de Meijer. O preço da opção é então calculado como uma média da fórmula de Black-Scholes sobre a distribuição da volatilidade, resultando em uma fórmula explícita para o preço em termos de uma função G de duas variáveis. Estudamos ainda o comportamento do preço teórico com os diversos parâmetros do modelo e fazemos uma breve comparação com dados empíricos do mercado brasileiro de opções. Na terceira parte da tese, estudamos um modelo estatístico para a distribuição dos incrementos de velocidades em fluidos turbulentos. Como hipótese básica do modelo, assumimos que a distribuição de incrementos de velocidade condicionada a um dado fluxo de energia é uma gaussiana com uma variância proporcional ao fluxo de energia e uma média que depende linearmente da variância. A dinâmica do fluxo de energia entre as diferentes escalas da hierarquia é descrita por um processo estocástico hierárquico semelhante àquele usado para o modelo de volatilidade estudado na parte dois da tese. Desse modo, a distribuição estacionária do fluxo de energia também é escrita em termos de uma função G de Meijer. A distribuição de probabilidade marginal dos incrementos de velocidade é obtida como uma composição estatística da distribuição condicional (gaussiana) com a distribuição do fluxo de energia (função G). Como resultado dessa composição, obtemos uma distribuição de probabilidade assimétrica que é escrita em termos de uma função G de Meijer de duas

variáveis. O nosso modelo descreve muito bem a assimetria observada nas distribuições empíricas dos incrementos de velocidade, tanto para dados experimentais quanto para dados de simulações númericas das equações de Navier-Stokes.

Palavras-chave: Sistemas Complexos Hierárquicos. Econofísica. Opções. Volatilidade Estocástica. Turbulência. Intermitência. Distribuições Não Gaussianas.

List of Figures

Content

1 General Introduction

In this thesis we shall discuss some generic statistical properties exhibited by so-called complex systems. One can find complex systems in several disciplines, such as physics, computer science, meteorology, sociology, economics, psychology, chemistry and biology [Friedrich et al., 2011]. In such systems all the components may interact with each other in different ways, leading to effects such as non-linearity, complexity, together with chaotic characteristics (e.g., sensibility to initial conditions), which makes it difficult to predict the dynamics of the system. One of the ways in which these systems can be studied is from the statistical physics point of view. In this framework, one can explore the prediction of the statistical properties of the system and, in addition, take advantage of the fact that there are different complex systems that exhibit the same statistical properties. These statistical resemblances among distinct complex systems have suggested the idea of certain universality between the different models and the methodologies to analyze these systems. For instance, a characteristic shared by these systems is that large events do happen more frequently than predicted by a Gaussian or normal distribution. Such deviations from Gaussianity are indeed observed in several phenomena [Bogachev et al., 2017, Rouse and Willitsch, 2017, Friedrich et al., 2011, Silva et al., 2004, Ghashghaie et al., 1996, Frever et al., 2011, Nakamura et al., 2016, Andersona et al., 2017, Sornette, 2002]. That is, the relevant variables in such systems follows non-Gaussian statistics displaying heavy tails, skewness and peaked probability density functions (PDFs). In this thesis we will deal with these so-called *stylized facts* in finance and turbulence data through different methodologies. In particular, we will propose some new theoretical models to describe certain important statistical features in these two areas.

A great deal of effort has been devoted to constructing physical models to explain the origin of non-Gaussianity. Two approaches along this line, which are both used in this thesis, are the so-called nonextensive statistical mechanics formalism [Beck, 2001, Beck, 2000, Tsallis, 1988, Tsallis, 2009] and the superposition of conventional statistics, a procedure known as superstatistics [C.Beck, 2004, Castaing et al., 1990, Beck, 2011, Wilczek, 2016]. In the first case we deal with the so-called q-Gaussian or Tsallis distribution, which is a type of generalized statistics that yields probability distributions with power law tails. On the other hand, the superstatistics approach can also be used to generate non-Gaussian distributions. The idea behind the superposition of probability densities has found empirical application in several areas, such as finance [Aas and Haff, 2006, Muzy et al., 2000, Dragulescu and Yakovenko, 2002], turbulence [Beck, 2001, Beck, 2000, Castaing et al., 1990, Chevillard et al., 2012] and other complex systems [Bogachev et al., 2017, Rouse and Willitsch, 2017, Friedrich et al.,

2011, Ghashghaie et al., 1996, Frever et al., 2011, Nakamura et al., 2016, Andersona et al., 2017]. More recently [Salazar and Vasconcelos, 2012, Macêdo et al., 2017], the superstatistical approach has been extended to multiscale systems—i.e., systems with multiple time and length scales—, giving rise to a large family of heavy-tailed distributions. In this formalism, a system can be considered as composed of several smaller subsystems, each one being in a local quasi-equilibrium with its immediate vicinity. Each of these subsystems is characterized by a time scale that differs considerably from that of the other subsystems [Vasconcelos et al., 2018, Salazar and Vasconcelos, 2012, Castaing et al., 1990]. Ordering these subsystems according to their time scales, from largest to shortest, the PDF of the subsystem with the shortest scale can be obtained by averaging its quasi-equilibrium distribution, say a Gaussian, over the distribution of the subsystems with the longer time scales. This procedure thus gives rise to non-Gaussian distributions.

The description of asymmetric or skewed distributions is a little more complicated. Besides the multiscale superstatistics, several other approaches have been used in physics and finance to generate skewed distributions, such as piecewise functions, mixtures of functions and conventional PDFs with argument modified [Borland and Bouchaud, 2007, Chevillard et al., 2006, Chevillard et al., 2012, Aas and Haff, 2006, Beck, 2000, Barndorff-Nielsen et al., 2004, Rouse and Willitsch, 2017, McCauley and Gunaratne, 2003]. In the turbulence case, where the skewness is an essential issue, elucidating its physical origins persists as a long-standing open question. Part of this thesis will be dedicated to obtaining theoretical models to describe non-Gaussianity and skewness in turbulence. In finance the problem lies in the fact that the prices of certain financial instruments, the so-called derivatives — because its value derives of the value of an underlying asset —, are evaluated averaging over the distribution of the underlying asset that exhibits non-Gaussian behavior. The non-Gaussianity together with the skewness lead to pricing models for these derivatives that are quite complex and in non-closed forms.

The main theme of this thesis will be concerned with developing theoretical models to describe non-Gaussian effects in both turbulent flows and the stock markets dynamics. A comparison between empirical data and our theoretical predictions will be presented whenever possible, and we shall also discuss the most important improvements of our approach in relation to previous models.

In the context of finance we shall study certain financial instruments called "options" which can be used for both investment strategies and risk management, representing nowadays a multi-trillion market. An option is a derivative contract that gives its holder the right, but not the obligation, to buy (call option) or sell (put option) an underlying asset at a specified strike price on a specified maturity date. Because the price of an option depends not only

on the spot price of the underlying asset but also on the intensity of its fluctuations (i.e., the volatility), it is paramount to have a good model for the underlying asset price dynamics in order to obtain a reliable model for the option fair price.

The standard model of finance, namely the Black-Scholes model, surmises that risky asset prices can be described by a geometric Brownian motion, implying that the asset's logarithmic returns follow an uncorrelated Gaussian process. Within this Gaussian framework, an analytical expression for the price of a European call option—the celebrated Black-Scholes formula—can be obtained [Black and Scholes, 1973]. In the last two decades or so, however, empirical evidence has accumulated showing that financial markets often display heavy-tailed distributions [Mantegna and Stanley, 2007, Cont, 2001, Vasconcelos, 2004], meaning that large price fluctuations occur more frequently than predicted by Gaussian statistics. These findings led to the consideration of non-Gaussian distributions as alternative models to describe price fluctuations [Malevergne et al., 2005, Malevergne and Sornette, 2006].

One such distribution that has attracted considerable attention is the so-called Tsallis distribution [Tsallis, 1988, Tsallis, 2009], also known as the q-Gaussian distribution, which has the interesting feature of decaying with power law tails (the q-Gaussian recovers the standard Gaussian distribution when its parameter q is taken equal to 1.) An option pricing model within the framework of the q-Gaussian distribution has been introduced by Borland [Borland, 2002a,Borland, 2002b], who derived an analytic expression for the option price which generalizes the Black-Scholes formula. Another important non-Gaussian option pricing model is the empirical model introduced by McCauley and Gunaratne [McCauley and Gunaratne, 2003] which assumes that the returns follow an exponential distribution. Other non-Gaussian approaches to pricing options include models based on Lèvy stable distributions [Matacz, 2000, Miranda and R.Riera, 2001], which also have power law tails, and the so-called stochastic volatility models where the volatility of the underlying asset price is regarded as a randomly fluctuating quantity [Heston, 1993, Hull and White, 1987]. Option pricing strategies based on a variational minimization of the risk over the option duration have been used in [Bouchaud and Sornette, 1994, Bouchaud et al., 1995].

Another important stylized fact of financial data is a phenomenon akin to intermittency in turbulent flows [Cont, 2001, Ghashghaie et al., 1996, Arneodo et al., 1996]. Fluid intermittency is characterized by the tendency of the distribution of velocity differences between two points to develop long non-Gaussian tails at short distances. Similarly, in financial markets intermittency is manifest in the fact that the empirical PDF of price returns—i.e., the logarithmic differences between prices at two instants separated by a given time lag—often depends on the time lag. For time lags of the order of minutes or less the empirical PDFs tend to display power-law tails, whereas for lags of the order of hours or a few days the central part of the PDF

is better described by an exponential distribution, with a Gaussian regime being recovered for longer time scales; see, e.g., references [Silva et al., 2004, Matia et al., 2004, Kleinert and Chen., 2007, A.A.G.Cortines and R.Riera, 2007, Ramos et al., 2016] for discussions of this phenomenon. The change in shape of the empirical return distributions from an exponential law at the daily scale to a Gaussian distribution for larger time lags has also been studied in the context of the Heston model for stochastic volatility [Dragulescu and Yakovenko, 2002]. The convergence from power-law tails to a Gaussian distribution has been empirically investigated in several stock indices, such as the Dow Jones and the NYSE [Queirós, 2005]. Intermittency effects in finance have also been studied by means of the Kramers-Moyal coefficients associated with the evolution equation for the PDF of the price returns, see, e.g., references [Sornette, 2001, Cortines et al., 2007, Cortines et al., 2008].

Intermittency effects pose a serious problem for option pricing: since options have a lifespan of a couple of months but are frequently traded on relatively short-time scales, it is not clear *a priori* which type of model one should use to price options in markets where the empirical PDFs vary considerably with the time scale. It is thus important to pursue empirical analyses of option markets in light of different pricing models—Gaussian and non-Gaussian ones. In this context, it is of particular interest to investigate how these pricing models fare with respect to the time to maturity. For instance, in a recent comparative study of the exponential and the Black-Scholes models as applied to the Brazilian option market [Ramos et al., 2016], it was found that close to maturity the exponential model performs better than the Black-Scholes model.

In the first part of this thesis we investigate the applicability of the q-Gaussian model to the Brazilian market. First we analyze the statistics of the Ibovespa index, which is the main stock index of the São Paulo Stock Exchange. We study historical series of both daily closing prices and intraday quotes at 15 minutes intervals. We observe that the empirical distribution of the intraday returns is well described by a q-Gaussian, whereas the daily returns follow an exponential distribution. After detecting this intermittency effect in the Ibovespa, we then proceed to analyze the option market on the Ibovespa index by studying a set of 345 option chains covering a period of two years of trading.

First we compared the q-Gaussian model (with $q > 1$) to the Black-Scholes formula ($q = 1$) and found that the former provides an improvement over the latter in only 30% of the cases. We then applied the exponential model to the option chains for which the q-Gaussian model surpasses the Black-Scholes model. Here we found that the exponential model better fits the data in 75% of the cases, implying that the q-Gaussian model performs simultaneously better than the Black-Scholes and the exponential models in less than 10% of all option chains analyzed here. Furthermore, we observe that the exponential model works significantly better

than the q-Gaussian model for option chains close to the expiration date, confirming a trend (in favor of the exponential model near maturity) that was seen in a previous comparison [Ramos et al., 2016] between the exponential model and the Black-Scholes model, as mentioned above.

In view of the intermittency exhibited by the market data, we propose an intermittency model to introduce this effect in the problem of option pricing. In other words, we include the stochastic nature of the volatility in a model for option pricing. For this, we consider a multiscale dynamical model to describe the dynamics of the stochastic volatility process. The model is justified by the idea of an information cascade between the different agents of financial markets, a notion which has been employed in previous works, such as [Ghashghaie et al., 1996, Cont and Bouchaud, 2000, Breymann et al., 2000, Muzy et al., 2000, Arnéodo et al., 1998, Lux, 2001, Bacry et al., 2013]. So we can use an analogy between energy cascades in physical phenomena (as the Kolmogorov energy cascade in turbulence) and information cascades in finance. Under this parallel, the volatility is assumed to be described by a multiscale model for complex systems recently developed by [Macêdo et al., 2017, Salazar and Vasconcelos, 2012]. With this model, the stationary PDF for the volatility is obtained in closed form in terms of the Meijer G-function [Prudnikov et al., 1989]. Macêdo et al., used this distribution to obtain a model for the returns distribution and applied it to analyze Ibovespa time series of intraday quotes at every 30 seconds. To do this, they used the procedure known as statistical composition, or superstatistics [C.Beck, 2004], assuming that the dynamics of returns is faster than that of the variance (the volatility). Consequently, it is possible to write the marginal distribution of returns as a statistical superposition of the variance distribution and a quasi-equilibrium distribution for the returns conditioned to a variance value. A more detailed discussion is presented in chapter 4.

Our approach to include the random nature of volatility in the context of option pricing is to consider it as a stochastic variable in the Black-Scholes formula. The stochastic process describing it is the multiscale model discussed above and therefore its stationary distribution can be written in terms of the G-function. Assuming that the volatility is a slowly fluctuating variable, we are able to compute the option price as an average of the Black-Scholes formula over this variable distribution. With this procedure we find an expression for the option price, at least formally, which is written in terms of a definite integral of the bivariate Meijer G-function [Mittal and Gupta, 1972]. We present some results of the model as a function of the different parameters and compare it with the results yielded from the Black-Scholes formula. In particular, we notice that it behaves similarly to classical models for stochastic volatility such as the Heston and Hull-White models. For instance, it displays the so-called *volatility smiles*, which can be customized by the variation of the different parameters. We also apply our model to fit some options data of the Brazilian market showing that our results are always

better than those of the Black-Scholes formula. The preliminary results shown here suggest further analyses including more data, the direct comparison with other stochastic volatility models and improvements of the numerical implementation of the bivariate Meijer G-function.

As to turbulent flows, we study the PDF of velocity differences between two points separated by a given distance. Our research aims to reproduce two critical properties of the velocity increments statistics: i) The strongly non-Gaussian behavior and ii) the skewness shown by its distribution. In this context, several models have been proposed. For example [Beck, 2000] employed a distribution of the Tsallis class, and a model based in the approximate log-normality of the energy dissipation has been proposed in [Castaing et al., 1990]. Likewise, in [Chevillard et al., 2006] the distribution of velocity increments is written as a superposition of the derivatives of a Gaussian function. Despite all this, a quantitative description of intermittency and skewness in velocity increments distributions is still a challenge. Here we propose a way to obtain a distribution maintaining the main statistical features observed empirically. Our model is built considering the hierarchical model for intermittency proposed in [Macêdo et al., 2017] and discussed above in the context of volatility in financial markets, but in this case the stochastic variable is the energy dissipation rate. In the same paper, Macêdo et al. dealt with the velocity increments distributions in a symmetric fashion. This was attained with the statistical composition of a zero-mean Gaussian distribution with slowly fluctuating variance, and the distribution of these variances obtained from the hierarchical model. Here we also adopted the superstatistics procedure with the same distribution for the energy dissipation rate but with a conditional Gaussian distribution with a slowly fluctuating variance and with an average depending linearly on the variance. In this way, by performing the statistical composition we obtain an asymmetric distribution written in terms of a bivariate Meijer G-function. We analyze some properties of the model, such as the particular case when only one scale is considered in the stochastic hierarchy driving the energy flux. In this circumstance, the distribution is found to be expressed in terms of a Bessel function of the second kind, similar to the Generalized Hyperbolic Skew Student's t-distribution (GH) in [Aas and Haff, 2006, Ernst and v. Hammerstein Ernst August, 2004]. This kind of distribution appears in applications of turbulence and financial markets. Their asymptotic analysis exhibits different behaviors in each of the tails, being one heavy and one semi-heavy tail. The general case with several scales in the hierarchy driving the energy flux also shows this behavior, as discussed in this thesis.

This thesis is organized as follows. In chapter 2 we present a brief review of the main concepts related to the problem of option pricing as well as three statistical models proposed with this end, namely the Black-Scholes model, the exponential model, and the option model based on the q-Gaussian distribution. The Hull-White and Heston models for stochastic volatility

are also briefly discussed. In chapter 3 an empirical analysis of both daily and intraday returns of the Ibovespa is performed in light of the Gaussian, exponential and q-Gaussian models, alongside with an analysis of the Brazilian option market using three option pricing formulas: the Black-Scholes, exponential and the Borland q-Gaussian model. In chapter 4 we put forward our hierarchical model for option pricing. We start reviewing the dynamical model for the volatility and the underlying assumptions of our approach. Also, the model results are computed as a function of the different parameters and a brief comparison with empirical data is done. Chapter 5 is an introduction to the concepts related to fluid turbulence phenomena. A review of the hierarchical model for the energy dissipation rate is presented along with the symmetrical version for the distribution of velocity increments proposed by [Macêdo et al., 2017]. In chapter 6 we discuss our asymmetric statistical model for the velocity increments in turbulence. We compare the model predictions with numerical data from direct numerical simulations (DNS) of the Navier-Stokes equations as well as with experimental data. In chapter 7 we summarize our main findings, drawing conclusions and perspectives.

2 Option and Derivatives: An Introduction

2.1 Random Nature of Stock Prices

Before beginning with the mathematical theory of options and derivatives we need to introduce several economic concepts about financial markets. We shall also discuss some mechanisms by which financial instruments are exchanged or traded and some features of the fluctuating nature of financial markets. In financial markets different financial instruments or assets are traded such as stocks, commodities and exchange rate of money. The chance to obtain a profit on an investment in an asset depends on the risk level of the asset. Assets therefore can be risk-free or can carry some risk. For example, a bank account may be considered risk free since the bank pays a specific interest rate and the holder has a predictable profit. On the other hand, goods like stocks involve a certain degree of risk because their prices are subjected to unpredictable fluctuations. In this case, the chances of earning or losing depend for example on the investment strategy, the risk tolerance, or our ability to predict the market behavior. For this reason, trading with stocks is attractive to aggressive investors who take advantage of the fluctuating nature of the prices through transactions from which they hope to make some profit.

The trading of stocks are usually done in organized exchanges, such as, the New York Stock Exchange (NYSE) and the Sao Paulo Stock Exchange (BOVESPA). The average behavior of a market is given by the so-called indexes. For example, a stock index represents the mean price of a set of stocks. Each index is calculated with a specific methodology. For example the Bovespa Index (Ibovespa) is a total return index which measures the price movements of its stock components and in addition assumes that all gains are reinvested into the index. In general, the eligible stocks which may be selected as index constituents are those that meet an inclusion criteria (usually, the more actively traded and better representative stocks).

The current price of a stock reflects the overall value of a company and also depends on the future performance of this company. Thus, it is expected that an investor would like to know if it is worth investing in determined stock when he only has the information at present time. The difficulty here lies in the fact that stock prices show a certain degree of uncertainty. This is observed, for instance, when the historical series of a stock index is plotted as a function of time, as shown figure **2-1** for the Bovespa index from July 2012 to July 2017 (data downloaded from [BM&FBOVESPA, 2018]).

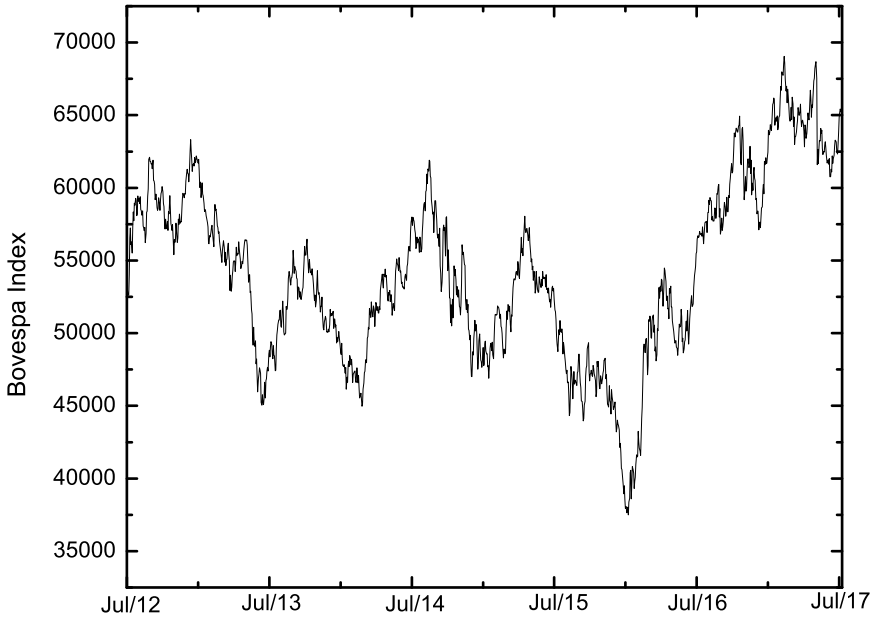

Figure 2-1 : Historical series of the Bovespa Index from July 2012 to July 2017.

It seems difficult to make a prediction about the future behavior of stock prices on the basis of the present information. However, it is possible to describe the dynamics of the prices using probabilistic ideas. To understand that, let us introduce some basic ideas and applications, including the modeling of option prices.

We can first consider the case of a bank account. If you have one dollar in a bank account, that pays an interest rate r, then the money $B = B(t)$ you have at time t increases at a rate

$$\frac{dB}{dt} = rB. \tag{2.1}$$

Therefore, the money in the account at time t is given by the solution of the differential equation (2.1), with the initial condition $B(0) = 1$. So that,

$$B(t) = e^{rt}. \tag{2.2}$$

In an analogous way, for the case of a stock with value S, its growth rate can be written as

$$\frac{dS}{dt} = R(t)S, \tag{2.3}$$

where $R(t)$ is the rate of return of the stock. Due to the random nature of financial markets, the rate $R(t)$ can be considered as composed of two parts. The first part, like the interest rate of a bank account is of predictable nature, and here it is denoted by μ. The second one,

which contains the fluctuating nature of the stock value, is introduced as a probabilistic noise $\xi(t)$. So the rate of return is expressed as the sum of these terms, i.e. $R(t) = \mu + \xi(t)$, and the variation of the stock price becomes

$$\frac{dS}{dt} = [\mu + \xi(t)]S. \tag{2.4}$$

The noise term $\xi(t)$, which is also associated to the risk of the stock price, is written as a white noise, like in the Brownian motion (see Appendix B).

2.2 Options Contracts

Besides stocks and commodities, there are other types of financial instruments which are traded in the same way. These securities are generically called derivatives because they derive their value from the price of some primary underlying asset. This is the case of the options contracts of which there are several kinds. Here we only consider option contracts known as *European options*. The characteristic of a European option is that it can only be exercised at the future date specified in the contract. Another case is, for example, an American option, which can be exercised at any time up to maturity. Below we give a formal definition of a European option.

A European call (put) option with exercise price K and expiration date T, written on an underlying asset with price S, is a contract that gives the holder the right to buy (sell) the underlying asset for the price K at time T.

Trading with these contracts is of great interest because through its selling and buying it is possible to design financial operations to obtain earnings or reduce the risk in an investment. To understand this, let us explain how an option works. Consider a call option with expiration time T on a stock whose price S_T at maturity is above the strike price K. In this case, the holder of the option will exercise his right to buy the stock from the underwriter at price K and sell it in the market at the spot price S_T, earning a profit equal to the difference $S_T - K$. On the other hand, if the price S_T is lower than the strike K, then the holder of the option would rather buy the asset in the current market if he so wishes. Thus the holder will not exercise his right and the option expires worthless. The payoff of a call option at maturity is therefore given by

$$Payoff_{call} = \max(S_T - K, 0). \tag{2.5}$$

The behavior of $Payoff_{call}$ as a function of S can be seen in figure **2-2**. Here we can say, that if the stock price S_T is less than the strike K, then the call function is equal to zero; otherwise, the function has the value given by the line with unitary slope, as indicated in equation (2.5). The thin line indicated for $t < T$ is the call option price at time t before of

expiration. This price is greater than the price at time T owing to considerations about the risk of the investment. In other words, the farther in time is the expiration date of the option, the more uncertain is the behavior of the stock and thus more risky is the option. Hence its price is higher for $t < T$ as compared to the payoff at $t = T$.

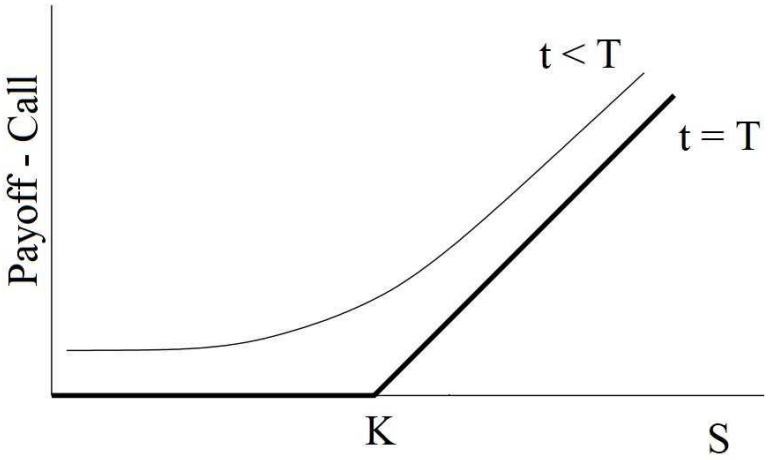

Figure 2-2 : Call payoff as a function of the stock price S.

In a similar way, the payoff of put options is written as

$$Payoff_{Put} = \max(K - S_T, 0). \tag{2.6}$$

This means that if the market stock price at the expiration time T is less than the strike K, the holder can buy the stock in the market at price S and sell to the option underwriter at price K pocketing a profit equal to the difference into (2.6). If otherwise, $S_T > K$, the option worth is zero. This is illustrated in figure **2-3**.

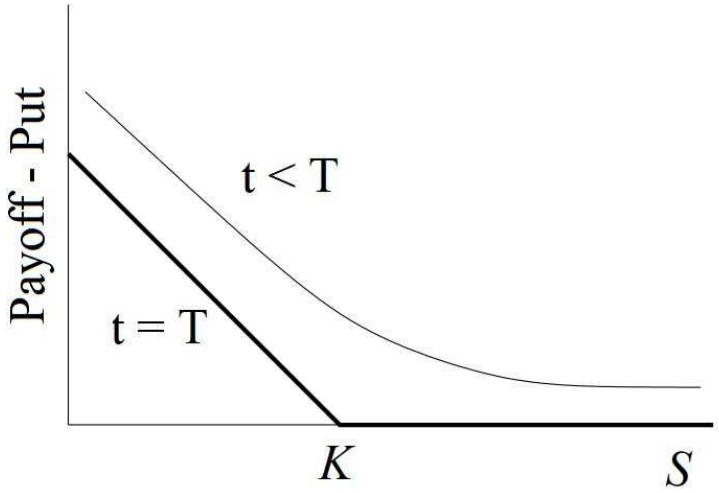

Figure 2-3 : Put payoff as a function of the stock price S.

We have omitted the fact that the holder of an option must pay a premium C for this contract. Thus, the net profit which the holder gets only occurs if $S_T > K + C$. So, the graph that represents the profit of an option must be modified by subtracting the premium C from the payoff graph, which is shown in figures **2-4** and **2-5** for the call option and put option respectively.

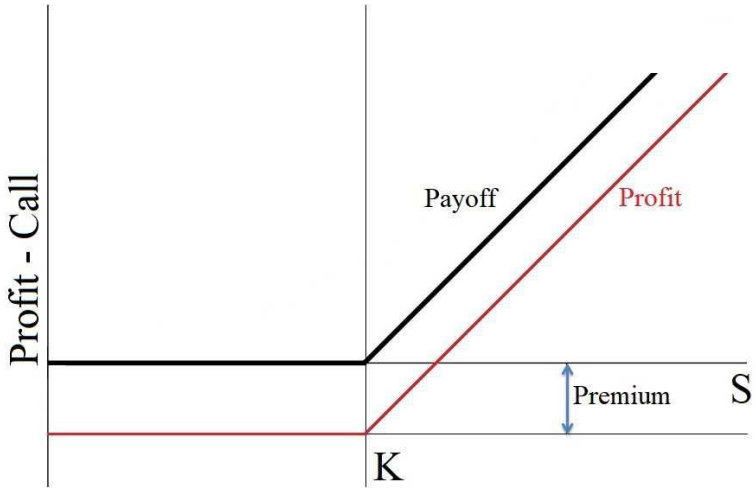

Figure 2-4 : Profit of a call option as function of the asset price S.

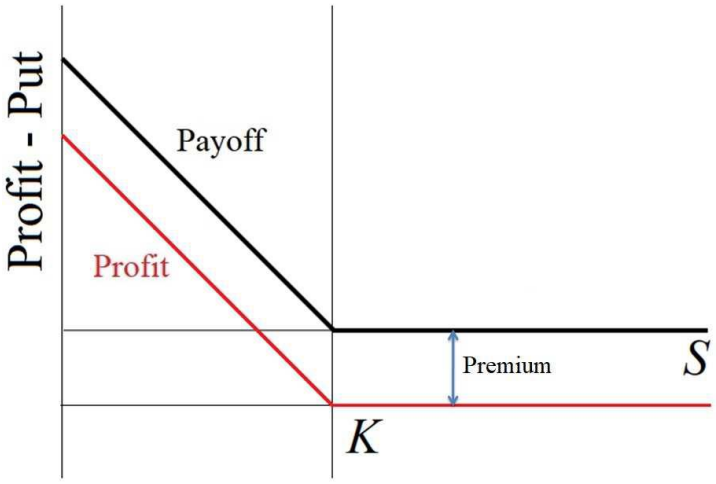

Figure 2-5 : Profit of a put option as function of the asset price S.

As already mentioned, the holder of an option must pay a price C for the option, since it entitles him to a right and hence a chance to make a profit. The question then is: What is the fair price C for both holder and the underwriter of the option?. For example, let us consider a transaction where a call option is traded. Here, it is expected that the buyer of the option would like to pay the lowest possible price for the option, which implies that he will have the greater profit on the investment. Contrarily, the underwriter of the option would like to receive the highest possible price for the premium of the option, so if the stock price in the market at time of maturity is higher, he would lose little money. Thus, the problem now is to determine the fair price of the option. Clearly, this depends on K and S_T, and intuitively on our ability to predict the future states of the market. A solution to this problem was given in 1973 in the famous papers by Black and Scholes [Black and Scholes, 1973] and Merton [Merton, 1973], for which Scholes and Merton won the Nobel prize in Economics in 1997. The main improvement of the so-called Black-Scholes model is that includes the random nature of the prices of the underlaying asset. However, due to some unrealistic assumptions about the market, generalizations of this model and other approaches have emerged. For instance, a strong assumption in the Black-Scholes model is that the volatility of prices is a constant, but empirical evidence shows that it also has a random nature. In order to deal with this problem, the so-called stochastic volatility models were introduced, such as the Hull-White and Heston models [Hull and White, 1987, Heston, 1993], and others derived directly from empirical analysis of the market. In the remainder of this chapter, we will review some of these approaches to the problem of option pricing. In the next chapter we will discuss the application of these models to perform a statistical analysis of the Brazilian stock and option

markets.

2.3 Gaussian Approach

2.3.1 The Black-Scholes model

The goal of Black and Scholes [Black and Scholes, 1973] was to calculate the price of options and other derivatives written on an underlying stock with market price $S(t)$. The model presupposes that in the market there are two assets, a bank account with a value $B(t)$ and a stock with price $S(t)$. The bank account is a risk-free asset which follows the stochastic differential equation (SDE) (2.1), which we rewrite as

$$dB = rBdt. \tag{2.7}$$

where r is the risk-free interest rate. The stock price $S(t)$ follows a Langevin type SDE like (2.4).

$$dS = \mu Sdt + \sigma SdW, \tag{2.8}$$

where $\mu > 0$ is the stock expected mean rate of return, $\sigma > 0$ is the volatility and $W(t)$ is the standard Brownian motion or Wiener process. The process (2.8) is known as the Geometrical Brownian Motion (GBM). It is worth to mention that the standard Brownian motion or Wiener process $\{W(t),\, t \leq 0\}$ satisfies the following properties:

i) W(0)=0.

ii) The increments $W(t) - W(s)$ are stationary and independent.

iii) For $t > s$, $W(t) - W(s)$ has a Gaussian distribution $N(0, \sqrt{t-s})$.

iv) The trajectories are continuous.

The conditions (ii) and (iii) indicate that the process $W(t)$ is distributed according to $N(0, \sqrt{t})$.

Let us now define the process

$$x = \ln \frac{S(t + \Delta t)}{S(t)}. \tag{2.9}$$

The variable $x(t)$ is called the logarithmic return of the price S at time lag Δt. (We shall refer to x simply as the return.) Using Ito's Lemma (see Appendix A), one can show that the stochastic process for the return is given by,

$$dx = \left(\mu - \frac{\sigma^2}{2}\right) dt + \sigma dW. \tag{2.10}$$

The stochastic integration of this process results,

$$x(t) = x(t_0) + \left(\mu - \frac{\sigma^2}{2}\right)(t - t_0) + \sigma[W(t) - W(t_0)]. \tag{2.11}$$

Therefore, taking into account the properties of $W(t)$, we can conclude that the returns $x(t)$ are distributed according to a normal distribution with mean $\mu' = (\mu - \frac{1}{2}\sigma^2)\Delta t$ and variance $\sigma^2\Delta t$:

$$f(x,t;\mu,\sigma) = \frac{1}{\sigma\sqrt{2\pi\Delta t}} \exp\left(-\frac{[x-(\mu-\frac{1}{2}\sigma^2)\Delta t]^2}{2\sigma^2\Delta t}\right), \tag{2.12}$$

The equivalent distribution of the price S is obtained using $\widetilde{f}(S)dS = f(\ln S)d(\ln S)$. So, we obtain

$$\widetilde{f}(S,t;\mu,\sigma) = \frac{1}{\sqrt{2\sigma^2\Delta t}}\,\frac{1}{S}\,\exp\left(\frac{\left[\ln\frac{S}{S_0} - \left(\mu - \frac{\sigma^2}{2}\right)\Delta t\right]^2}{2\sigma^2\Delta t}\right). \tag{2.13}$$

The option price in the Black-Scholes model achieves a closed formula denoted by $C(S,t;K,T) \equiv C(S,t)$, which represents the present value for a European call option with strike price K, expiration date T, for a given price S of an underlying stock. Then, given the process (2.8) for the underlying stock, it is possible to write a SDE for the corresponding call option C by the Itô equation in the Appendix A, which reads

$$dC = \left[\frac{\partial C}{\partial t} + \mu S\frac{\partial C}{\partial S} + \frac{1}{2}\sigma^2 S^2\frac{\partial^2 C}{\partial S^2}\right]dt + \sigma S\frac{\partial C}{\partial S}dW. \tag{2.14}$$

A second order partial differential equation so-called Black-Scholes equation can be written for the option price C following the stochastic process above. There are two alternative derivations of the Black-Scholes equation (BSE), the first considering a delta-hedging portfolio and the second one assuming a replicating portfolio [Vasconcelos, 2004]. Here we only discuss the case considering a delta-hedging portfolio with which the risk of the investment can be eliminated, see appendix D. By assuming a delta-hedge strategy, the portfolio consists on taking a long position on the option $C(t)$ and a short position on a number Δ of stocks with price S. Here, Δ is the quantity of stocks for which the value of our portfolio will be protected. In addition, if the portfolio is self-financed, i.e. all trades are financed by selling or buying assets of the portfolio, its value Π takes the form

$$\Pi = C(S,t) - \Delta \cdot S. \tag{2.15}$$

Such that the dynamics of portfolio obeys the relation

$$d\Pi = dC - \Delta\, dS. \tag{2.16}$$

The dynamics of the portfolio can be written by substituting (2.8) and (2.14) into equation (2.16), yielding

$$d\Pi = \left[\frac{\partial C}{\partial t} + \mu S\frac{\partial C}{\partial S} + \frac{1}{2}\sigma^2 S^2\frac{\partial^2 C}{\partial S^2} - \Delta\mu S\right]dt + \sigma S\left[\frac{\partial C}{\partial S} - \Delta\right]dW. \tag{2.17}$$

Therefore, the risk is eliminated if the probabilistic term which contains dW is equal to zero, or in other words by choosing

$$\frac{\partial C}{\partial S} = \Delta. \tag{2.18}$$

In this case, equation (2.17) simplifies to

$$d\Pi = \left[\frac{\partial C}{\partial t} + \frac{1}{2}\sigma^2 S^2 \frac{\partial^2 C}{\partial S^2}\right] dt. \tag{2.19}$$

Since the portfolio is risk-free or purely deterministic, it must yield the same rate of return as the bank account. This means that the rate of change of the portfolio value follows the relation

$$d\Pi = r\Pi dt. \tag{2.20}$$

Comparing with (2.19) one finds that

$$r\Pi = \frac{\partial C}{\partial t} + \frac{1}{2}\sigma^2 S^2 \frac{\partial^2 C}{\partial S^2}. \tag{2.21}$$

Now integrating (2.16) and using (2.18), we have

$$\Pi = C - \frac{\partial C}{\partial S} S. \tag{2.22}$$

After substituting the relation above into (2.21), we finally obtain

$$\frac{\partial C}{\partial t} + \frac{1}{2}\sigma^2 S^2 \frac{\partial^2 C}{\partial S^2} + rS\frac{\partial C}{\partial S} - rC = 0, \tag{2.23}$$

which is known as the Black-Scholes differential equation. Its solution with the boundary condition

$$C(S,T) = \max(S - K, 0), \tag{2.24}$$

can be found by transforming (2.23) into a linear parabolic equation, which can in turn be transformed into the heat equation whose solution is known. Thus, this solution gives the price of a European option depending on the maturity T, the strike K, the underlying asset price S, the interest rate r and also on the volatility σ (variance of the Gaussian distribution of logarithmic return). After performing the calculations outlined above, one finds that the call option price predicted by the Black-Scholes model reads

$$C_{BS}(S, K, r, t; \sigma) = S\, N(d_1) - K\, e^{-r(T-t)} N(d_2), \tag{2.25}$$

where $N(x)$ is the cumulative distribution of a normal random variable

$$N(x) = \frac{1}{2\pi} \int_{-\infty}^{x} e^{-\frac{y^2}{2}} dy \tag{2.26}$$

and

$$d_1 = \frac{\ln(S/K) + \left(r + \frac{1}{2}\sigma^2\right)(T-t)}{\sigma\sqrt{T-t}} \tag{2.27}$$

$$d_2 = \frac{\ln(S/K) + \left(r - \frac{1}{2}\sigma^2\right)(T-t)}{\sigma\sqrt{T-t}} \tag{2.28}$$

2.3.2 Risk-neutral valuation

The result in (2.25) can be also obtained by using the risk neutral valuation [Cox and Ross, 1976]. In this approach, the expected return of the option value should be the same as that of a risk-free asset or a bank account. Thus, given the option on an underlying asset S and maturity T, whose value at time $t < T$ is $C(S,t)$, its expected value at maturity $C(S(T),T) = \langle \max(S(T)-K,0)\rangle_{\mathbb{Q}}$, will be

$$\langle \max(S(T)-K,0)\rangle_{\mathbb{Q}} = C(S,t)\, e^{r\Delta t}. \tag{2.29}$$

Here, $\langle \dots \rangle_{\mathbb{Q}}$ denotes the average under the appropriate measure $\mathbb{Q}$ where the discounted price $\tilde{S}(t) = e^{-r\Delta t}\, S(t)$ is a martingale [Vasconcelos, 2004]. The risk-free interest rate is r and $\Delta t = T - t$.

Now, we can determine the option price at time $t < T$ discounting its mean value $C(S,T)$ from the maturity T with an interest rate r,

$$C(S,K,r,t) = e^{-r\Delta t}\langle \max(S-K,0)\rangle_{\mathbb{Q}}. \tag{2.30}$$

The martingale measure $\mathbb{Q}$ is such that the price follows the log-normal distribution (2.13) with the rate of return being equal to the the interest rate of a risk-free asset $\mu = r$. Thus, according to this measure the returns follow a normal distribution:

$$p(x,t;r,\sigma) = \frac{1}{\sqrt{2\pi\Delta t\sigma^2}} \exp\left(-\frac{[x-(r-\frac{\sigma^2}{2})\Delta t]^2}{2\sigma^2\Delta t} \right). \tag{2.31}$$

The payoff of the option written as a function of the return $x = \ln \frac{S(t+T)}{S(t)} = \ln \frac{S}{S_0}$, take the form

$$C(S,K,r,t) = \max(S_0 e^x - K, 0), \tag{2.32}$$

and consequently the mean price of the option as shown in (2.30), becomes

$$C(r,K,S_0;\sigma) = e^{-r\Delta t} \int_{-\infty}^{\infty} \max(S_0 e^x - K, 0)\, p(x,t;\mu,\sigma)\, dx. \tag{2.33}$$

The option is worth only if $S_0 e^x - K > 0$, hence the integral above can be written as

$$C(r,K,S_0;\sigma) = e^{-r\Delta t} \int_{\ln(\frac{K}{S_0})}^{\infty} (S_0 e^x - K) \frac{1}{\sqrt{2\pi\Delta t\sigma^2}} \exp\left(-\frac{[x-(r-\frac{\sigma^2}{2})\Delta t]^2}{2\sigma^2\Delta t} \right) dx. \tag{2.34}$$

Performing the integration we obtain

$$C_{BS}(S_0,K,r,t;\sigma) = S_0\, N(d_1) - K\, e^{-r(T-t)} N(d_2). \tag{2.35}$$

where $N(x)$ is the cumulative distribution (2.26) and d_1, d_2 are given by (2.27) and (2.28) respectively. This is, we have obtained the same Black-Scholes formula in (2.25), but now using only the risk-neutral approach and the assumption that the logarithmic returns follows a Gaussian statistics. In a similar way, the risk-neutral valuation can be also used in cases when the logarithmic returns follows non-Gaussian statistics. In the following sections we analyze particular cases of the exponential and power law distribution.

2.4 An Empirical Exponential Model

Among the non-Gaussian approaches to describe the dynamics of logarithmic returns in financial markets, we shall mention the empirical exponential model introduced by [McCauley and Gunaratne, 2003]. In this section, we review this exponential model for the distribution of returns and also the corresponding option formula obtained from the risk-neutral valuation.

2.4.1 Exponential distribution of returns

The proposal of McCauley and Gunaratne in [McCauley and Gunaratne, 2003] uses an exponential distribution $f(x)$ written in the form

$$f(x) = \begin{cases} A\, e^{\gamma(x-\delta)} & \text{if} \quad x < \delta \\ B\, e^{-\nu(x-\delta)} & \text{if} \quad x > \delta \end{cases} \tag{2.36}$$

where A, B and δ are constants. In this case, the normalization condition $\int_{-\infty}^{\infty} f(x)dx = 1$, after imposing the condition $\langle x \rangle = \delta$, leads to the following normalization constants:

$$A = \frac{\gamma^2}{\gamma + \nu} \tag{2.37}$$

$$B = \frac{\nu^2}{\gamma + \nu}. \tag{2.38}$$

And the variance of the exponential distribution is found to be

$$\mathrm{Var}[x] = \frac{2}{\gamma\nu}. \tag{2.39}$$

2.4.2 Exponential option pricing

A closed formula for a European call option can also be obtained under the assumption that the returns of the underlying asset follow the exponential distribution given in (2.36). The option price can be found using the risk neutral valuation, discounting the expected option value $C(T)$ from the maturity T with a constant rate r [McCauley and Gunaratne, 2003]. So,

employing the equation (2.30) and using the exponential distribution (2.36) to calculate the average of the payoff, the exponential model for option pricing yields the following expression for the price C of a European call option:

$$C\, e^{r\Delta t} = \begin{cases} Se^{\delta}\, \frac{\gamma^2(\nu-1)+\nu^2(\gamma+1)}{(\gamma+\nu)(\gamma+1)(\nu-1)} + \frac{K\gamma}{(\gamma+1)(\gamma+\nu)} \left(\frac{K}{S}e^{-\delta}\right)^{\gamma} & , \quad S > Ke^{-\delta} \\ \\ \frac{K\nu}{(\nu-1)(\gamma+\nu)} \left(\frac{K}{S}e^{-\delta}\right)^{-\nu} & , \quad S < Ke^{-\delta} \end{cases} \tag{2.40}$$

Using the risk-neutral condition where the expected stock price $\langle S(t)\rangle$ behaves like a risk-free investment increasing exponentially at the rate of carrying r, we can write a relation for δ as a function of γ and ν as

$$r = \frac{1}{\Delta t}\int_t^T \mu(s)ds = \frac{1}{\Delta t}\ln\left(\frac{\langle S(t+\Delta t)\rangle}{S(t)}\right) = \frac{1}{\Delta t}\left(\delta + \ln\left(\frac{\gamma\nu+(\nu-\gamma)}{(\gamma+1)(\nu-1)}\right)\right) \tag{2.41}$$

where r is the risk-free interest rate, $\Delta t = T - t$ and μ is the expected rate of return of the stock. In this way, as r is known by the investors, δ can be fixed by determination of the parameters γ and ν.

2.5 A Power Law Model for Option Pricing

Other non-Gaussian alternative is to consider that the logarithmic returns follow a power-law distribution. Using this assumption Borland in [Borland, 2002a] presented a model for option pricing where the distribution of return is given by the q-Gaussian or Tsallis distribution [Tsallis, 1988]. Here we summarize the main ideas of the model, more details can be found for instance in [Borland, 2002a, Borland, 2002b].

2.5.1 Power law distribution

The q-Gaussian statistics arises by considering a stochastic process for the logarithmic returns $Y(t) = \ln\left(\frac{S(t+\Delta t)}{S(t)}\right)$ given by the following Itô-Langevin equation:

$$dY = \mu dt + \sigma P_q(Y,t)^{\frac{1-q}{2}} dW(t). \tag{2.42}$$

where $W(t)$ is the Wiener process and $P_q(Y,t)$ is the macroscopic probability of the process Y. The parameters q, μ and σ are constants of the model.

Using the Chapman-Kolmogorov theorem [Gardiner, 1985], it is possible to prove that this process has an associated Fokker-Planck equation (FPE) given by

$$\frac{\partial P(Y,t)}{\partial t} = -\mu\frac{\partial[P(Y,t)]}{\partial Y} + \frac{\sigma^2}{2}\frac{\partial^2[P(Y,t)^{2-q}]}{\partial Y^2}. \tag{2.43}$$

The solution of this equation results in a power law distribution:

$$P(Y,t) = \frac{1}{Z(t)}\left[1 - \frac{\beta(t)}{\sigma^2}(1-q)(Y - Y_0 - \mu t)^2\right]^{\frac{1}{1-q}}, \tag{2.44}$$

where

$$Z(t) = [(2-q)(3-q)ct]^{\frac{1}{3-q}} \tag{2.45}$$

and

$$\beta(t) = \frac{c}{Z^2(t)}. \tag{2.46}$$

Defining the variable

$$\Omega(t) = \frac{Y - \mu t}{\sigma} \tag{2.47}$$

the SDE in (2.42) can be written as

$$dY = \mu dt + \sigma d\Omega \tag{2.48}$$

with

$$d\Omega = P_q(\Omega,t)^{\frac{1-q}{2}} dW(t). \tag{2.49}$$

From (2.47) we immediately have

$$d\Omega = d\left(\frac{Y - \mu t}{\sigma}\right). \tag{2.50}$$

Thus, the new variable Ω obeys the following Fokker-Planck equation:

$$\frac{\partial}{\partial t}P_q(\Omega,t|\Omega',t') = \frac{1}{2}\frac{\partial^2}{\partial\Omega^2}P_q(\Omega,t|\Omega',t')^{2-q}. \tag{2.51}$$

It is easy to show that this equation has the solution

$$P_q(\Omega,t|\Omega',t') = \frac{1}{Z_q(t)}\left[1 - \beta_q(t)(1-q)(\Omega - \Omega')^2\right]^{\frac{1}{1-q}} \tag{2.52}$$

where $Z_q(t)$ is related to the normalization of the distribution (2.52) and $\beta_q(t)$ is related to the definition of the variance of this distribution. They can be written as

$$Z_q(t) = \left[(2-q)(3-q)c_q(t-t')\right]^{\frac{1}{3-q}} \tag{2.53}$$

and

$$\beta_q(t) = \frac{c_q}{Z_q^2(t)}. \tag{2.54}$$

We can also write these in the form

$$Z(t) = \frac{\sqrt{\pi}\,\Gamma\left(\frac{3-q}{2q-2}\right)}{\Gamma\left(\frac{1}{q-1}\right)\sqrt{(q-1)\,\beta(t)}} \tag{2.55}$$

$$\beta_q(t) = \frac{1}{2\,\sigma_q^2(t)\,Z(t)^{q-1}}. \tag{2.56}$$

So, using (2.54), (2.55) and (2.56), we have

$$c_q = \frac{\pi\,\Gamma^2\left(\frac{3-q}{2q-2}\right)}{(q-1)\,\Gamma^2\left(\frac{1}{q-1}\right)}. \tag{2.57}$$

Considering $\Omega' = 0$ at $t' = 0$, then it is possible to write (2.52) in the way

$$P_q(\Omega, t) = \frac{1}{Z_q(t)}\left[1 - \frac{\beta_q(t)}{\sigma^2}(1-q)(Y-\mu t)^2\right]^{\frac{1}{1-q}}, \tag{2.58}$$

whose variance is

$$\langle (Y-\mu t)^2 \rangle = \begin{cases} \frac{\sigma^2}{(5-3q)\,\beta(t)} & , q < \frac{5}{3} \\ \infty & , q \geq \frac{5}{3} \end{cases}. \tag{2.59}$$

Therefore, the variance of the q-Gaussian distribution is only finite for $q < \frac{5}{3}$.

Now that we have a model for the returns based on the q-Gaussian statistics, we can derive a corresponding formula for the price of an option. This is done in the next section.

2.5.2 Call options pricing

An option pricing model has been obtained by Borland [Borland, 2002b] considering that the distribution of the logarithmic returns $Y(t)$ is described by a q-Gaussian distribution. In this model the stock price $S(t)$ should be calculated in some measured $\mathbb{Q}$, where it becomes a martingale, yielding

$$S(T) = S_0 \exp\left(rT - \frac{\sigma^2}{2}\int_0^T P_q^{1-q} dt + \sigma\Omega(T)\right). \tag{2.60}$$

Here $S(T) \equiv S(t + \Delta t)$ is the stock price at maturity T, $S_0 \equiv S(t)$ is the price at present time and r is the risk-free rate, and $\Omega(t)$ is a stochastic process which follows the q-Gaussian distribution (2.52). Now the integral involved into (2.60) can be calculated choosing $t' = 0$ and $\Omega' = 0$, yielding

$$\begin{aligned} \int_0^T P_q^{1-q} dt &= \int_0^T \left[(2-q)(3-q)ct\right]^{\frac{q-1}{3-q}} dt - (1-q)\int_0^T \frac{\beta(t)\Omega(t)^2}{Z(t)^{1-q}} dt \\ &= \left[(2-q)(3-q)c\right]^{\frac{q-1}{3-q}} \int_0^T t^{\frac{q-1}{3-q}} dt - (1-q)\int_0^T \frac{\beta(t)\Omega(t)^2}{Z(t)^{1-q}} dt \\ &= \frac{3-q}{2}\left[(2-q)(3-q)c\right]^{\frac{q-1}{3-q}} t^{\frac{2}{3-q}} - (1-q)\int_0^T \frac{\beta(t)\Omega(t)^2}{Z(t)^{1-q}} dt. \end{aligned} \tag{2.61}$$

Using (2.53) and defining

$$\begin{aligned}\alpha &= \frac{1}{2}(3-q)\left[(2-q)(3-q)c\right]^{\frac{q-1}{3-q}} \\ &= \frac{1}{2}(3-q)Z^{q-1}t^{\frac{q-1}{3-q}},\end{aligned} \tag{2.62}$$

equation (2.61) can be written as

$$\int_0^T P_q^{1-q}dt = \alpha T^{\frac{2}{3-q}} - (1-q)\int_0^T \frac{\beta(t)\Omega(t)^2}{Z(t)^{1-q}}dt. \tag{2.63}$$

As $P_q(\Omega(s), s)$ is the distribution of variable $\Omega(s)$ in the scale of time s, an equivalent distribution in a scale T can be written, such that the variable $\Omega(T) = \sqrt{\frac{\beta(s)}{\beta(T)}}\Omega(s)$ also follows a Tsallis distribution like (2.52). So the integral in (2.63) becomes,

$$\int_0^T P_q^{1-q}dt = \alpha T^{\frac{2}{3-q}} - (1-q)\int_0^T \frac{\beta(T)\Omega(T)^2}{Z(t)^{1-q}}dt. \tag{2.64}$$

The product $\beta(T)\Omega(T)^2$ is a constant and therefore it can be excluded from the integral in the second term, i.e.

$$\int_0^T P_q^{1-q}dt = \alpha T^{\frac{2}{3-q}} - (1-q)\beta(T)\Omega(T)^2\int_0^T \frac{dt}{Z(t)^{1-q}}. \tag{2.65}$$

The integral into (2.65) is computed using the definition for $Z(t)$ in (2.53) and the definition of α in (2.62). So, it results

$$\int_0^T P_q^{1-q}dt = \alpha T^{\frac{2}{3-q}}\left[1-(1-q)\beta(T)\Omega(T)^2\right], \tag{2.66}$$

which implies that the equation for the price $S(t)$ in (2.60) can be write in the form

$$S(T) = S_0\exp\left(rT + \sigma\Omega(T) - \frac{\sigma^2}{2}\alpha T^{\frac{2}{3-q}}\left[1-(1-q)\beta(T)\Omega(T)^2\right]\right). \tag{2.67}$$

Choosing $q = 1$ one obtains the same martingale used in the Black-Scholes model, where S follows a driftless geometric Brownian motion and $\Omega(t)$ is a Wiener process $W(t)$. With $q > 1$ (power law case) there appears the term depending on $\Omega(T)^2$ in addition to terms into the Black-Scholes case, as a consequence of the noise-induced drift.

Now we can use the risk-neutral valuation to write the option price in the form

$$C = \langle e^{-rT}(S(T) - K)\rangle, \quad \text{for} \quad S(T) > K, \tag{2.68}$$

where the stock price $S(T)$ at maturity T is given by (2.67). Equation (2.68) can also be written as

$$C = \langle e^{-rT} S(T) \rangle - \langle e^{-rT} K \rangle. \tag{2.69}$$

Then, using the condition $S(T) > K$, we can use (2.67) to obtain

$$rT + \sigma\Omega(T) - \frac{\sigma^2}{2}\alpha T^{\frac{2}{3-q}} \left[1 - (1-q)\beta(T)\Omega(T)^2\right] - \ln\frac{K}{S0} > 0. \tag{2.70}$$

The inequality above is satisfied between the two roots of Ω,

$$\Omega_{1,2} = \frac{-1}{(1-q)\alpha T^{\frac{2}{3-q}}\sigma\beta(T)} \pm \left[\frac{1}{(1-q)\alpha^2 T^{\frac{4}{3-q}}(1-q)^2\sigma^2\beta(T)^2} - \frac{2}{(1-q)\alpha T^{\frac{2}{3-q}}\sigma^2\beta(T)}\left(rT + \ln\frac{S}{K} - \frac{\sigma^2}{2}\alpha T^{\frac{2}{3-q}}\right)\right]^{\frac{1}{2}}. \tag{2.71}$$

Using (2.71), the first average in (2.69) is:

$$\langle e^{-rT} S(T) \rangle = \frac{S}{Z(T)} \int_{\Omega_1}^{\Omega_2} \exp\left(\sigma\Omega(T) - \frac{\sigma^2}{2}\alpha T^{\frac{2}{3-q}} \left[1 - (1-q)\beta(T)\Omega(T)^2\right]\right) \times \left[1 - (1-q)\beta(T)\Omega(T)^2\right]^{\frac{1}{1-q}} d\Omega(T). \tag{2.72}$$

The second term yields

$$\langle e^{-rT} K \rangle = \frac{e^{-rt} K}{Z(T)} \int_{\Omega_1}^{\Omega_2} \left(1 - \beta(T)(1-q)\Omega^2\right)^{\frac{1}{1-q}} d\Omega. \tag{2.73}$$

Here $\beta(T)$, $Z(T)$, c_q and α were defined in relations (2.54),(2.57), (2.61) and (2.62), respectively.

The relations (2.72) and (2.73) can be written in terms of a normalized noise process with mean equal to zero and unit variance. This can be made using the following transformation of variable

$$\Omega_N = \Omega(T)\sqrt{\frac{\beta(T)}{\beta_N}}. \tag{2.74}$$

Choosing the condition of normalized variance we obtain $\beta_N = 1/(5-3q)$ and the option price finally results

$$C(S, K, T; \sigma, q) = S(t) M_q(d_1, d_2, b(\Omega_N)) - e^{-rT} K N_q(d_1, d_2), \tag{2.75}$$

where

$$M_q(d_1, d_2, b(\Omega_N)) = \frac{1}{Z_N} \int_{d_1}^{d_2} e^{b(\Omega_N)} \left[1 - (1-q)\beta_N \Omega_N^2\right]^{\frac{1}{1-q}} d\Omega_N, \tag{2.76}$$

$$N_q(d_1, d_2) = \frac{1}{Z_N} \int_{d_1}^{d_2} \left[1 - (1-q)\beta_N \Omega_N^2\right]^{\frac{1}{1-q}} d\Omega_N \tag{2.77}$$

and

$$b(\Omega_N) = \sigma\sqrt{\frac{\beta_N}{\beta(T)}}\Omega_N - \frac{\sigma^2}{2}\alpha T^{\frac{2}{3-q}}\left(1-(1-q)\beta_N\Omega_N^2\right). \tag{2.78}$$

The limits of integration $d_{1,2}$ are given by

$$d_{1,2} = \Omega_{1,2}\sqrt{\frac{\beta(T)}{\beta_N}} \tag{2.79}$$

So far, we have introduced the formalism of three statistical approaches for the description of returns and option prices in financial markets. We show in the next chapter that by using them, we can make a detailed analysis of the Brazilian stock and option markets. This will give us a better understanding of the market, which can be useful to think about investment strategies.

2.6 Stochastic Volatility Models

It is observed in financial markets data that when the volatility is plotted as a function of time, it exhibits a random behavior like that shown by the prices. Because of this, it is necessary to consider the dynamics of the volatility to be described by a stochastic process, i.e., now the volatility is regarded as a randomly fluctuating quantity. As a consequence of this, the dynamics of prices is also affected, which makes the distribution of returns non-Gaussian as observed in empirical data. Furthermore, the price of derivatives which depends on the asset price becomes dependent also on the volatility distribution. Therefore, it is expected that also affects for instance the prices of the options. To introduce the effect of the stochastic volatility in the option prices we shall discuss two classical models in finance, namely the Hull-White and Heston models [Hull and White, 1987, Heston, 1993]. Here we review the main features of these models and some preliminary ideas, which we will use for the development of the hierarchical model for option pricing in chapter 4. We also recall the result in [Vicente et al., 2006], in which a Heston model for volatility with two different time scales is considered.

2.6.1 Hull-White model

In the Hull-White model, the dynamics of a security price S and its instantaneous variance $v = \sigma^2$, is described by the following stochastic processes,

$$dS = \mu\, S\, dt + \sqrt{v}\, S\, dW_1, \tag{2.80}$$

$$dv = -\gamma\,(v - v_0)\, dt + \kappa\, v\, dW_2. \tag{2.81}$$

Here dW_1 and dW_2 are two Winner processes, which are assumed in general to be correlated and so obey the relation

$$\langle dW_1 dW_2 \rangle = \rho\, dt. \tag{2.82}$$

The parameters μ, γ and κ may be dependent on time t and the volatility v, and ρ is the correlation between the Wiener processes dW_1 and dW_2.

To obtain a partial differential equation for the price of a derivative asset $f(S, v, t)$, on a stock S following the dynamics discussed above, Hull and White [Hull and White, 1987] assumed that the volatility is not a traded asset. They showed that the price of the derivative security f, depending on the state variables S and v, must satisfy the differential equation,

$$\frac{\partial f}{\partial t} + \frac{1}{2}\left[v\, S^2 \frac{\partial^2 f}{\partial S^2} + 2\rho v^{3/2}\kappa S \frac{\partial^2 f}{\partial S \partial v} + \kappa^2 v^2 \frac{\partial^2 f}{\partial v^2}\right] - rf = -rS\frac{\partial f}{\partial S} - \gamma v^2 \frac{\partial f}{\partial v}. \tag{2.83}$$

This derivative asset can be for example an option with payoff $f(S_T, v_T^2, T) = \max(S_T - K, 0)$. Thus, the solution to (2.83) for this option at time t, may be derived by using the risk-neutral valuation procedure. So, Hull and White proposed the solution

$$f(S, v, t) = e^{-r(T-t)} \int f(S_T, v_T, T) p(S_T|S, v) dS_T, \tag{2.84}$$

where $p(S_T|S, v)$ is the conditional distribution of S_T at expiration given the security price S and variance v at time t. The conditional distribution of S_T depends on both the process driving S and the process driving v. As it is not possible to obtain this distribution depending on the two variables, $p(S_T|S, v)$ is obtained by the statistical composition

$$p(S_T|S, v) = \int g(S_T|S, \bar{v}) h(\bar{v}|v) d\bar{v}, \tag{2.85}$$

where $h(\bar{v}|v)$ is the distribution of the mean variance $\bar{v}$ given the value of the variance v at time t. The price distribution conditioned to the mean volatility $g(S_T|S, \bar{v})$ is a log-normal distribution when the correlation ρ between the volatility and the price S_T is equal to zero. The mean variance $\bar{v}$ over the life time of the derivative security is defined by the stochastic integral,

$$\bar{v} = \frac{1}{T-t}\int_t^T v(\tau) d\tau. \tag{2.86}$$

Thus, the solution suggested by Hull and White is obtained substituting (2.85) into (2.84) yielding,

$$f(S, v, t) = \int \left[e^{-r(T-t)} \int f(S_T, v_T, T) g(S_T|\bar{v}) dS_T\right] h(\bar{v}|v) d\bar{v}. \tag{2.87}$$

Note that the term in square bracket is the Black-Scholes price for a given $\bar{v}$:

$$C_{BS}(S, K, t|\bar{v}) = e^{-r(T-t)} \int f(S_T, \bar{v}, T) g(S_T|\bar{v}) dS_T \tag{2.88}$$

One can thus write

$$f(S,v,t) = \int C_{BS}(S,K,t|\bar{v})h(\bar{v})d\bar{v} \tag{2.89}$$

where we omitted the dependence of the distribution h on v.

The problem in the Hull-White's formulation is that the distribution of $\bar{v}$ is unknown. To circumvent this, they performed a series expansion of the Black-Scholes price about the expected value of $\bar{v}$. This allowed them to write an approximate formula for the option price as a function of the moments of $\bar{v}$, which can be calculated assuming that γ and k are constants in the stochastic process driving the volatility. Later in this thesis, we shall use a similar idea to obtain our hierarchical model for the volatility dynamics. But, instead of using the distribution of the mean volatility $\bar{v}$, we used the equilibrium distribution of the volatility v at the shortest time scale. In other words, the option price will be given as the average of the Black-Scholes price over the distribution of the volatility v. But, first, let us in the following section review another classical model for stochastic volatility namely the Heston model.

2.6.2 Heston model

Another model of stochastic volatility was presented by Heston [Heston, 1993]. In this model, the dynamics of an asset with price S and stochastic volatility v is described by the following system of SDEs [Cox et al., 1985],

$$dS = \mu\, S\, dt + \sqrt{v}\, S\, dW_1, \tag{2.90}$$

$$dv = -\gamma\, [v - v_0]\, dt + \kappa\, \sqrt{v_0\, v}\, dW_2, \tag{2.91}$$

with

$$\langle dW_1 dW_2 \rangle = \rho\, dt. \tag{2.92}$$

In the stochastic process (2.90) for the asset price S, μ is the drift rate of S, v is the stochastic volatility and dW_1 is a Brownian motion process. In the process (2.91) for the volatility, v_0 is the long-run mean of v, γ is the rate of reversion and κ is called the volatility of volatility. Here, the correlation between the two variables S and v is given by ρ.

As in the case of the Hull-White model and using standard arbitrage arguments, it can be proved that the value of a derivative asset f must satisfy the partial differential equation,

$$\begin{aligned} &\frac{1}{2}vS^2\frac{\partial^2 f}{\partial S^2} + \rho\,\kappa\, v\, S\, \frac{\partial^2 f}{\partial S \partial v} + \frac{1}{2}\kappa^2 v \frac{\partial^2 f}{\partial v^2} + rS\frac{\partial f}{\partial S} \\ &\qquad + [\gamma(\theta - v) - \lambda(S,v,t)]\, \frac{\partial f}{\partial v} - rf + \frac{\partial f}{\partial t} = 0, \end{aligned} \tag{2.93}$$

where the term $\lambda(S,v,t)$ represents the price of volatility risk which is proportional to the volatility v. Heston assumed that if the derivative f is a call option $C(S,v,t)$, with strike K

and maturity at time T, thus it must satisfy the differential equation (2.93). Therefore, by analogy with the Black-Scholes model Heston uses a trial solution in the form

$$C(S,\nu,t) = SP_1 - KP(t,T)P_2. \tag{2.94}$$

Here, the first term is the spot asset upon optimal exercise and the second term is the present value of the strike price. Using the logarithmic return $x = \ln(S)$ and replacing (2.94) into (2.93), one finds that the equation above satisfies (2.93), if the functions P_j (with $j = 1, 2$), are written as

$$P_j(x,v,T;\ln[K]) = \frac{1}{2} + \frac{1}{\pi}\int_0^\infty Re\left[\frac{e^{-i\phi\ln[K]}f_j(x,v,T;\phi)}{i\phi}\right]d\phi. \tag{2.95}$$

The function $f_j(x,v,T;\phi)$ is the characteristic function of P_j, which satisfies the same partial differential equation (2.93). This integral is difficult to evaluate because of its limits of integration. However, methods such as the one proposed by Carr and Madan in [Carr and Madan, 1999] using the Fourier transform can be used to estimate the price of an option in this model.

2.6.3 Heston model with two relaxation times

Empirical evidence that suggests a Heston model with more than one time scale is found in the work of [Vicente et al., 2006]. In this, the Heston model is applied to study the dynamics of market prices fluctuation in the Brazilian market. In particular, they studied the autocorrelation function of the logarithmic returns variance of the Bovespa index data from January 1990 to January 2005.

The stationary autocorrelation function of the volatility for the standard Heston model is found to be,

$$C(\tau|\gamma,v_0,\kappa) = \frac{e^{-\gamma\tau}}{\beta}, \tag{2.96}$$

where γ is the rate of reversion, v_0 is the long run mean, $\beta = \frac{2\gamma}{\kappa^2}$ and κ is the volatility of volatility.

They found however that the empirical autocorrelation of the volatility function is not well described by formula (2.96). They observed, by fitting the data, that this autocorrelation is better described by a sum of two exponentials:

$$C(\tau|\gamma,v_0,\kappa) = c_1\, e^{-\gamma_2\tau} + c_2\, e^{-\gamma_2\tau}. \tag{2.97}$$

Based on this finding, they suggested that a Heston model with two scales of relaxation times should be used to describe the volatility process. The resulting dynamics can then be written

as

$$dS = \mu\, S\, dt + \sqrt{v_2}\, S\, dW_0, \tag{2.98}$$

$$\begin{aligned} dv_1 &= -\,\gamma_1\,[v_1 - v_0]\,dt + \kappa_1\sqrt{v_0\, v_1}\, dW_1 \\ dv_2 &= -\,\gamma_2\,[v_2 - v_1]\,dt + \kappa_2\sqrt{v_1\, v_2}\, dW_2. \end{aligned} \tag{2.99}$$

This result is an important starting point for our aim to introduce a hierarchical model for volatility and therefore a hierarchical model of option pricing. In chapter 4, we consider models where the dynamics of the asset prices S follows a stochastic process like (2.98) and the dynamics of the volatility v is described for a system of several stochastic processes as those given in (2.99). In our model each process has a characteristic relaxation time and assuming that the relaxation times are considerably different (time scales well separated), we can obtain an analytical model for the option price as will be discussed in detail in chapter 4.

2.7 Implied Volatility

According to the Black-Scholes model, a single volatility value would be sufficient to describe the prices of a set of options with same maturity time and traded the same day. However, the market option prices differ slightly from the prediction of the Black-Scholes model. In other words, this means that the volatility cannot be the same for all the options in the set. An estimate of the volatility for the price of the underlying asset of an option is the so-called implied volatility. This is defined as the value of the volatility of the underlying asset that when is replaced into the Black-Scholes formula it gives a theoretical value equal to the current market price of the option. In other words, the implied volatility σ_{imp} is the value of the volatility σ obtained by solving it into the equation

$$C_{BS}(S, K, r, t; \sigma) - C_{Market} = 0. \tag{2.100}$$

When the implied volatility σ_{imp} of a set of options with same maturity (see figure **2-6**a) is plotted as a function of the strike K, a smile-like curve emerges, an effect known as "volatility smile" and depicted in figure **2-6**b. There are two hypotheses as to why this effect appears. From a practical viewpoint this is explained considering that in-the-money ($K < S$) and out-of-the-money ($K > S$) options have a higher demand. So, the price of the option increases and also its implied volatility. A more technical explanation involves the non-Gaussian character of the distribution of returns of the asset price. In other words, this may explain why extreme fluctuations are very probable in financial markets.

In the course of this thesis, we will use this concept as a criterion to establish discrepancies between empirical data and the theoretical predictions of the different models for option

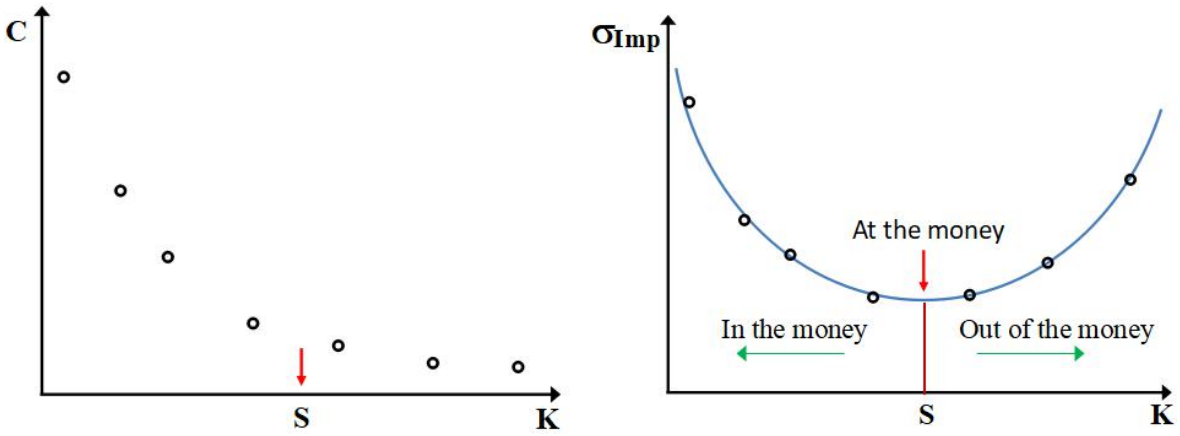

(a) (b)

Figure 2-6 : (a) Set of options with same maturity and (b) corresponding smile of volatility.

pricing considered here. For example, in the following chapter where we will discuss the application of the non-Gaussian models reviewed in sections 2.4 and 2.5 to analyze the statistics of the Brazilian option markets. Later in chapter 4, we will also use this concept to determine the properties of our hierarchical model for option pricing.

3 Non-Gaussian Option Models in the Brazilian Market

3.1 Introduction

In this chapter, we show an analysis of Ibovespa data in the light of the non-Gaussian models presented in chapter 2. In section 3.2, an empirical analysis of both the daily and intraday returns of the Ibovespa is performed in light of these three models. In section 3.3 we briefly describe our option data and the methodology used to study them. The results of our analysis of the Brazilian option market are presented in section 3.4.

3.2 Statistical Analysis of the Ibovespa Returns

To begin our analysis of the Brazilian market, let us recall that the logarithmic return $x(t)$ of the price S at time lag τ is defined as

$$x_\tau(t) = \ln S(t+\tau) - \ln S(t). \tag{3.1}$$

So, for example, if we have a daily data series for the prices of a stock, the daily logarithmic return ($\tau = 1\,\text{day}$) is given by the difference between the logarithm of the prices computed at successive days. Here, we have analyzed logarithmic returns obtained from two historical series of the Ibovespa: i) a series of daily closing prices from January 1968 up to February 2004, totaling 8889 data points, and ii) a series of intraday quotes at every 15 minutes covering the years from 1998 to 2001, containing 19995 data points. We fitted the empirical distributions for both series with the three theoretical distributions given in equations (2.31, 2.36, 3.5). Analyzing the quality of the respective fit, we determined which model best describes the empirical data in each case. When performing empirical analyses of returns, it is often convenient to normalize the returns to unit variance. With this is possible to fix some parameters in the models analyzed. Let us discuss briefly this:

For example, in the Gaussian case (2.31), with returns of unit variance, we define a new variable:

$$x = \frac{Y}{\sqrt{\mathrm{V}ar[Y]}} = \frac{Y}{\sqrt{\sigma^2 t}}, \tag{3.2}$$

whose PDF then becomes

$$p(x,t) = \frac{1}{\sqrt{2\pi}} \exp\left(-\frac{(x-\mu')^2}{2}\right), \tag{3.3}$$

where

$$\mu' = \frac{\left(\mu - \frac{1}{2}\sigma^2\right)\sqrt{t}}{\sigma}.$$

One then sees that the normalized mean μ' is proportional to $\sqrt{t}$, which becomes negligibly small for small timescales. Because of this property, we shall often assume that the normalized returns at short time lags have zero mean, which is a valid approximation for the empirical data, as we will see later.

For the exponential case, the original distribution (2.36) can be easily normalized to unit variance by setting

$$\gamma\nu = 2. \tag{3.4}$$

In applying formula (2.36) to the normalized empirical returns, we shall consider that the returns have zero mean, i.e., $\delta = 0$, in which case the exponential distribution (with unity variance) is left with only one free parameter (either γ or ν) to be determined from the fitting procedure.

Now consider the power law distribution with normalized returns, $x = (Y - \mu t)/\sqrt{\langle (Y - \mu t)^2 \rangle}$. One then has $\beta = 1/(5 - 3q)$, Z is given by (2.54) and so one has the following normalized distribution:

$$P_q(x) = \frac{\Gamma\left(\frac{1}{q-1}\right)}{\sqrt{\pi}\,\Gamma\left(\frac{3-q}{2q-2}\right)} \sqrt{\frac{q-1}{5-3q}} \left[1 - \left(\frac{1-q}{5-3q}\right) x^2\right]^{\frac{1}{1-q}}. \tag{3.5}$$

One then sees that the q-Gaussian with zero mean and unity variance has only one free parameter, namely the parameter q.

Using the data series of daily closing prices from January 1968 up to February 2004 we proceed to calculate the logarithmic returns series by using the relation (3.1), in the scale $\tau = 1\,day$ and the corresponding PDF of this set data. We chose to calculate a normalized to variance and centered PDF, by which, we subtracted the arithmetic mean of returns to the data series and we divided by its variance. To contrast the PDF with the statistical models (Gaussian an non-Gaussian) the least squares fit was used as presented in Appendix E.

Figure **3-1** shows the empirical distribution of daily returns (circles) and the respective fits by the exponential distribution (thick blue line) and the q-Gaussian (thin red line); also shown for comparison is a Gaussian of unity variance (dashed black line). It is clear from this figure that the empirical distribution deviates quite significantly from a Gaussian, whilst both the exponential and q-Gaussian distributions are in good agreement with the data. The exponential distribution, however, gives a better fit to the data in the sense that it yields a greater coefficient of determination (see Appendix E): $R^2 = 0.9917$ for the exponential distribution, whereas $R^2 = 0.9889$ for the q-Gaussian. In figure **3-1** the exponential distribution was fitted with formula (2.36) after setting $\delta = 0$ (zero mean) and $\nu = 2/\gamma$ (unity variance), which leaves γ as the only fitting parameter, whereas for the q-Gaussian we used (3.5) which

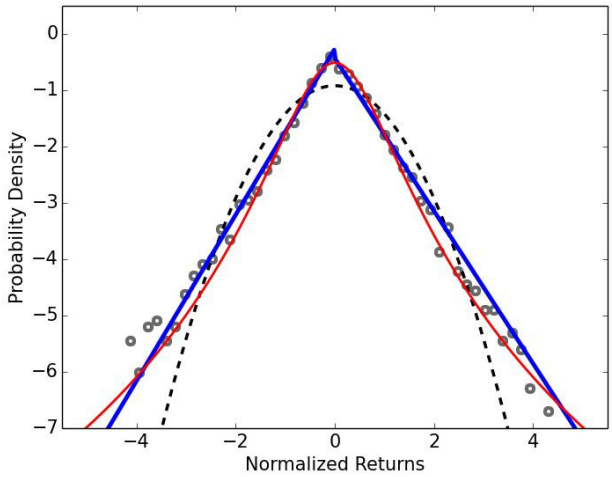

Figure 3-1 : Empirical distribution of daily returns of the Ibovespa index (circles) and respective fits with exponential (thick blue line) and q-Gaussian (thin red line) distributions. The dashed line represents a Gaussian with unity variance. The fitting parameters are $\gamma = 1.47 \pm 0.01$ (exponential distribution) and $q = 1.473 \pm 0.008$ (q-Gaussian).

has q as the only parameter. In both fitting procedures we have used the method of the golden section search [Press et al., 2007] to determine the respective values of γ and q that minimize the sum of squared residuals for each distribution; the corresponding fitting parameters are $\gamma = 1.47 \pm 0.01$ and $q = 1.473 \pm 0.008$.

Using a similar procedure that for daily return, we analyze the logarithmic returns for the intraday quotes at 15 minute intervals. This is shown in figure **3-2** with the same plot convention as in figure **3-1**. Here the empirical distribution shows much heavier tails than in the case of daily returns. From the visual inspection of figure **3-2** one clearly sees that the q-Gaussian gives a better description of the data in comparison with the exponential distribution. This is confirmed by the fact that $R^2 = 0.9982$ for the q-Gaussian, while $R^2 = 0.9359$ for the exponential fit. Here one finds $q = 1.572 \pm 0.002$, which is considerably larger than the value for q obtained for the daily returns, thus showing that the distribution of returns at shorter scales does indeed have more pronounced tails. Evidence of power law tails in the intraday quotes of the Ibovespa has also been observed, e.g., in references [A.A.G.Cortines and R.Riera, 2007, Tabak et al., 2009].

As the time lag increases, the power law distribution should converge to a Gaussian, i.e., $q \to 1$, with an exponential distribution appearing at some intermediate crossover scale. In order to study this effect, we have computed the empirical returns at time lags $\tau = 2^n \times 15\,\text{min}$ with $n = 1, \ldots, 10$ and fitted each data set with the q-Gaussian distribution. Examples of some empirical distributions and respective fits are shown in figure **3-3**a for

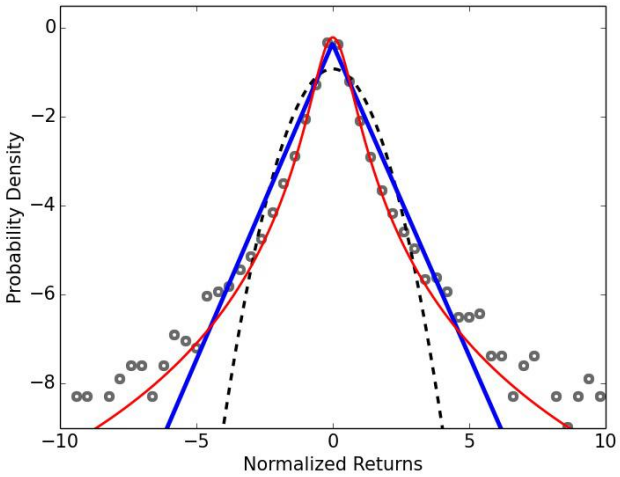

Figure 3-2 : Empirical distribution of intraday returns of the Ibovespa index at a time lag of 15 minutes, with the same plot convention as in Fig. **3-1**. Here the fitting parameters are $\gamma = 1.43 \pm 0.04$ and $q = 1.572 \pm 0.002$.

$\tau = 15, 60, 240, 480, 960, 3840$ min. A plot of q as a function of τ is shown in Fig. **3-3**b. One sees from this figure that q decreases toward unity as τ increases. That is, for long time lags such that the correlations between the logarithmic returns vanish, we recover the Gaussian case as expected from the central limit theorem. (Note that the resulting series of returns become increasingly less representative as τ increases which makes the fitting procedure less reliable for large τ, but nonetheless the trend $q \to 1$ is clearly verified.)

For comparison, we have also fitted the distribution of returns at different time lags τ with the exponential model. In figure **3-4** we plot the respective figure of merit R^2 as a function of the lag τ for both the q-Gaussian model (circles) and the exponential model (crosses). One sees from this figure that the exponential model gives a very good fit to the data for scales of the order of a few hours, where its R^2 value is approximately the same as that obtained from the q-Gaussian model (and both very close to 1). Here the q-Gaussian model performs slightly better than the exponential model at this scale, while the opposite occurs for the daily data shown in figure **3-1**. This is probably because the intraday series covers a relatively small period of time (three years), which makes the return distributions for larger time lags statistically less significant. Nevertheless, it is evident from the combined analysis of the daily and intraday quotes that the empirical distribution of the Ibovespa at scales from a few hours to a few days is well described by an exponential distribution.

The analysis above confirms the fact that the shape of the distribution of the Ibovespa returns varies with the time scale: it exhibits power law tails at short time scales (of the

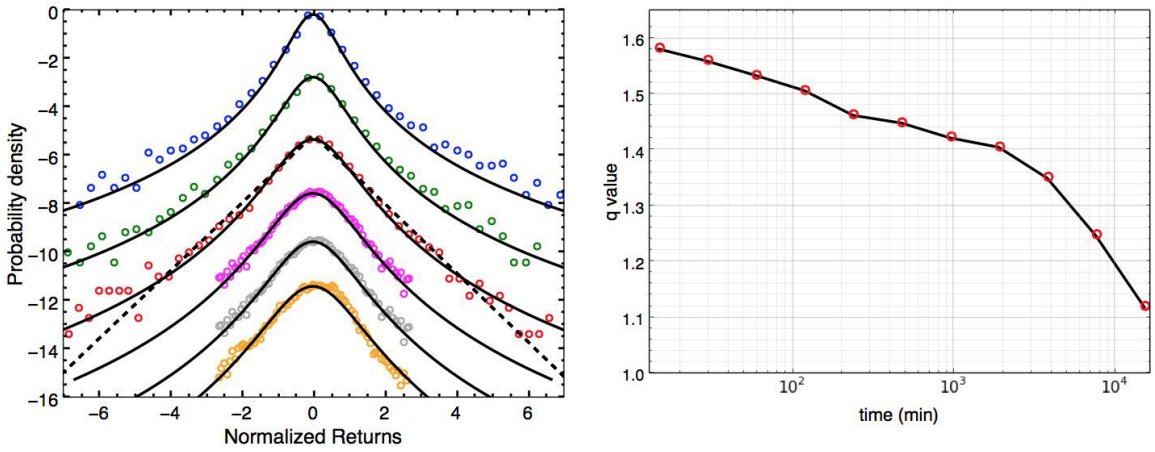

(a) (b)

Figure 3-3 : (a) Distributions of returns (open circles) for time-lags of length τ = 15, 60, 240, 480, 960, 3840 minutes (from top to bottom) calculated from the intraday quotes at 15 minutes of the Ibovespa index, together with the respective fits (solid curves) by the q-Gaussian model. The dashed line indicates the fit by the exponential model for τ = 240 min. The curves have been arbitrarily shifted vertically for clarity. (b) Time evolution of q-parameter as a function of the time lag $\tau = 2^n \times 15$ min, for $n = 0, 1, ..., 10$.

order of minutes or less), follows an exponential decay at mesoscales (from hourly to daily scale), and then tends to a Gaussian at large (monthly) scales as one would expect from the central limit theorem. Similar behavior was observed for example for data of Intel (INTC) and Microsoft (MSFT) traded at NASDAQ, and IBM and Merck (MRK) traded at NYSE in [Silva et al., 2004]. Also for The Dow-Jones index data, S&P 500, NYSE index daily data and Ibovespa data for other periods [Dragulescu and Yakovenko, 2002, Cortines et al., 2007, Mantegna and Stanley, 2002, Miranda and R.Riera, 2001].

3.3 Option Data and Methodology

Since the main stock index of the São Paulo Stock Exchange is the Ibovespa index, we analyze data series of options whose underlying asset is that index. Our study includes market prices of European call options traded daily in the period spanning two years of trading (2005-2006). Options on the Ibovespa index are of the European type and are denoted by the symbol IBOV followed by a letter and a number. The letter indicates the date of expiration according to the following convention: letters from A to L indicate call options expiring on the months from January to December, respectively. Options on the Ibovespa always

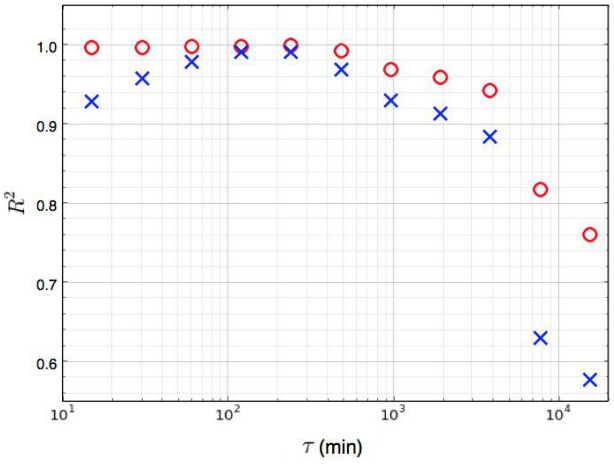

Figure 3-4 : Figure of merit R^2 for the fits of the returns at time lag τ by the q-Gaussian model (circles) and the exponential model (crosses).

expire on the Wednesday closest to the 15th day of the corresponding month of expiration. The number following the letter corresponds to the exercise price. For instance, the option IBOVL37 of year 2006 denotes the option whose expiration date was December 13, 2006 (the closest Wednesday to December 15, 2006), and whose strike price was BRL 37000.

The traded options that have the same expiration date form what is called an option series. A set of options belonging to the same series that are traded on a particular day is called an *option chain* [Ramos et al., 2016]. Each option chain has a set of premiums (closed market price) as a function of the strike price. For instance, figure **3-5** shows the option chain of the IBOVL series for year 2006 at 38 days before expiration. The circles indicate the market prices, the dashed red line represents the intrinsic value of the option, corresponding to the difference between the current price (indicated by the blue arrow) and the strike price.

In the two-year period analyzed in our study there were 850 option chains, each containing a number of points (i.e., traded strikes) ranging from 1 to 11. Here, however, we considered only option chains with at least five strikes, so as to make the statistical analysis more significant. This subset contains 345 option chains. To analyze the option data we adopted a methodology similar to that used in [Ramos et al., 2016], which we briefly summarize here. For a given admissible option chain (i.e., with 5 or more strikes), we fit the corresponding set of prices C_i versus strike K_i with the theoretical formulas predicted by the models described in section 2.2. For instance, in fitting the Black-Scholes formula (2.25) to a given option chain we assume that the volatility σ is the same for all options in the chain and determine σ by a least-square fit using the golden section search method [Press et al., 2007]. Similarly, for

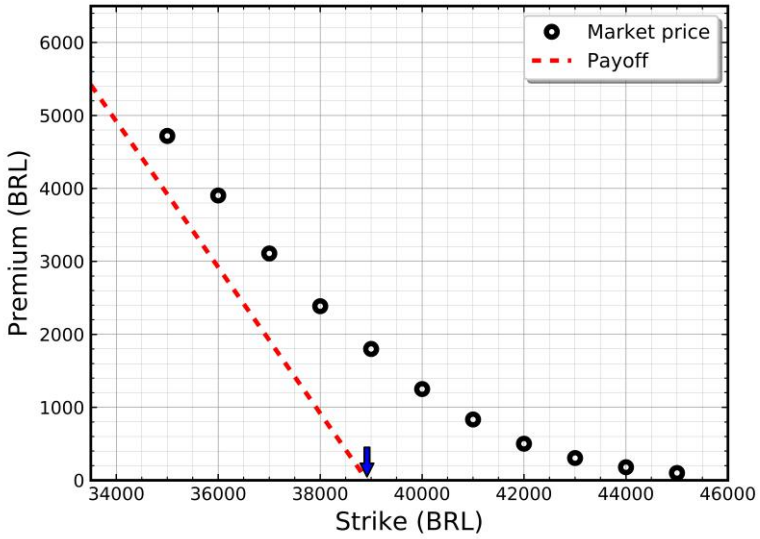

Figure 3-5 : Option chain of the IBOVL series for year 2006 at 38 days before expiration.

the exponential and q-Gaussian models we fit formulas (2.40) and (2.75) to the option data using the Nelder-Mead optimization method [Nelder and Mead, 1965] to obtain the optimal values of the parameters (γ, ν) and q, respectively. In all fits performed here, the risk-free interest rate r was assumed to be the Brazilian Interbank Deposit Rate [BM&FBOVESPA, 2018] valid at the time of the option chain.

In comparing the performances of the models for a given option chain, we look at the respective coefficients of determination R^2 produced by the corresponding best fits (see Appendix E). We recall that the closer R^2 is to unity the better is the fit. Thus, we shall say that a model that yields a higher R^2 performs better than a model whose best fit has a lower R^2. In the next section we shall present a comparative analysis of how the three option pricing models discussed in section 2.2 apply to the Brazilian market.

3.4 Empirical Analysis of Option Prices

As mentioned above, from our original database we selected the option chains with 5 or more strikes and for each one of them we fitted the option premiums with the theoretical formulas predicted by the three option pricing models discussed above and then compared the respective fits. First we discuss the performance of the q-Gaussian option model with respect to the standard Black-Scholes model.

We recall that the q-Gaussian distribution recovers the Gaussian for $q = 1$. Thus, if the fit of the option pricing formula (2.75) for a given option chain returns a value of q that is

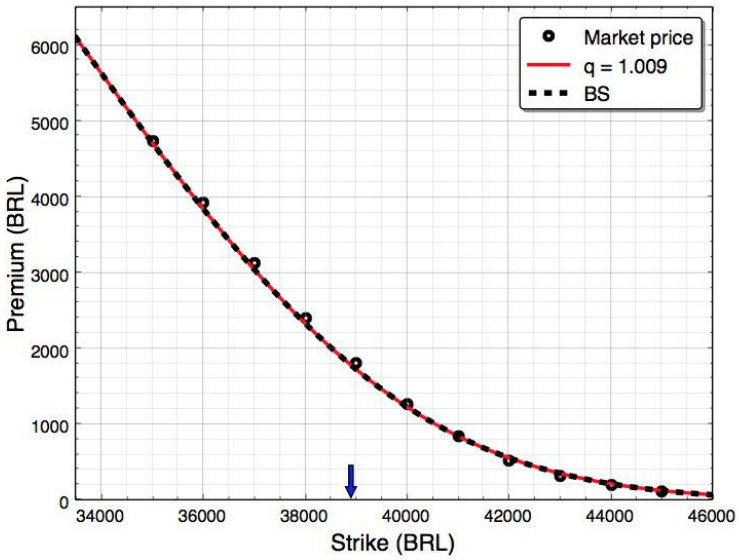

Figure 3-6 : Market prices (circles) for the option chain of the IBOVL series for year 2006 at 38 days before expiration. Also shown are the respective fits by the Black-Scholes formula (dashed black line) and by the option pricing formula based on the q-Gaussian distribution (solid red line). The arrow indicates the corresponding spot price.

sufficiently close to unity, i.e., $q \approx 1$, we conclude that the Black-Scholes model describes well this option chain. As a practical rule we adopt the following criterion: if the q-value obtained from the fitting procedure is within 5% from unity, we shall assume that the Black-Scholes model is more suitable in such cases (and effectively consider $q = 1$). One example of this case is given in figure **3-6**, where we show the market prices (circles) for the option chain belonging to the IBOVL series for the year 2006 at 38 days prior to maturity. Here the fit by the q-Gaussian model (red solid line) yields $q = 1.009$, meaning that in practice the Black-Scholes formula describes the data better than the general formula for any $q > 1$. Also shown for comparison in figure **3-6** is the fit obtained by directly employing the Black-Scholes formula (dashed line), which is indeed indistinguishable from the fit found using the general formula based of the q-Gaussian model.

If a value $q > 1$ is obtained for a given option chain, we then conclude that in this case it is more advantageous to use the general q-Gaussian model as it fits better the data than does the Black-Scholes formula ($q = 1$). One example of this case is presented in figure **3-7** where we show the option chain belonging to the IBOVL series for year 2005 at 49 days prior to maturity. The best fit by the q-Gaussian model (red line) yields $q = 1.422$. For comparison, we also show in figure **3-7** the fit with the Black-Scholes formula (dashed line). Although both models agree reasonably well with the empirical data, the q-Gaussian model

provides a slightly better fit, which is confirmed by comparing the respective coefficients of determination: $R^2 = 0.9992$ for the q-Gaussian model, whereas and $R^2 = 0.9984$ for the Black-Scholes model. Although both models give a value of R^2 very close to one another (and close to unity), it is nonetheless legitimate to discern between the two models on the basis of this figure of merit; see, e.g., reference [Ramos et al., 2016] for further discussion on this point.

An alternative way to display the results presented in figure **3-7**a is shown in figure **3-7**b, where we plot the corresponding implied volatilities for the empirical data (open circles), the Black-Scholes model (black dashed line) and the q-Gaussian model (red solid curve). It is clear from this figure that the q-Gaussian model adjusts better the implied volatilities, and so it does indeed give a better description of the market option prices in comparison with the Black-Scholes model.

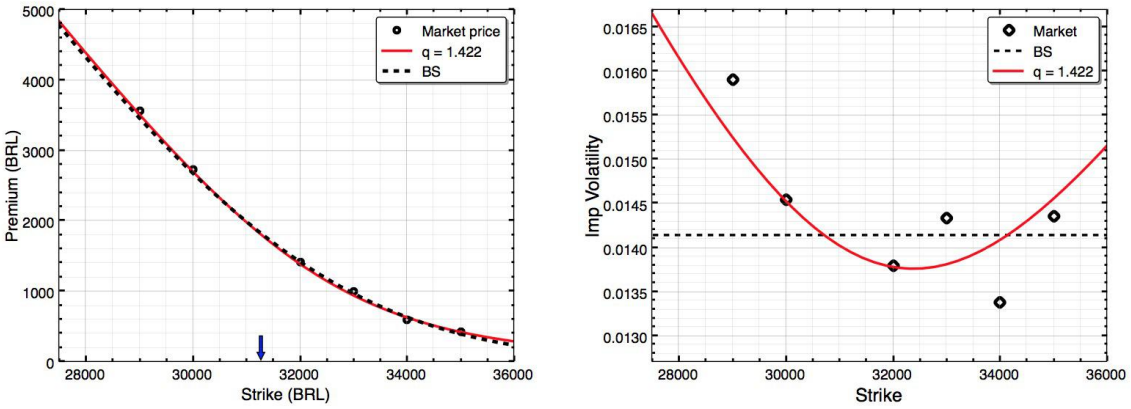

(a) (b)

Figure 3-7 : (a) Market prices (circles) for the option chain of the IBOVL series for year 2005 at 49 days before the expiration date, together with fits by the Black-Scholes and q-Gaussian models. (b) Corresponding implied volatilities for the option chain shown in panel (a).

In order to make a more extensive comparison between the Black-Scholes and the q-Gaussian models, we have performed least-square fits of formula (2.75) for all 345 admissible option chains in our data set. In figure **3-8**a we show the values of q as a function of the time to expiration, Δt, of the corresponding option chain. Values of $q > 1$ are denoted by blue crosses, whereas the cases with $q = 1$ (according to the criterion above) are indicated in red circles. In figure **3-8**b we show the histogram corresponding to the values $q > 1$ obtained in figure **3-8**a. Although larger values of q (implying heavier tails) tend to be favored—notice that the mode lies in the interval $[1.56, 5/3)$,— there is nonetheless a considerable spread in the values of $q > 1$. This implies that, in general, different option chains may require different

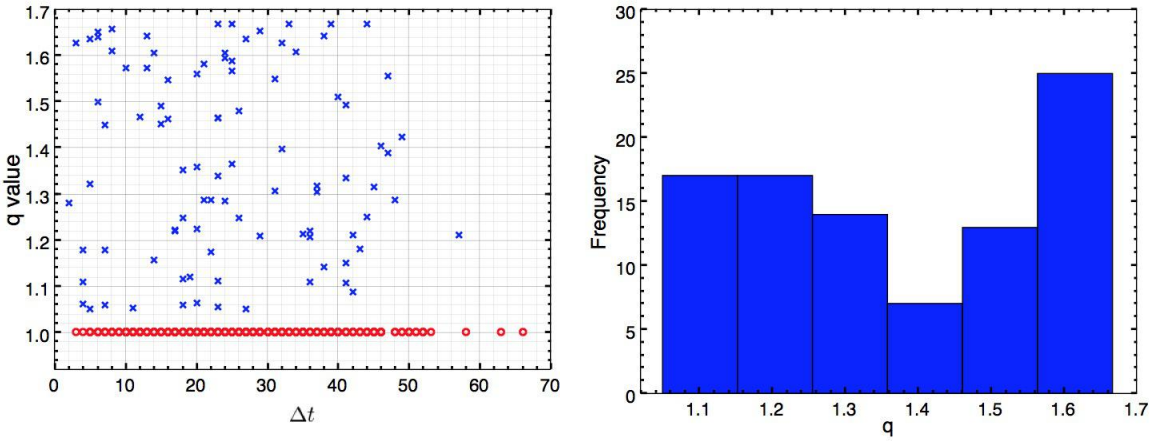

(a) (b)

Figure 3-8 : (a) Values of the q parameter as a function of the time Δt to expiration. Values with $q > 1$ are indicated by blue crosses and $q = 1$ by red circles. (b) Corresponding histogram of q values for the cases where $q > 1$.

values of q. This is in contrast with the approach adopted in [Borland, 2002a, Borland, 2002b] where the value of q is estimated from the return distribution of the underlying asset and hence it is assumed to be the same for all options on this asset.

To make a comparative analysis of the performance of the two models as a function of the time to maturity, we plot in figure **3-9** the percentage of cases with $q > 1$ among all option chains for each Δt (red squares). The dashed horizontal line in the figure corresponds to the 50% line. One sees from this plot that the q-Gaussian model tends to perform better than the Black-Scholes model for options close to maturity, since for $\Delta t < 9$ days the points (squares) lie above or at the 50% line. This trend is more clearly seen when one looks at the cumulative frequency of the cases with $q > 1$, as shown by the black circles in figure **3-9**. This curve gives the percentage of the cases with $q > 1$ among all option chains with a time to maturity less than or equal to a given Δt. One sees from this plot that the q-Gaussian model performs better in the majority of the cases for all times up to 8 days prior to maturity, as the cumulative frequency remains above 50% up to this point. For larger Δt the Black-Scholes model adjusts better the data in the majority of cases. This analysis shows furthermore that among all options chains analyzed the q-Gaussian model (with $q > 1$) gives a better fit to the data, as compared to the Black-Scholes formula, in only 27% of the cases; see the last circle in figure **3-9**.

For the cases where the q-Gaussian model yields $q > 1$, thus surpassing the Black-Scholes model, we have investigated how it compares to the exponential model. To this end, we have

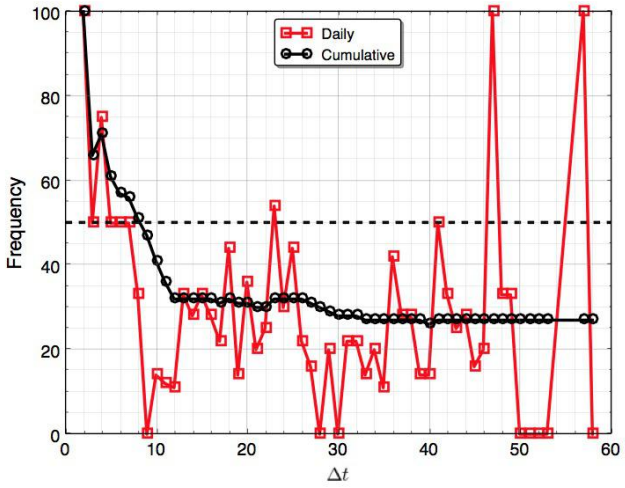

Figure 3-9 : Percentage of option chains fitted by the q-Gaussian model with $q > 1$ as a function of the time Δt to maturity. The red squares are the results for each Δt and the black circles are the cumulative frequency from 0 to Δt; see text.

also fitted the option chains in this class ($q > 1$) with the price formula from the exponential model and compared the corresponding fits by both models. The result of this comparison is shown in figure **3-10**, where we plot the percentage of cases for which the exponential model gives a better fit to the option data. As in figure **3-9**, the red squares correspond to the frequency for each Δt, whereas the black circles are the cumulative frequency from 0 to Δt. One first result from this analysis is that the exponential model adjusts better the option data in 75% of all cases; see last circle in figure **3-10**. The superiority of the exponential model over the q-Gaussian model is particularly striking for option chains near maturity. For instance, one sees from figure **3-10** that the exponential model fits better the data in 90% of all options chains with less than 16 days to expiration and in 100% of the cases within 6 days to maturity or less.

One example of an option chain very close to maturity is shown in figure **3-11**a for the IBOVJ series of year 2005 at 6 days before expiration. Here one sees that the exponential model does indeed provide a much better fit to the option prices than the q-Gaussian model. Notice, in particular, that the q-Gaussian model performs rather poorly for in-the-money options, whereas the exponential model seems to have more 'flexibility' in that it describes well both in-the-money and out-of-the-money options. This flexibility of the exponential model is also clearly seen in figure **3-11**b, where we plot the market implied volatilities together with the respective implied volatility computed from both models. Notice that the market implied volatility is highly asymmetrical in this case. In contrast to the q-Gaussian model which is

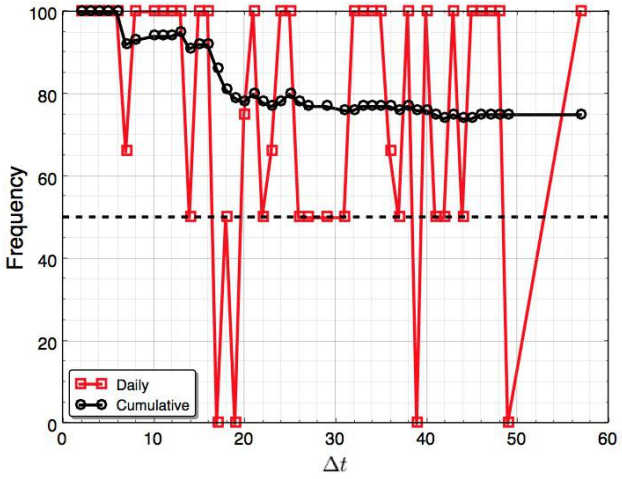

Figure 3-10 : Percentage of option chains better fitted by the exponential model in comparison to the q-Gaussian model as a function of the time Δt to maturity. The red squares are the results for each Δt and the black circles are the cumulative frequency from 0 to Δt.

symmetric, the exponential model is non-symmetric by definition, see eq. (2.36), and hence it is more capable of describing the skewed volatility smile.

For option chains farther from expiration the discrepancy between the two models is in general less pronounced, as illustrated in figure **3-12**a for the IBOVL series of year 2006 at 26 days prior to maturity. Here both models provide reasonably good fits to the empirical data, with the exponential model performing slightly better in the sense that it yields a higher coefficient of determination, namely $R^2 = 0.9991$, as compared to $R^2 = 0.9989$ for the q-Gaussian model. In this case the volatility smile has a more symmetrical pattern, as shown in figure **3-12**b, thus explaining why both models give reasonably good descriptions of the market option prices. Overall, however, the exponential model has a much better performance than the q-Gaussian model, as discussed above.

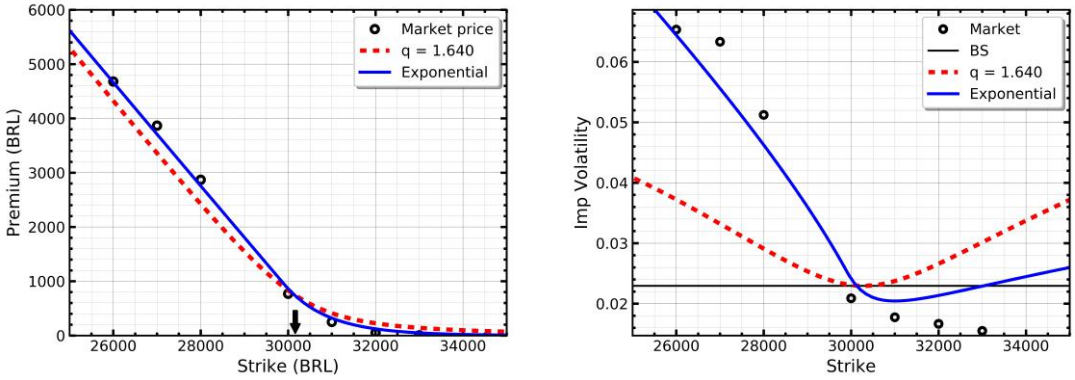

(a) (b)

Figure 3-11 : (a) Comparison between best fits to the market option prices (circles) by the q-Gaussian model (red dashed line) and the exponential model (solid blue line) for the option chain of the IBOVJ series for year 2005 at 6 days before expiration. The arrow indicates the corresponding spot price. (b) Corresponding implied volatilities for the empirical data (circles), the q-Gaussian model (red dashed line), and the exponential model (solid blue line).

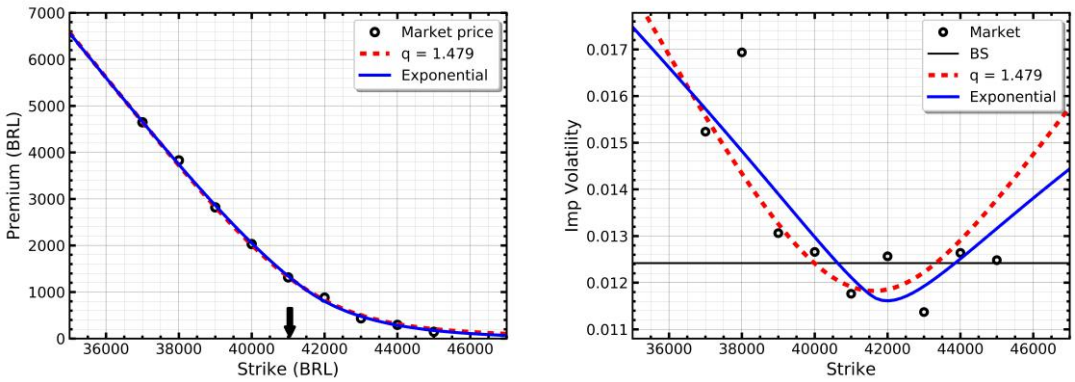

(a) (b)

Figure 3-12 : (a) Best fits to the market option prices (circles) by the q-Gaussian model (red dashed line) and the exponential model (solid blue line) for the option chain of the IBOVL series of year 2006 at 26 days before expiration. (b) Corresponding implied volatilities for the empirical data (circles), the q-Gaussian model (red dashed line), and the exponential model (solid blue line).

4 Hierarchical Models for Option Pricing

4.1 Introduction

In this chapter, we develop a hierarchical model for option pricing, where the volatility of the price of the underlying asset is described as a multi-scale stochastic process. This can be made considering the empirical evidence that shows the existence of hierarchical structures in the data series of financial markets. This kind of hierarchical behavior is also found for example in the turbulence phenomenon. This is a reason why methods from turbulence have been used to study financial markets. Some examples of this can be found for example in the papers of [Macêdo et al., 2017, Ausloos and Ivanova, 2003, Dragulescu and Yakovenko, 2002, Ghashghaie et al., 1996, Arnéodo et al., 1998]. The idea to use concepts from turbulence is justified by the fact that there are some similar features between the two phenomena: fluctuations in turbulent flows (of velocity increments and energy dissipation rate) and in financial markets (of returns and volatility). For example, in fully developed turbulence, the dissipation rate displays intermittent high fluctuations, yielding fat tails in the distribution of velocity increments. Similarly, financial time series exhibits switching between quiet phases with low volatility and turbulent phases with bursts of volatility. These bursts, known as clustering volatility tend to persist in time giving rise to heavy tails in the distribution of financial data, indicating that extreme variations of price are much more probable than one would expect from a Gaussian-like distribution. Also in finance, price and volatility are negatively correlated, i.e. when price decreases the volatility increases. This effects called leverage leads to a negative skewness in the distribution of returns [Vulpiani and Livi, 2003]. Similarly, in turbulence the distribution of longitudinal velocity increments is also skewed toward negative values.

The features above suggest that we can consider the volatility in financial markets to be equivalent of the energy flux in turbulence and therefore its dynamics can be described by cascading processes as is usual in its mechanical analog. Here, instead of an energy cascade, we have an information cascade from longer to shorter time scales [Muzy et al., 2000, Chunxia et al., 2007]. Indeed, the idea of information cascades is not new, this appeared with the hypothesis of a heterogeneous market [Müller et al., 1997]. This hypothesis considers the fact that in markets there are many agents that differ in several aspects, which have an effect on the market volatility. Some of these aspects can be their risk aversions, economic expectations, market information and time horizons. For example, the daily trader will observe market volatility on a very short time scale while a long-term investor will not watch the market often enough to even perceive short-term volatility. This generates a 'flux of information'

from large to small time scales, which can be modeled by a cascading process [Breymann et al., 2000]. In this thesis, such a cascade process will be described using a hierarchical model consisting of several coupled stochastic differential equations, where the dynamics at a given scale is coupled only to the dynamics of the scale immediately above it.

In what follows, we adopt the idea of cascades of information to obtain the multi-scale model of volatility that will lead us to introduce a hierarchical model in the context of options and derivatives. For this, we first show our general assumptions to propose our approach for option pricing. Then, we review the hierarchical model used to describe the dynamics of the volatility process. With this, we obtain expressions for the price of options and we show some theoretical results as a function of the parameters of the model. Finally, we make a brief comparison with empirical data and some of the conventional models analyzed in chapter 2.

4.2 General Approach for Option Pricing

Here we show a general approach to solve the problem of options pricing in the case where the volatility of prices is described by more than one stochastic process. Let us consider an asset whose dynamics of its price S is described by the process,

$$dS = \mu S dt + S\sqrt{v} dW, \tag{4.1}$$

where μ is the expected return, v is the volatility of the price and $W(t)$ is the Wiener process. We shall consider a general case when the volatility v is described by some stochastic process whose stationary PDF is given by $f(v)$. (The specific form of the stochastic process followed by the volatility v will be discussed later). Furthermore, if we suppose that the dynamics of the asset price (4.1) is much faster than the dynamics of the volatility, we can consider that over short time periods, the statistics of the price S achieves a local equilibrium for the corresponding value of v. In other words, the short-time distribution of the price is given by the conditional distribution $g(S|v)$. We shall assume that $g(S|v)$ is the log-normal distribution corresponding to the solution of the stationary Fokker-Planck equation associated with the process (4.1), as we showed in section 2.3.

This assumption known as hypothesis of time scales separation, allows us to calculate the marginal distribution of the asset price in the form

$$p(S) = \int g(S|v) f(v)\, dv. \tag{4.2}$$

With this, we can apply the risk-neutral approach to obtain the price of the option on the underlying asset as

$$C(S, K, r, t) = e^{-r(T-t)} \int C(S, K) p(S) dS. \tag{4.3}$$

Here $C(S,K) = \max(S-K,0)$ and r is the risk-free interest rate. Substituting (4.2) into (4.3), we can write our approach for the price $C(S,K,r,t)$ of an option as

$$\begin{aligned} C(S,K,r,t) &= \int \left[e^{-r(T-t)} \int C(S,K) g(S|v) dS \right] f(v) dv \\ &= \int C_{BS}(S,K,r,t|v)\, f(v)\, dv. \end{aligned} \tag{4.4}$$

where $C_{BS}(S,K,r,t|v)$ may be seen as the Black-Scholes price conditioned to the volatility v.

The next step to solve the problem raised in (4.4) is to determine a hierarchical physical model for the dynamics of the volatility and with this the stationary distribution $f(v)$. To this end, we adopt the hierarchical model for fluctuations introduced in [Salazar and Vasconcelos, 2012, Macêdo et al., 2017] and the concept of information cascades in finance to describe the dynamics of the volatility v.

To conclude this general discussion, let us emphasize that similar approaches have been used for example by Hull-White and Scott [Hull and White, 1987,Scott, 1987]. The difference with respect to their approaches is that in (4.4) they use the distribution $f(\bar{v})$ of the mean volatility over time $\bar{v}$, which cannot be written in analytical form, whereas here we average the Black-Scholes price over the equilibrium distribution $f(v)$ of the volatility, which can be solved exactly; see below. Since the previous authors [Hull and White, 1987, Scott, 1987] did not have an explicit formula for the distribution of the mean volatility $f(\bar{v})$, they had to use approximations. Another similar approach was considered by Madan-Carr-Chang for the variance gamma model for option pricing in [Madan et al., 1998]. In this case, they compute the average of the Black-Scholes formula over the distribution of a random time, which is distributed as a gamma process. They obtain a close formulation for the option price as a hypergeometric function of two variables, namely the Humbert function. Here, instead, we have adopted the idea of [Macêdo et al., 2017], who used the equilibrium distribution of the volatility (for a certain class of hierarchical stochastic process; see below), to compute the distribution of the logarithmic returns $x = \ln S$ using the integral (4.2). Using this approach, they obtain excellent agreement with the empirical data of Ibovespa index. The difference with our model is that they used for the conditional probability $g(x|v)$ of the logarithmic returns a normal distribution with zero mean. Furthermore, they only analyzed the distribution of returns. Here we are interested in option pricing in a multi-scale setting. We shall therefore compute directly the average of the Black-Scholes price, which implies that our conditional distribution for the returns is a normal distribution with mean different to zero.

4.3 Multi-Scale Model for Fluctuations

In this section, we discuss the generalized hierarchical model that will be useful in the remainder of this work. We start by presenting the model in the general context of complex systems as was developed by [Salazar and Vasconcelos, 2012, Macêdo et al., 2017] and in the course of this we will discuss how it will be useful for our purposes. We consider a system that has N well-separated time scales τ_i, $i = 1, \ldots, N$, in addition to the large scale τ_0, which are sorted from smallest to the largest $\tau_i << \tau_{i-1}$. In this model, the dynamics of an arbitrary variable ϵ is described by a generalized stochastic process, which is written as a set of SDEs in the form

$$d\epsilon_i = F_i(\epsilon_0, ..., \epsilon_N, t)dt + G_i(\epsilon_0, ..., \epsilon_N, t)dW_i, \quad i = 1, \ldots, N. \tag{4.5}$$

Each level $i = 1, \ldots, N$ of the hierarchy has associated with it a random variable ϵ_i and an independent Wiener process W_i. For instance, in turbulence the variable ϵ_i represents the energy flux at each level of energy cascade, whereas in finance it describes the volatility at each time scale, as we will see later.

The terms $F_i(\epsilon_0, ..., \epsilon_N, t)$ and $G_i(\epsilon_0, ..., \epsilon_N, t)$ are functionals chosen in such a way that they must satisfy some dynamical constrains [Salazar and Vasconcelos, 2010]. These are:

i) Time translation symmetry.

$$\partial_t G_i(\epsilon_0, \cdots, \epsilon_N, t) = \partial_t F_i(\epsilon_0, \cdots, \epsilon_N, t) = 0 \tag{4.6}$$

ii) Local interaction.

$$G_i(\epsilon_0, \cdots, \epsilon_N, t) = G_i(\epsilon_{i-1}, \epsilon_i) \tag{4.7}$$

$$F_i(\epsilon_0, \cdots, \epsilon_N, t) = F_i(\epsilon_{i-1}, \epsilon_i) \tag{4.8}$$

iii) Scale invariance.

$$G_i(\lambda\epsilon_{i-1}, \lambda\epsilon_i) = \lambda G_i(\epsilon_{i-1}, \epsilon_i) \tag{4.9}$$

$$F_i(\lambda\epsilon_{i-1}, \lambda\epsilon_i) = \lambda F_i(\epsilon_{i-1}, \epsilon_i) \tag{4.10}$$

iv) Condition of equilibrium.

$$\langle\epsilon_i\rangle = \epsilon_0 \quad \text{for} \quad t \to \infty \tag{4.11}$$

v) Positivity of ϵ_i.

$$P(\epsilon_i < 0) = 0, \quad \forall\, t, \quad \text{if} \quad \epsilon_j(t = 0) \geq 0 \tag{4.12}$$

Indeed it is possible to show that such a system of equations under the conditions above exists only if it is written as

$$d\epsilon_i = -\gamma_i(\epsilon_i - \epsilon_{i-1})dt + \kappa_i \epsilon_i^{\alpha} \epsilon_{i-1}^{1-\alpha} dW, \tag{4.13}$$

where γ_i, κ_i are positive real constants. The stochastic process written in this form guarantees that overall conditions above are satisfied. The first three conditions are easily verified. The condition (iv) establishes that for $t \to \infty$ the mean $\langle \epsilon_i \rangle$ relaxes to its equilibrium value ϵ_0 for all $i = 1, ..., N$; this is guaranteed by the linear deterministic term in (4.13), as one can easily verify. To verify that condition (v) is satisfied, suppose that $\epsilon_i = 0$ at some point in time, with $\epsilon_{i-1} \neq 0$. Then, the second term in (4.13) vanishes and the first one ensures a positive increment, which guarantees that ϵ_i never becomes negative. The parameter α is required to be $0 \leq \alpha \leq 1$ to avoid the divergence of the stochastic process ($G(0,0) = 0$). In addition, we shall require that the coefficients of the Fokker-Planck equation associated with the stochastic process (4.13) are analytic functions of ϵ_i, which is only satisfied by certain values of the parameter α. These values are:

i) $\boldsymbol{\alpha = 1}$. With this value the stochastic variable ϵ_i of each scale of the hierarchy follows a SDE in the form:

$$d\epsilon_i = -\gamma_i(\epsilon_i - \epsilon_{i-1})dt + \kappa_i \epsilon_i dW_i(t), \quad i = 1, \ldots, N. \tag{4.14}$$

Assuming the hypothesis that the characteristic times of the different scales are well separated, the variable ϵ_i of the i-th scale fluctuates much faster that the variable ϵ_{i-1} of the scale above it. Thus, we can use the Itô lemma to find the associated Fokker-Planck equation for the conditional distribution $f(\epsilon_i|\epsilon_{i-1})$ of ϵ_i for a fixed value of ϵ_{i-1}, which in this case is given by

$$\partial_t f_i - \partial_{\epsilon_i}[\gamma_i(\epsilon_i - \epsilon_{i-1})f_i] - \frac{1}{2}\partial^2_{\epsilon_i}[\kappa_i^2 \epsilon_i^2 f_i] = 0. \tag{4.15}$$

The stationary solution of (4.15) is an inverse gamma PDF $f_i(\epsilon_i|\epsilon_{i-1})$ as shown in Appendix F, which reads

$$f_i(\epsilon_i|\epsilon_{i-1}) = \frac{(\beta_i \epsilon_{i-1})^{\beta_i+1}}{\Gamma(\beta_i + 1)} \epsilon_i^{-\beta_i - 2} e^{-\beta_i \epsilon_{i-1}/\epsilon_i}, \tag{4.16}$$

where $\beta_i = \frac{2\gamma_i}{\kappa_i^2}$ and $\Gamma(x)$ is the gamma function.

The particular case with $N = 1$, where the stochastic variable is described by only one process of the form shown in (4.14) is just the Hull-White process for volatility discussed in section 2.6.1. The general case with $N > 1$ has not, to the best of our knowledge, been considered before. We shall refer to this case ($N > 1$) as the hierarchical Hull-White model; see section 4.4.

ii) $\boldsymbol{\alpha = \frac{1}{2}}$. Now the stochastic process for the variable ϵ_i becomes

$$d\epsilon_i = -\gamma_i(\epsilon_i - \epsilon_{i-1})dt + \kappa_i \sqrt{\epsilon_i\, \epsilon_{i-1}} dW_i(t), \quad i = 1, \ldots, N. \tag{4.17}$$

Here we also have a stochastic process (4.17) for each level i of the hierarchy. So, with the same assumption of well-separated time scales like in the previous case, the Fokker-Planck

equation for the conditional distribution $f_i(\epsilon_i|\epsilon_{i-1})$ is given by

$$\partial_t f_i - \partial_{\epsilon_i}[\gamma_i(\epsilon_i - \epsilon_{i-1})f_i] - \partial^2_{\epsilon_i}[\kappa_i^2 \epsilon_i \epsilon_0 f_i] = 0. \tag{4.18}$$

The stationary solution $f_i(\epsilon_i|\epsilon_{i-1})$ in this case is the gamma distribution (see Appendix F):

$$f_i(\epsilon_i|\epsilon_{i-1}) = \frac{(\beta_i/\epsilon_{i-1})^{\beta_i}}{\Gamma(\beta_i)} \epsilon_i^{\beta_i - 1} e^{-\beta_i \epsilon_i/\epsilon_{i-1}}. \tag{4.19}$$

with $\beta_i = \frac{2\gamma_i}{\kappa_i^2}$.

Now if we compare the stochastic process (4.17) with the stochastic model for volatility by Heston as shown (2.91), we find that with the appropriated variables the latter is a particular case of the hierarchical model (4.17) with $N = 1$. We shall therefore refer to the general model (4.17) with $N > 1$ as the hierarchical Heston model; see section 4.5. We shall mention that the original Heston model (i.e, with $N = 1$) has also been used as a dynamical model for the evolution of ecological systems in [Azaele et al., 2006], where it is obtained an exact solution for the Fokker-Planck equation (4.18). However, here we are only interested in the stationary solution of the Fokker-Planck equation.

4.4 Hierarchical Hull-White Model

4.4.1 Hierarchical Hull-White model for the volatility

As discussed above, adopting the idea of an information cascade in the problem of financial markets we can justify a hierarchical model for the dynamics of the volatility. From the generalized stochastic process (4.13) we showed that this can be used to introduce a multi-scale Hull-White process considering the case when the parameter $\alpha = 1$. Thus, let us introduce our cascade model as consisting of a set of Hull-White processes of volatility $v_1, ..., v_N$, that follow the SDEs:

$$\begin{aligned} dv_1 &= -\gamma_1(v_1 - v_0)dt + \kappa_1 v_1 dW_1 \\ dv_2 &= -\gamma_2(v_2 - v_1)dt + \kappa_2 v_2 dW_2 \\ &\vdots \qquad\qquad\qquad \vdots \\ dv_N &= -\gamma_N(v_N - v_{N-1})dt + \kappa_N v_N dW_N. \end{aligned} \tag{4.20}$$

We assume furthermore that the process v_i is much faster than the process v_{i-1}, in other words, we consider that $\gamma_i \gg \gamma_{i-1}$. This means that the variable v_i at a small scale i achieves the equilibrium so quickly, that the variable v_{i-1} in the next larger scale $i - 1$ is approximately constant. In this case, as discussed in section 4.3, the stationary marginal

distribution $f(v_i|v_{i-1})$ is given by an inverse gamma distribution:

$$f_i(v_i|v_{i-1}) = \frac{(\beta_i v_{i-1})^{\beta_i+1}}{\Gamma(\beta_i+1)} v_i^{-\beta_i-2} e^{-\beta_i v_{i-1}/v_i}. \tag{4.21}$$

Also, the distribution of volatilities $f_N(v_N)$ can be calculated as a statistical composition with the distributions of all the other scales $i = 1, \ldots, N-1$, by using the relation:

$$f_N(v_N) = \int_0^\infty dv_{N-1} \ldots \int_0^\infty dv_1 \; f_N(v_N|v_{N-1}) \ldots f_1(v_1|v_0). \tag{4.22}$$

We show in the Appendix G that the successive integration of (4.22) with $f(v_i|v_{i-1})$ as given in (4.21) can be done using the method of the Mellin transform. With this procedure, the PDF for the hierarchical system of N scales (4.20), can be written in terms of the Meijer G-function as

$$f_N(v_N) = \frac{\Omega}{v_0\omega} G^{0,N}_{N,0}\left(\begin{matrix} -\boldsymbol{\beta_N} - \mathbf{1} \\ - \end{matrix} \middle| \frac{v_N}{v_0\omega} \right) \tag{4.23}$$

where we use bold font to denote the vector of parameters $\boldsymbol{\beta_N} = (\beta_1, \ldots, \beta_N)$. Also $\Omega = 1/\prod_{i=1}^N \Gamma(\beta_i+1)$ and $\omega = \prod_{i=1}^N \beta_i$. An empty line (-) in the argument of the Meijer G-function means that as $m = q = 0$, the elements vector $\vec{b}_q$ is empty (see definition in Appendix H, equation (H.1)).

We emphasize that this hierarchical model converges to the log-normal distribution in the limit $N \to \infty$, as shown in [Salazar and Vasconcelos, 2010]. So, the distribution of volatility recovers the stationary limit of the exponential Ornstein-Uhlenbeck process introduced by Scott, in which case it becomes log-normal [Scott, 1987, Masoliver and Perelló, 2006].

4.4.2 Option pricing in the hierarchical Hull-White model

In section 2.6.1 we reviewed the original Hull-White model for option pricing where the dynamics of the underlying asset of the option S and its volatility v is described by a geometrical Brownian motion (2.80) and a Hull-White process (2.81), respectively. Now in its hierarchical version, the dynamics of the asset price S is also described by a geometrical Brownian motion but its volatility is driven by the hierarchical process (4.20). So, we have the following system of SDE:

$$\begin{aligned} dS &= \mu S dt + S\sqrt{v_N} dW \\ dv_N &= -\gamma_N(v_N - v_{N-1})dt + \kappa_N v_N dW_N \\ &\vdots \qquad\qquad\qquad \vdots \\ dv_2 &= -\gamma_2(v_2 - v_1)dt + \kappa_2 v_2 dW_2 \\ dv_1 &= -\gamma_1(v_1 - v_0)dt + \kappa_1 v_1 dW_1 \end{aligned} \tag{4.24}$$

where we write the process beginning from the smallest to the largest scale and assuming that these are well-separated.

As discussed in section 4.2, in order to obtain the price of an option in our hierarchical Hull-White model we need to perform the integral (4.4), substituting $f_N(v_N)$ by equation (4.23), which corresponds to the stationary PDF of the volatility v_N, that now is described by a multi-scale process. This reads

$$C(S,K,r,t,N) = \frac{\Omega}{v_0\omega}\int_0^\infty C(S,K,r,t|v_N)G^{0,N}_{N,0}\left(\begin{matrix}-\boldsymbol{\beta_N}-\mathbf{1}\\ -\end{matrix}\middle|\frac{v_N}{v_0\omega}\right)dv_N, \tag{4.25}$$

with $\Omega = 1/\prod_{i=1}^N \Gamma(\beta_i+1)$ and $\omega = \prod_{i=1}^N \beta_i$.

Using that $C(S,K,r,t|v_N)$ is the Black-Scholes price for the option conditioned on the volatility v_N, it is possible to carry out the integral in (4.25) explicitly. The final result as a function of the spot price S, the strike K, the risk-free interest rate r, the time t and the number N of scales in the hierarchy, can be written as (see Appendix I):

$$C(S,K,r,t,N) = S\,\Theta_1(a,b) - Ke^{-r\tau}\,\Theta_2(a,b) + S\,\Psi_1(b) - Ke^{-r\tau}\,\Psi_2(b), \tag{4.26}$$

where $\tau = T-t$ and

$$a = \frac{[\ln\left(\frac{S}{K}\right) + r\tau]}{\sqrt{\omega v_0 \tau}}$$
$$b = \frac{\sqrt{\omega v_0\tau}}{2}. \tag{4.27}$$

We have also defined the generalized functions:

$$\Theta_1(a,b) = \frac{\Omega}{\sqrt{2\pi}}\times\int_0^a da'\,e^{-a'b}\mathbb{G}_{\boldsymbol{N}}\left(\frac{2}{b^2},\frac{a'^2}{2}\right), \tag{4.28}$$

$$\Theta_2(a,b) = \frac{\Omega}{\sqrt{2\pi}}\times\int_0^a da'\,e^{a'b}\mathbb{G}_{\boldsymbol{N}}\left(\frac{2}{b^2},\frac{a'^2}{2}\right), \tag{4.29}$$

where $\mathbb{G}_{\boldsymbol{N}}(x,y)$ is a short-hand notation for the bivariate Meijer G-function:

$$\mathbb{G}_{\boldsymbol{N}}(x,y) = G^{0,N:0,1:1,0}_{N,0:1,0:0,1}\left(\begin{matrix}(-\boldsymbol{\beta}-\mathbf{\frac{1}{2}}) & : & (1) & : & (--)\\ (--) & : & (--) & : & (0)\end{matrix}\middle|x,y\right). \tag{4.30}$$

The bold notation $(-\boldsymbol{\beta}-\mathbf{\frac{1}{2}})$ denotes the vector with N elements $((-\beta_1-\frac{1}{2}),\ldots,(-\beta_N-\frac{1}{2}))$. In addition, we have introduced the functions $\Psi_{1,2}(b)$ defined respectively by

$$\Psi_{1,2}(b) = \frac{1}{2}\left[1 \pm \frac{\Omega}{\sqrt{\pi}}G^{1,N+1}_{N+2,1}\left(\begin{matrix}(-\boldsymbol{\beta},\frac{1}{2};1)\\ 0\end{matrix}\middle|\frac{2}{b^2}\right)\right], \tag{4.31}$$

where $\boldsymbol{\beta} = (\beta_1, \ldots, \beta_N)$.

An alternative form for the option price in terms of a series expansion is calculated in the appendix I. Although we did not use this result in our calculations, it is obtained as an infinite series of univariate Meijer G-functions. Explicitly, it reads:

$$C(S, K, r, t, N) = S\Psi_1(a, b) - Ke^{-r\tau}\Psi_2(a, b). \tag{4.32}$$

where

$$\begin{aligned}\Psi_1(a,b) = -\frac{\Omega}{\sqrt{2\pi}} \sum_{l=1}^{\infty} \frac{(-1)^l}{l!} \left(\frac{1}{2}\right)^l \frac{1}{b^{2l+1}} \Gamma(2l+1, ab) \\ \times G_{N+1,0}^{0,N+1}\left(1, -\boldsymbol{l} - \boldsymbol{\beta} - \tfrac{\mathbf{1}}{\mathbf{2}}, \frac{2}{b^2}\right),\end{aligned} \tag{4.33}$$

$$\begin{aligned}\Psi_2(a,b) = \frac{\Omega}{\sqrt{2\pi}} \sum_{l=1}^{\infty} \frac{(-1)^l}{l!} \left(\frac{1}{2}\right)^l \frac{1}{b^{2l+1}} \Gamma(2l+1, -ab) \\ \times G_{N+1,0}^{0,N+1}\left(1, -\boldsymbol{l} - \boldsymbol{\beta} - \tfrac{\mathbf{1}}{\mathbf{2}}, \frac{2}{b^2}\right)\end{aligned} \tag{4.34}$$

with Ω, a, b and $\boldsymbol{\beta}$ defined as in (4.26).

4.5 Hierarchical Heston Model

4.5.1 Hierarchical Heston model for the volatility

Under the same assumptions used for the hierarchical Hull-White model, a cascade process for volatility can be described by a hierarchical Heston model. Remember that the Heston model in finance is one particular case of the cases discussed in section 4.3. Now we can write a hierarchical model composed by a set of independent Heston processes:

$$\begin{aligned} dv_1 &= -\gamma_1(v_1 - v_0)dt + \kappa_1\sqrt{v_1\, v_0}dW_1 \\ dv_2 &= -\gamma_2(v_2 - v_1)dt + \kappa_2\sqrt{v_2\, v_1}dW_2 \\ \vdots &\qquad\qquad \vdots \\ dv_N &= -\gamma_N(v_N - v_{N-1})dt + \kappa_N\sqrt{v_N\, v_{N-1}}dW_N. \end{aligned} \tag{4.35}$$

In this case, the stationary conditional distribution of volatility $f(v_i|v_{i-1})$ is given by a gamma distribution:

$$f_i(v_i|v_{i-1}) = \frac{(\beta_i/v_{i-1})^{\beta_i}}{\Gamma(\beta_i)} v_i^{\beta_i - 1} e^{-\beta_i v_i / v_{i-1}}. \tag{4.36}$$

The generalized PDF for the scale v_N is obtained by integrating successively over all the smaller scales $i = 1, \ldots, N-1$ in (4.22). As we show in Appendix G, the integral can be

made solving the integration of two scales by using only the Mellin transform and writing the result in the form of a Meijer G-function. The following integrals into (4.22) are solved by using the properties of Meijer G-function in Appendix H. Finally, with this it is obtained the distribution of volatilities for the scale N:

$$f(v_N) = \frac{\omega\Omega}{v_0} G^{N,0}_{0,N}\left(\begin{matrix} - \\ \boldsymbol{\beta_N} - \mathbf{1} \end{matrix} \middle| \frac{\omega v_N}{v_0} \right), \tag{4.37}$$

with $\omega = \prod_{j=1}^{N} \beta_j$, $\Omega = \prod_{j=1}^{N} 1/\Gamma(\beta_j)$ and $\boldsymbol{\beta_N} = (\beta_1, \ldots, \beta_N)$.

4.5.2 Option pricing in the hierarchical Heston model

Now let us introduce the multi-scale version of the Heston model for option pricing discussed in section 2.6.2. Here the dynamical process for the price of the underlying asset is the same that in the case above but the dynamics process for the volatility is given by the hierarchical stochastic process with N scales (4.35). Thus, the complete model for the asset price is

$$\begin{aligned} dS &= \mu S dt + S\sqrt{v_N} dW \\ dv_N &= -\gamma_N(v_N - v_{N-1})dt + \kappa_N \sqrt{v_N\, v_{N-1}} dW_N. \\ \vdots &\qquad\qquad \vdots \\ dv_2 &= -\gamma_2(v_2 - v_1)dt + \kappa_2 \sqrt{v_2\, v_1} dW_2 \\ dv_1 &= -\gamma_1(v_1 - v_0)dt + \kappa_1 \sqrt{v_1\, v_0} dW_1. \end{aligned} \tag{4.38}$$

Using the same hypothesis that in the Hull-White case, the option price in the above model is obtained by performing the integral (4.4), but where now the distribution $f_N(\epsilon_N)$ of the stochastic volatility is the generalized function given in (4.37). With this, the integral (4.4) becomes

$$C(S,K,r,t,N) = \frac{\omega\Omega}{v_0} \int_0^\infty C(S,K,r,t|v_N) G^{N,0}_{0,N}\left(\begin{matrix} - \\ \boldsymbol{\beta} - \mathbf{1} \end{matrix} \middle| \frac{\omega v_N}{v_0} \right) dv_N, \tag{4.39}$$

where $\omega = \prod_{j=1}^{N} \beta_j$, $\Omega = 1/\prod_{j=1}^{N} \Gamma(\beta_j)$. As we show in Appendix J, by a procedure similar to the previous case, the final result for the integral above can be expressed in the form

$$C(S,K,r,t,N) = S\,\Theta_1(a,b) - Ke^{-r\tau}\,\Theta_2(a,b) + S\,\Psi_1(b) - Ke^{-r\tau}\Psi_2(b), \tag{4.40}$$

where $\tau = T - t$ and

$$a = \sqrt{\frac{\omega}{v_0 \tau}} \left[\ln\left(\frac{S}{K}\right) + r\tau \right], \qquad b = \frac{1}{2}\sqrt{\frac{v_0 \tau}{\omega}}. \tag{4.41}$$

We defined the function $\Theta_1(a, b)$ as

$$\Theta_1(a,b) = \frac{\Omega}{\sqrt{2\pi}} \int_0^a da'\, e^{-a'b}\, \mathbf{G_N}\left(\frac{2}{a^2}, \frac{b^2}{2}\right), \tag{4.42}$$

while the function $\Theta_2(a, b)$ is given by

$$\Theta_2(a,b) = \frac{\Omega}{\sqrt{2\pi}} \int_0^a da'\, e^{a'b}\, \mathbf{G_N}\left(\frac{2}{a'^2}, \frac{b^2}{2}\right). \tag{4.43}$$

Here again we use de symbol $\mathbf{G_N}(x, y)$ to denote the bivariate Meijer G-function

$$\mathbf{G_N}(x,y) = G^{0,N:0,1:1,0}_{N,0:1,0:0,1}\left(\begin{matrix} (-\boldsymbol{\beta} + \mathbf{\frac{3}{2}}) & : & (1) & : & (--) \\ (--) & : & (--) & : & (0) \end{matrix} \middle| x, y \right). \tag{4.44}$$

where $(-\boldsymbol{\beta} + \mathbf{\frac{3}{2}})$ represents the vector with N elements $((-\beta_1 + \frac{3}{2}), \ldots, (-\beta_N + \frac{3}{2}))$. Also, the functions $\Psi_{1,2}(b)$ are given respectively by

$$\Psi_{1,2}(b) = \frac{1}{2}\left[1 \pm \frac{\Omega}{\sqrt{\pi}} G^{N+1,1}_{2,N+1}\left(\begin{matrix} \frac{1}{2}; 1 \\ \boldsymbol{\beta}, 0 \end{matrix} \middle| \frac{2}{b^2} \right) \right], \tag{4.45}$$

with $\boldsymbol{\beta} = (\beta_1, \ldots, \beta_N)$.

Therefore, the solution for a European call option calculated as the average of the Black-Scholes formula under the assumption that the volatility follows a hierarchical Heston process reads as in (4.40), with the respective terms defined by (4.42), (4.43) and (4.45).

4.6 Properties of the Hierarchical Heston Model

In this section we show results generated by our model for the option prices as a function of the different parameters, such as the maturity T, the strike price K, the β parameter and the number N of scales considered in the hierarchical process for the volatility. Also, we analyze the implied volatility of the hierarchical model, which is defined as the value of volatility that when used into the Black-Scholes formula will give the same option price as that of our model. With this, we show that our model yields the so called implied volatility surface that represents the implied volatility as a function of the maturity and the strike price. This is

an important issue in modeling option prices because the implied volatility is a measure to estimate the future variability of the asset price underlying an option.

For the results discussed in the rest of this section, we computed the option price using formula (4.40). The bivariate Meijer G-function that appears was computed by implementing its definition as a double Mellin-Barnes-type contour integral via computer routines written in Python and Matlab like in [Chergui et al., 2016]. To the univariate Meijer G-function that appears in $\Psi_{1,2}$ we used the package of arbitrary precision *mpmath* of Python [Johansson et al., 2013].

First, we present the dependence of the option price on the number N of scales considered in the hierarchical model. In this case, we evaluated (4.40) using as test parameters the rate of interest $r = 0.01$, the spot price $S = 1$, the long-time mean $\sigma^2 = v_0$ of the volatility as $v_0 = 0.06$, and the parameter $\beta = 1.78$. The maturity was evaluated in the interval $T \in (0.2, 2.0)$ years and the strikes in the interval $K \in (0.45, 1.60)$.

Results of our model are shown in figure **4-1**. For example, figure **4-1**a shows the call price as a function of the strike K at maturity $T = 0.2$, including several scales in the model (N = 1,. . . ,8). The dashed straight line represents the option price at the maturity T, which is often called the intrinsic value of the option. The result from the Black-Scholes formula with volatility equal to the square root of the long-range mean $\sigma = \sqrt{v_0}$ (red dashed line) is also shown for comparison . Note in this figure that for an "at the money" option (i.e, with price $K = S$) and options whose price is near the spot price, our hierarchical model gives lower prices than the Black-Scholes formula being this difference more prominent as the number of scales increases. For "out of the money" options (with strike higher than the spot price S), where the option is essentially worthless (above $K \sim 1.15$), the model with several scales leads to higher prices than those computed by the Black-Scholes. A similar behavior, although not as visible, occurs for "in the money" options ($K < S$, far from the spot price S).

Let us now consider figure **4-1**b where we show the call prices in the case of a long maturity, namely $T = 2.0$. In this case, we can see that the prices generated by our model are further from the Black-Scholes formula. That is, the difference between the Black-Scholes price and the hierarchical model value is higher than in the case with $T = 0.2$. In addition, this difference extends to values far from the spot price.

The effects described above are better seen in figure **4-2**, where we have plotted the price difference between our model and the Black-Scholes formula $C_{hH} - C_{BS}$, for the two cases shown in figure **4-1**. In the case of short maturity ($T = 0.2$), see figure **4-2**a, our formula (4.40) gives lower prices than the Black-Scholes model for strikes in the interval $K \in (0.90, 1.15)$. Therefore the difference between the prices becomes negative $C_{hH} - C_{BS} < 0$. Out of this interval ($K < 0.90$ and $K > 1.15$), the price generated by our hierarchical model crosses the

Black-Scholes price yielding higher values and hence $C_{hH} - C_{BS} > 0$.

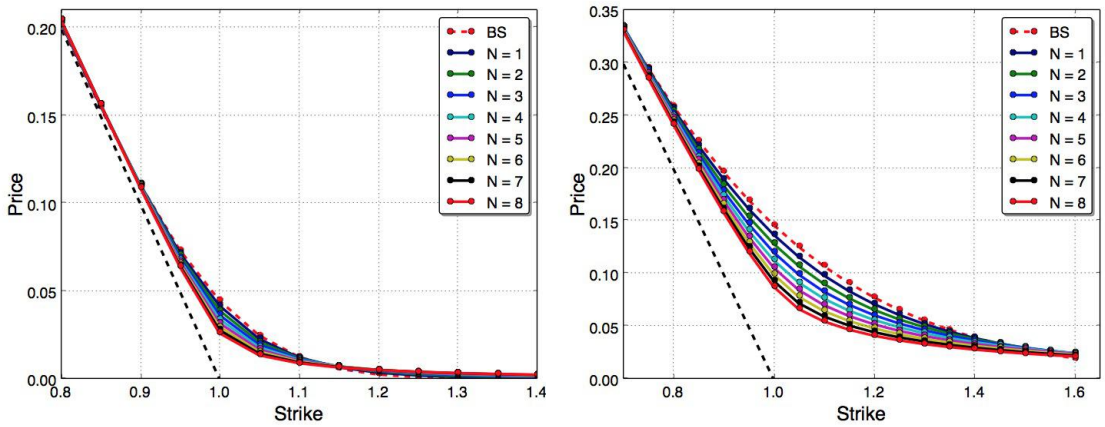

(a) (b)

Figure 4-1 : Option price on the hierarchical Heston model as a function of the strike K for different values of N. In all the cases we used $S = 1$. We show the case with maturity: (a) $T = 0.2$. (b) $T = 2.0$.

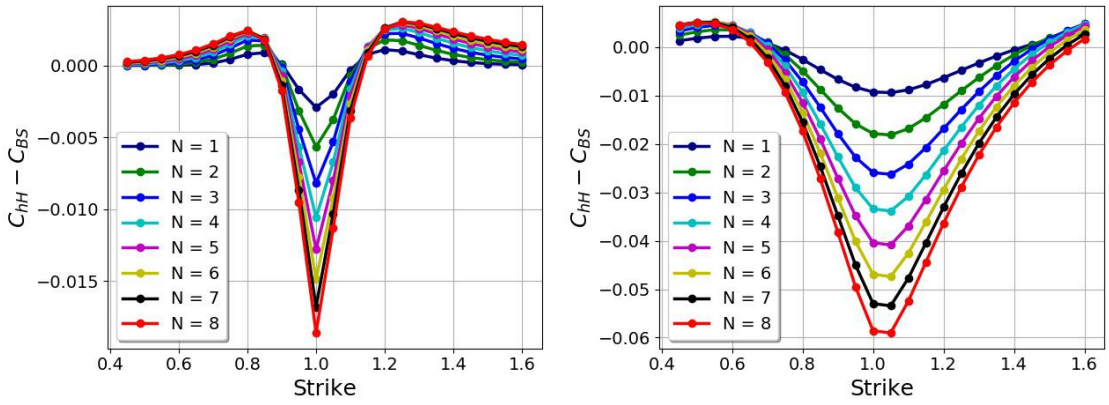

(a) (b)

Figure 4-2 : Difference between the option prices generated by the hierarchical model and those generated by the Black Scholes formula: (a) For the same conditions of the prices shown in figure **4-1**a. (b) For the same conditions of the prices shown in figure **4-1**b.

Figure **4-2**b shows price differences $C_{hH} - C_{BS}$ for the case $T = 2.0$. Here, we can see that near the spot price the difference between the hierarchical model and the Black-Scholes formula becomes higher than in the case $T = 0.2$. That is, for long maturity our model gives much lower prices than the Black Scholes price. Also, here the crossing point between the

prices are in $K \sim 0.7$ to the left and $K \sim 1.50$ to the right, much further from the spot price than in the case $T = 0.2$. Therefore, comparing figures **4-2**a and **4-2**b we can conclude that the difference $C_{hH} - C_{BS}$ is more noticeable as the maturity increases.

As we have shown above, the option price given by our model differs from the prediction of the Black-Scholes formula. This difference yields the "volatility smile" discussed in section 2.7, which is an effect only due to the stochastic nature of the volatility. Therefore, it is interesting to analyze the behavior of the implied volatility generated by the hierarchical model as a function of the number of scales. For this, let us compute the implied volatility of the hierarchical Heston model (4.40), as the value of σ obtained by solving it into the equation

$$C_{BS}(r, T, S, \sigma) - C_{model}(N, v_0, \beta) = 0 \tag{4.46}$$

where $C_{BS}(r, T, S, \sigma)$ is the Black-Scholes formula for the option price and $C_{model}(N, v_0, \beta)$ the price generated by our model with the parameters v_0, β in the different scales N. So, we computed the implied volatility for the corresponding cases in figures **4-1**a and **4-1**b, which is shown in figures **4-3** and **4-4**, respectively. The model produces volatility smiles since the implied volatility varies as a function of the strike K. In addition, we observe that indeed the 'strength' of the smile depends on the number of scales included in the stochastic volatility process. Figure **4-3** for example shows the implied volatility as a function of the strike K and $N = 1, \ldots, 8$, for an option with expiration at time $T = 0.2$. Here the Black-Scholes volatility defined as $\sigma = \sqrt{v_0}$ is represented by the red dashed line. We can see that the smile volatility is more prominent as N increases. The minimum of the smile appears at $K = 1$ and then it increases as K achieves values far from S. Note in particular that there is a small region near the spot price where the implied volatility achieves lower values than the volatility used in the Black-Scholes formula. For in and out of the money options (far from S), the implied volatility is higher than the Black-Scholes volatility. Figure **4-4** shows the implied volatility curves generated for an option with expiration at $T = 2.0$, which shows a similar behavior, in the sense that the volatility smiles are more pronounced as N increases, but now these are flatter than in the case with short maturity.

The results above then show that our model yields similar results to those of the original Heston model, since the differences with respect to the Black-Scholes model have the same behavior as shown in [Heston, 1993]. Furthermore, the improvement of our formulation is that by including several scales in the dynamics of the volatility, the model is able to enhance the difference of prices and therefore generates richer patterns of implied volatility.

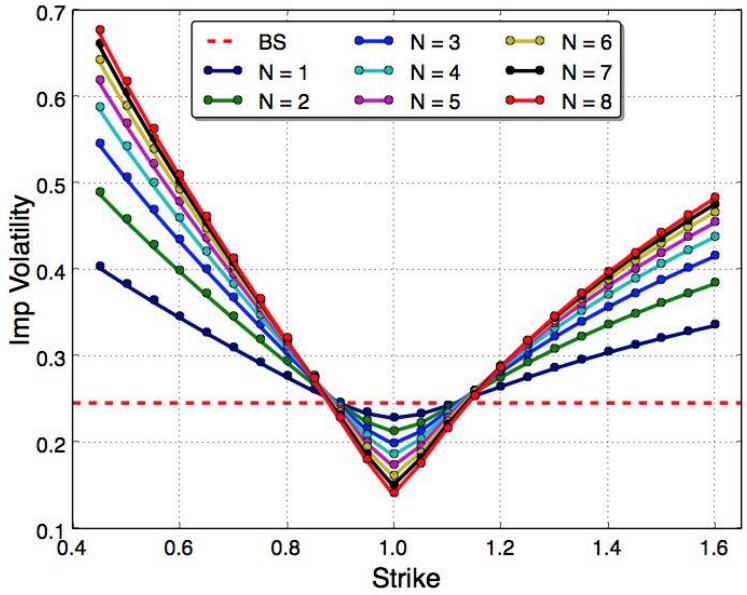

Figure 4-3 : Implied volatilities of the hierarchical Heston model as a function of strike K and N. Here we use $T = 0.2$.

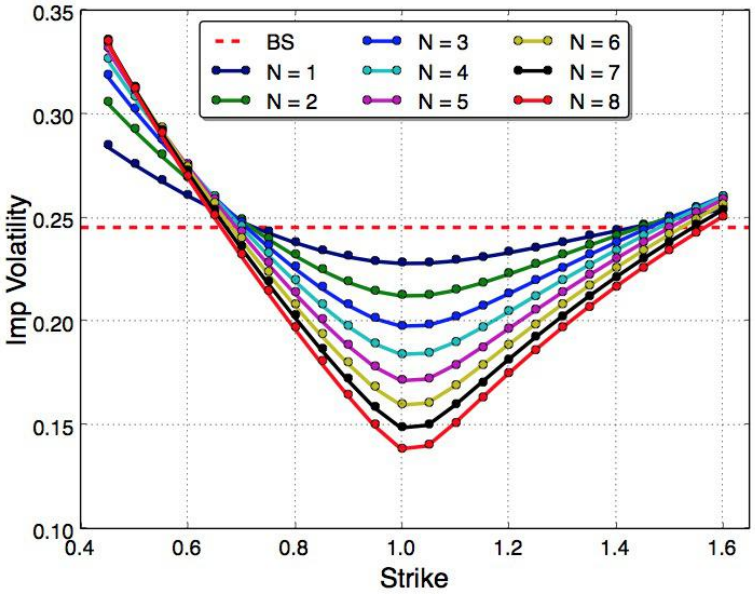

Figure 4-4 : Implied volatilities of the hierarchical Heston model as a function of strike K and N. Here we use $T = 2.0$.

4.7 Properties of the Hierarchical Hull-White Model

In this section, we discuss the features of our model by considering a Hull-White stochastic process for the volatility. We have used the same test parameters than in the previous case, which will help us later to establish differences between the results generated by the hierarchical Heston model and the hierarchical Hull-White models. But first, let us show the properties of this latter and its comparison with the Black-Scholes model.

Now the option prices are computed using the hierarchical Hull-White model given by equation (4.26) together with expressions (4.28), (4.29) and (4.31). Results of this are shown in figure **4-5**, where we have plotted a set of option prices with maturity $T = 0.2$ (figure **4-5**a) and $T = 2.0$ (figure **4-5**b). The behavior of the prices in this model is similar to the case based in a Heston model since in this case our model also gives higher prices than the Black-Scholes formula for in and out of the money options and lower values near the spot price $S = 1$. This is clearly noticed in figures **4-6**a and **4-6**b where we show the differences between the results of our model (4.26) and the Black-Scholes formula for the same cases in figure **4-5**. Therefore, our results also agree with the general behavior shown by the original Hull-White model for the case when the correlation between the asset price and its volatility is equal to zero [Hull and White, 1987].

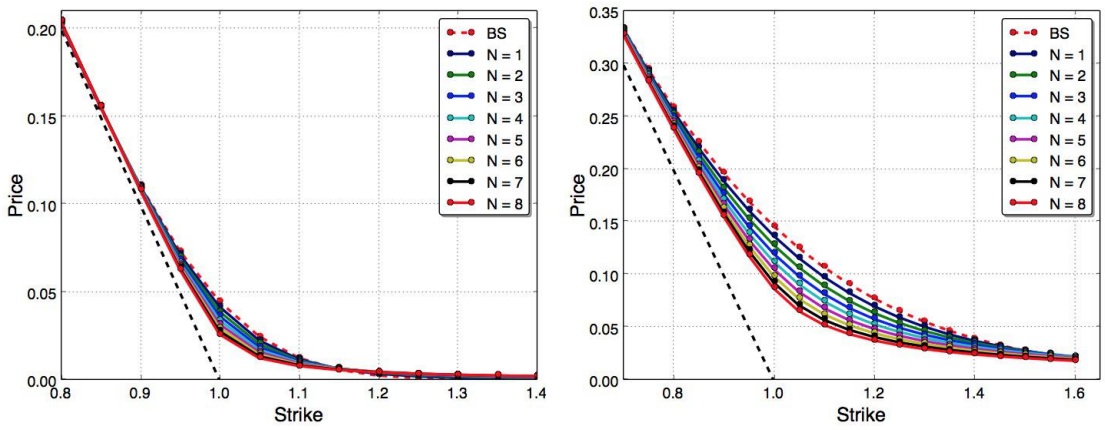

(a) (b)

Figure 4-5 : Hull-White option price on an asset of value $S = 1$ as a function of the strike K and the number of scales N. (a) Maturity $T = 0.2$. (b) Maturity $T = 2.0$.

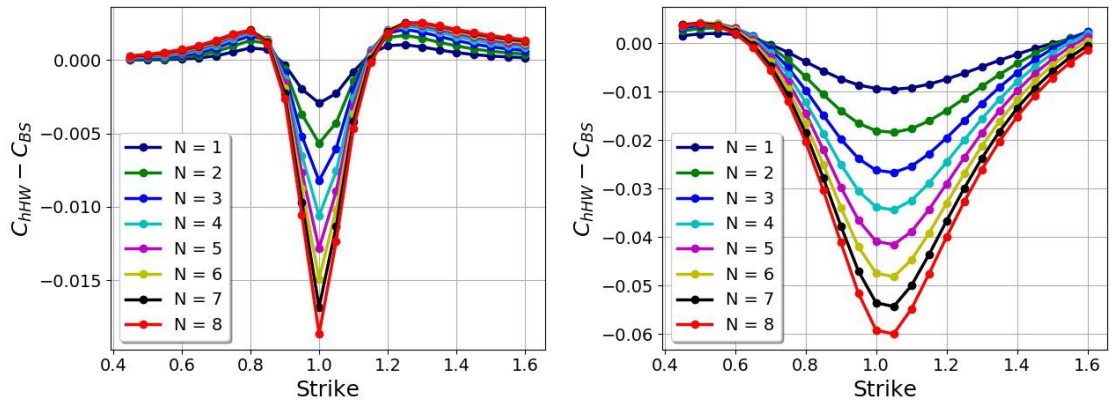

(a) (b)

Figure 4-6 : Difference between the option price generated by the hierarchical model with a Hull-White stochastic process and those generated by the Black Scholes formula: (a) For the same parameters of figure **4-5**a. (b) For the same parameters of figure **4-5**b.

The corresponding implied volatilities of the cases shown in figure **4-5** are plotted in figures **4-7** and **4-8**, for the maturities $T = 0.2$ and $T = 2.0$, respectively. Here we show that our model exhibits different volatility smiles depending on the number of scales in the hierarchical stochastic process. In fact, the implied volatility patterns are more pronounced as N increases. In the first case, where $T = 0.2$, our model yields implied volatility less than the Black-Scholes volatility σ near the spot price, i.e. for $K \in (0.90, 1.15)$. On the other hand, outside this interval, i.e. for in and out of the money options, the implied volatility obtained with the hierarchical model becomes higher than the volatility σ used in the Black-Scholes formula. For the case of long maturity, i.e. $T = 2.0$, the patterns of volatility are smoother than those displayed when $T = 0.2$. In this case, our model gives implied volatility less than the Black-Scholes volatility in a larger interval of the strike prices, $K \in (0.70, 1.50)$. Outside this interval, the implied volatility of our model becomes higher than the Black-Scholes volatility. In other words, as maturity increases the implied volatility of our model tends to the constant value σ. However, we can also customize the concavity of the implied volatility curve including more scales in our model.

As we saw above, our models yield the main features shown for the classical models for stochastic volatility. In particular, these give lower prices than the Black-Scholes model for strikes near to the spot price and higher option prices for in and out of the money options. In addition, we showed that our models produce the so-called volatility smiles patterns, which can be customized by the number of scales N in the model. Looking at the results of our two hierarchical models, we see similar properties, but now we want to know the difference between them. For this, in the next section, we compute their differences in the option prices

and in the volatility smiles.

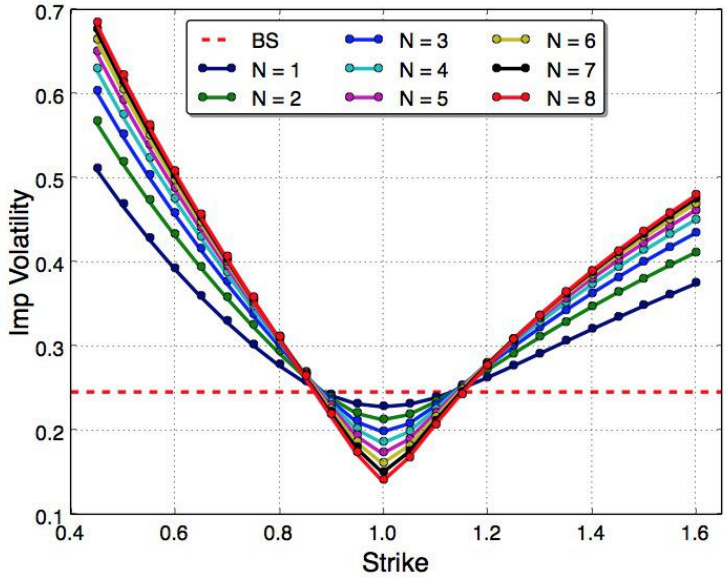

Figure 4-7 : Implied volatilities of hierarchical Hull-White model as a function of strike K and the number of scales N. Here we considered the case with maturity T=0.2

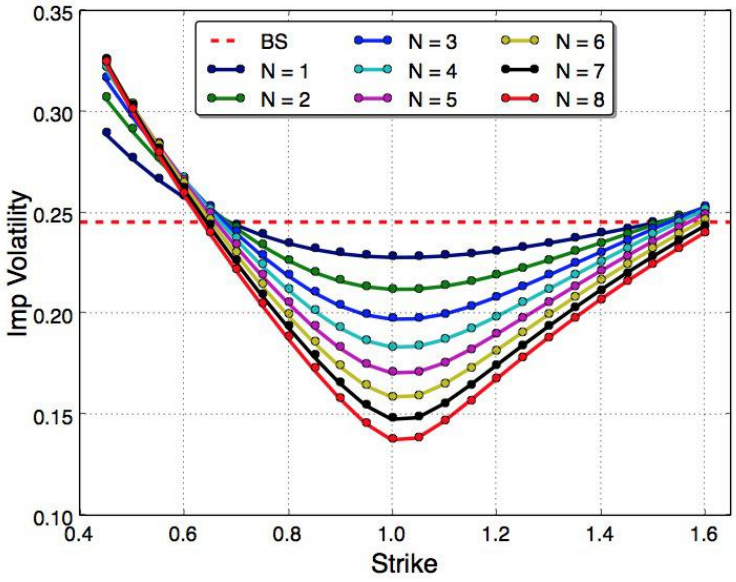

Figure 4-8 : Implied volatilities of the hierarchical Hull-White model as a function of strike K and the number of scales N. Here we considered the case with maturity T=2.0.

4.8 Comparison Between the Hierarchical Hull-White and Heston Models

As was noticed in the previous section, the two hierarchical models give a relatively similar behaviour for the option price as a function of K and T. However, a closer look reveals differences that are directly related to the PDF of the volatility used to obtain the respective models, i.e. a gamma or inverse gamma distribution. It is expected that a different stochastic process for the volatility v yields a different contribution to the stochastic process of the asset price S. Therefore, the distribution of returns implicitly used to average the Black-Scholes formula gives different results for the option price (4.4).

The deviations between our two hierarchical models are more visible when we compute the differences between the call prices generated by the Hull-White and the Heston approaches ($C_{hHW} - C_{hH}$). Using the results of sections 4.6 and 4.7, we have obtained the figures **4-9**a and **4-9**b where $C_{hHW} - C_{hH}$ is plotted as a function of the strike for the cases $T = 0.2$ and $T = 2.0$, respectively. In fact, we can see that in both cases the quantity $C_{hHW} - C_{hH}$ becomes negative near the spot price, meaning that the hierarchical Heston model yields slightly higher prices than those obtained from the hierarchical Hull-White model. Contrarily, far from the spot price, i.e. for in and out of the money options, the difference becomes positive, indicating that the hierarchical Hull-White formula C_{hHW} gives higher values than the Heston model C_{hH}. Note that at spot price the two models give approximately the same price for short maturity (see figure **4-9**a), whereas for longer maturity (figure **4-9**b), they differ considerably. This can be explained as follows. We have from the Black-Scholes formula (2.25) that for $K = S$ the term $\ln(S/K) \to 0$ and therefore the price becomes only dependent on the maturity T and the volatility v. Thus, for short maturity the difference between the two terms of the Black-Scholes formula is negligible. Conversely, as maturity increases the difference between the two terms in the Black-Scholes model becomes greater and therefore in this case the option price is more affected by the process driving the volatility. Now recall that in both of our models, the final option price is obtained as an average of the Black-Scholes formula over the corresponding distribution $f(v_N)$ of the volatility. The preceding argument then shows that the difference $C_{hHW} - C_{hH}$ between the predicted prices of the hierarchical Hull-White and Heston models is negligible for options with short maturity. This can be seen in figure **4-9**a, where there seems to be no difference between the prices of both models for $K = S$. Contrarily, if the maturity of the option is greater, the difference between the terms of the Black-Scholes formula is more affected by the process of volatility and as consequence we can see noticeable differences between the two models when $K = S$, as shown in figure **4-9**b.

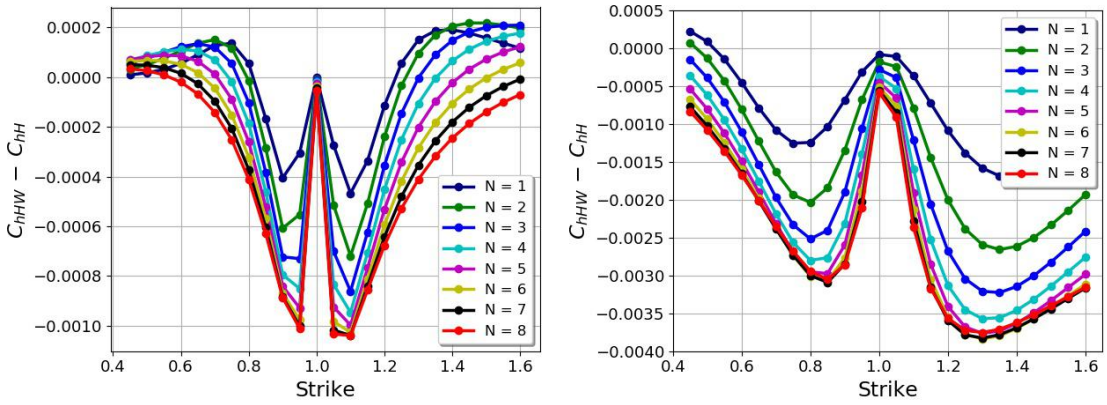

(a) (b)

Figure 4-9 : Difference between the option prices generated by the hierarchical Hull-White and Heston models. (a) Price differences between figures **4-5**a and **4-1**a. Maturity T= 0.2 and (b) Price differences between figures **4-5**b and **4-1**b. T=2.0.

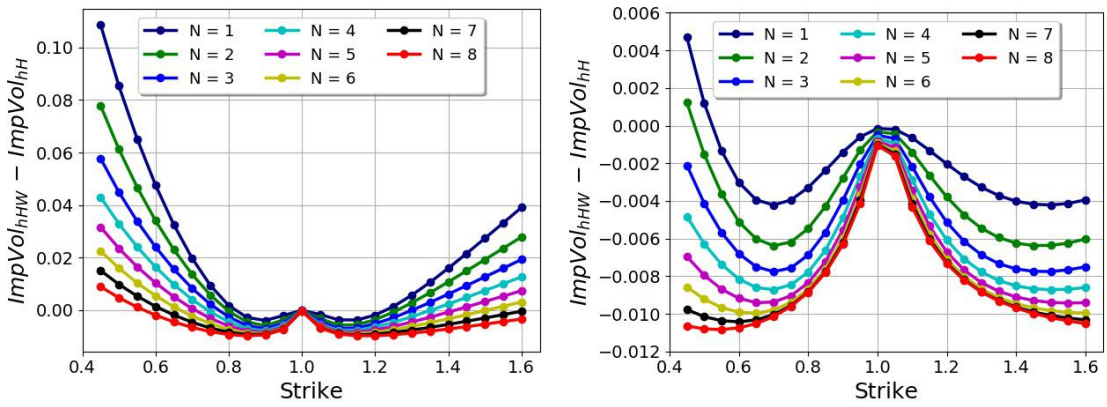

(a) (b)

Figure 4-10 : Difference between the implied volatility generated by the hierarchical Hull-White and the Heston formulas. (a) Implied volatility differences between figures **4-7** and **4-3**. Maturity T = 0.2 and (b) Implied volatility differences between figures **4-8** and **4-4**. T=2.0

Another form to determine differences in our models is by comparing their implied volatility patterns. So, for example, we can compute the difference between the implied volatility of the two models $ImpVol_{hHW} - ImpVol_{hH}$. These differences are plotted as a function of the strike K in figures **4-10**a and **4-10**b for the maturities $T = 0.2$ and $T = 2.0$, respectively. Here we can see that near the spot price $K \sim S$, the difference in implied volatility between our models becomes negative, i.e. $ImpVol_{hHW} - ImpVol_{hH} < 0$. By comparing with the

difference of prices shown in figure **4-9**, we notice that this is the same region where the prices are negative $C_{hHW} - C_{hH} < 0$. Conversely, for in and out of the money options (K far from S), where $C_{hHW} > C_{hH}$, the difference between the implied volatilities becomes positive, that is, $ImpVol_{hHW} > ImpVol_{hH}$. This can be explained by noting that the call price in the Black-Scholes model is a growing function of the volatility. Thus, if the price difference between our models is positive, the implied volatility difference will also be positive. Similarly, if the difference in price between our models becomes negative, the difference of their volatilities will also be negative.

To gain a better understanding of the dependence of these two models on the parameters K and T, we analyzed the implied volatility surface corresponding to the function of implied volatility $\sigma_{imp}(K, T)$ for both models. A volatility surface in addition to displaying the volatility smile also shows the so-called term structure of volatility, which puts on view how the implied volatility changes for options on the same asset but with a different maturity. The volatility surfaces of our two models are shown in figure **4-11**, where we have plotted the implied volatility as a function of the strike $K \in (0.45, 1.60)$ and the maturity $T \in (0.2, 2.0)$, for $N = 1$. The results for the Hull-White and Heston models are shown in figures **4-11**a and **4-11**b, respectively. These display clearly some differences between the volatility surfaces generated by the two models. For instance, for in and out of the money options, the hierarchical Hull-White model achieves higher values of implied volatility than the hierarchical Heston model. This is more evident if we look at volatility smiles corresponding to short maturities (for example $T = 0.2$). For long maturity the surfaces in both cases becomes flatter (see for example at $T = 2.0$). Other difference between the results for the implied volatility of our models is that the surfaces generated by the hierarchical Hull-White model seems flatter than the those obtained from the hierarchical Heston model. Similar effects are seen when we use several scales, for example $N = 8$, which is shown in figures (**4-12**a) and (**4-12**b) for the Hull-White and Heston models, respectively, although the differences between these are more difficult to notice by simple inspection.

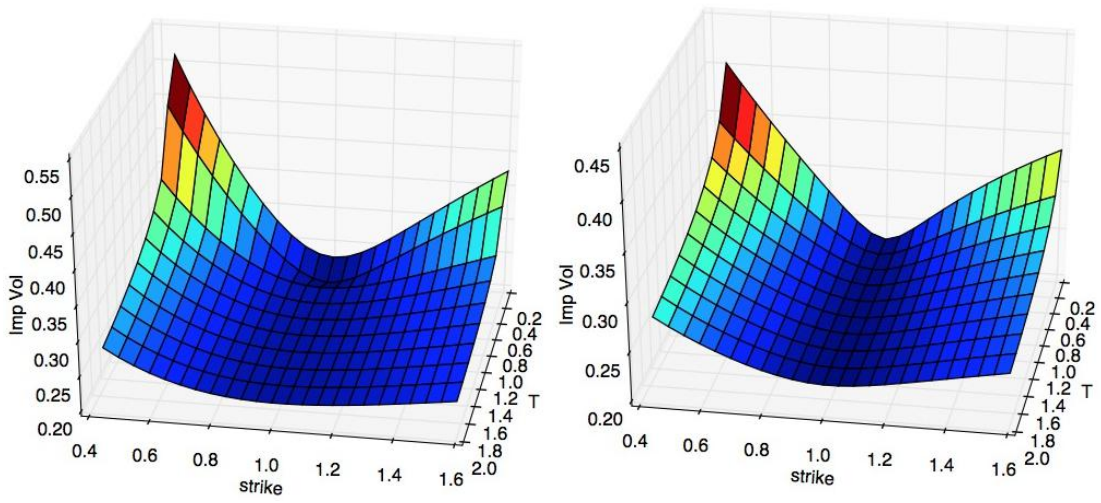

(a) (b)

Figure 4-11 : Implied volatility as a function of the strike K and the maturity T from the model with (a) the Hull-white and (b) the Heston process. The parameters used were $S_0 = 1$, $N = 1$, $T = 0.2 - 2.0$ and $K = 0.45 - 1.60$.

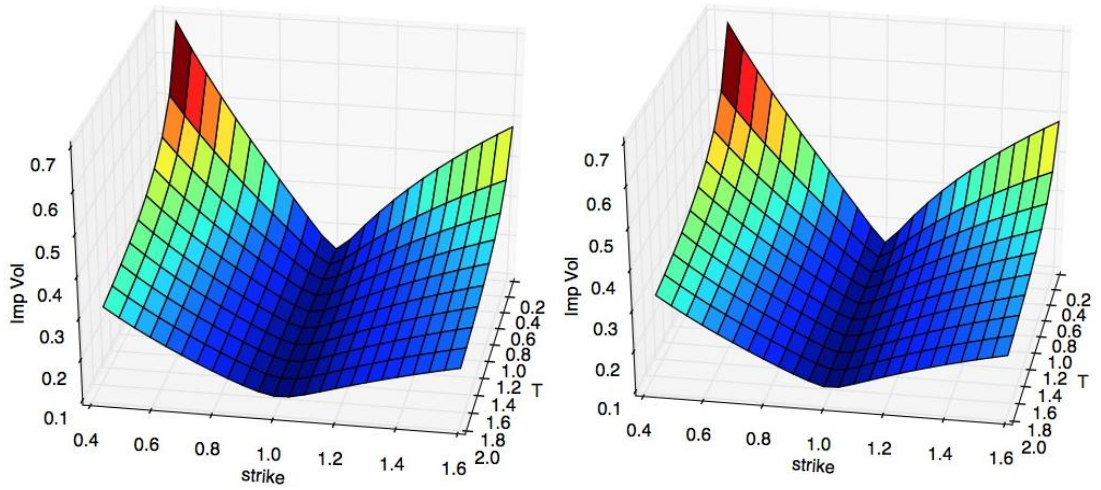

(a) (b)

Figure 4-12 : Implied volatility as a function of the strike K and the maturity T from the model with (a) the Hull-white and (b) the Heston process. The parameters used were $S_0 = 1$, $N = 8$, $T = 0.2 - 2.0$ and $K = 0.45 - 1.60$

4.9 Dependence on the β Parameter

Here we show the effect of the parameter β on the prices generated by our models. The parameter β appears when we solve the Fokker-Planck equation associated with the SDE for each case in section 4.3. Let us remember that there we defined $\beta = \frac{2\gamma}{\kappa^2}$, where γ is the reversion rate of the stochastic process and κ is related to the volatility of volatility. Therefore, the information about each stochastic process is in the value assigned to the parameter β. We also recall that the value of β governs the heavy-tail behavior of the probability distribution of the price returns, as discussed in [Macêdo et al., 2017].

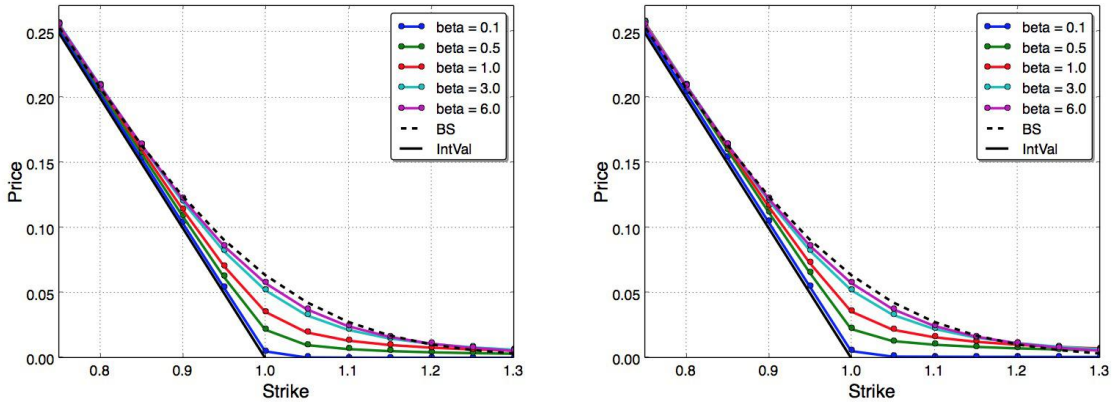

(a) (b)

Figure 4-13 : Option price as a function of β obtained by using: (a) The hierarchical Hull-White model and (b) The hierarchical Heston model. The parameters used were $S = 1$, $N = 5$ and maturity $T = 0.4$. Here BS denotes the Black-Scholes model and IntVal is the intrinsic value of the option.

We compute option prices by our hierarchical models as a function of the strike K, for different values of β using as test parameters $S = 1$, $N = 1$, $T = 0.4$. The strike ranges in the interval $K \in (0.7, 1.3)$ and the chosen β values were $\beta = (0.1, 0.5, 1.0, 3.0, 6.0)$. In figure **4-13** we show the prices generated by the hierarchical Hull-White model (left) and the hierarchical Heston model (right) with the different values of β. Here we find that for small values of β the option price generated by our models tends to the intrinsic value of the option. Contrarily, for large values of β ($\beta \to \infty$) the price given by our models tends to the Black-Scholes value. This behavior can be understood in terms of the reversion rate γ and the volatility of volatility κ. For example, a large value of β means a small value of κ, and therefore the volatility becomes less volatile. Large β also means that the reversion rate γ takes a large value, thus the volatility process relax quickly to its mean value v_0. So, according to the

two previous situations described, a high β value implies that the volatility process does not fluctuate and therefore the volatility becomes constant, and so we recover the Black-Scholes model as shown in figure **4-13**. The limit $\beta \to 0$ means that the reversion rate γ takes a small value or the volatility of volatility parameter κ takes high values. In this situation, volatility hardly moves back towards the average value v_0, extreme events of the market will be more probable and the volatility smile becomes more pronounced. This implies that far from the spot price S, i.e. for in and out of the money options, the option price increases, whereas for options with strike close to the spot price, the price decreases tending to the intrinsic value, as shown figure **4-13**.

4.10 Comparison with Market Prices

In this section we present a brief comparison between our hierarchical option pricing models and the market prices. To this end, we select some option chains of the Brazilian options market analyzed in chapter 3 and in a similar way we applied the least squares method to determine the parameters of the hierarchical models. The goodness of fit is determined by the standard error $SER = \sqrt{\chi^2/n}$, where n is the number of strikes in the chain. The standard error SER is used to compare the results given by the hierarchical models with the fit made by the conventional models, namely the Black-Scholes and the exponential models.

For example, we select a chain of options on the Ibovespa index traded on 05/25/06, corresponding to fifteen days before the maturity date on 06/14/06. The risk-free interest on 05/25/06 was $r = 0.0006$ and the spot price was $S = 37568.66$. Then, we fitted this options chain using the two hierarchical models presented above, which is shown in figure **4-14**. For the hierarchical Heston model we fitted up to $N = 7$ obtaining the parameters $\sigma_{hH} = \sqrt{v_0} = 0.014$ and $\beta = 7.718$. With these optimal parameters, we plotted the prices chain of our model, which is shown in figure **4-14**a (red line). Fitting by the hierarchical Hull-White approach we found for $N = 1$ the parameters $\sigma_{hHW} = \sqrt{v_0} = 0.014$ and $\beta = 0.737$. The corresponding theoretical prediction is shown in figure **4-14**b (red line). In order to compare with the conventional models analyzed in chapter 3, we have also plotted the Black-Scholes fit (dashed black line) from which we obtained the volatility value $\sigma_{BS} = 0.013$ and the exponential model (blue line) whose optimal parameters were $\nu = 0.124$ and $\gamma = 22.509$. Between the hierarchical models, we found that the Hull-White model fits the market prices slightly better than the Heston model, in the sense that it yields a lower standard error, namely $SER_{hHW} = 57.928$, as compared to $SER_{hH} = 58.001$ for the hierarchical Heston model. Both of our models provide better fits than the Black-Scholes formula for which we found $SER_{BS} = 65.094$, but they are not as good as the exponential model for which

$SER_{Exp} = 32.447$. In fact we can see that the curves corresponding to the hierarchical models (red line) in figures **4-14**a and **4-14**b seem to yield similar results that are reflected in their standard errors closed to each other.

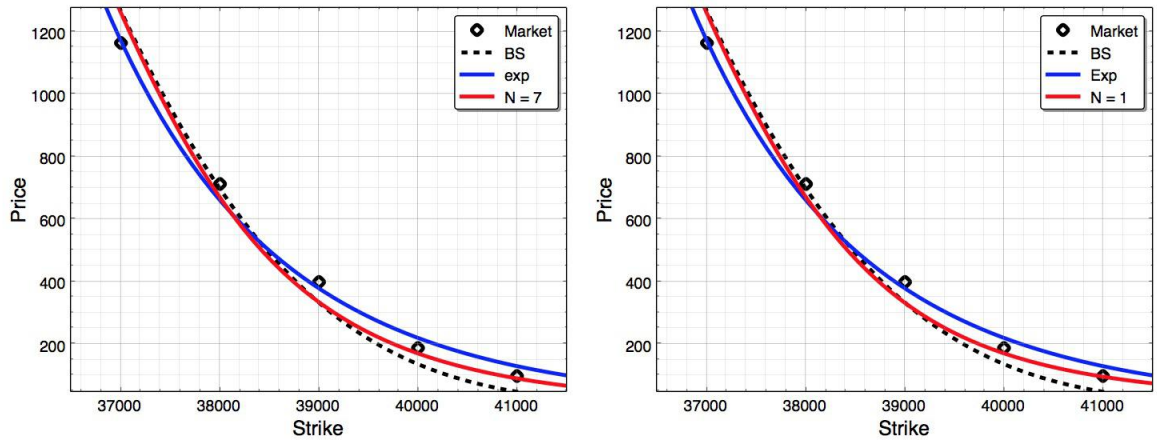

(a) (b)

Figure 4-14 : Bovespa option chain traded on 05/25/06 at 15 days before expiration (dots) and fit by methods: Black-Scholes (dashed black line); Exponential (blue line). And comparison with: (a) Heston model fit with $N = 7$; (b) Hull-White fit with $N = 1$ (red lines).

An alternative way to display the results presented in figure **4-14** is to plot the implied volatilities of each model as a function of the strike K. For this, we computed the implied volatilities by equating the price values generated by a given model $C_{model}(\mathbf{x})$ to the Black-Scholes formula $C_{BS}(K, S, T, r, \sigma)$ and solving for the volatility σ_{Imp}. In other words, we solve the equation:

$$C_{BS}(K, S, T, r, \sigma_{Imp}) - C_{model}(\mathbf{x}) = 0, \tag{4.47}$$

where $\mathbf{x}$ is the set of optimal fit parameters corresponding to each model.

Using the procedure described above we obtain the corresponding implied volatilities of the option prices in figure **4-14**, which is shown in figure **4-15**. In this figure we used the same convention of colors as in figure **4-14**, i.e we used points for the implied volatilities of the empirical data, black dashed line for the Black-Scholes volatility, blue line for the implied volatility of the exponential model and red line for the implied volatility of our hierarchical model. It is clear from this figure that our hierarchical models try to adjusts better the implied volatilities in comparison with the Black-Scholes formula, but the exponential model describes better the market data. We note however that the exponential model has the disadvantage that it is an empirical model in the sense that the exponential distribution is not obtained

from a dynamical process, contrarily to our hierarchical models whose associated distributions are derived from a set of stochastic differential equations.

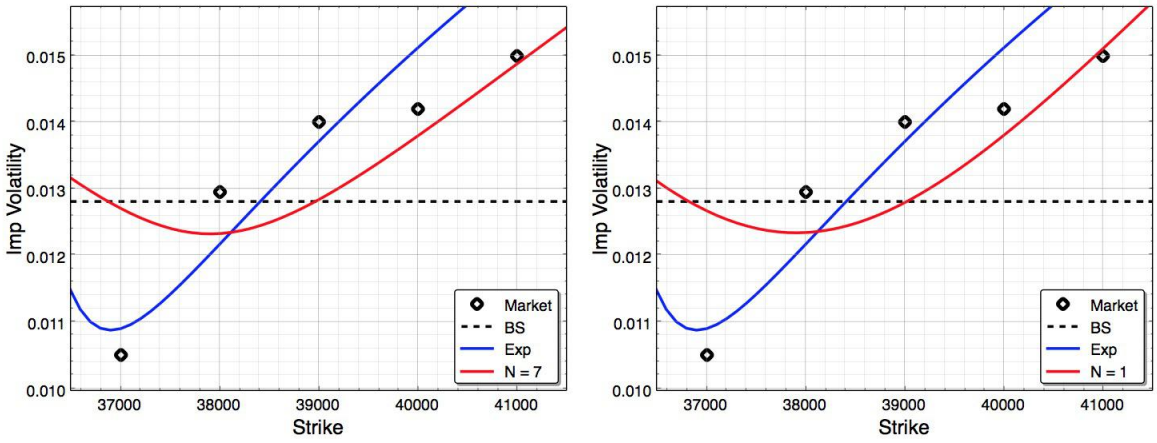

(a) (b)

Figure 4-15 : (a) Smile of volatility corresponding to data in figure **4-14**a; (b) Smile of volatility corresponding to data in figure **4-14**b.

Another example where we have applied our models is shown in figure **4-16**. As in the former case, we analyze an option chain traded on 09/11/06 on a stock with spot price $S = 40815.5$, interest rate $r = 0.0005$ and with time to expiration of 24 days on 13/12/06. Figure **4-16**a shows a comparison between the market prices (points) and the fits performed using the hierarchical Heston (red line), the Black-Scholes (black dashed line) and exponential (blue line) models. In this case, fitting the hierarchical Heston model up to $N = 6$ yields the parameters, $\sigma_{hH} = \sqrt{v_0} = 0.060$ and $\beta = 0.478$. Using the Black-Scholes formula we found $\sigma_{BS} = 0.019$, while for the exponential fit the parameters were $\gamma = 1.039$ and $\nu = 20.118$. On the other hand, figure **4-16**b shows a similar comparison but now with the fit performed employing the hierarchical Hull-White model. With this model we found the optimal parameters $N = 6$, $\sigma_{hHW} = 0.087$ and $\beta = 0.393$. Here both our models provide better fits compared to the Black-Scholes formula for options in and at the money. For options out of the money both models overestimate the option prices. By visual inspection of figure **4-16** the hierarchical Heston model shows good agreement with the empirical data for options in and at the money and similar results to those given by the exponential formula. For options out of the money our Heston formula becomes worse than the Hull-White one. The empirical exponential model again proves to be better, which it is confirmed by the fact that $SER_{Exp} = 79.364$, whereas the hierarchical Heston model yields $SER_{hH} = 252.437$ and the hierarchical Hull-White model gives $SER_{hHW} = 259.458$. For the fit by the Black-Scholes model we found

$SER_{BS} = 366.839$, worse than the hierarchical and exponential models. In conclusion, we can say that although our models improve the goodness of fit in comparison to the Black-Scholes model, the exponential model is capable of providing a better agreement with the data due to its asymmetric character as discussed in chapter 3. We recall however that the exponential model has the drawback that it is an empirical approach without a dynamical origin, as mentioned above.

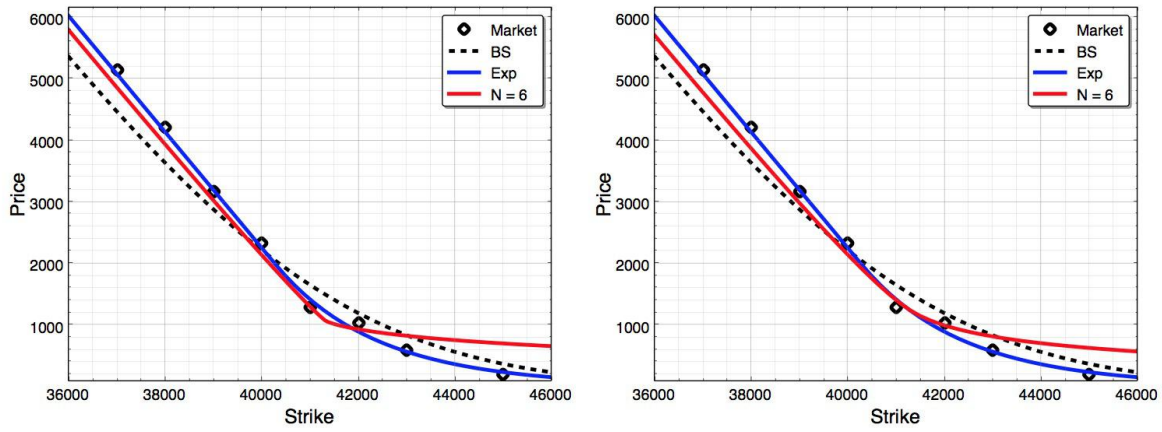

Figure 4-16 : Ibovespa option chain traded on 09/11/06 at 24 days before expiration. (a) hierarchical Heston model fit and conventional methods. (b) hierarchical Hull-White fit and conventional methods.

In figure **4-17** we show the corresponding volatility smiles of the fits in figure **4-16**. Here it is more noticeable that the hierarchical Heston model better describes the empirical volatility than the hierarchical Hull-White does. Both hierarchical models represent an improvement with respect to the Black-Scholes formula for in and at the money options, but for out of the money options they overestimate the value of the implied volatility. Overall, however, in this case, the hierarchical Hull-White model performs more poorly than the hierarchical Heston model.

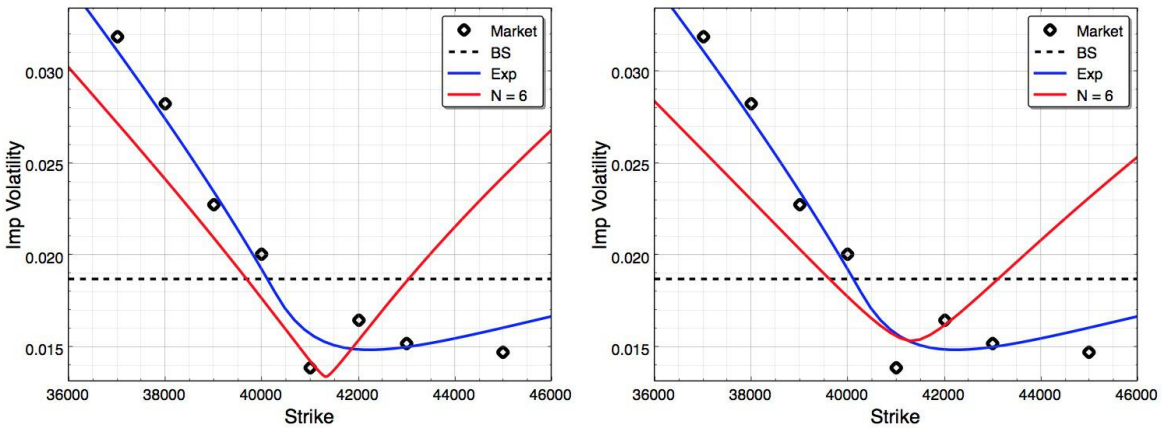

(a) (b)

Figure 4-17 : (a) Smile of volatility corresponding to data in figure **4-16**a; (b) Smile of volatility corresponding to data in figure **4-16**b.

5 Introduction to Statistical Turbulence

5.1 Turbulence Bases

Turbulence is a complex phenomenon that is commonly considered a chaotic or random motion of fluids. But actually turbulent fluids involve a lot of interesting features and concepts that define turbulence from the physics viewpoint. In order to give a definition of turbulence, let us mention the concept introduced in [McComb, 2014]. This reads:

Turbulence is the manifestation of the spatial-temporal chaotic behavior of fluid flows at large Reynolds numbers, i.e., of a strongly nonlinear dissipative system with an extremely large number of degrees of freedom (most probably) described by the Navier-Stokes equations.

To better understand this concept let us illustrate some of the characteristic features of fluid turbulence next:

1. From common observations, turbulence is seen as a motion of eddies of different sizes and speeds. Its study goes back to early times appearing for example in sketches of the water near a fall, in Leonardo Da Vinci water studies. In fact, it was there that the term *turbolenza* appeared for the first time [Yaglom, 2001]. From detailed experimental setups and in the language of physics, we can say that turbulence is a problem of many lengths and time scales. Experiments by Reynolds with laminar flow through a pipe show different regimes of turbulence which are characterized by a single velocity (e.g. the velocity at the center of the pipe) and a single length (e.g. the radius of the pipe), as shown in figure **5-1**. The dimensionless quantity which defines the different regimes of flow is named the Reynolds number

$$Re = Ud/\nu, \tag{5.1}$$

where U is the mean velocity, d is the diameter of the pipe and ν is the kinematic viscosity of the fluid [Tsinober, 2009].

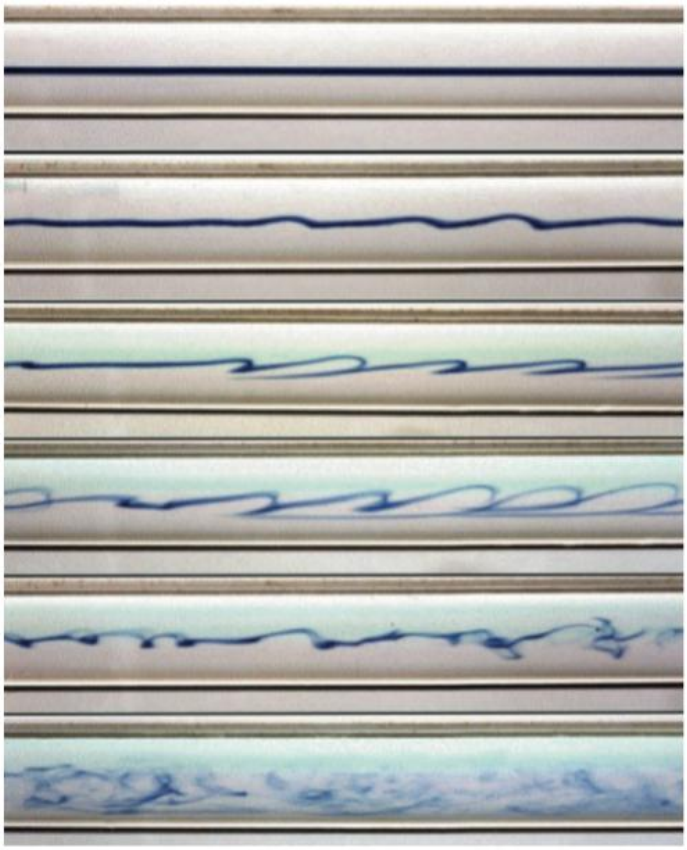

Figure 5-1 : Reynolds experiment in a circular pipe. The smallest mean velocity corresponds to the upper frame where the flow regime is laminar, the largest mean velocity corresponds to the lower frame where the flow regime is turbulent [Tsinober, 2009].

2. Turbulent flows are found to be highly dissipative. For example, in the laminar regime the pressure difference Δp at a distance, l, along the pipe of diameter d is proportional to the mean velocity, U, whereas in the turbulent regime it is much larger and is approximately proportional to $U^{7/4}$ in pipes with smooth walls and to U^2 in pipes with rough walls. The latter means that the rate of energy losses, $\Delta p d^2 U$, i.e., the rate of energy dissipation in the turbulent regime in pipes with rough walls is proportional to U^3/d and is independent of viscosity. In the turbulent regime the dissipation may be orders of magnitude larger than their laminar counterparts at the same Reynolds number.

3. Turbulent flows are strongly mixing in nature. The classic experiment by Reynolds shows that a dye-line injected at the center of a laminar pipe-flow becomes broken up in turbulence and rapidly spreads across the pipe. This mixing property is naturally associated with high rates of radial heat and mass transfer and resistance to flow because of radial momentum transfer. Another example is the figure **5-2** where the evolution of a jet coming

out of an orifice on the left is shown. It can be observed that the flow develops large scale structures which further break down resulting in fully developed turbulence.

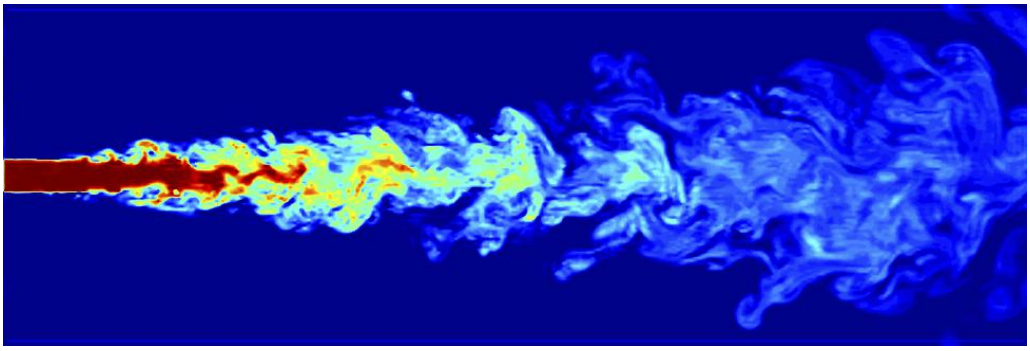

Figure 5-2 : Coexistence of different flow regimes: Laminar, transitional and turbulent regimes in a circular jet [Lawrence Livermore National Laboratory, 2018].

4. The fluid velocity is a random function of space and time. Experimental and theoretical evidence shows that the PDF of the velocity increments is non-Gaussian. For example figures **5-3** and **5-4** show the histogram of velocity increments generated from experimental data measured by [Chanal et al., 1997] and numerical simulations of the Navier-Stokes equations done by [Li et al., 2008]. In these figures we have also plotted the corresponding Gaussian fit (red line), where it is evident that it does not describe the data histogram. In addition, these figures show a slight skewness as expected from the Kolmogorov's 4/5 law (see above), which will be an important issue for our proposal of a theoretical model for the PDF of velocity increments in turbulence.

5. Due to the continuum nature of fluids, there are correlations between fluid motions at different points and times. These correlations vanish when increases the separation of measuring points or the time lag, and are characterized by correlation lengths and correlation times.

6. The nonlinearity of the flow motion produces as a result an interaction between the many degrees of freedom and scales (of time or space). For example, in atmospheric flows the relevant scales range from hundreds of kms to parts of a mm, i.e., there exist many degrees of freedom which are strongly interacting.

These and other features are discussed in many bibliographic sources, such as [Frisch, 1995, McComb, 2014, Tsinober, 2009], some of these additional features include, for example, notions of similarity and isotropy, which will be reviewed in the following sections.

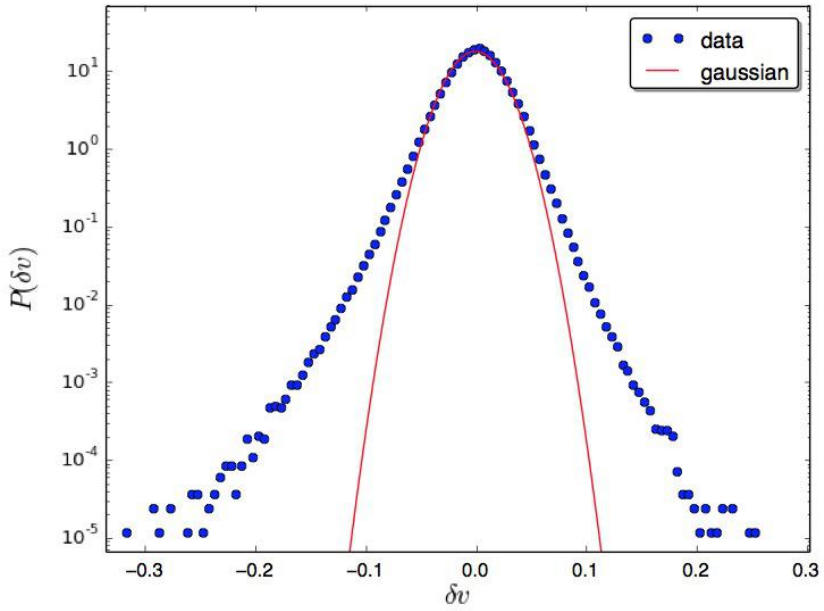

Figure 5-3 : Empirical distribution of velocity increments (dots) and Gaussian fit (red line).

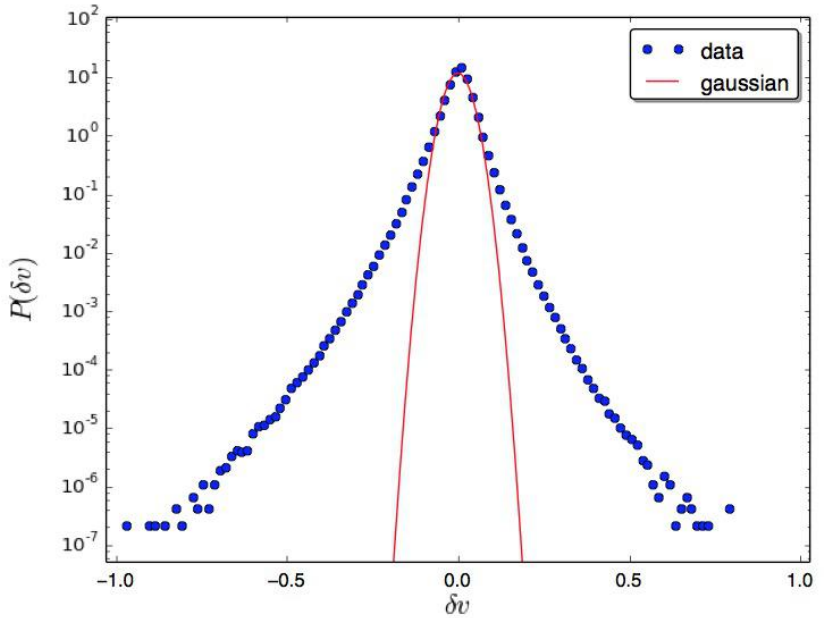

Figure 5-4 : Histogram of velocity increments generated by simulations of the Navier-Stokes equations (dots) and Gaussian fit (red line).

5.2 Navier-Stokes Equations

As an introduction, we present in this section the Navier-Stokes equations, which describe the dynamics of an incompressible Newtonian viscous fluid and are obtained by the following physical assumptions: conservation of mass, Newton's second law and the constitutive relations of the fluid. The state of the fluid is characterized by its density $\rho(t, \vec{r})$ and fluid velocity $\vec{v}(t, \vec{r})$. Under the assumption of incompressibility (constant density), the equations of motion (Newton's second law) that govern for a Newtonian fluid simplify to the incompressible Navier-Stokes equations:

$$\partial_t \vec{v} + \vec{v} \cdot \vec{\nabla} \vec{v} = -\vec{\nabla} p + \nu \nabla^2 \vec{v}, \tag{5.2}$$

and

$$\vec{\nabla} \cdot \vec{v} = 0, \tag{5.3}$$

where $\partial_t = \frac{\partial}{\partial t}$, $\vec{v} = \vec{v}(x, y, z, t)$ is the velocity field in the 3-dimensional space $p = p(x, y, z, t)/\rho$ is the pressure divided by the density ρ and ν is the kinematic viscosity of the fluid $\nu = \eta/\rho$.

The Navier-Stokes equations have a symmetry group, which consists of the following transformation group $g \in G$ of $\vec{v}$

$$\textit{Space translations}: \quad g_{\vec{a}}^{space} \vec{v}(\vec{r}, t) = \vec{v}(\vec{r} - \vec{a}, t) \tag{5.4}$$

$$\textit{Time translations}: \quad g_{\tau}^{time} \vec{v}(\vec{r}, t) = \vec{v}(\vec{r}, t - \tau) \tag{5.5}$$

$$\textit{Galilean transformation}: \quad g_{\vec{u}}^{Gal} \vec{v}(\vec{r}, t) = \vec{v}(\vec{r} - \vec{u}t, t) + \vec{u} \tag{5.6}$$

$$\textit{Space reflection}: \quad P\vec{v}(\vec{r}, t) = -\vec{v}(-\vec{r}, t), \quad P \equiv \textit{parity operator} \tag{5.7}$$

$$\textit{Space rotations}: \quad g_R^{rot} \vec{v}(\vec{r}, t) = R\vec{v}(R^{-1}\vec{r}, t), \quad R \in (SO)3 \tag{5.8}$$

$$\textit{Scale invariance}: \quad g_{\lambda}^{scale,h} \vec{v}(\vec{r}, t) = \lambda^h \vec{v}(\lambda^{-1}\vec{r}, \lambda^{h-1}t), \quad \lambda \in \Re. \tag{5.9}$$

The pressure does not appear above since it can be expressed as a function of v in the Navier-Stokes equations. In fact, its transformations are the same as those for the scalar variable $v^2 = |\vec{v}|^2$. The proof of some of the properties above is immediate such as the spatial and temporal translations which do not depend explicitly on time and space coordinates.

The Galilean transformation can be proved as follows. Using $\vec{v'} = \vec{v}(\vec{r} - \vec{u}t) + \vec{u}$ we get

$$\partial_t \vec{v'}(\vec{r}, t) = \partial_t \vec{v}(\vec{r} - \vec{u}t, t) - (\vec{u} \cdot \vec{\nabla})\vec{v}(\vec{r} - \vec{u}t, t) \tag{5.10}$$

$$(\vec{v'}(\vec{r}, t) \cdot \vec{\nabla})\vec{v'}(\vec{r}, t) = [\vec{v}(\vec{r} - \vec{u}t, t) + \vec{u}] \cdot \vec{\nabla}\vec{v}(\vec{r} - \vec{u}t, t). \tag{5.11}$$

adding these equations amounts to the left-hand side of the Navier-Stokes equations, and since the right-hand side is straightforwardly invariant, this proves the Galilean symmetry. The

scale invariance is demonstrated in the same way. Setting $\vec{v'} = \lambda^h \vec{v}(\lambda^{-1}\vec{r}, \lambda^{h-1}t)$, we obtain

$$\partial_t \vec{v'}(\vec{r},t) = \lambda^{2h-1}\partial_t \vec{v}(\lambda^{-1}\vec{r}, \lambda^{h-1}t) \tag{5.12}$$

$$(\vec{v'}(\vec{r},t)\cdot\vec{\nabla})\vec{v'}(\vec{r},t) = \lambda^{2h-1}\vec{v}(\lambda^{-1}\vec{r}, \lambda^{h-1}t)\cdot\vec{\nabla}\vec{v}(\lambda^{-1}\vec{r}, \lambda^{h-1}t) \tag{5.13}$$

$$\vec{\nabla}p'(\vec{r},t) = \lambda^{2h-1}\vec{\nabla}p(\lambda^{-1}\vec{r}, \lambda^{h-1}t) \tag{5.14}$$

$$\nu\nabla^2\vec{v'}(\vec{r},t) = \lambda^{h-2}\nu\nabla^2\vec{v}(\lambda^{-1}\vec{r}, \lambda^{h-1}t). \tag{5.15}$$

For finite viscosity $\nu > 0$, only $h = -1$ removes the factors involving the scaling factor λ. This allows us to define the Reynolds number keeping it the same for different scales, that is

$$Re = \frac{UL}{\nu}, \tag{5.16}$$

where L is the domain size and U is the characteristic velocity. Now choosing $L' = \lambda L$ and $U' = \lambda^h U$, the Reynold's number with this scaling becomes

$$Re' = \lambda^{h+1}\frac{UL}{\nu} = \lambda^{h+1}Re = Re, \text{ if } h = -1. \tag{5.17}$$

This scale invariance is equivalent to the principle of hydrodynamic similarity by which two flows with the same geometry and same Reynolds number but different scale of longitude and velocity are similar and related only by a scaling transformation.This also has as consequence that at sufficiently high Reynolds number, the viscosity term is neglected and therefore any exponent h may be chosen.

Other results derived from the Navier-Stokes equations are for instance some conservation laws [Frisch, 1995]. Considering periodic boundary conditions for the quantities involved in the dynamic of the system, it is possible to demonstrate that the Navier-Stokes equations satisfy the following conservation laws:

i) Conservation of moment.

$$\frac{d}{dt}\langle\vec{v}\rangle = 0 \tag{5.18}$$

ii) Conservation of energy.

$$\frac{d}{dt}\langle\frac{1}{2}v^2\rangle = -\nu\langle|\vec{\omega}|^2\rangle, \tag{5.19}$$

where $\langle\rangle$ is the spatial average and $\vec{\omega} = \vec{\nabla}\times\vec{v}$ is the vorticity. The mass does not appear since the Navier-Stokes equations are normalized to the density. Equation (5.19) gives the conservation of the overall system energy and shows the dissipation of energy as a consequence of the viscosity, as expected.

The energy balance equation (5.19) does not contain any contribution from the nonlinear term in the Navier-Stokes equation because this term vanishes since we have periodic functions whose spatial average is equal to zero. Up to this point, we do not know the role of

nonlinearities in relation to the energy. For that, it is necessary to define the concept of scale and to analyze the energy flux among different scales of motion without affecting the global energy budget.

5.3 Energy Budget Scale by Scale.

The energy budget in the fluid may be understood from the spectral analysis of the dynamical variables which describe the state of the fluid. It is done by the decomposition of these variables in a discrete Fourier representation considering periodic conditions for the fluid. So, applying this treatment to de Navier-Stokes equations with an external force $\vec{f}$, it is possible to obtain de so-called scale-by-scale energy budget equation, that describes the dynamics of the energy in the fluid. From this treatment, the concept of scale is defined to be related to the cutoff wavenumber (maximum and minimum) considered in the Fourier series, this is $l \sim K^{-1}$. So, for a given scale, or considering up to a specific wavenumber cutoff it is possible to obtain the dynamics for the energy in this scale. As shown in [Frisch, 1995], this reads

$$\partial_t E_K + \Pi_K = -2\nu\Omega_K + F_K \tag{5.20}$$

where the total energy E_K, accumulated up to the wavenumber K is defined as

$$E_K = \frac{1}{2}\sum_{k\leq K} |\vec{v}_{\vec{k}}|^2; \tag{5.21}$$

Ω_K is the enstrophy accumulated up to K:

$$\Omega_K = \frac{1}{2}\sum_{k\leq K} k^2|\vec{v}_{\vec{k}}|^2; \tag{5.22}$$

F_K is the rate of energy injected up to K

$$F_K = \frac{1}{2}\sum_{k\leq K} \vec{f}_{\vec{k}} \cdot \vec{v}_{\vec{-k}}. \tag{5.23}$$

Finally, the energy flux through the scale K^{-1} toward smaller scales is defined as:

$$\Pi_K = \langle \vec{v}_K^{<} \cdot (\vec{v}_K^{<} \cdot \vec{\nabla}\vec{v}_K^{>})\rangle + \langle \vec{v}_K^{<} \cdot (\vec{v}_K^{>} \cdot \vec{\nabla}\vec{v}_K^{>})\rangle, \tag{5.24}$$

where the symbols " $>$ " and " $<$" indicate wave vectors $k > K$ and $k \leq K$ in the Fourier decomposition of the velocity function.

Equation (5.20) means that the rate of change of the energy at scales down to $l \sim K^{-1}$ is equal to the energy injected into these scales by the force (F_K) minus the energy dissipated within such scales ($2\nu\Omega_K$) minus the flux of energy (Π_K) to smaller scales due to nonlinear

terms into the Navier-Stokes equations. This last term appears as a mechanism of interaction between successive scales and directly connects the description given by the Navier-Stokes equations and the common hypothesis in turbulence theory such as the assumption of the energy cascade. In particular, such energy cascade allows describing the variation of the energy flux from long to short scales in the so-called inertial range. This phenomenon known as intermittency can be seen as the variability of the turbulence with the scale, that is, as the existence of a multi-scale process [Batchelor and Townsend, 1949].

The construction of a hierarchical model of intermittency is done by [Salazar, 2010,Salazar and Vasconcelos, 2010] starting from equation (5.20). They assumed that in the limit of infinite Reynolds number the contribution of the viscosity becomes negligible. In addition, considering that the energy is injected only in the integral scale l_0, the dynamics of the energy in a scale is only determined by differences between the incoming and outgoing energy flux Π_K in that scale, in other words by the energy flux through a scale or cascade level.

5.4 Kolmogorov's 1941 Theory (K41)

In 1941 Kolmogorov, after having done many contributions to mathematics and the theory of stochastic processes, decided to venture into the study of turbulent flows. Kolmogorov's theory is based on three important hypotheses combined with dimensional arguments and experimental observations [Kolmogorov, 1941b, Kolmogorov, 1941a].

For homogenous turbulence, the turbulent kinetic energy is on average the same everywhere. For isotropic turbulence, eddies also behave similarly in all directions. Kolmogorov argued that the directional biases of the large scales are lost in the chaotic scale-reduction process as energy is transferred to successively smaller eddies. *Hence Kolmogorov's hypothesis of local isotropy states that at sufficiently high Reynolds numbers, the small-scale turbulent motions ($l \ll l_0$) are statistically isotropic* [Pope, 2000]. Here l_0 is the scale used as the reference to define the smaller scales and is called the integral scale. In practice, this is related to the dimensions of the system where the fluid is flowing. The term local isotropy means isotropy at small scales, whereas at large scale the turbulence may still be anisotropic.

The observable quantity to be studied in an experimental setup of turbulence is the velocity increment, $\delta\vec{v}$, between two spatial points separated by a distance l,

$$\delta\vec{v}(\vec{r},\vec{l}) = \vec{v}(\vec{r}+\vec{l}) - \vec{v}(\vec{r}). \tag{5.25}$$

Kolmogorov's hypotheses of homogeneous and isotropic turbulence mean that there is no preferential direction, hence the velocity increments depend only on the modulus of $\vec{l}$: $\delta\vec{v}(\vec{r},\vec{l}) = \delta\vec{v}(\vec{r},l)$. To simplify the notation we shall denote $\delta\vec{v}(l) \equiv \delta\vec{v}(\vec{r},l)$.

Kolmogorov also argued that the statistics of the small-scale motions are universal: they are similar in every high Reynolds number turbulent flow, independent of the mean flow field and the boundary conditions. These constitute the result of two hypothesis, as discussed next. "The first similarity hypothesis which states that in every turbulent flow at sufficiently high Reynolds number, the statistics of the small scale motions ($l \ll l_0$) have a universal form that is uniquely determined by the dissipation rate ϵ and the kinematic viscosity ν" [Pope, 2000].

This theory implicitly assumes that turbulence is statistically self-similar at smaller scales. This essentially means that the statistics is scale-invariant in the inertial range. Statistical scale-invariance implies that the scaling of the velocity increments should occur with a unique scaling exponent h, so that when l is scaled by a factor λ, $\delta\vec{u}$ should have the same statistical distribution as $\lambda^h \delta\vec{u}(l)$, where h does not depend on the scale.

The second hypothesis as described in [Tsinober, 2009, Pope, 2000], reads:
"Kolmogorov's second similarity hypothesis states that in every turbulent flow at sufficiently high Reynolds number, the statistics of the smaller scale motions ($\eta \ll l \ll l_0$) have a universal form that is uniquely determined by the average rate of dissipation ϵ and by the specific scale l".
Here

$$\eta = \nu^{3/4}/\langle\epsilon\rangle^{1/4} \tag{5.26}$$

is the so-called Kolmogorov dissipation scale. From these hypotheses, using dimensional arguments one can obtain a relation for the second order structure function, defined as the second moment of the velocity increments $\langle(\delta\vec{v}(l))^2\rangle$. As this quantity has dimensions of $[L]^2[T]^{-2}$ the only combination of ϵ and l which results in a quantity with the same dimension is $\epsilon^{2/3}l^{2/3}$, therefore

$$\langle(\delta v(l))^2\rangle = C\epsilon^{2/3}l^{2/3} \tag{5.27}$$

for longitudinal increments $\delta v(l) = d\vec{v}(\vec{r}, l) \cdot \hat{l}$, where C is a dimensionless constant. From the Kolmogorov theory it also follows a result for the high-order structure functions, which scale as

$$\langle(\delta v(l))^p\rangle \sim l^{\zeta_p}, \tag{5.28}$$

where ζ_p is known as the scaling exponent and it gets the value $\zeta_p = p/3$ for the K41 theory. This model was not able to reflect the observed phenomenon of intermittency, and therefore new models were devised in which the exponents ζ_p did present a non-linear dependency on p. Thus, it was necessary a modification of the K41 Kolmogorov's theory, known as Kolmogorov's K62 theory [Kolmogorov, 1941a, Kolmogorov, 1941b].

In his first 1941 paper [Kolmogorov, 1941a], Kolmogorov only treated (at least explicitly) the second-order function, although all his hypotheses were formulated for statistical proper-

ties of velocity increments and therefore for structure functions of higher order. Instead, the 1941a paper was followed by the most remarkable quantitative prediction obtained as a direct consequence of the Navier-Stokes equations for the inertial range $l_0 \ll l \ll \eta$ [Kolmogorov, 1941b]. An exact formula for the third moment of the velocity increments known as the 4/5 law:

$$\langle(\delta v(l))^3\rangle = -\frac{4}{5}\,\epsilon\, l. \tag{5.29}$$

This result will serve later as part of the justification for our statistical asymmetric model for turbulence. Although this relation introduces the idea of universality for the multiplicative constant $-4/5$, experimental results exhibit large variability from the range of l in which this is valid, even at rather high Reynolds numbers [Tsinober, 2009, Kholmyansky and Tsinober, 2008]. Several possible causes for deviations from the 4/5 law are discussed for example in [Frisch, 1995, Tsinober, 2009]. In fact this is one of the issues in turbulence which has kept the turbulence community quite busy until now.

5.5 Kolmogorov-Obukhov (K62) theory

In 1962 Kolmogorov presented his theory of intermittency, since then called K62, in response to criticisms from Landau about the assumption in the K41 theory in which he considered constant energy dissipation [Landau and Lifshitz, 1987]. Landau argued that due to the random nature of energy transfers to smaller scales, the fluctuation of energy dissipation should increase as the ratio l/l_0 decreases. In addition, there was experimental evidence which showed that the amplitude of temporal fluctuations of the velocity field exhibited abrupt variations [Obukhov, 1962, Gurvich, 1960]. Then, Obukhov, a doctoral student of Kolmogorov adduced that such variations could be explained if the rate of dissipation ϵ had a certain variance about the mean [Obukhov, 1941]. With this, Kolmogorov introduced into his theory a modified form of the dissipation rate averaged over a sphere of radius l, denoted by $\epsilon_r(\vec{r}_0, t)$ [McComb, 2014]. This was defined as

$$\epsilon_r(\vec{r}_0, t) = \frac{3}{4\pi r^3}\int_{r'\leq r} d^3r'\epsilon(\vec{r}_0 + \vec{r}') \tag{5.30}$$

where the sphere is centered in $\vec{r}_0$ and $\epsilon(\vec{r}_0 + \vec{r}') \equiv \epsilon$ is the instantaneous energy dissipation rate, given by

$$\epsilon = \frac{\nu}{2}\sum_{i,j}\left(\frac{\partial v_j}{\partial x_i} + \frac{\partial v_i}{\partial x_j}\right)^2. \tag{5.31}$$

Kolmogorov also proposed that for small scales, $l \ll l_0$, the logarithm of $\epsilon_r(\vec{r}_0, t)$ had a normal distribution, with variance given by

$$\sigma_l^2 = A + \mu \ln\left(\frac{l_0}{l}\right), \tag{5.32}$$

where μ is a universal constant. This assumption in the literature is known as the log-normal hypothesis or hypothesis of log-normality. As result of this hypothesis, the statistical moments of the energy dissipation and the velocity fluctuations, which characterize the turbulent regime, should be replaced by

$$\langle \epsilon_l^q \rangle = \epsilon_0^q (l/l_0)^{\tau_q} \tag{5.33}$$

and

$$\langle (\delta v(l))^p \rangle = (\epsilon_0 l)^{p/3} (l/l_0)^{\zeta_p}, \tag{5.34}$$

respectively, where the scaling exponents τ_q and ζ_p are given by

$$\tau_q = \frac{\mu}{2}(q - q^2) \tag{5.35}$$

and

$$\zeta_p = \frac{p}{3} + \frac{\mu}{18}(3p - p^2). \tag{5.36}$$

For Lagrangian turbulence, in which the velocity fluctuations are measured over the same particle in different instants of time, the structure functions for the increments of velocity are described as a function of the temporal scale in which the increments are measured. In this case the Kolmogorov similarity hypothesis is written as

$$\langle \delta v_\tau^p \rangle = (\epsilon_0 \tau)^{p/3} (\tau/T)^{\zeta_p}, \tag{5.37}$$

where the scaling exponent for the log-normal model reads

$$\zeta_p = \frac{p}{2} + \frac{\lambda^2}{2}(2p - p^2), \tag{5.38}$$

and λ is a free parameter of the model. An example of the behavior of these scaling exponents is shown in figure **5-5**.

The log-normal hypothesis presents some conceptual difficulties [Frisch, 1995, Mandelbrot, 1999]. For instance, it violates the condition which states that the scaling exponent ζ_p is a nondecreasing function of p, related to obtaining the incompressible Navier-Stokes equation. Despite the critiques to this model, it would lead to further models of intermittency such as the β model and fractal models discussed in [Parisi and Frisch, 1983, Mandelbrot, 1999, Frisch et al., 1978, She and Lévêque, 1994], which are not considered in this work.

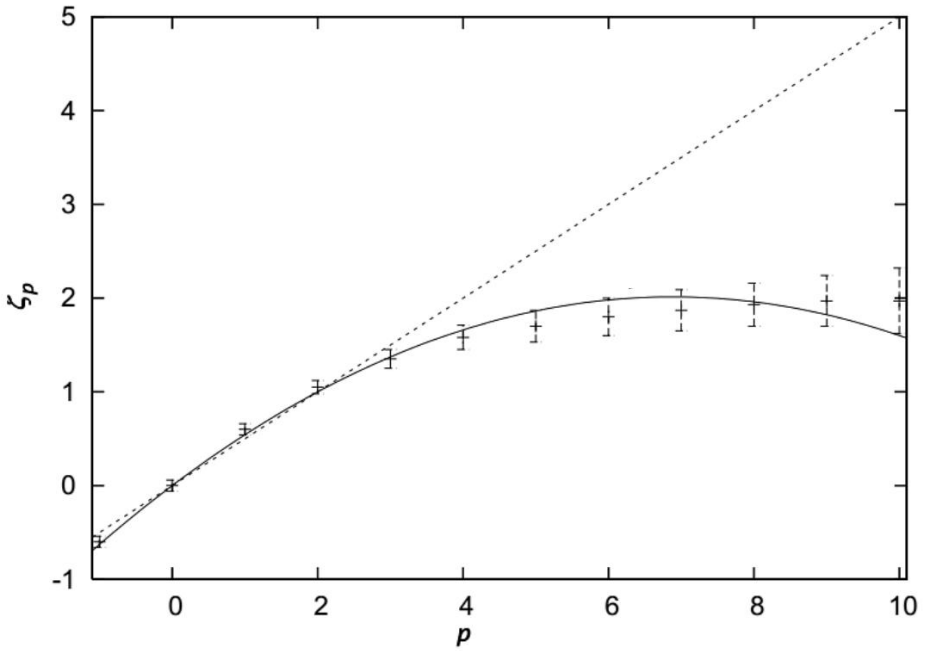

Figure 5-5 : Lagrangian scaling exponents ζ_p as measured by [Xu et al., 2006] and as predicted by the Beck's superstatistical model for $\lambda^2 = 0.085$ (solid line) [Beck, 2007]. No intermittency (dashed line).

Up to here, we have given a brief introduction to the theory of turbulence. Our motivation is to give enough background material to justify the following sections where we introduce a hierarchical model of turbulence. In our formalism we regard the hypothesis of Kolmogorov and the concept of intermittency, but considering a multiscale dynamical model for the stochastic fluctuations of the energy fluxes between scales.

5.6 Hierarchical Model for the Energy Flux.

Here we recall the hierarchical model presented in section 4.3, but now in the context of turbulence. In this case, the fluctuating variable is the energy dissipation rate and its dynamics described by a system of N stochastic processes as in the case of the volatility in the previous chapter. In section 5.7 we review the symmetric statistical model for the distribution of velocity increments obtained by [Macêdo et al., 2017, Salazar and Vasconcelos, 2010]. Later in chapter 6 we will develop these concepts to introduce an asymmetric model.

5.6.1 Inverse gamma class.

A hierarchical model can be introduced based on the concept of energy cascades proposed by [Richardson, 1922]. A turbulent flow represented as an energy cascade including several scales (N) is illustrated in the picture below. The initial cascade level ϵ_0 is the scale where the energy flux is injected and where the flow exhibits its largest eddies. These eddies, in turn, transfers energy to smaller eddies in the following level ϵ_1 (process explained by the non-linear terms in the equation of motion) and so on to the smallest scale ϵ_N, after which energy is dissipated into heat by viscous effects. Mathematically, the model can be described by a system of N SDEs similar to those in (4.14). We then consider the following model

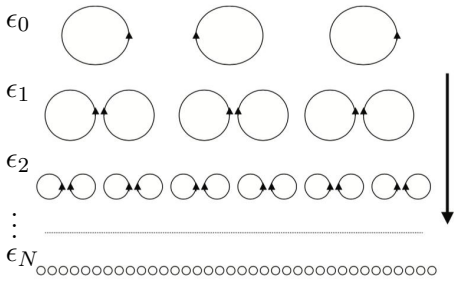

$$\begin{aligned} d\epsilon_1 &= -\gamma_1(\epsilon_1 - \epsilon_0)dt + \kappa_1\epsilon_1 dW_1 \\ d\epsilon_2 &= -\gamma_2(\epsilon_2 - \epsilon_1)dt + \kappa_2\epsilon_2 dW_2 \\ &\vdots \qquad\qquad\qquad \vdots \\ d\epsilon_N &= -\gamma_N(\epsilon_N - \epsilon_{N-1})dt + \kappa_N\epsilon_N dW_N, \end{aligned} \tag{5.39}$$

with the characteristic times satisfying $\gamma_i^{-1} \ll \gamma_{i-1}^{-1}$. This means that the processes in smaller scales occur faster than in the larger scales. Using this hypothesis, we can assume that the energy flux of a smaller scale i achieves the equilibrium so quickly that the energy flux in a larger scale $i-1$ is approximately constant. So, the marginal PDF of the energy flux in scale N under the hypothesis above is given by the general integral

$$f_N(\epsilon_N) = \int_0^\infty d\epsilon_{N-1} \ldots \int_0^\infty d\epsilon_1 \; f_N(\epsilon_N|\epsilon_{N-1}) \ldots f_1(\epsilon_1|\epsilon_0), \tag{5.40}$$

where the conditional probability $f(\epsilon_i|\epsilon_{i-1})$ for the scale i is given by an inverse gamma distribution (4.16); see [Salazar, 2010] for further discussions.

Particular case: Two scales model

Now we consider the hierarchical model (5.39) for the particular case when there are only two scales, i.e., $N = 2$. In this case the two stochastic processes ϵ_2 and ϵ_1 are related by the following system of equations:

$$\begin{aligned} d\epsilon_2 &= -\gamma_2(\epsilon_2 - \epsilon_1)dt + \kappa_2\epsilon_2 dW_2 \\ d\epsilon_1 &= -\gamma_1(\epsilon_1 - \epsilon_0)dt + \kappa_1\epsilon_1 dW_1. \end{aligned} \tag{5.41}$$

Each process above has an associated Fokker-Planck equation whose stationary solution is given by an inverse gamma distribution, see Appendix F for more details. For example, the

solution for the PDF of the stochastic process ϵ_2 conditioned on $\epsilon_1 = \text{cte}$ is an inverse gamma distribution in the form

$$f_2(\epsilon_2|\epsilon_1) = \frac{(\beta_2\epsilon_1)^{\beta_2+1}}{\Gamma(\beta_2+1)}\epsilon_2^{-\beta_2-2}e^{-\beta_2\epsilon_1/\epsilon_2}, \tag{5.42}$$

and similarly, for the distribution of ϵ_1 conditioned on ϵ_0 we have

$$f_1(\epsilon_1|\epsilon_0) = \frac{(\beta_1\epsilon_0)^{\beta_1+1}}{\Gamma(\beta_1+1)}\epsilon_1^{-\beta_1-2}e^{-\beta_1\epsilon_0/\epsilon_1}. \tag{5.43}$$

Assuming that the time scales of the processes are well separated, which is satisfied if $\gamma_2 >> \gamma_1$, the marginal PDF, $f_2(\epsilon_2)$, for the process ϵ_2 reads

$$f_2(\epsilon_2) = \int_0^\infty f_2(\epsilon_2|\epsilon_1)f_1(\epsilon_1|\epsilon_0)d\epsilon_1. \tag{5.44}$$

Replacing (5.42) and (5.43) into (5.44) and performing the integration gives

$$f_2(\epsilon_2) = C\epsilon_2^{-2-\frac{\beta_2+\beta_1}{2}}K_{\beta_2-\beta_1}\left(2\sqrt{\frac{\beta_2\beta_1\epsilon_0}{\epsilon_2}}\right), \tag{5.45}$$

where the normalization constant is given by

$$C = 2\left(\frac{\beta_1\epsilon_0}{\beta_2}\right)^{\frac{\beta_2-\beta_1}{2}}\left[\frac{\beta_2^{\beta_2+1}}{\Gamma(\beta_2+1)}\right]\left[\frac{(\beta_1\epsilon_0)^{\beta_1+1}}{\Gamma(\beta_1+1)}\right]. \tag{5.46}$$

This expression has an equivalent and more convenient representation as a Meijer G-function in the following form (see Appendix G):

$$f_2(\epsilon_2) = \frac{1}{\epsilon_0\beta_1\beta_2\Gamma(\beta_1+1)\Gamma(\beta_2+1)}G_{2,0}^{0,2}\left(\begin{matrix}-\beta_1-1,-\beta_2-1\\ -\end{matrix}\middle|\frac{\epsilon_2}{\beta_1\beta_2\epsilon_0}\right). \tag{5.47}$$

To illustrate the complexity of the model, consider the next scale involving the process ϵ_3, whose conditional PDF is

$$f_3(\epsilon_3|\epsilon_2) = \frac{(\beta_3\epsilon_2)^{\beta_3+1}}{\Gamma(\beta_3+1)}\epsilon_3^{-\beta_3-2}e^{-\beta_3\epsilon_2/\epsilon_3}. \tag{5.48}$$

The marginal distribution $f_3(\epsilon_3)$ is obtained by integrating the product of (5.45) and (5.48) with respect to ϵ_2, i.e., the expression

$$f_3(\epsilon_3) = \frac{C\,(\beta_3)^{\beta_3+1}\,\epsilon_3^{-\beta_3-2}}{\Gamma(\beta_3+1)}\int_0^\infty \epsilon_2^{\beta_3-1-\frac{\beta_2+\beta_1}{2}}e^{-\beta_3\epsilon_2/\epsilon_3}K_{\beta_2-\beta_1}\left(2\sqrt{\frac{\beta_2\beta_1\epsilon_0}{\epsilon_2}}\right)d\epsilon_2. \tag{5.49}$$

This integral is easier to solve using the Meijer G-function notation of $f_2(\epsilon_2)$ in (5.47) and the properties of the Meijer G-function shown in Appendix H. So the integral above becomes an

integral of the product of two G-functions, which can be solved using property (G.17). With this procedure, the final result for $f_3(\epsilon_3)$ is given in terms of another Meijer G-function (for details see Appendix G), in the form:

$$f_3(\epsilon_3) = \frac{1}{\epsilon_0\beta_1\beta_2\beta_3\Gamma(\beta_1+1)\Gamma(\beta_2+1)\Gamma(\beta_3+1)} \times G_{3,0}^{0,3}\left(\begin{matrix}-\beta_1-1,-\beta_2-1,-\beta_3-1\\ -\end{matrix}\middle|\frac{\epsilon_3}{\beta_1\beta_2\beta_3\epsilon_0}\right). \tag{5.50}$$

Model with N scales

We show in appendix G that the successive integration of (5.40) can be done using the Mellin transform and the Meijer G-function. In this representation, we take advantage of some Meijer G-function properties. In particular, we use the so-called convolution property which states that when a product of two G-functions is integrated, the result is another Meijer G-function, as shown in (G.17). In this way, the PDF for the hierarchical system with N scales (5.39) can be written in terms of the Meijer G-function, proceeding as in (5.47) and (5.50). So the stationary distribution $f_N(\epsilon_N)$ of the inverse gamma class becomes:

$$f_N(\epsilon_N) = \frac{\Omega}{\epsilon_0\omega}G_{N,0}^{0,N}\left(\begin{matrix}-\boldsymbol{\beta_N}-\mathbf{1}\\ -\end{matrix}\middle|\frac{\epsilon_N}{\epsilon_0\omega}\right) \tag{5.51}$$

where $\Omega = \prod_{i=1}^{N}\frac{1}{\Gamma(\beta_i+1)}$, $\omega = \prod_{i=1}^{N}\beta_i$ and $\boldsymbol{\beta_N} = (\beta_1,\ldots,\beta_N)$.

5.6.2 Gamma class

In reference [Macêdo et al., 2017] it was shown that in addition to the model (5.39), another class of dynamical model for the energy flux is allowed. In this case, the system of SDEs consists of N processes of the type shown in equation (4.17). More specifically, we have the following set of SDEs

$$\begin{aligned} d\epsilon_1 &= -\gamma_1(\epsilon_1-\epsilon_0)dt + \kappa_1\sqrt{\epsilon_1\,\epsilon_0}dW_1 \\ d\epsilon_2 &= -\gamma_2(\epsilon_2-\epsilon_1)dt + \kappa_2\sqrt{\epsilon_2\,\epsilon_1}dW_2 \\ &\vdots \qquad\qquad\qquad \vdots \\ d\epsilon_N &= -\gamma_N(\epsilon_N-\epsilon_{N-1})dt + \kappa_N\sqrt{\epsilon_N\,\epsilon_{N-1}}dW_N. \end{aligned} \tag{5.52}$$

The marginal probability density $f_N(\epsilon_N)$ at the smallest scales can be written in the same way as (5.40), with $f(\epsilon_i|\epsilon_{i-1})$ following a gamma distribution like (4.19),

$$f_i(\epsilon_i|\epsilon_{i-1}) = \frac{(\beta_i/\epsilon_{i-1})^{\beta_i}}{\Gamma(\beta_i)}\epsilon_i^{\beta_i-1}e^{-\beta_i\epsilon_i/\epsilon_{i-1}}. \tag{5.53}$$

The successive integration of $f_N(\epsilon_N)$ in (5.40) may also be given through the Mellin transformation and the Meijer G-function. To illustrate this, we first solve the integration of two scales (i.e., $N = 2$) in the appendix G using only the Mellin transformation, obtaining a result in the form of a Meijer G-function. The subsequent integrals for $N > 2$, see (5.40), are solved by using the properties of the Meijer G-function. The final result for the distribution $f_N(\epsilon_N)$ for an arbitrary number N of scales is

$$f_N(\epsilon_N) = \frac{\omega\,\Omega}{\epsilon_0} G^{N,0}_{0,N}\left(\begin{matrix} - \\ \boldsymbol{\beta_N - 1}\end{matrix}\middle|\frac{\omega\,\epsilon_N}{\epsilon_0}\right), \tag{5.54}$$

with $\omega = \prod_{j=1}^{N}\beta_j$, $\Omega = \prod_{j=1}^{N} 1/\Gamma(\beta_j)$ and $\boldsymbol{\beta} = (\beta_1, \ldots, \beta_N)$.

5.7 Hierarchical Model for Velocity Increments: Symmetric Version.

We have shown in figures **5-3** and **5-4**, that the distribution of longitudinal velocity increments $\delta v_r(x) \equiv \delta v = v(x+r) - v(x)$ measured at a small separation r, for a turbulent fluid does not follow a Gaussian distribution. In the Landau picture this occurs due to fluctuations of the dissipation rate ϵ for r from the inertial range going down to the dissipative scale η. As an improvement, Kolmogorov considered in 1962 the fluctuations of the energy flux, making a hypothesis about the probability density for the rate of dissipation. His original hypothesis consists in assuming that the rate of dissipation follows a log-normal distribution, but without deriving it from a dynamical model for the dissipation [Landau and Lifshitz, 1987, Kolmogorov, 1962].

In more recent works [Castaing et al., 1990, Beck, 2001, C.Beck, 2004, Macêdo et al., 2017, Salazar and Vasconcelos, 2010], the concept of compounding, or superstatistics was introduced in turbulence modeling. Under this idea, the fluctuations of the local energy flux ϵ have a distribution $f(\epsilon)$ and are assumed to occur on a long timescale, such that locally the system can achieve a quasi-equilibrium with an approximately constant value of ϵ. In this scenario, one can assume that locally the system exhibits a Gaussian conditional probability distribution for the velocity increments $P(\delta v|\epsilon)$:

$$P(\delta v|\epsilon) = \frac{1}{\sqrt{2\pi\epsilon}} \exp\left(-\frac{(\delta v)^2}{2\epsilon}\right). \tag{5.55}$$

The marginal distribution of δv can then be obtained after integration over the PDF of the energy flux $f(\epsilon)$ in the form

$$P(\delta v) = \int_0^\infty P(\delta v|\epsilon) f(\epsilon) d\epsilon. \tag{5.56}$$

As we have argued in the previous section, the statistics of ϵ can be obtained from a general class of stochastic processes justified by general physical assumptions [Macêdo et al., 2017, Salazar and Vasconcelos, 2010]. Hence, as said before, there are two possible PDFs for the energy flux given by relations (5.51) and (5.54). So now we can employ these distributions together with (5.55) to compute the marginal distribution of the velocity increments in (5.56). In following the sections, we review this procedure which yields the symmetric distribution $P(\delta v)$ proposed in [Macêdo et al., 2017, Salazar and Vasconcelos, 2010].

5.7.1 Power-law class

In this case, the symmetric distribution of the velocity increments is obtained by considering the conditional distribution $P(\delta v|\epsilon_N)$ to be a Gaussian (5.55). The energy flux ϵ_N is then given by the distribution $f_N(\epsilon_N)$, such that the marginal $P_N(\delta v)$ written as the statistical composition (5.56) becomes

$$P_N(\delta v) = \frac{1}{\sqrt{2\pi}} \int_0^\infty \epsilon_N^{-1/2} \exp\left(-\frac{(\delta v)^2}{2\epsilon_N}\right) f_N(\epsilon_N) d\epsilon_N. \tag{5.57}$$

The distribution of the energy flux $f_N(\epsilon_N)$ is given by the inverse gamma class function (5.51), which yields

$$P_N(\delta v) = \frac{1}{\sqrt{2\pi}} \frac{\Omega}{\epsilon_0 w} \int_0^\infty \epsilon_N^{-1/2} \exp\left(-\frac{(\delta v)^2}{2\epsilon_N}\right) G_{N,0}^{0,N}\left(\begin{matrix} -\boldsymbol{\beta_N} - \mathbf{1} \\ - \end{matrix}\middle| \frac{\epsilon_N}{\epsilon_0 w}\right) d\epsilon_N. \tag{5.58}$$

The exponential in this integral can be written as a Meijer G-function, see (H.3), and the term $\left(\frac{\epsilon_N}{\epsilon_0 w}\right)^{-1/2}$ can be incorporated into the last G-function using property (H.5). With these changes, we have

$$P_N(\delta v) = \frac{1}{\sqrt{2\pi}} \frac{\Omega}{(\epsilon_0 w)^{3/2}} \int_0^\infty G_{0,1}^{1,0}\left(\begin{matrix} - \\ 0 \end{matrix}\middle| \frac{(\delta v)^2}{2\epsilon_N}\right) G_{N,0}^{0,N}\left(\begin{matrix} -\boldsymbol{\beta_N} - \frac{\mathbf{3}}{\mathbf{2}} \\ - \end{matrix}\middle| \frac{\epsilon_N}{\epsilon_0 w}\right) d\epsilon_N. \tag{5.59}$$

Now, we can invert the argument in the first G-function using property (H.7):

$$P_N(\delta v) = \frac{1}{\sqrt{2\pi}} \frac{\Omega}{(\epsilon_0 w)^{3/2}} \int_0^\infty G_{1,0}^{0,1}\left(\begin{matrix} 1 \\ - \end{matrix}\middle| \frac{2\epsilon_N}{(\delta v)^2}\right) G_{N,0}^{0,N}\left(\begin{matrix} -\boldsymbol{\beta_N} - \frac{\mathbf{3}}{\mathbf{2}} \\ - \end{matrix}\middle| \frac{\epsilon_N}{\epsilon_0 w}\right) d\epsilon_N. \tag{5.60}$$

Using property (H.6) to integrate the expression above, we can write

$$P_N(\delta v) = \frac{\Omega}{\sqrt{2\pi\epsilon_0 w}} G_{1,N}^{N,1}\left(\begin{matrix} 1 \\ \boldsymbol{\beta_N} + \frac{\mathbf{3}}{\mathbf{2}} \end{matrix}\middle| \frac{2\epsilon_0 w}{(\delta v)^2}\right). \tag{5.61}$$

Finally using again the property (H.7), the argument of this function can be inverted, and we have the solution:

$$P_N(\delta v) = \frac{\Omega}{\sqrt{2\pi\epsilon_0 w}} G_{N,1}^{1,N}\left(\begin{matrix} -\boldsymbol{\beta_N} - \frac{\mathbf{1}}{\mathbf{2}} \\ 0 \end{matrix}\middle| \frac{(\delta v)^2}{2\epsilon_0 w}\right). \tag{5.62}$$

This is one of the models proposed in [Macêdo et al., 2017] named power law class because its asymptotic behavior shows power law tails (see appendix K). In the particular case when $N = 1$, it yields the known Tsallis distribution [Tsallis, 1988] that indeed is a power law distribution.

5.7.2 Stretched exponential class

Proceeding similarly to the previous subsection, but now replacing $f_N(\epsilon_N)$ by (5.54) into the statistical composition (5.57), the marginal distribution $P_N(\delta v)$ can be written as

$$P_N(\delta v) = \frac{1}{\sqrt{2\pi}} \frac{w\Omega}{\epsilon_0} \int_0^\infty \epsilon_N^{-1/2} \exp\left(-\frac{(\delta v)^2}{2\epsilon_N}\right) G_{0,N}^{N,0}\left(\begin{matrix} - \\ \boldsymbol{\beta_N} - \mathbf{1} \end{matrix}\middle| \frac{w\epsilon_N}{\epsilon_0}\right) d\epsilon_N. \tag{5.63}$$

The exponential function is again written as a Meijer G-function using (H.3) and a term $\left(\frac{w\epsilon_N}{\epsilon_0}\right)^{-1/2}$ can be absorbed into the last G-function using property (H.5). With these changes, we have

$$P_N(\delta v) = \frac{\Omega}{\sqrt{2\pi}} \left(\frac{w}{\epsilon_0}\right)^{3/2} \int_0^\infty G_{0,1}^{1,0}\left(\begin{matrix} - \\ 0 \end{matrix}\middle| \frac{(\delta v)^2}{2\epsilon_N}\right) G_{0,N}^{N,0}\left(\begin{matrix} - \\ \boldsymbol{\beta_N} - \mathbf{\frac{3}{2}} \end{matrix}\middle| \frac{w\epsilon_N}{\epsilon_0}\right) d\epsilon_N. \tag{5.64}$$

The argument of the first G-function can be inverted using property (H.7), resulting in

$$P_N(\delta v) = \frac{\Omega}{\sqrt{2\pi}} \left(\frac{w}{\epsilon_0}\right)^{3/2} \int_0^\infty G_{1,0}^{0,1}\left(\begin{matrix} 1 \\ - \end{matrix}\middle| \frac{2\epsilon_N}{(\delta v)^2}\right) G_{0,N}^{N,0}\left(\begin{matrix} - \\ \boldsymbol{\beta_N} - \mathbf{\frac{3}{2}} \end{matrix}\middle| \frac{w\epsilon_N}{\epsilon_0}\right) d\epsilon_N. \tag{5.65}$$

Now the integral involving the product of two Meijer G-functions (H.6), gives us

$$P_N(\delta v) = \frac{\Omega}{\sqrt{2\pi}} \left(\frac{w}{\epsilon_0}\right)^{1/2} G_{N+1,0}^{0,N+1}\left(\begin{matrix} -\boldsymbol{\beta_N} + \mathbf{\frac{3}{2}}, 1 \\ - \end{matrix}\middle| \frac{2\epsilon_0}{w(\delta v)^2}\right). \tag{5.66}$$

After inverting the argument of the G-function with property (H.7), the solution finally reads

$$P_N(\delta v) = \frac{\Omega}{\sqrt{2\pi}} \left(\frac{w}{\epsilon_0}\right)^{1/2} G_{0,N+1}^{N+1,0}\left(\begin{matrix} - \\ \boldsymbol{\beta_N} - \mathbf{\frac{1}{2}}, 0 \end{matrix}\middle| \frac{w(\delta v)^2}{2\epsilon_0}\right). \tag{5.67}$$

This class of model was named the stretched exponential class in [Macêdo et al., 2017] because its asymptotic behavior is a stretched exponential, as shown in appendix K.

6 Asymmetric Statistical Model for Turbulence

6.1 Introduction

In the previous chapter we presented the main ideas necessary for the development of the following sections, namely a hierarchical model for the intermittency of the dissipation rate and the concept of superstatistics or statistical composition. We also reviewed the symmetric model for the distribution of the velocity increments proposed by [Macêdo et al., 2017]. Now we want to introduce an asymmetric version of the hierarchical model for the statistics of velocity increments, starting from some basic physical facts about the turbulent state.

When energy is forcefully injected into a fluid, e.g., by pumping, stirring or heating it, a series of instabilities take place in the ensuing flow which lead to a turbulent state where the fluid velocity fluctuates wildly in time and space. It has long been recognized, since Kolmogorov's pioneer work [Kolmogorov, 1941a], that the probability distribution of the velocity differences in isotropic turbulence is skewed toward negative values. Physically, this asymmetry is believed to stem from vortex stretching, but obtaining the form of the distribution remains a challenge. Here we introduce a stochastic model of turbulence that yields an analytic expression for the skewed distribution of the velocity increments. The model is based on the experimental observation that, locally, the velocity distribution is a Gaussian with slowly fluctuating mean and variance [Naert, 2005]. Properly averaging over the slow variables then yields the desired velocity distribution, which is shown to be in agreement with both experimental and numerical data.

6.2 Conditional and Marginal PDF for the Velocity Increments

In section 5.7 we reviewed a symmetric version of the distribution of velocity increments. In that case a conditional Gaussian distribution with zero mean is considered as the kernel of the statistical composition (5.56). Such a composition of centered Gaussian PDFs can only yield a centered fat tailed distribution. Here instead we are interested in asymmetric distributions. We shall thus consider the more general case when the conditional distribution of the velocity increments $P(\delta v_r|\epsilon_r)$ is assumed to be described by a Gaussian distribution of the form:

$$P(\delta v_r|\epsilon_r) = \frac{1}{\sqrt{2\pi\sigma^2_{\delta v_r|\epsilon_r}}} \exp\left[-\frac{(\delta v_r - \langle \delta v_r|\epsilon_r\rangle)^2}{2\sigma^2_{\delta v_r|\epsilon_r}}\right], \tag{6.1}$$

where the variance of the distribution is given by

$$\sigma^2_{\delta v_r|\epsilon_r} \equiv \langle (\delta v_r)^2|\epsilon_r\rangle - \langle \delta v_r|\epsilon_r\rangle^2.$$

The specific forms of the random variables $\langle \delta v_r | \epsilon_r \rangle$ and $\sigma^2_{\delta v_r|\epsilon_r}$ are dictated by physical arguments. For instance, first we write the conditional expectation $\langle \delta v_r | \epsilon_r \rangle$ in the form:

$$\langle \delta v_r | \epsilon_r \rangle = \mu \left(\epsilon_r - \epsilon_0 \right), \tag{6.2}$$

where μ is a constant and the mean value of ϵ_r is required to be $\epsilon_0 = \langle \epsilon_r \rangle$. Equation (6.2) is to be understood in the measure-theoretic sense, meaning that the random variable $\langle \delta v_r | \epsilon_r \rangle$ is a coarser version of δv_r [Feller, 1968]. Relation (6.2) automatically ensures that the (unconditional) mean of δv_r is zero:

$$\langle \delta v_r \rangle = 0,$$

as required by isotropy. Furthermore, it is reasonable to assume that the conditional variance $\sigma^2_{\delta v_r|\epsilon_r}$ is associated with the energy flux rate into scale r, and so we identify

$$\sigma^2_{\delta v_r|\epsilon_r} = \epsilon_r. \tag{6.3}$$

Note that eqs. (6.2) and (6.3) imply the following relation between the conditional expectation $\langle \delta v_r | \epsilon_r \rangle$ of the velocity increments and the conditional variance $\sigma^2_{\delta v_r|\epsilon_r}$:

$$\langle \delta v_r | \epsilon_r \rangle = \mu \left(\sigma^2_{\delta v_r|\epsilon_r} - \epsilon_0 \right). \tag{6.4}$$

In view of (5.56), the marginal PDF of the velocity increments is then given by

$$P(\delta v_r) = \int_0^\infty \frac{1}{\sqrt{2\pi\epsilon_r}} \exp\left[-\frac{\left(\delta v_r - \mu(\epsilon_r - \epsilon_0)\right)^2}{2\epsilon_r} \right] f(\epsilon_r) d\epsilon_r, \tag{6.5}$$

or alternatively

$$\begin{aligned} P(\delta v_r) &= \int_0^\infty \frac{1}{\sqrt{2\pi\epsilon_r}} \exp\left[-\frac{1}{2}\left(\frac{\delta v_r + \mu\epsilon_0}{\sqrt{\epsilon_r}} - \mu\sqrt{\epsilon_r} \right)^2 \right] f(\epsilon_r) d\epsilon_r \\ &= \frac{e^{\mu(\delta v_r + \mu\epsilon_0)}}{\sqrt{2\pi}} \int_0^\infty {\epsilon_r}^{-1/2} \exp\left[-\frac{(\delta v_r + \mu\epsilon_0)^2}{2\epsilon_r} - \frac{\mu^2\epsilon_r}{2} \right] f(\epsilon_r) d\epsilon_r. \end{aligned} \tag{6.6}$$

Note that

$$\begin{aligned} \mathrm{var}[\delta v_r] &= \langle (\delta v_r)^2 \rangle = \langle \epsilon_r \rangle + \mu^2 \langle (\epsilon_r - \epsilon_0)^2 \rangle \\ &= (1 - 2\mu^2)\epsilon_0 + \mu^2(\langle \epsilon_r^2 \rangle + 1). \end{aligned} \tag{6.7}$$

Furthermore, as the moments of a Gaussian distribution are known, the unconditioned moments of $P(\delta v_r)$ are easily computed. For instance, the third and fourth moments are

$$\begin{aligned} \langle (\delta v_r)^3 \rangle &= \mu^3 \langle (\epsilon_r - \epsilon_0)^3 \rangle + 3\mu \langle \epsilon_r (\epsilon_r - \epsilon_0) \rangle \\ &= \mu^3 \langle \epsilon_r^3 \rangle + 3\mu(1 - \mu^2\epsilon_0) \langle {\epsilon_r}^2 \rangle + \mu\epsilon_0^2(2\mu\epsilon_0 - 3) \end{aligned} \tag{6.8}$$

$$\begin{aligned}\langle(\delta v_r)^4\rangle &= \mu^4\langle(\epsilon_r-\epsilon_0)^4\rangle + 6\mu^2\langle\epsilon_r(\epsilon_r-\epsilon_0)^2\rangle + 3\langle\epsilon_r^2\rangle \\ &= \mu^4\langle\epsilon_r^4\rangle + 2\mu^2(3-2\mu^2\epsilon_0)\langle\epsilon_0^3\rangle + 3(3\mu^4\epsilon_0^2 - 4\mu^2\epsilon_0 + 1)\langle\epsilon_r^2\rangle - 3\mu^2\epsilon_0^3(2\mu^2\epsilon_0 - 2)\end{aligned} \tag{6.9}$$

where $\langle\epsilon^n\rangle$ is the n-th moment of the distribution of ϵ.

As in the symmetric model discussed in section 5.7, here we also consider two types of distribution for the function $f(\epsilon_r)$: (i) the inverse gamma class given by the expression (5.51) and (ii) the gamma class given by (5.54). The moments of these functions are easily computed, resulting in [Salazar and Vasconcelos, 2010]

$$\langle\epsilon_N^p\rangle = \langle\epsilon_0^p\rangle\prod_{j=1}^{p-1}\left(\frac{\beta}{\beta-j}\right)^N, \tag{6.10}$$

for the inverse gamma case, and

$$\langle\epsilon_N^p\rangle = \langle\epsilon_0^p\rangle\prod_{j=1}^{p-1}\left(\frac{\beta+j}{\beta}\right)^N \tag{6.11}$$

for the gamma case.

6.3 Distribution of Velocity Increments: Particular Case $N = 1$

6.3.1 Inverse gamma class

Considering the particular case when $N = 1$, we have seen that the distribution of variances $f(\epsilon_r)$ becomes an inverse gamma distribution given by the relation

$$f(\epsilon_r) = \frac{(\epsilon_0\beta)^{\beta+1}}{\Gamma(\beta+1)}{\epsilon_r}^{-\beta-2}e^{-\frac{\beta\epsilon_0}{\epsilon_r}}. \tag{6.12}$$

Replacing this into (6.6) the PDF $P(\delta v_r)$, becomes

$$P(\delta v_r) = \frac{(\epsilon_0\beta)^{\beta+1}e^{\mu(\delta v_r+\mu\epsilon_0)}}{\sqrt{2\pi}\Gamma(\beta+1)}\int_0^\infty {\epsilon_r}^{-\beta-\frac{5}{2}}\exp\left[-\frac{1}{\epsilon_r}\left(\frac{(\delta v_r+\mu\epsilon_0)^2}{2}+\beta\epsilon_0\right)-\frac{\mu^2\epsilon_r}{2}\right]d\epsilon_r. \tag{6.13}$$

This integral looks like the following Bessel integral:

$$\int_0^\infty x^{\nu-1}e^{-\frac{\alpha}{x}-\gamma x}dx = 2\left(\frac{\alpha}{\gamma}\right)^{\frac{\nu}{2}}K_\nu(2\sqrt{\alpha\gamma}) \tag{6.14}$$

Hence we can rewrite (6.13) as

$$P(\delta v_r) = \sqrt{\frac{2}{\pi}}\frac{(\epsilon_0\beta)^{\beta+1}e^{\mu(\delta v_r+\mu\epsilon_0)}}{\Gamma(\beta+1)}\left[\frac{|\mu|}{\sqrt{(\delta v_r+\mu\epsilon_0)^2+2\beta\epsilon_0}}\right]^{\beta+\frac{3}{2}}K_{\beta+\frac{3}{2}}\left(|\mu|\sqrt{(\delta v_r+\mu\epsilon_0)^2+2\beta\epsilon_0}\right), \tag{6.15}$$

where we recall that $K_{-\nu}(z) = K_\nu(z)$.

It is possible to show that the distribution (6.15) has a different functional form for the tails, having a semi-heavy tail to the right and a heavy tail to the left for the case $\mu < 0$, as discussed next. We recall that the Bessel function of the second kind K_ν has the following asymptotic behavior:

$$K_v(z) \sim \sqrt{\frac{\pi}{2z}} e^{-z},\ z \to \infty. \tag{6.16}$$

Using this in (6.15) and defining $\delta v_r \equiv x$, we find that

$$P(x) \sim \frac{1}{|x|^{\beta+2}} e^{\mu x} e^{-|\mu||x|}, \quad \text{for} \quad |x| \to \infty \tag{6.17}$$

Therefore, we obtain two different asymptotic behaviors depending on μ. More explicitly, we have the following cases: i) $\mu < 0$

$$P(x) \sim \begin{cases} \frac{1}{|x|^{\beta+2}} & , \quad \text{if} \quad x \to -\infty \\ \frac{1}{|x|^{\beta+2}} e^{-2|\mu|x} & , \quad \text{if} \quad x \to +\infty \end{cases} \tag{6.18}$$

ii) $\mu > 0$

$$P(x) \sim \begin{cases} \frac{1}{|x|^{\beta+2}} e^{-2\mu|x|} & , \quad \text{if} \quad x \to -\infty \\ \frac{1}{|x|^{\beta+2}} & , \quad \text{if} \quad x \to +\infty \end{cases} \tag{6.19}$$

6.3.2 Gamma class

Now we consider the variances distributed as a gamma distribution

$$f(\epsilon_r) = \frac{(\beta/\epsilon_0)^\beta}{\Gamma(\beta)} {\epsilon_r}^{\beta-1} e^{-\frac{\beta\epsilon_r}{\epsilon_0}}. \tag{6.20}$$

The PDF $P(\delta v_r)$ of the velocity increments is obtained, in analogy to the previous case, by integration of (6.6), with (6.20) being the distribution of the variances. We then have

$$P(\delta v_r) = \frac{(\beta/\epsilon_0)^\beta e^{\mu(\delta v_r + \mu\epsilon_0)}}{\sqrt{2\pi}\,\Gamma(\beta)} \int_0^\infty {\epsilon_r}^{\beta-\frac{3}{2}} \exp\left[-\frac{(\delta v_r + \mu\epsilon_0)^2}{2\epsilon_r} - \epsilon_r\left(\frac{\mu^2}{2} + \frac{\beta}{\epsilon_0}\right)\right] d\epsilon_r. \tag{6.21}$$

Now, using the Bessel integral (6.14) again, we obtain the following solution for $P(\delta v_r)$:

$$P(\delta v_r) = \sqrt{\frac{2}{\pi}} \frac{(\beta/\epsilon_0)^\beta e^{\mu(\delta v_r + \mu\epsilon_0)}}{\Gamma(\beta)} \left[\frac{|\delta v_r + \mu\epsilon_0|}{\sqrt{\mu^2 + 2\beta/\epsilon_0}}\right]^{\beta-\frac{1}{2}} K_{\beta-\frac{1}{2}}\left(\sqrt{\mu^2 + 2\beta/\epsilon_0}\,|\delta v_r + \mu\epsilon_0|\right). \tag{6.22}$$

As in the previous case, by using (6.16) and $\delta_r v \equiv x$, it is possible to show that the asymptotic behavior of this distribution is now given by

$$P(x) \sim |x|^{\beta-1} e^{\mu x} e^{-\sqrt{\mu^2+2\beta/\epsilon_0}\,|x|}, \tag{6.23}$$

which implies the following two cases:

$$P(x) \sim \begin{cases} |x|^{\beta-1} e^{-(\sqrt{\mu^2+2\beta/\epsilon_0} \pm |\mu|)|x|} & , \quad \text{if} \quad \mu < 0 \quad \text{and} \quad x \to \pm\infty \\ |x|^{\beta-1} e^{-(\sqrt{\mu^2+2\beta/\epsilon_0} \mp \mu)|x|} & , \quad \text{if} \quad \mu > 0 \quad \text{and} \quad x \to \pm\infty \end{cases} \tag{6.24}$$

6.4 Distribution of Velocity Increments: General Case $N > 1$

6.4.1 Inverse gamma class

We have seen in the section (5.6.1) that the distribution $f(\epsilon_r)$ of the energy flux can be written as a generalized inverse gamma distribution. So, denoting $f_N(\epsilon_N) \equiv f(\epsilon_r)$ we can write

$$f_N(\epsilon_N) = \frac{1}{\epsilon_0\, \omega\, \Gamma(\boldsymbol{\beta}+\mathbf{1})} G^{0,N}_{N,0}\left(\begin{matrix} -\boldsymbol{\beta}-\mathbf{1} \\ - \end{matrix} \middle| \frac{\epsilon_N}{\epsilon_0\, \omega} \right) \tag{6.25}$$

with

$$\omega = \prod_{j=1}^{N} \beta_j \tag{6.26}$$

and

$$\Gamma(\boldsymbol{\beta}+\mathbf{1}) = \prod_{j=1}^{N} \Gamma(\beta_j + 1). \tag{6.27}$$

Using this definition, the integral (6.6) becomes

$$P_N(\delta v_r) = \frac{e^{\mu(\delta v_r + \mu\epsilon_0)}}{\sqrt{2\pi}} \int_0^\infty {\epsilon_N}^{-1/2} \exp\left[-\frac{(\delta v_r + \mu\epsilon_0)^2}{2\epsilon_N} - \frac{\mu^2 \epsilon_N}{2} \right] f(\epsilon_N) d\epsilon_N, \tag{6.28}$$

or

$$P_N(\delta v_r) = \frac{e^{\mu(\delta v_r + \mu\epsilon_0)}}{\sqrt{2\pi}\, \epsilon_0\, \omega\, \Gamma(\boldsymbol{\beta}+\mathbf{1})} \int_0^\infty {\epsilon_N}^{-1/2} \exp\left[-\frac{(\delta v_r + \mu\epsilon_0)^2}{2\epsilon_N} - \frac{\mu^2 \epsilon_N}{2} \right] \times G^{0,N}_{N,0}\left(\begin{matrix} -\boldsymbol{\beta}-\mathbf{1} \\ - \end{matrix} \middle| \frac{\epsilon_N}{\epsilon_0\, \omega} \right) d\epsilon_N. \tag{6.29}$$

The exponential term in this integral can be written as a product of two exponentials, which in turn can be expressed as a Meijer G-function. Doing this, we obtain

$$P_N(\delta v_r) = \frac{e^{\mu(\delta v_r + \mu\epsilon_0)}}{\sqrt{2\pi}\, \epsilon_0\, \omega\, \Gamma(\boldsymbol{\beta}+\mathbf{1})} \int_0^\infty \epsilon_N^{-\frac{1}{2}} G^{1,0}_{0,1}\left(\begin{matrix} - \\ 0 \end{matrix} \middle| \frac{(\delta v_r + \mu\epsilon_0)^2}{2\,\epsilon_N} \right) G^{1,0}_{0,1}\left(\begin{matrix} - \\ 0 \end{matrix} \middle| \frac{\mu^2 \epsilon_N}{2} \right) \times G^{0,N}_{N,0}\left(\begin{matrix} -\boldsymbol{\beta}-\mathbf{1} \\ - \end{matrix} \middle| \frac{\epsilon_N}{\epsilon_0\, \omega} \right) d\epsilon_N. \tag{6.30}$$

For convenience it is better to write this expression as a function of $1/\epsilon_N$. So, we can use the property (H.7) to write the last two Meijer G-functions as a function of the inverse of their arguments. With this equation (6.30) becomes

$$P_N(\delta v_r) = \frac{e^{\mu(\delta v_r+\mu\epsilon_0)}}{\sqrt{2\pi}\,\epsilon_0\,\omega\,\Gamma(\boldsymbol{\beta}+\mathbf{1})}\int_0^\infty \epsilon_N^{-\frac{1}{2}}\, G_{0,1}^{1,0}\left(\begin{matrix}-\\0\end{matrix}\middle|\frac{(\delta v_r+\mu\epsilon_0)^2}{2\,\epsilon_N}\right) G_{1,0}^{0,1}\left(\begin{matrix}1\\-\end{matrix}\middle|\frac{2}{\mu^2\epsilon_N}\right) \times G_{0,N}^{N,0}\left(\begin{matrix}-\\\boldsymbol{\beta}+\mathbf{2}\end{matrix}\middle|\frac{\epsilon_0\,\omega}{\epsilon_N}\right) d\epsilon_N. \tag{6.31}$$

Then using the change of variable $y = 1/\epsilon_N$ and re-ordering the integrand, one has

$$P_N(\delta v_r) = \frac{e^{\mu(\delta v_r+\mu\epsilon_0)}}{\sqrt{2\pi}\,\epsilon_0\,\omega\,\Gamma(\boldsymbol{\beta}+\mathbf{1})}\int_0^\infty y^{-\frac{3}{2}}\, G_{0,N}^{N,0}\left(\begin{matrix}-\\\boldsymbol{\beta}+\mathbf{2}\end{matrix}\middle|\epsilon_0\,\omega\,y\right) G_{1,0}^{0,1}\left(\begin{matrix}1\\-\end{matrix}\middle|\frac{2}{\mu^2}y\right) \times G_{0,1}^{1,0}\left(\begin{matrix}-\\0\end{matrix}\middle|\frac{(\delta v_r+\mu\epsilon_0)^2}{2}y\right) dy. \tag{6.32}$$

Now, a term of the form $(\epsilon_0\omega\,y)^{-\frac{3}{2}}$ can be included into the first Meijer G-function by the property (H.5), yielding

$$P_N(\delta v_r) = \sqrt{\frac{\epsilon_0\,\omega}{2\pi}}\,\frac{e^{\mu(\delta v_r+\mu\epsilon_0)}}{\Gamma(\boldsymbol{\beta}+\mathbf{1})}\int_0^\infty G_{0,N}^{N,0}\left(\begin{matrix}-\\\boldsymbol{\beta}+\mathbf{\frac{1}{2}}\end{matrix}\middle|\epsilon_0\,\omega\,y\right) G_{1,0}^{0,1}\left(\begin{matrix}1\\-\end{matrix}\middle|\frac{2}{\mu^2}\,y\right) \times G_{0,1}^{1,0}\left(\begin{matrix}-\\0\end{matrix}\middle|\frac{(\delta v_r+\mu\epsilon_0)^2}{2}\,y\right) dy \tag{6.33}$$

This integral has a solution as a bivariate Meijer G-function. Using the definition (H.12) and the property (H.15) [Mittal and Gupta, 1972], the integral above becomes

$$P_N(\delta v_r) = \frac{e^{\mu(\delta v_r+\mu\epsilon_0)}}{\sqrt{2\pi}\Gamma(\boldsymbol{\beta}+\mathbf{1})}\,\frac{1}{\sqrt{\epsilon_0\,\omega}}\,\mathbb{G}_{\boldsymbol{N}}\left(\frac{2}{\mu^2\,\epsilon_0\,\omega}, \frac{(\delta v_r+\mu\epsilon_0)^2}{2\epsilon_0\,\omega}\right), \tag{6.34}$$

where we have used $\mathbb{G}_{\boldsymbol{N}}(x,y)$ to denote the bivariate Meijer G-function, which reads

$$\mathbb{G}_{\boldsymbol{N}}(x,y) = G_{N,0:1,1:0,1}^{0,N:0,1:1,0}\left(\begin{matrix}(-\boldsymbol{\beta}-\mathbf{\frac{1}{2}}) & : & (1) & : & (--)\\ (--) & : & (--) & : & (0)\end{matrix}\middle| x, y\right). \tag{6.35}$$

Asymptotic behaviour

The asymptotic expansion of our function (6.34) can be obtained by using the saddle point method to approximate the integral (6.28). The details of this calculations are shown in Appendix K. Here we only show briefly the main steps. The function (6.25) can be expanded

when $\epsilon \to \infty$ as:

$$f(\epsilon_N) \sim G_{N,0}^{0,N}\left(\begin{matrix}-\boldsymbol{\beta}-\mathbf{1} \\ -\end{matrix}\middle|\frac{\epsilon_N}{\epsilon_0\omega}\right) = G_{0,N}^{N,0}\left(\begin{matrix}- \\ \boldsymbol{\beta}+\mathbf{2}\end{matrix}\middle|\frac{\epsilon_0\omega}{\epsilon_N}\right) \sim \sum_{k=1}^{N} C_k \left(\frac{\epsilon_N}{\epsilon_0\,\omega}\right)^{-\beta-2}. \tag{6.36}$$

Replacing this approximation into (6.28) and using the saddle point method to expand the integral, we find that for $\mu < 0$ the asymptotic behavior of our model is given by

$$P_N(\delta v_r) \sim \left(\sum_{j=1}^{N} \frac{c_j}{|\delta v_r|^{\beta_j+2}}\right) \times \begin{cases} 1 & ,\text{for } \ \delta v_r \to -\infty \\ e^{-2|\mu|\delta v_r} & ,\text{for } \ \delta v_r \to \infty \end{cases}. \tag{6.37}$$

Therefore, the result (6.37) shows that, for $\mu < 0$, our distribution exhibits a power-law behavior for $\delta v_r < 0$ and an exponentially tempered power-law behavior for $\delta v_r > 0$.

6.4.2 Gamma class

Now we want to use the generalized gamma class distribution for the energy flux (5.54) to replace $f(\epsilon_r)$ in the integral (6.6). Let us recall that the distribution of the energy flux in this case is given by

$$f(\epsilon_N) = \frac{\omega}{\epsilon_0\,\Gamma(\boldsymbol{\beta})} G_{0,N}^{N,0}\left(\begin{matrix}- \\ \boldsymbol{\beta}-\mathbf{1}\end{matrix}\middle|\frac{\omega\epsilon_N}{\epsilon_0}\right), \tag{6.38}$$

where

$$\omega = \prod_{j=1}^{N}\beta_j \quad \text{and} \quad \Gamma(\boldsymbol{\beta}) = \prod_{j=1}^{N}\Gamma(\beta_j). \tag{6.39}$$

The integral (6.6) can thus be written as

$$\begin{aligned} P_N(\delta\tilde{v}_r) = \left(\frac{\omega}{\epsilon_0}\right)^{\frac{3}{2}} \frac{e^{\mu(\delta\tilde{v}_r+\mu\epsilon_0)}}{\sqrt{2\pi}\,\Gamma(\boldsymbol{\beta})} \int_0^{\infty} G_{0,N}^{N,0}\left(\begin{matrix}- \\ (\boldsymbol{\beta}-\mathbf{\frac{3}{2}})\end{matrix}\middle|\frac{\omega\,\epsilon_N}{\epsilon_0}\right) G_{1,0}^{0,1}\left(\begin{matrix}(1) \\ -\end{matrix}\middle|\frac{2\epsilon_N}{(\delta\tilde{v}_r+\mu\epsilon_0)^2}\right) \\ \times G_{0,1}^{1,0}\left(\begin{matrix}- \\ (0)\end{matrix}\middle|\frac{\mu^2\,\epsilon_N}{2}\right) d\epsilon_N. \end{aligned} \tag{6.40}$$

This integral resembles the previous one in (6.33) and can also be written in terms of the bivariate Meijer G-function, in the form

$$P_N(\delta\tilde{v}_r) = \sqrt{\frac{\omega}{2\pi\epsilon_0}} \frac{e^{\mu(\delta\tilde{v}_r+\mu\epsilon_0)}}{\Gamma(\boldsymbol{\beta})} \mathbb{G}_{\boldsymbol{N}}\left(\frac{2\epsilon_0}{\omega(\delta\tilde{v}_r+\mu\epsilon_0)^2}, \frac{\mu^2\epsilon_0}{2\omega}\right), \tag{6.41}$$

where

$$\mathbb{G}_{\boldsymbol{N}}(x,y) = G_{N,0:1,0:0,1}^{0,N:0,1:1,0}\left(\begin{matrix}(-\boldsymbol{\beta}+\mathbf{\frac{3}{2}}) & : & (1) & : & (--) \\ (--) & : & (--) & : & (0)\end{matrix}\middle| x, y\right). \tag{6.42}$$

Asymptotic behaviour

As in the case $N = 1$, it is possible to show that the distribution (6.41) has different behaviors in the tails. For this, first we write the asymptotic form ($x \to \infty$) of the Meijer G-function in (6.38). As shown in [Kilbas and Saigo, 2004],

$$G_{0,N}^{N,0}\left(\begin{matrix} - \\ (\boldsymbol{\beta}-\mathbf{1}) \end{matrix}\middle| x\right) \sim x^{\frac{1}{N}\left(N\left(\beta-\frac{3}{2}\right)+\frac{1}{2}\right)} e^{-Nx^{\frac{1}{N}}}. \tag{6.43}$$

Inserting this into (6.6) and using the saddle point method, the resulting integral may be approximated as

$$P_N(\delta\tilde{v}_r) \sim |\delta\tilde{v}_r|^{\beta-\frac{3}{2}+\frac{1}{N}} \exp\left[-N\left(\frac{\omega|\delta\tilde{v}_r|}{\epsilon_0|\mu|}\right)^{1/N}\right] \times \begin{cases} 1 & , \quad \text{for} \quad \delta\tilde{v}_r \to -\infty \\ e^{-2|\mu|\delta\tilde{v}_r} & , \quad \text{for} \quad \delta\tilde{v}_r \to \infty \end{cases}, \tag{6.44}$$

for $\mu < 0$. The details of calculation are shown in Appendix K.

6.5 Other Approaches to Describe Intermittency and Skewness

The aim of this section is to review other models that have been used in the literature to deal with the non-Gaussian character and the skewness of the distribution of velocity increments $P(\delta v_r)$. Let us for example discuss the model proposed by [Castaing et al., 1990]. To do this, let us first briefly mention the symmetric version of their model. In such a model, the PDF $P(\delta v_r)$ is also constructed as a statistical composition of a Gaussian distribution of velocity increments conditioned to a given value of variance, and the distribution of the variance fluctuations, like in (5.56). The variance is also related to the energy transfer rate ϵ, which is assumed to be log-normality distributed. Thus, in this approach, the symmetric distribution of velocity increments reads

$$P_\lambda(\delta v_r) = \frac{1}{2\pi\lambda}\int_0^\infty e^{-\frac{(\delta v_r)^2}{2\sigma^2}} e^{-\frac{\ln^2(\sigma/\sigma_0)}{2\lambda^2}} \frac{d\sigma}{\sigma^2}, \tag{6.45}$$

where $\sigma_0 = \langle\sigma\rangle$ and λ is the variance of $\ln\sigma$. The asymmetric version of the model (6.45) is introduced as an ansatz, under certain physical assumptions. In particular, they considered that there exists a direct relationship between the variance fluctuations and the scale r. This allows them to write the conditional Gaussian distribution in (6.45) as

$$P(\delta v_r|\sigma) \propto e^{-\frac{(\delta v_r)^2}{2\sigma^2}\left(1-\frac{d\ln\sigma}{dr}\, l(\delta v_r)\right)}, \tag{6.46}$$

where $l(\delta v_r)$ is the separation between the measurement points of the velocity increments. Using dimensional arguments, it is possible to write the second term in the exponential above, in the form

$$\frac{d\ln\sigma}{dr}\, l(\delta v_r) = a_s \frac{\delta v_r/\sigma}{(1+\delta v_r^2/\sigma^2)^{1/2}} \tag{6.47}$$

where a_s is an universal positive number, independent of σ and r in the inertial range. With this modification, the statistical composition for $P(\delta v_r)$ becomes

$$P_\lambda(\delta v_r) = \frac{A(a_s)}{2\pi\lambda} \int_0^\infty e^{-\frac{(\delta v_r)^2}{2\sigma^2}\left(1-a_s\frac{\delta v_r/\sigma^2}{(1+\delta v_r^2/\sigma^2)^{1/2}}\right)} e^{-\frac{\ln^2(\sigma/\sigma_0)}{2\lambda^2}} \frac{d\sigma}{\sigma^2}, \tag{6.48}$$

The model above showed good agreement with experimental data, however, it presents some problems related to the main features characterizing the empirical distribution of velocity increments. For instance, the mean value $\langle \delta v_r \rangle$ is different from zero, while the isotropy requires that the distribution has zero average. The explanation for the skewness is introduced considering a particular space dimension, therefore it cannot be applied to two and three dimensions, where the skewness origin is different. In addition, we emphasize that this model does not have an analytical closed form, as in our proposal presented in previous sections.

An additional approach to address the asymmetry problem is presented by [Beck, 2000]. There, the model derived by considering a dynamical model of the velocity increments $\delta v_r \equiv u$, where this stochastic variable follows the Langevin type equation in the form:

$$\frac{du}{dt} = -\gamma u + F_{chaot}(t), \tag{6.49}$$

where γ is a damping constant and $F_{chaot}(t)$ is not a Gaussian noise but something deterministic chaotic, which changes on a typical time scale $\tau << -\gamma$. Under this assumption, it can be shown that the rescaled variable $u' = 2u \to u$ follows the invariant probability density function with unity variance

$$P(u) = \frac{1}{\sqrt{2\pi}} e^{-\frac{1}{2}u^2 + c\sqrt{\gamma\tau}\left(u - \frac{1}{3}u^3\right)} + O(\gamma\tau). \tag{6.50}$$

Notice the term $c\sqrt{\gamma\tau}\left(u - \frac{1}{3}u^3\right)$ correcting the Gaussian term in the equation above, which is responsible for the asymmetric of the distribution. The constant c is a constant which is not dimensionless and therefore is not universal.

In addition, Beck [Beck, 2000] dealt with the non-Gaussian behavior using a generalized distribution of the Tsallis or q-Gaussian kind as those discussed in section 2.5. Using such a distribution it is possible to obtain stretched distributions as well as concave distributions, as the Gaussian limit when $q = 1$. Then, he used the same correction term as in (6.50) into the argument of the q-Gaussian distribution. With these changes, Beck's asymmetric model becomes

$$P(u) = \frac{1}{Z_q}\left[1 - \beta(1-q)\left(\frac{1}{2}u^2 - \frac{c}{\sqrt{R_\lambda}}\left(u - \frac{1}{3}u^3\right)\right)\right]^{-\frac{1}{1-q}}, \tag{6.51}$$

where Z_q is related to the normalization condition of $P(u)$, the parameter β is determined by the condition that the distribution should have unity variance. The Taylor scale Reynolds

number R_λ is related to the dimensionless parameter $\gamma\tau$ in the form $\sqrt{\gamma\tau} \sim R_\lambda^{-1}$. This is so, since γ is related to the kinematic viscosity ν and τ can be computed as the ratio between the Taylor scale λ and the mean velocity. The symmetric case is recovered when the Reynolds number $R_\lambda \to \infty$, case in which the unity variance condition is satisfied if $\beta = 2/(5-3q)$, as discussed in section 2.5.

This model seems to match the empirical data, and the parameter q can be seen as a measurement of the cascade level in a turbulent flow. However, later in 2001 Beck published a symmetric version of the model, where the power law distribution (q-Gaussian) is computed using the concept of superstatistics [Beck, 2001]. The symmetric model has however been criticized because it is in disagreement with experimental observations for example when it is applied to some Lagrangian turbulence data [Crawford et al., 2002]. It is observed that generalizations are needed to fit the empirical data [Salazar, 2010, Salazar and Vasconcelos, 2010]. Therefore, one could think that the asymmetric expression (6.51) may present similar problems as those of the symmetric case.

Finally, let us briefly comment a more recent model proposed by [Chevillard et al., 2006]. This model brings together various approaches to obtain a PDF of the velocity increments. In the first place, the overall distribution of velocity increments $P_l(\delta v_l)$ related to the scale l is constructed by the mixture of a distribution for the symmetric part $P_l^+(\Delta_l)$ (even function) and other for the asymmetric part $P_l^-(\Delta_l)$ (odd function). Such that the overall distribution becomes

$$P_l(\delta v_l) = P_l^+(\delta v_l) + P_l^-(\delta v_l). \tag{6.52}$$

The distributions $P_l^+(\delta v_l)$ and $P_l^-(\delta v_l)$ are constructed using the multifractal picture of the turbulence dynamics [Chevillard et al., 2012, Chevillard et al., 2006, Borgas, 1993], besides the superstatistics approach like in the first case presented in this section.

The alternatives approaches to generate asymmetric distributions reviewed above all have, unfortunately, some problems either due to its own formalism or because of some missing information that the model does not consider. This is why the goal of deriving asymmetric distributions from physically reasonable assumptions remains a long-standing problem. In this sense, our motivation was to develop an alternative description of the PDF of velocity increments to incorporate the idea of an energy cascade into a dynamical model, so as to explain the emergence of non-Gaussian effects, such as skewness and heavy tails. Our model was constructed in such a way that we can obtain an analytical expression in terms of certain special functions for the distribution of velocity increments, as discussed in the previous section. In the following section, we will test our model against turbulence data, both experimental and numerical. A more direct comparison between our model and other asymmetric models, such as those discussed in this section, will be however left for future research.

6.6 Applications to Turbulence Data

Here we will analyze two sets of data and compare the empirical distributions of velocity increments in both cases with the theoretical prediction of our models proposed above. The first data set is obtained from numerical simulations of the Navier-Stokes equations and the second one is obtained from velocity measurements in a turbulent flow of an axisymmetric jet with helium at low temperature.

6.6.1 Construction of the series of variances

To compare our theory with turbulence data, we adopt a similar procedure as in [Macêdo et al., 2017, Gonzalez et al., 2007] with the aim of choosing the best parameters in our model by using quantities obtained from the available data. As the integral (6.5) contains the distribution $f(\epsilon_r)$, we first need to compute, from the original velocity data, a subsidiary data set for the variable ϵ_r. To do that, first we divide the time series of velocity increments $\delta v(t) = v(t) = v(t+\tau) - v(t)$ (τ is the smallest scale) into overlapping intervals (or boxes) of size M, and for each such interval we compute an estimator of the variance:

$$\epsilon(t) = \frac{1}{M}\sum_{j=0}^{M-1}[\delta v(t-j\delta t) - \overline{\delta v}(t)]^2, \tag{6.53}$$

where

$$\overline{\delta v}(t) = \frac{1}{M}\sum_{j=0}^{M-1}\delta v(t-j\delta t). \tag{6.54}$$

So, for each choice of M we have a data set of variances from which one can compute the distribution $f(\epsilon_r)$. We then numerically compound the distribution of the series $\epsilon(t)$ with a Gaussian function of nonzero mean, as suggested by (6.5), for various values of μ, and select the value of μ for which the corresponding superposition integral best fits the distribution $P(\delta v)$ of the original series $\delta v(t)$. We repeat this procedure for several M and select the optimal M and μ that give the best overall fit to $P(\delta v)$. With this, we can fix two parameters into (6.5), μ and ϵ_0, where the latter is the arithmetic mean of the ϵ series corresponding to the optimal M.

Now for a given choice of N and depending on the type of model (gamma or inverse gamma class), the parameter β is fixed from the second moment of $f_N(\epsilon_N)$, which is given by

$$\langle \epsilon_N^2 \rangle = {\epsilon_0}^2 \left(\frac{\beta+1}{\beta}\right)^N, \tag{6.55}$$

for the case when $f_N(\epsilon_N)$ is a gamma class distribution in the form of (6.38), and by

$$\langle \epsilon_N^2 \rangle = {\epsilon_0}^2 \left(\frac{\beta}{\beta-1}\right)^N, \tag{6.56}$$

if $f_N(\epsilon_N)$ is an inverse gamma type distribution in the form of (6.25).

In other words, once obtained the parameters (M, μ and ϵ_0), the next step is to determine the parameter β by solving it in (6.55) or (6.56) for different values of N. The second moment $\langle \epsilon_N^2 \rangle$ of the distribution of ϵ is also computed directly from the data set corresponding to the optimal M. With this we complete a set of parameters $(N, \mu, \beta, \epsilon_0)$ where $N = \{1, 2, 3, \dots\}$. Finally, using these parameters, we plot and compare the prediction of the two models for $f_N(\epsilon)$ and $P_N(\delta v)$ up to the value of N that gives the best performance in both, the distribution of variances and the distribution of velocity increments.

6.6.2 Application to numerical data

Let us first consider the DNS data obtained from the Johns Hopkins University turbulence research group's database [Li et al., 2008]. It consists of about $\sim 3 \times 10^8$ points obtained from the simulation of an homogeneous and isotropic turbulent flow with Taylor based Reynolds number $R_\lambda \approx 418$ simulated in a periodic cube of 1024^3 lattice points over five large eddy turnover times and whose smallest resolved scale corresponds to roughly twice the Kolmogorov dissipative scale.

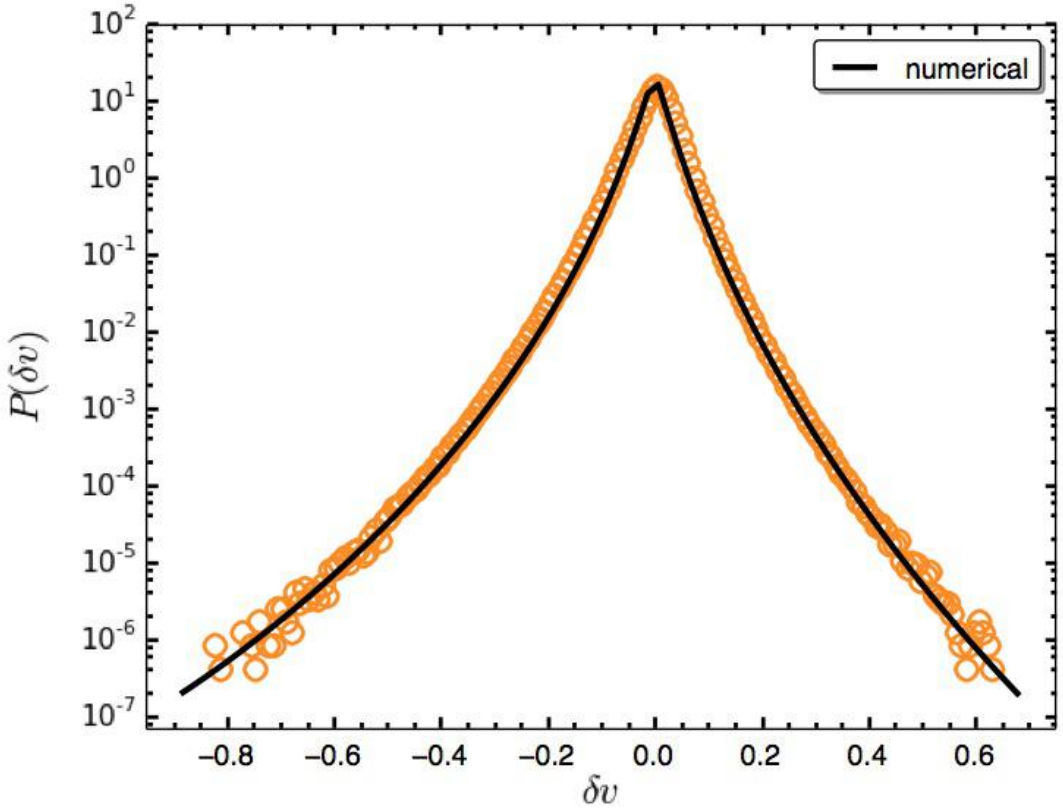

Figure 6-1 : Numerical statistical composition of empirical distribution of ϵ_r and the Gaussian kernel as shown by (6.5).

With the methodology discussed in the previous section we found an excellent agreement of our model and the empirical distribution of velocity increments δv for $M = 19$ and $\mu = -2.124$. In figure **6-1** we plot the statistical numerical composition (6.6) obtained by integrating the empirical distribution of ϵ and a numerical Gaussian kernel. The optimal value of M can be interpreted as an estimation of the scale associated with fluctuations in the background variable ϵ_N.

Our model was developed under certain assumptions about the distribution of velocity increments conditioned on the value of the energy flux rate ϵ. Let us now analyze in more detail our assumptions about the conditional probability density and its parameters. It is worth emphasizing that no fit is performed in figure **6-1**. Here we are merely plotting the theoretical prediction for $P(\delta v_r)$ obtained from the superposition of the subsidiary series $\epsilon(x)$ with the Gaussian kernel, as described in the preceding paragraph, for the optimal values of M and μ. The fact that very good agreements are obtained for the distributions of both δv_r and ϵ (as will be shown in figure **6-3**) is a strong testament to the overall validity and

self-consistency of the model. To further test the assumptions of our model, we plot in figure **6-2**a the conditional distribution $P(\delta v|\epsilon)$ for various values of ϵ, where we have rescaled and shifted the different distributions so that they would have the same mean (zero) and variance (unit). One sees from the figure that all such rescaled distributions collapse fairly well onto a Gaussian (red curve), in agreement with (6.1). In figure **6-2**b, the conditional average $\langle \delta v|\epsilon\rangle$ (top) and variance $\sigma^2_{\delta v|\epsilon}$ as functions of ϵ are also shown (bottom). While the behaviour of $\langle \delta v|\epsilon\rangle$ does not seem linear as assumed, there is a consistent decay to which (6.2) may be seen as an approximation in the region where ϵ is more frequent. The linear behaviour of the conditional variance $\sigma^2_{\delta v|\epsilon}$ with ϵ assumed in (6.3) is, on the other hand, well verified.

Once we have determined the optimal M and μ, and thus obtained the auxiliary series of variances ϵ, we then need to investigate what is the value of N (number of scales) that best describes the empirical distribution of both velocity increments and energy flux. This procedure is described next.

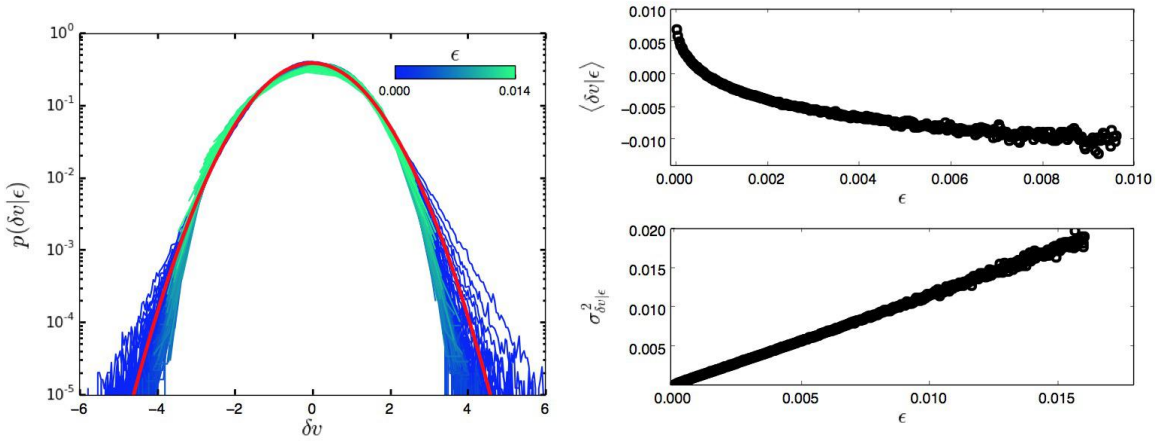

(a) (b)

Figure 6-2 : (a) Probability function of velocity increments conditioned to ϵ. (b) Conditional average $\langle \delta v|\epsilon\rangle$ as a function of ϵ (upper) and conditional variance $\sigma^2_{\delta v|\epsilon}$ as a function of ϵ (lower).

For each chosen N, the corresponding value of the parameter β was determined by requiring that the theoretical (gamma or inverse gamma) and empirical distributions have the same second moment $\langle \epsilon_r^2\rangle$ and mean ϵ_0, where $\epsilon_0 = 1.086 \times 10^{-3}$ is the arithmetic mean of the variances series calculated for $M = 19$. With this procedure, we find that the best performance is given by the model for the gamma class. To see this, we compared the theoretical predictions for both the velocities distribution (6.41) and the variances distribution (6.38) with their corresponding equivalent empirical histograms. This is shown in figure **6-3**, where the cases $N = 3, 4, 5$ (up-bottom) are plotted for the velocities distribution (left panels), and

for the distribution of the background variable ϵ_r (right panels). By comparing the different cases, we find that the case $N = 4$ better fits both the PDF of velocity increments and the distribution of variances, as shown in figures **6-3**c and **6-3**d, respectively. For this case, the corresponding parameter β obtained from the second moment of the distribution of ϵ_r was $\beta = 2.981$. The case $N = 3$ in figures **6-3**a and **6-3**b, fits reasonably the distribution of velocity increments but does not fit the distribution of variances in the tails, especially for small ϵ. Similarly, the case $N = 5$ shows good agreement with the distribution of the velocity increments (see figure **6-3**e) but for the distribution of variances the model gives lower values than the empirical distribution for small ϵ (see figure **6-3**f). Thus, we conclude that $N = 4$ yields the best fit for both the velocity increments and variances distribution.

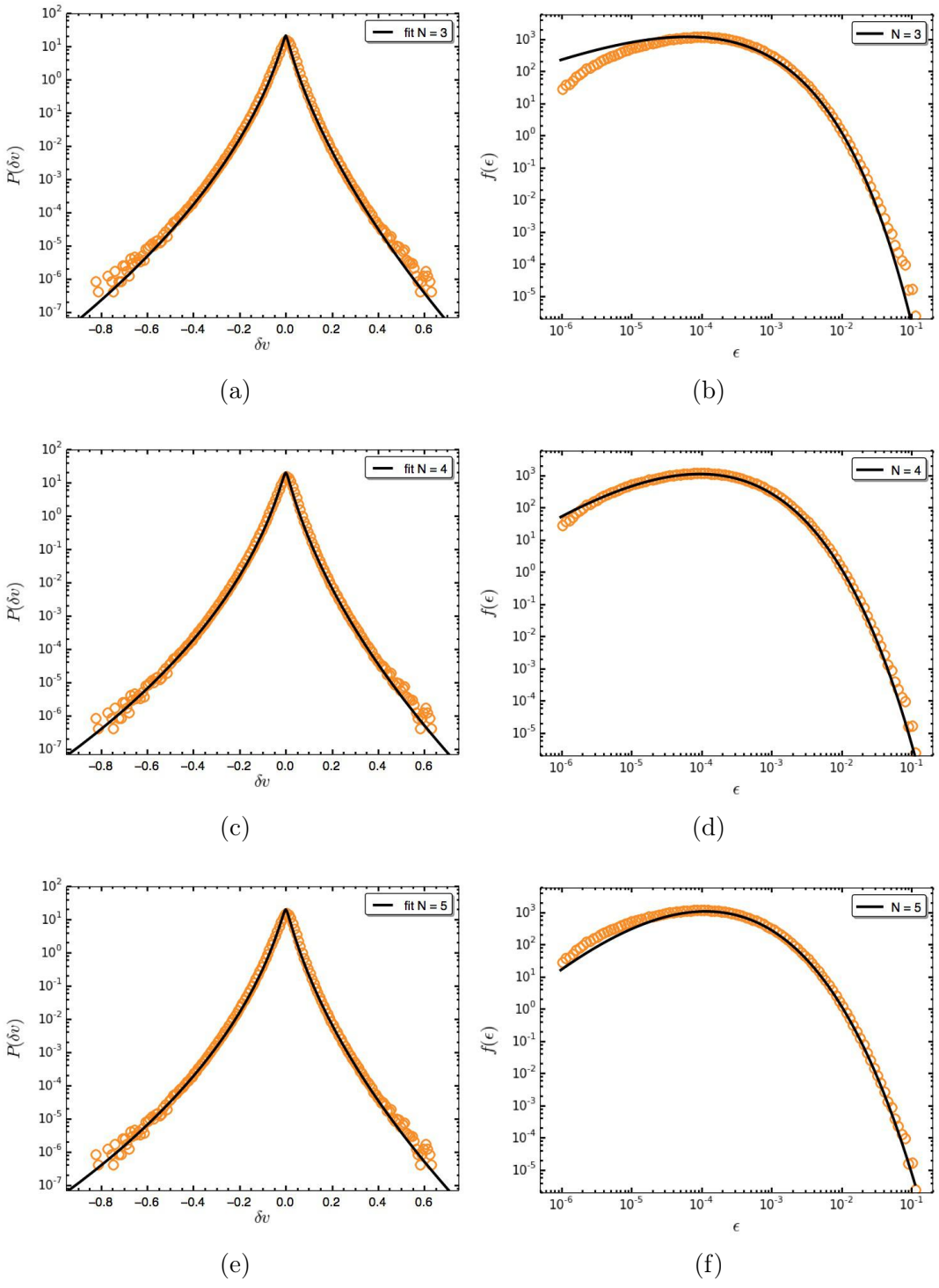

Figure 6-3 : Distribution of velocity increments (left) and variances (right), for $N = 3, 4, 5$ (top-bottom). The parameters $\epsilon_0 = 1.086 \times 10^{-3}$ and $\mu = -2.124$ were obtained from the numerical composition of the empirical distribution of variances and a non-zero mean Gaussian distribution as in (6.5). $\beta = 2.981$ was determined by equating the second moment of the empirical $f(\epsilon_r)$ to the expression (6.55).

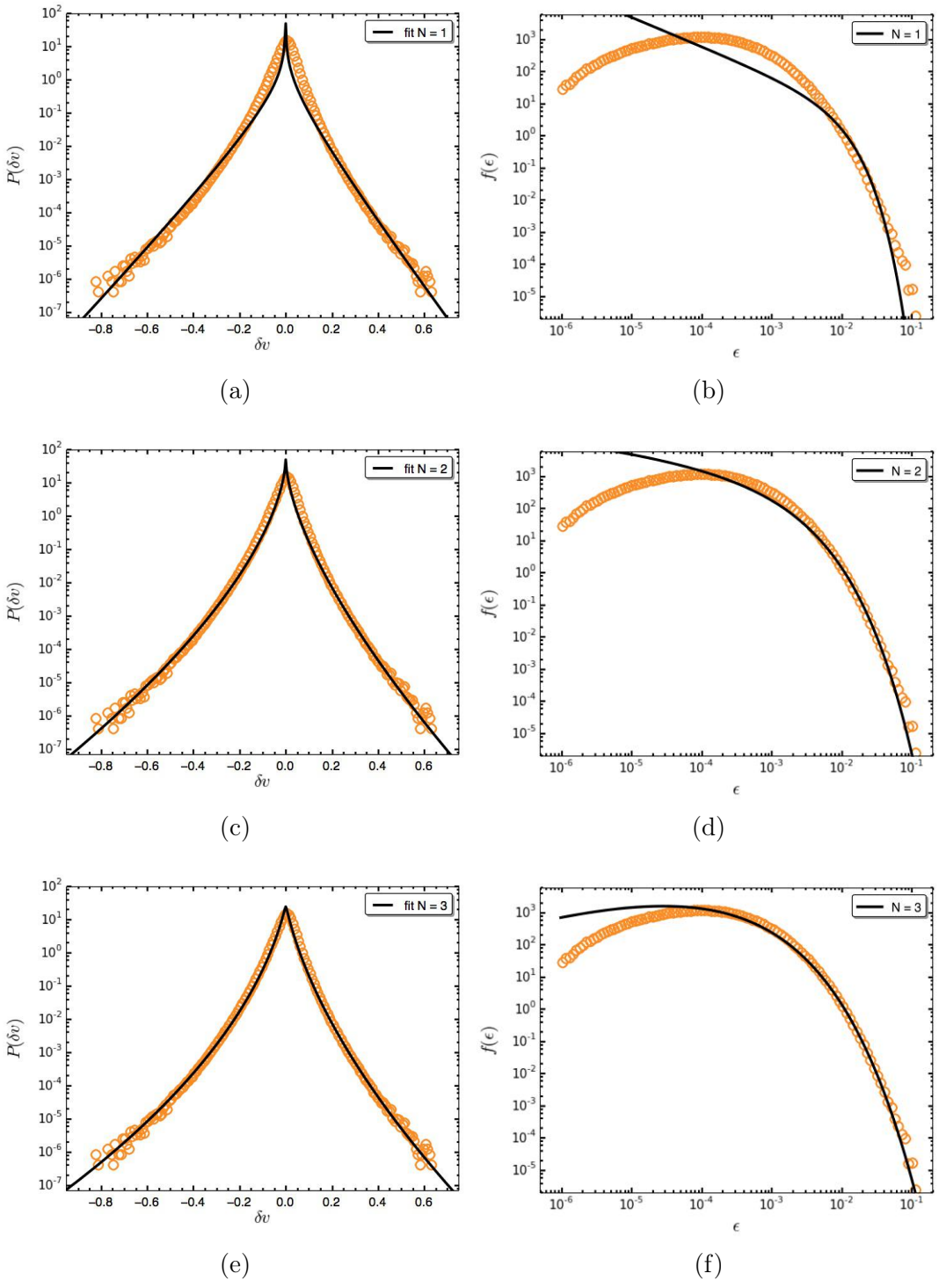

Figure 6-4 : Fitting of the velocity increments distribution using the gamma class model (left panels). Theoretical predictions for the distribution of variances (right panels).

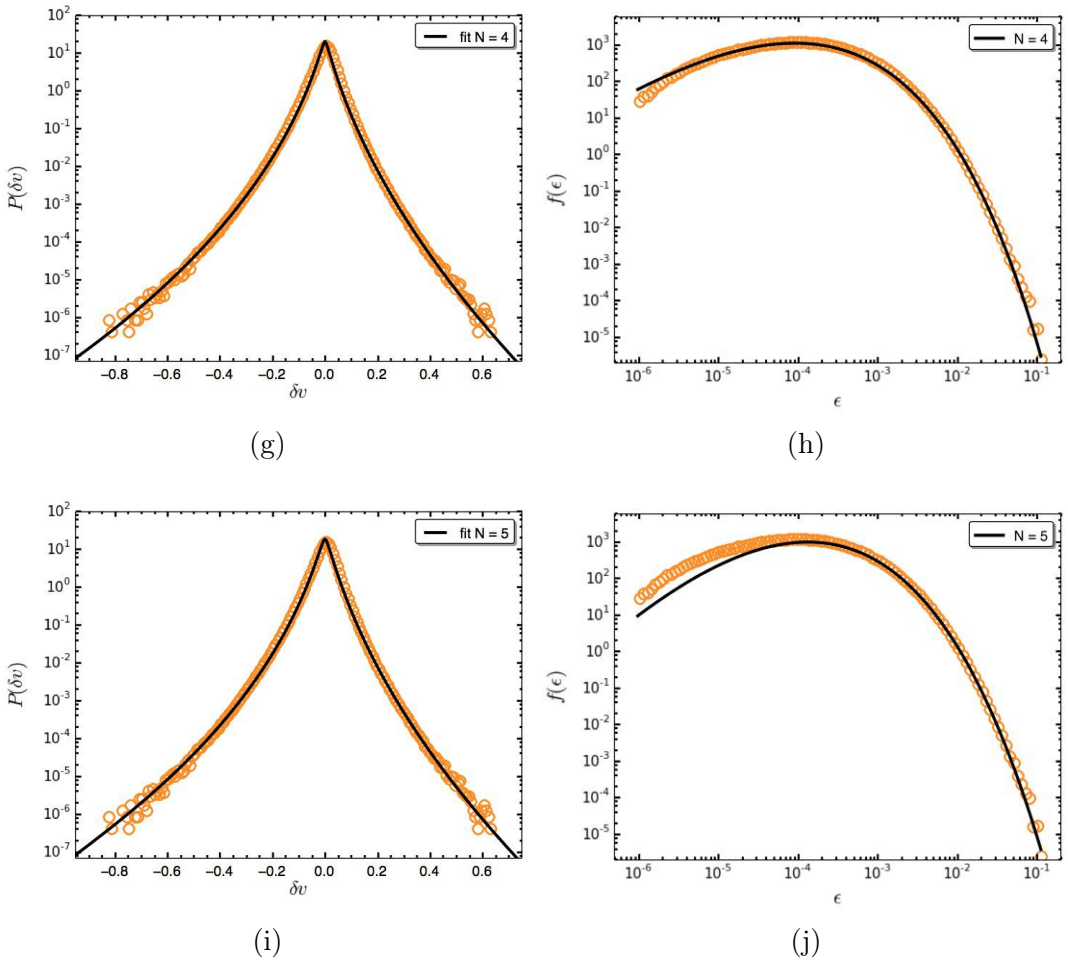

Figure 6-4 : Fitting of the velocity increments distribution using the gamma class model (left panels). Theoretical predictions for the distribution of variances (right panels).

As we anticipated using the methodology explained above, the hierarchical model of the gamma class gives the best description of the empirical histograms. Another form to see that is, for instance, by directly fitting the empirical distribution of the velocity increments with both models (6.34) and (6.41). In this way, for a given N we obtain the optimal values of β, ϵ_0 and μ that provide the best performance of the velocity increments histogram. The distribution of the variances is then plotted using the optimal values of β and ϵ_0 in the corresponding formula for $f(\epsilon_r)$. The model that best describes the data series is determined by comparing simultaneously the theoretical predictions for the PDFs of velocity increments and variances with its corresponding empirical counterpart. Results of this different methodology are shown in figure **6-4**, where we have fitted the distribution of velocity increments (left panels) with the gamma class (6.41), for the cases $N = 1, 2, 3, 4, 5$ (top-bottom). In this figure, we also show the corresponding prediction for the distribution of variances given by the model (6.38),

(right panels). It is clear the improvement of the fit as N increases, particularly at the center of the distribution. As when computing the parameter β from the second moment of the distribution of variances, the best fit is achieved for the case $N = 4$ in figures **6-4**g and **6-4**h. For this case, the parameters obtained were $\epsilon_0 = 1.120 \times 10^{-3}$, $\mu = -2.027$ and $\beta = 2.920$, very close to those determined by the former methodology.

So far, we have found similar results with the two methodologies for the estimation of the best N. In both cases we found good agreement between our model (6.41) and the empirical distribution obtained from the DNS. Let us now investigate the model based on the inverse gamma class for the distribution $f_N(\epsilon_r)$. For this, a free fit of the data using the model in (6.34) was performed, which is shown in figure **6-5**. We have plotted the cases $N = 1, 2, 3, 4, 5$ (top-bottom) for the distribution of velocity increments (left panels) and the corresponding model (6.25) for the distribution $f_N(\epsilon_r)$ (right panels). Here we can see that although the distribution of the velocity increments is reasonably well fitted, especially for large N, we have a rather poor fit of the distribution of variances, where only the right tail of the empirical distribution $f(\epsilon_r)$ is properly reproduced. We thus conclude that the hierarchical model of the inverse gamma class does not give a good description of the numerical data. In other words, the hierarchical model of the gamma class performs better in this case.

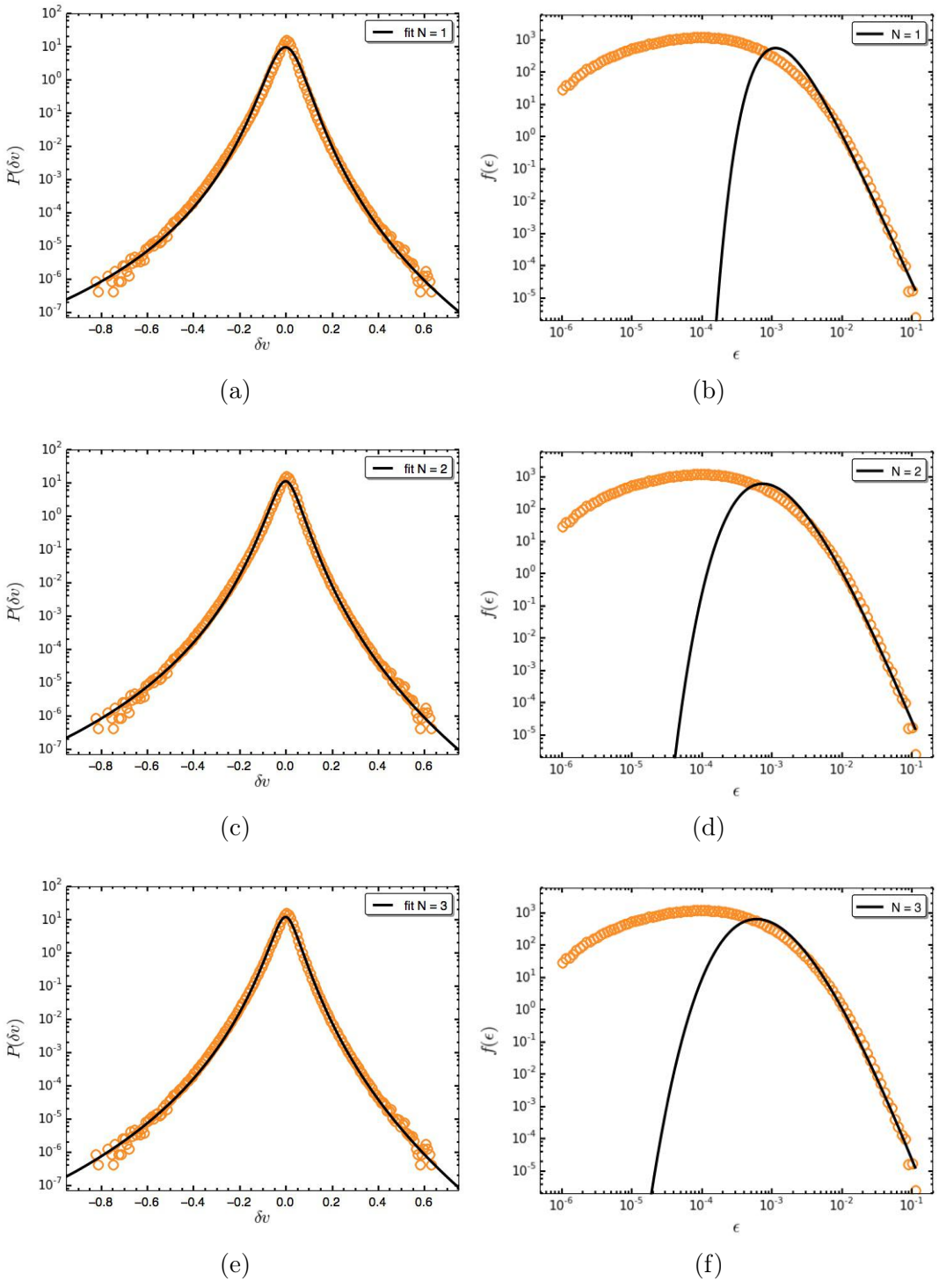

Figure 6-5 : Fitting of the velocity increments distribution using the inverse gamma class model (left panels). Theoretical predictions for the distribution of variances (right panels).

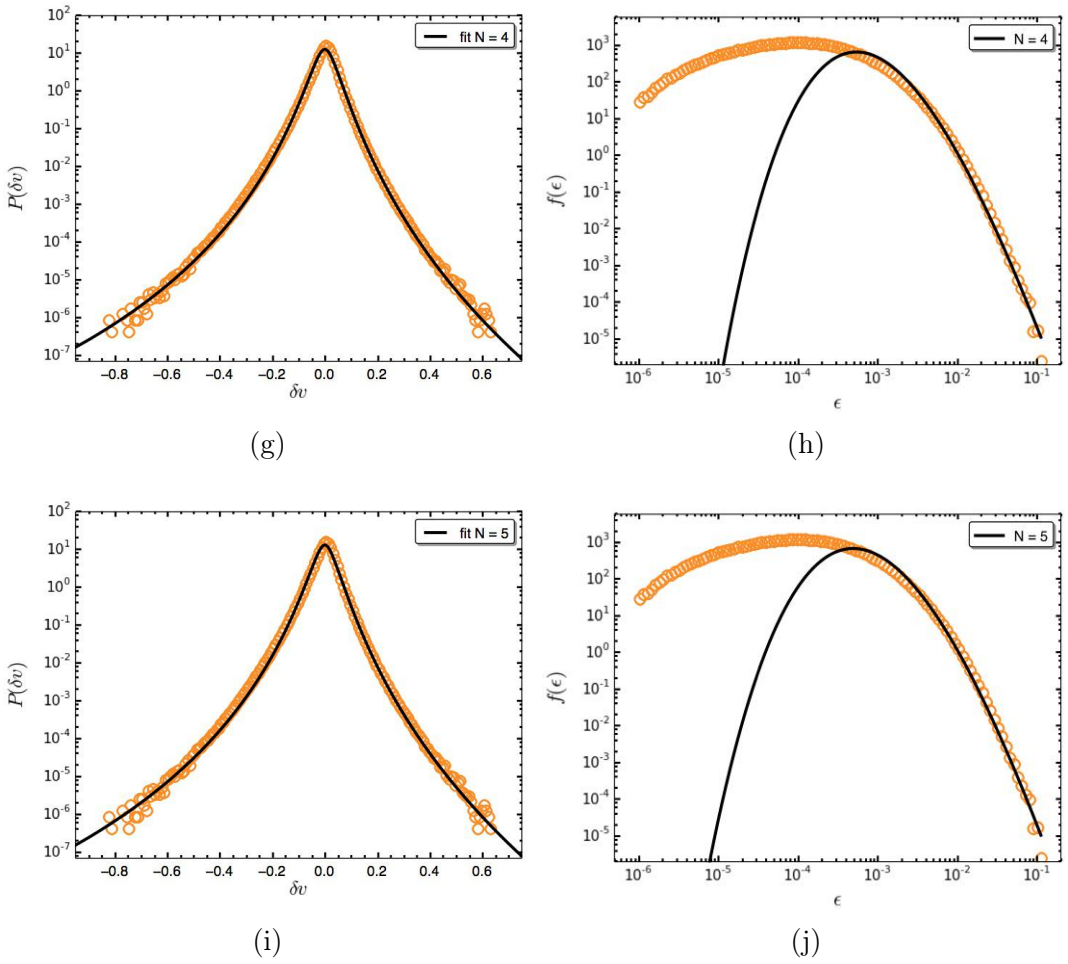

Figure 6-5 : Fitting of the velocity increments distribution using the inverse gamma class model (left panels). Theoretical predictions for the distribution of variances (right panels).

6.6.3 Application to experimental data

We now turn to the analysis of experimental turbulence data. In figure **5-3** we showed the distribution of velocity increments (points) measured by a hot-wire probe in a low temperature gaseous helium jet [Chanal et al., 1997]. The data set contains 10^7 points obtained from an experimental run performed at the Taylor-scale Reynolds number $R_\lambda = 703$, with a sampling rate of 271.5 kHz which corresponds to $r = 6.5$ μm (as obtained from Taylor's frozen turbulence hypothesis); for more details about the experiments see [Chanal et al., 1997]. In this case, the model based on the inverse gamma class (6.34) gives a better description of the experimental data, as will be shown below.

The parameters of the model were obtained from the series of variances $\epsilon(t)$, as explained in the previous section for the case of the DNS data. The first part of the procedure to

determine the parameters, as described in section 6.6.1, is to make the statistical composition (6.5) of the empirical distribution $f(\epsilon_r)$ of variances with the Gaussian kernel for different box sizes M and find the μ value that fits better the empirical PDF of the velocity increments $\delta_r v$. We then select the value of M and corresponding μ that yield the overall best fit. With this procedure, a optimal box size $M = 19$ was determined and the parameters showing the best agreement with the empirical PDF for the velocity increments were $\mu = -4.535$ and $\epsilon_0 = 4.896 \times 10^{-4}$.

Once the optimal M and the values of μ and ϵ_0 are obtained, we need to determine the parameter β for a given N. For each chosen N, β is calculated requiring that the second moment of (6.25), given by (6.56), should be equal to the second moment computed from the series of variances. Figure **6-6** shows the model predictions for $P(\delta v_r)$ given by (6.34) (left panels) and the corresponding distribution $f_N(\epsilon_r)$ given by (6.25) (right panels) for several N values. In the distribution of velocity increments $P_N(\delta v_r)$, we see improvements as N increases, especially in the tails. However, while the left tail of the variances distribution improves as N increases, the right tail gets worse. So in view of these overall considerations, we select $N = 5$ as the best choice for N in this case; see figures **6-6**i and **6-6**j. The value of β in this case is $\beta = 12.016$.

As a test of the results above a free fit of the empirical distribution of velocity increments was performed using both models (6.34) and (6.41). First we consider the case of the model based on the inverse gamma process, whose results are shown in figure **6-7**. Here, in the left column, we plot the empirical PDF of the velocity increments together with the theoretical fit. In the right column we show the empirical PDF for the series of variances with the corresponding prediction of the inverse gamma model from (6.25), employing the parameters obtained from the fits in the left panels. The fits show good results for the distribution of velocity increments $P(\delta_r v)$ in all cases $N = 1, 2, 3, 4, 5$, describing very well the skewness of the empirical distribution. However, by looking at the distribution of variances $f_N(\epsilon_r)$ we notice that the agreement is not as good. For example, the case N = 1 poorly fits the left tail, which improves when $N = 2$ and so on until $N = 5$. In other words, using a free fit procedure to determine the model parameters, we also observe that $N = 5$ gives the best description of the experimental data. In fact, we found similar values of the parameters when determined by the two procedures described above. For the case $N = 5$ we found $\beta = 12.016$ by fitting the second moment of the variances and $\beta = 10.008$ by the free fit methodology.

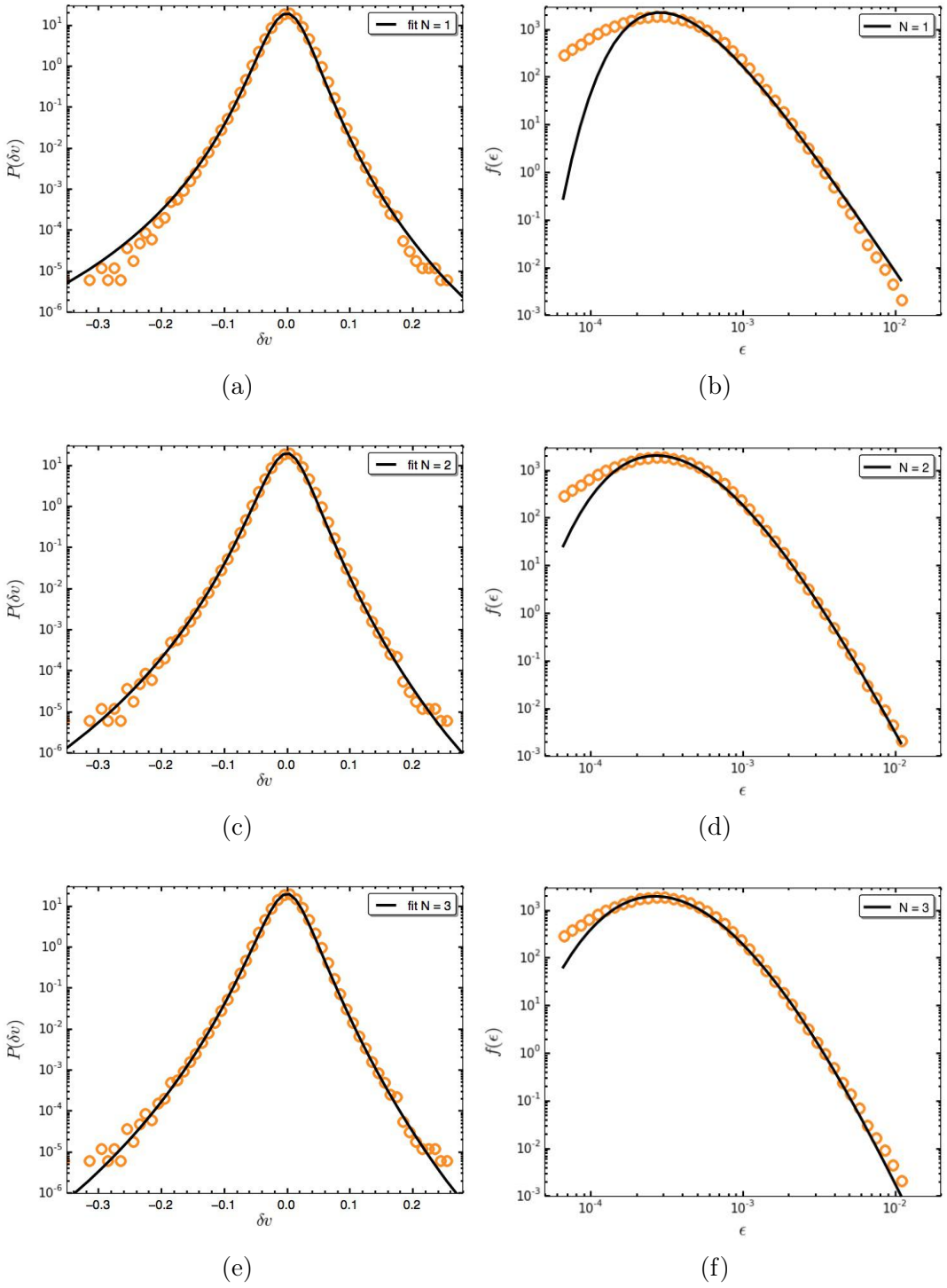

Figure 6-6 : Left panels: PDF of the velocity increments for the experimental data (circles) and fit by the hierarchical model of the inverse gamma class . Here we fit the second moment of the series of variance with the theoretical formula (6.56). Right panels: Empirical distribution of variances (circles) and theoretical prediction (curves) corresponding to the left panel.

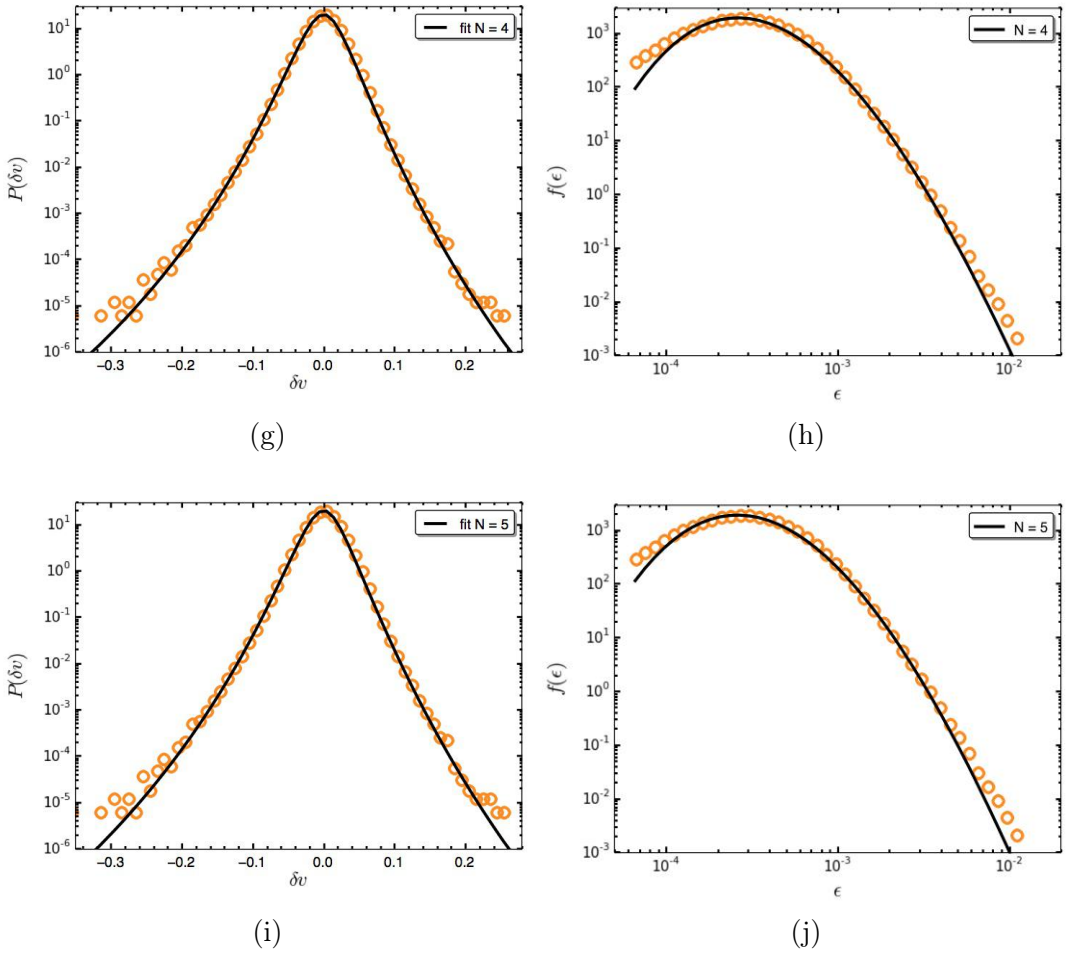

Figure 6-6 : Left panels: PDF of the velocity increments for the experimental data (circles) and fit by the hierarchical model of the inverse gamma class . Here we fit the second moment of the series of variance with the theoretical formula (6.56). Right panels: Empirical distribution of variances (circles) and theoretical prediction (curves) corresponding to the left panel.

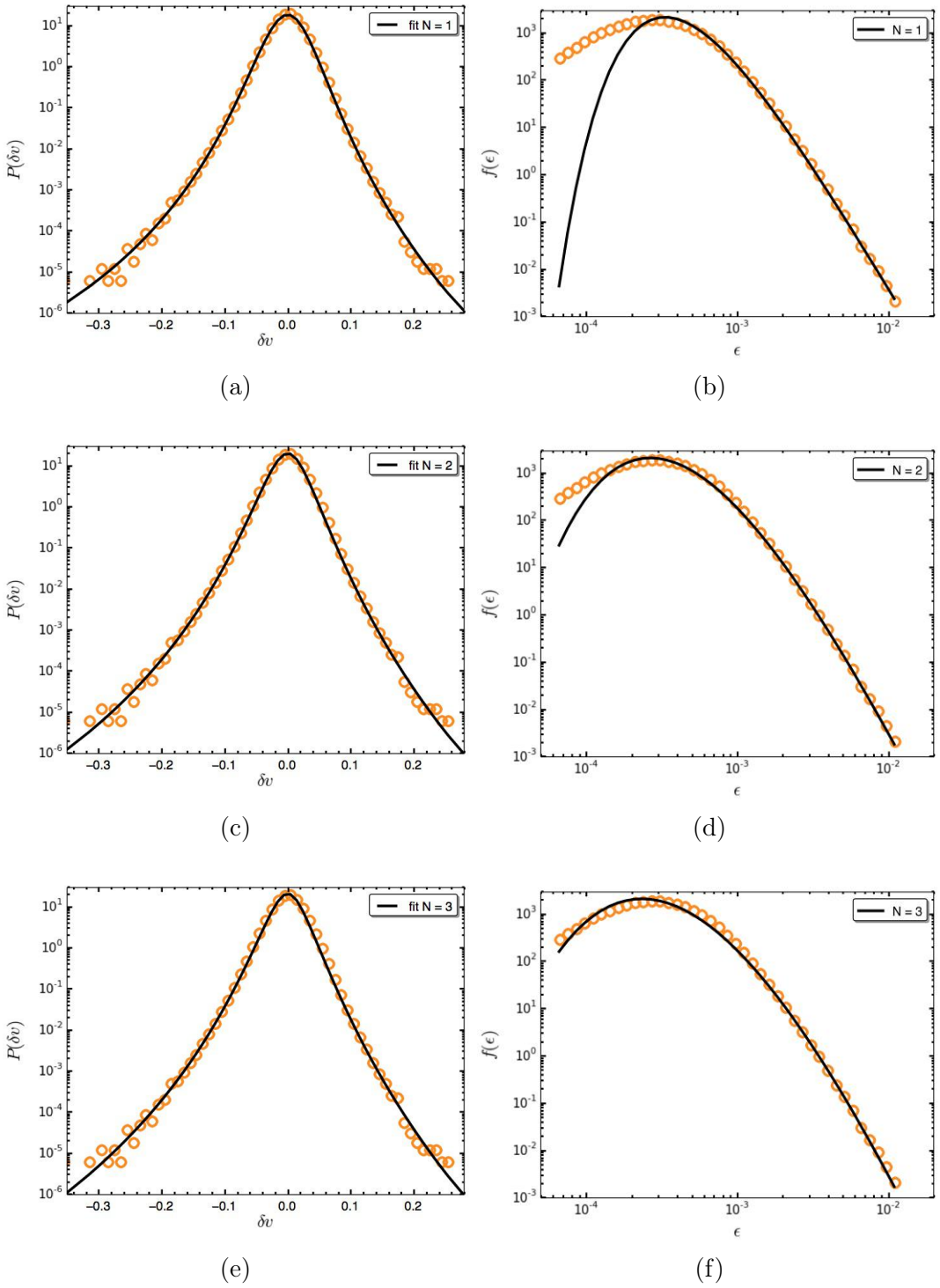

Figure 6-7 : Left panels: Free fits of the velocity increments histogram of the experimental data using the model based on the inverse gamma distribution. Right panels: Theoretical prediction for the variances distribution corresponding to the left panels.

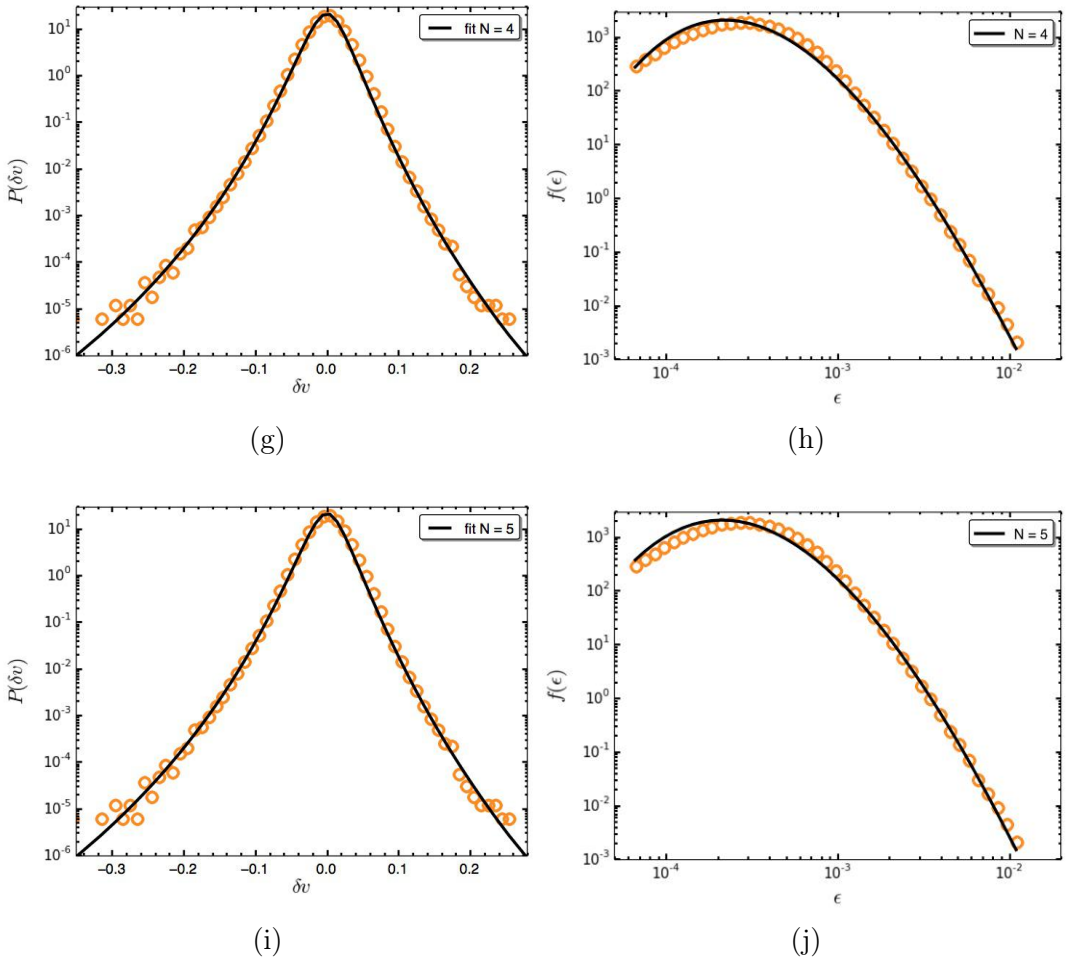

Figure 6-7 : Left panels: Free fits of the velocity increments histogram of the experimental data using the model based on the inverse gamma distribution. Right panels: Theoretical prediction for the variances distribution corresponding to the left panels.

To illustrate why the gamma type model does not fit very well the distribution of velocity increments, a free fit using equation (6.41) was carried out, where for each given N all the parameters (μ, ϵ_0, β) are obtained directly. For example, in the left column of figure **6-8** we show the empirical distribution of velocity increments and the corresponding fits for $N = 1, 2, 3, 4, 5$ (top-bottom). While in the right column the corresponding PDFs of variances predicted by the model (6.38) with the parameters ϵ_0 and β obtained from the fits on the left. Notice that the theoretical distribution of velocity increments for this model is rather sharp-pointed, specially for small N, and does not give a good match to the empirical data. As the value of N increases the performance of the model improves. However, at the top part of the distribution $P(\delta v_r)$ the agreement remains somewhat poor. Furthermore, for the variance distribution $f_N(\epsilon_N)$ the model does not show a good agreement with the empirical

distribution, not even for large N.

In summary, the hierarchical model of the gamma class does not seem capable to describe the experimental data analyzed above. This confirms the result anticipated earlier that the model based on the inverse gamma distribution of variances is more appropriated in this case.

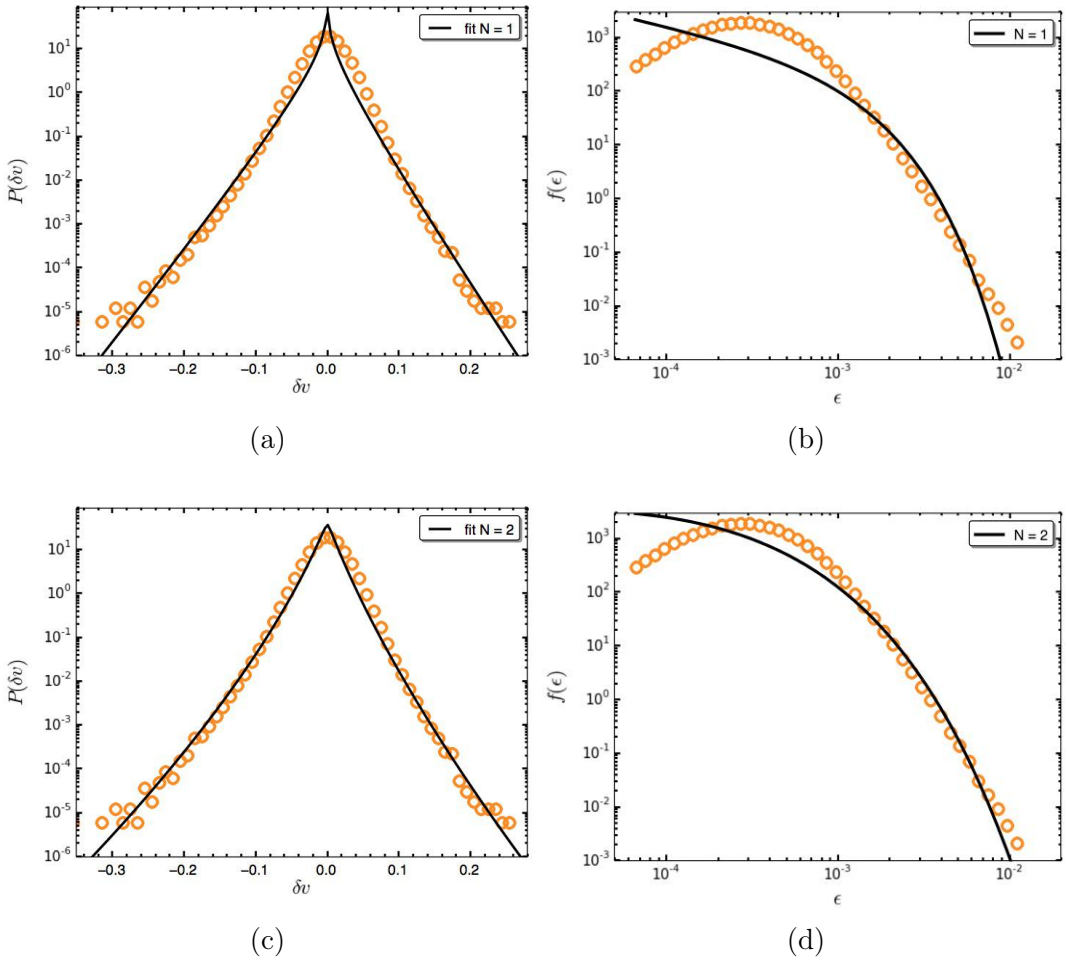

Figure 6-8 : Left panels: Free fits of the velocity increments histogram of the experimental data using the model based on the gamma distribution. Right panels: Theoretical prediction for the variances distribution corresponding to the left panels.

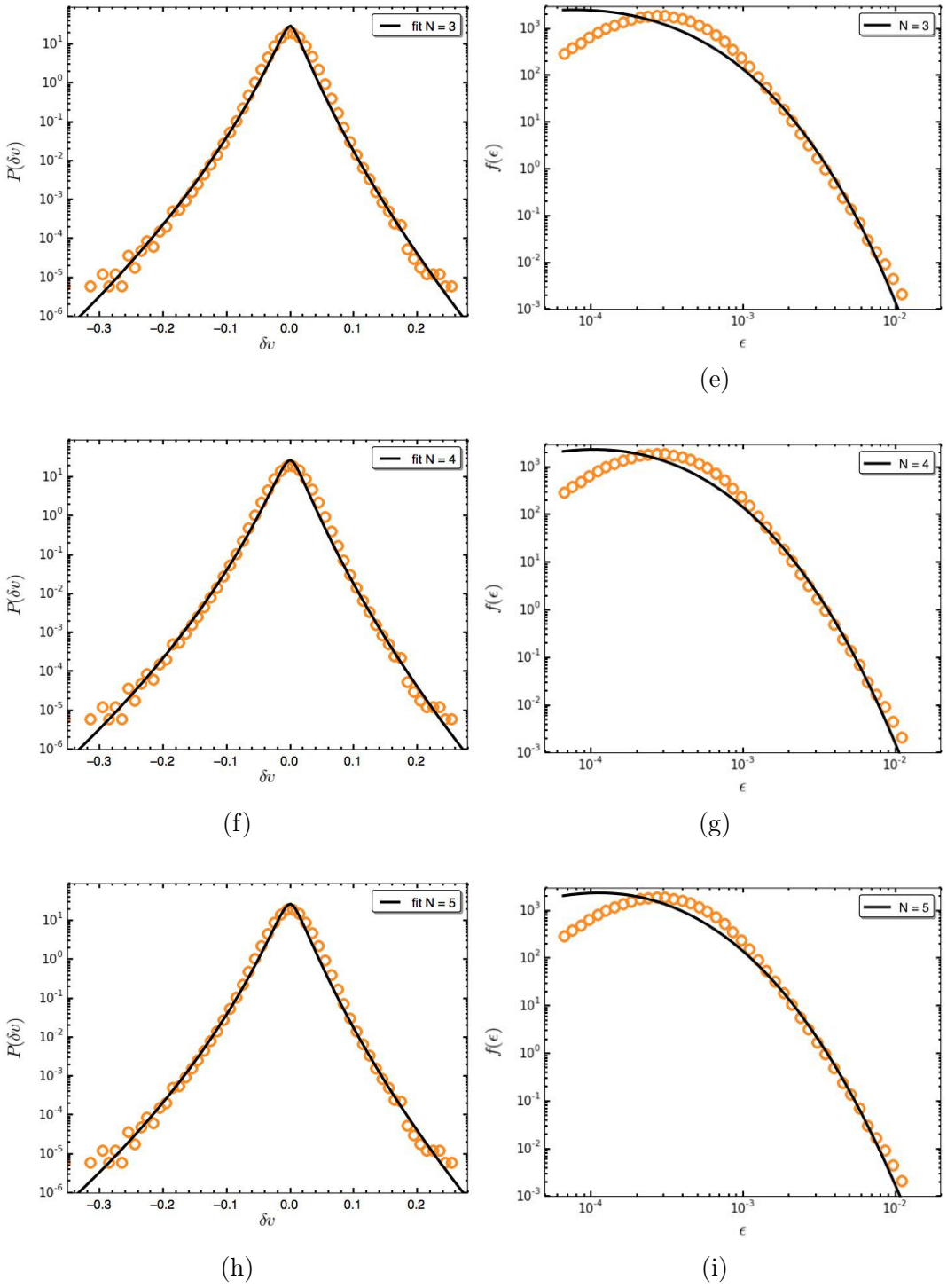

Figure 6-8 : Left panels: Free fits of the velocity increments histogram of the experimental data using the model based on the gamma distribution. Right panels: Theoretical prediction for the variances distribution corresponding to the left panels.

7 Conclusions and Perspectives

7.1 Analysis of Brazilian Markets

We have performed an empirical analysis of the Brazilian market option in light of three option pricing models, namely the standard Black-Scholes model, which assumes that the returns are Gaussian distributed, and two non-Gaussian models based on the exponential and the q-Gaussian distributions, respectively. As the q-Gaussian distribution (with $q > 1$) has power law tails—a common feature of financial data—, particular emphasis was given to the comparison between this model and the other two models whose underlying distributions have exponential decays.

First we analyzed how the q-Gaussian model compares to the Black-Scholes model ($q = 1$). This comparison was made by fitting the pricing formula given by the q-Gaussian model to each option chain in our database and then analyzing the returned q-value for each case. If the best fit yields $q \approx 1$ for a given option chain, it means that the Black-Scholes describes well the corresponding empirical data, whilst a value of $q > 1$ indicates that the q-Gaussian model better fits the data. We found that the value $q = 1$ is observed in over 70% of all option chains analyzed, thus meaning that in only about 30% of the cases the q-Gaussian model (with $q > 1$) represents an improvement with respect to the Black-Scholes formula.

For the cases when $q > 1$, we then compared the q-Gaussian model with the exponential model. Here we found that in only 25% of these cases the q-Gaussian model gives a better fit to the data than the exponential model. The two results above combined thus show that the overall performance of the q-Gaussian model is rather poor, for in only about 7% of all option chains analyzed it performs simultaneously better than both the Black-Scholes and the exponential models.

We have found, in particular, that for options near maturity the exponential model performs much better than the q-Gaussian model. For example, we found that the former model better fits the empirical data for *all* option chains within 6 days to maturity. A previous comparative study of the exponential and Black-Scholes models [Ramos et al., 2016] revealed a similar trend, with the exponential model performing better than the Black-Scholes model for times closer to the expiration date. These two results, in combination, thus show that for options near maturity the exponential model gives the best overall description of the option prices. This finding is in line with the observation that the empirical distribution of the daily Ibovespa returns is better described (particularly in its central part) by an exponential distribution.

In light of the results above, one is led to conclude that option pricing models based on

power-law distributions appear to be less relevant for real markets. This might be related to the fact that heavy-tailed distributions usually occur at shorter time scales as compared to the typical option trading frequency. Another reason for the poor performance of the q-Gaussian model in comparison with the exponential model is related to the fact that the market implied volatility for option chains near maturity exhibits a strongly nonsymmetric pattern as a function of the strike price—i.e, the volatility smile is skewed. The q-Gaussian model, being symmetric, cannot describe such asymmetric patterns, whereas the exponential model is asymmetric by definition and hence can cope with skewed volatility smiles.

Although we have restricted our study of the Brazilian options market to the years 2005 and 2006, we believe that our main result, namely that options near maturity are better described by the exponential model, should hold in present times. In this regard, it is perhaps worth pointing out that the Brazilian stock market has become relatively more efficient after the liberalization reforms of the early 1990's [Costa and Vasconcelos, 2003], although short periods of increased inefficiency may eventually occur [Cajueiro and Tabak, 2004]. The statistical features of the Ibovespa index should thus be somewhat robust in recent times, and so the results reported here are expected to be of general validity.

Here we have analyzed only options on a stock index, namely the Ibovespa index. It would be interesting to perform a similar analysis of options on individual stocks to verify whether the exponential model applies to these options as well. For example, options on the stocks of Petrobras and Vale (two of the largest companies listed on the São Paulo Stock Exchange) are very liquid and hence are natural candidate for future investigation. The results described here should also apply to other financial markets where exponential distributions have been observed [Silva et al., 2004, Matia et al., 2004, Kleinert and Chen., 2007, Dragulescu and Yakovenko, 2002].

Another important point for further studies concerns the question of developing investment strategies based on the exponential model which may allow one to trade options more efficiently. Such trading strategies should be particularly relevant near the expiration date, since in this case the exponential model has been shown to perform significantly better than the two other models analyzed here.

As already mentioned, we have found evidence that the superiority of the exponential model over the q-Gaussian model seems to stem from the fact that the market implied volatility smile is skewed to the left—a feature that cannot be captured by the symmetric q-Gaussian model. It would be interesting therefore to compare the exponential model with other option pricing models with skew, such as the constant elasticity of variance model [Cox and Ross, 1976,Beckers, 1980] and the q-Gaussian model with skew [Borland and Bouchaud, 2007]. It has been observed, however, that the q-Gaussian model allows arbitrage, and a corrected version

has been proposed [Vellekoop and Nieuwenhuis, 2007] but where explicit pricing formulas are no longer available. It would nevertheless be interesting to include this modified model as well in future studies. It would also be useful to consider other non-Gaussian option pricing models, such as models based on the stretched exponential distribution [Malevergne et al., 2005, Malevergne and Sornette, 2006] and nonparametric pricing strategies based on the minimization of risk [Bouchaud and Sornette, 1994, Bouchaud et al., 1995]. Such an extended comparison between different option models will be left for future studies.

7.2 Hierarchical Model for Option Pricing

In chapter 4, we introduced a general class of hierarchical models for option pricing defined as an average of the Black-Scholes price over the stationary distribution of the stochastic volatility v. The dynamics of the volatility is described by a hierarchical stochastic process composed by a set of coupled Heston or Hull-White processes. Using the hypothesis of time scales separation, we can write the functional form of the stationary distribution of the volatility at short scales in terms of a Meijer G-function. With this, we can use our approach (4.4) to compute the average of the Black-Scholes formula, whose result can be expressed as a sort of cumulative function of the bivariate Meijer G-function. In this way, we introduced a hierarchical theory to the problem of option pricing in financial markets.

We found that our model shows similar effects in the prices and in the implied volatility surfaces to those yielded from the original Heston and Hull-White models. In particular, we have shown that the hierarchical models considered here generate lower prices for options at the money than the model Black-Scholes and higher prices for options in the money and out of the money than the Black-Scholes model. This behavior is also shown in the original articles [Hull and White, 1987, Heston, 1993] and it solves one of the known problems of the Black-Scholes model reporting the so-called volatility smile. In addition, we have shown that our models have the advantage that this effect (volatility smile) can be customized by the inclusion of different scales ($N > 1$) or by variation of the β parameter. Therefore our model provides a richer description of the features of the option chains and the surfaces of volatility.

7.3 Asymmetric Statistical Model for Turbulence

In conclusion, an asymmetric hierarchical model for the velocity increments was developed in closed form, using the procedure known as statistical composition. The theoretical formula was obtained from the statistical composition of a Gaussian distribution with non-zero mean and either one of two distributions: the gamma and the inverse gamma class. We have shown that the Gaussian distribution is indeed a reasonable approximation for the distribution of

velocity increments conditioned on the energy flux (variance). For the experimental and numerical data the inverse gamma and gamma distributions, respectively, describe the distribution of the variances of the velocity increments. Our model thus shows a good agreement with the empirical distribution of velocity increments in turbulent flows and, in addition, it is able to explain the crucial negative skewness of velocity increments while maintaining a zero mean.

The model was built considering the distribution of velocity increments, $P(\delta v|\epsilon)$, conditioned on the energy transfer rate ϵ to be a Gaussian with non-zero mean. A linear model for the conditional average ensured a vanishing average for the increments, regardless of the model considered for the energy transfer rate. We then coupled the Gaussian model to a previously developed hierarchical model for the energy transfer over different scales, which allowed us to obtain closed analytical expressions for the velocity increment distribution in terms of the bivariate Meijer G-functions. Asymptotic analysis shows that the model based on the inverse gamma distribution exhibits an exponentially tempered power-law decay in the right tail and a power-law one in the left tail. On the other hand, the model obtained using the gamma class distribution displays stretched exponential behavior in both tails. These two behaviors are associated with 'universality classes' of the hierarchical model and both have been observed in our study. Although it is not clear which class should be used a priori, we may conjecture that it depends on the Reynolds number as well as on the scale over which the velocity increments are computed. However, further investigations are needed in this direction.

7.4 Perspectives

1. **Other asymmetric models**

   As discussed in chapter 6, our asymmetric distribution is capable of describing the main features of the empirical histograms of the velocity increments and the energy dissipation rate. To attain a closed formula, we assume that the conditioned distribution of the velocity increments is a Gaussian with variance proportional to the dissipation rate and mean depending linearly on the variance. We found that in fact the first hypothesis is verified in the available series as shown in figure **6-2** , i.e., $\sigma^2_{\delta v|\epsilon} \sim \epsilon$. However, the assumption for the conditional mean $\langle \delta v|\epsilon \rangle \sim \epsilon$, although may be seen as a reasonable approximation, does not match the behavior estimated from data. To cope with this, it would be worth to analyze other functional forms for $\langle \delta v|\epsilon \rangle$. For example, we can consider models like that discussed in Appendix L, where the conditional mean depends on the square-root of ϵ, i.e., $\langle \delta v|\epsilon \rangle \sim \sqrt{\epsilon}$. Using this hypothesis, it is possible to

derive a formula for the distribution of velocity increments as a bivariate Fox H-function. More studies on similar models, including arbitrary powers for the conditional variance and mean, are very interesting perspectives.

Another improvement may be achieved by considering alternative models for the distribution of the dissipation rate providing a better description of the empirical data, mainly in the tails. This means finding other classes of hierarchical stochastic processes to describe the dynamics of the energy flux which meet the dynamical constraints discussed in section 4.3, and deriving analytical expressions for its corresponding stationary distribution. With such results, one must be able to compute the marginal PDF by the statistical composition procedure like in the cases considered in this thesis, i.e., attaining closed formulas. Also, we are interested in applying our models to other systems exhibiting intermittency or where our asymmetrical distributions may be used.

Another very interesting perspective for future investigations is for instance the possibility of bridging our asymmetrical model to the field-theoretical approach developed in [Wilczek, 2016], where Gaussian fields are combined to create intermittent (but still symmetric) fields.

2. **Hierarchical model for option pricing**
   In chapter 4, we obtained expressions for the option premium which we wrote as definite integrals of the bivariate Meijer G-function. We also presented some results computed with our formulation and the comparison with empirical data where we showed the different effects on the prices and the implied volatility. We are now interested in forming a more detailed analysis of the model, applying it to different option chains as we did to analyze the Brazilian market in chapter 3. However, to this end, the numerical evaluation of the bivariate Meijer G-function via the Mellin-Barnes integral or another method should be improved. In other words, we need to develop computational routines that allow us to evaluate expressions such as (4.44) and (4.30) for a wide range of parameter with satisfactory precision and in reasonable computing time. Once the numerical issues are properly dealt with, the strengths and weaknesses of our theory will become more clear as compared to the Black-Scholes, exponential, power-law, and even the classical models for stochastic volatility such as Heston, CEV and VG [Carr and Madan, 1999, Beckers, 1980, Madan et al., 1998].

References

[A.A.G.Cortines and R.Riera, 2007] A.A.G.Cortines and R.Riera (2007). Non-extensive behavior of a stock market index at microscopic time scales. *Physica A*, 377:181–192.

[Aas and Haff, 2006] Aas, K. and Haff, I. H. (2006). The generalized hyperbolic skew student's t-distribution. *Journal of Financial Econometrics*, 4(2):275–309.

[Andersona et al., 2017] Andersona, S. C., Branch, T. A., Cooperc, A. B., and Dulvya, N. K. (2017). Black-swan events in animal populations. *PNAS*, 144(12):3252–3257.

[Arneodo et al., 1996] Arneodo, A., Bouchaud, J.-P., R. Cont, J.-F. M., Potters, M., and Sornette, D. (1996). Comment on "turbulent cascades in foreign exchange markets". *eprint arXiv:cond-mat/9607120*.

[Arnéodo et al., 1998] Arnéodo, A., Muzy, J.-F., and Sornette, D. (1998). Direct causal cascade in the stock market. *The European Physical Journal B*, 2:277–282.

[Ausloos and Ivanova, 2003] Ausloos, M. and Ivanova, K. (2003). Dynamical model and nonextensive statistical mechanics of a market index on large time windows. *Physical Review E*, 68(046122).

[Azaele et al., 2006] Azaele, S., Pigolotti, S., Banavar, J. R., and Maritan, A. (2006). Dynamical evolution of ecosystems. *Nature*, 444:926–928.

[Bacry et al., 2013] Bacry, E., Kozhemyak, A., and Muzy, J. F. (2013). Log-normal continuous cascade model of asset returns: aggregation properties and estimation. *Quantitative Finance*, 13(5):795–818.

[Barndorff-Nielsen et al., 2004] Barndorff-Nielsen, O., Blaesild, P., and Schmiegel, J. (2004). A parsimonious and universal description of turbulent velocity incrementse. *Eur. Phys. J. B*, 41:345–363.

[Batchelor and Townsend, 1949] Batchelor, G. K. and Townsend, A. A. (1949). The nature of turbulent motion at large wave-numbers. *The Royal Society*, 199(1057):238–255.

[Beck, 2000] Beck, C. (2000). Application of generalized thermostatistics to fully developed turbulence. *Physica A*, 277(5):115–123.

[Beck, 2001] Beck, C. (2001). Dynamical foundations of nonextensive statistical mechanics. *Phys. Rev. Lett.*, 87:180601.

[Beck, 2007] Beck, C. (2007). Statistics of three-dimensional lagrangian turbulence. *Phys. Rev. Lett.*, 98(064502).

[Beck, 2011] Beck, C. (2011). Generalized statistical mechanics for superstatistical systems. *Phil. Trans. R. Soc. A*, 369:453–465.

[Beckers, 1980] Beckers, S. (1980). The constant elasticity of variance model and its implications for option pricing. *J. Finance*, 35:661–673.

[Black and Scholes, 1973] Black, F. and Scholes, M. (1973). The pricing of options and corporate liabilities. *J. Polit. Econ.*, 81:637–654.

[BM&FBOVESPA, 2018] BM&FBOVESPA (2018). Bm&fbovesp a nova bolsa. http://www.bmfbovespa.com.br.

[Bogachev et al., 2017] Bogachev, M. I., Markelov, O. A., Kayumov, A. R., and Bunde, A. (2017). Superstatistical model of bacterial DNA architecture. *Sci Rep.*, 7(43034):1–12.

[Borgas, 1993] Borgas, M. S. (1993). The multifractal Lagrangian nature of turbulence. *Phil. Trans. R. Soc. Lond.*, 342(1665):379–411.

[Borland, 2002a] Borland, L. (2002a). Option pricing formulas based on a non-Gaussian stock price model. *Phys. Rev. Lett.*, 89:98701.

[Borland, 2002b] Borland, L. (2002b). A theory of non-Gaussian option pricing. *Quant. Finance*, 2:415–431.

[Borland and Bouchaud, 2007] Borland, L. and Bouchaud, J. P. (2007). A non-gaussian option pricing model with skew. *Quantitative Finance*, 7:703.

[Bouchaud et al., 1995] Bouchaud, J. P., Iori, G., and Sornette, D. (1995). Real world options: smile and residual risk. *RISK*.

[Bouchaud and Sornette, 1994] Bouchaud, J. P. and Sornette, D. (1994). The black-scholes option pricing problem in mathematical finance: generalization and extensions for a large class of stochastic processes. *Journal de Physique I*, 4:863–881.

[Breymann et al., 2000] Breymann, W., Ghashghaie, S., and Talkner, P. (2000). A stochastic cascade model for FX dynamics. *Int. J. Theor. Appl. Finan.*, 03:357.

[Cajueiro and Tabak, 2004] Cajueiro, D. O. and Tabak, B. M. (2004). The hurst exponent over time: testing the assertion that emerging markets are becoming more efficient. *Physica A*, 336:521–537.

[Carr and Madan, 1999] Carr, P. and Madan, D. B. (1999). Option valuation using the fast Fourier transform. *Journal of Computational Finance*, 2:61–73.

[Castaing et al., 1990] Castaing, B., Gagne, Y., and Hopfinger, E. J. (1990). Velocity probability density functions of high Reynolds number turbulence. *Physica D*, 47:77.

[C.Beck, 2004] C.Beck (2004). Superstatistics: theory and applications. *Continuum Mechanics and Thermodynamics*, 16(3):293–304.

[Chanal et al., 1997] Chanal, O., Chabaud, B., Castaing, B., and Hébral, B. (1997). *Eur. Phys. J. B*, 68:2442.

[Chergui et al., 2016] Chergui, H., Benjillali, M., and Saoudi, S. (2016). Performance analysis of project-and-forward relaying in mixed mimo-pinhole and Rayleigh dual-hop channel. *IEEE Communications Letters*, 20(3):610–613.

[Chevillard et al., 2012] Chevillard, L., Castaing, B., Arneodo, A., LÃ©vêque, E., Pinton, J.-F., and Roux, S. G. (2012). A phenomenological theory of Eulerean and Lagrangian velocity fluctuations in turbulent flows. *C. R.Physique*, 13:899–928.

[Chevillard et al., 2006] Chevillard, L., Castaing, B., Lévêque, E., and Arneodo, A. (2006). Unified multifractal description of velocity increments statistics in turbulence: Intermittency and skewness. *Physica D*, 218:77.

[Chunxia et al., 2007] Chunxia, Y., Yingchao, Z., Hongfa, W., and Peiling, Z. (2007). *The Origin of Volatility Cascade of the Financial Market*. Springer Berlin Heidelberg, Berlin, Heidelberg.

[Cont, 2001] Cont, R. (2001). Empirical properties of asset returns: stylized facts and statistical issues. *Quant. Finance*, 1:223–236.

[Cont and Bouchaud, 2000] Cont, R. and Bouchaud, J.-P. (2000). Herd behavior and aggregate fluctuations in financial markets. *Macroeconomic Dynamics*, 4:170 – 196.

[Cortines et al., 2008] Cortines, A., Anteneodo, C., and Riera, R. (2008). Stock index dynamics worldwide: a comparative analysis. *Eur. Phys. J. B*, 65:289–294.

[Cortines et al., 2007] Cortines, A. A. G., Riera, R., and Anteneodo, C. (2007). From short to fat tails in financial markets: a unified description. *Eur. Phys. J. B*, 60:385–389.

[Costa and Vasconcelos, 2003] Costa, R. and Vasconcelos, G. (2003). Long-range correlations and non-stationarity in the brazilian stock market. *Physica A*, 329:231–248.

[Cox et al., 1985] Cox, J. C., Ingersoll, J. E., and Ross, S. A. (1985). A theory of the term structure of interest rates. *Econometrica*, 53(2):385–407.

[Cox and Ross, 1976] Cox, J. C. and Ross, S. A. (1976). The valuation of options for alternative stochastic processes. *Journal of Financial Economics*, 3:145–166.

[Crawford et al., 2002] Crawford, A. M., Mordant, N., Bodenschatz, E., and Reynolds, A. M. (2002). Comment on "dynamical foundations of nonextensive statistical mechanics". *arXiv:physics/0212080*.

[Dragulescu and Yakovenko, 2002] Dragulescu, A. A. and Yakovenko, V. M. (2002). Probability distribution of returns in the heston model with stochastic volatility. *Quantitative Finance*, 2:443–453.

[Ernst and v. Hammerstein Ernst August, 2004] Ernst, E. and v. Hammerstein Ernst August (2004). *Generalized Hyperbolic and Inverse Gaussian Distributions: Limiting Cases and Approximation of Processes*, pages 221–264. Birkhäuser Basel, Basel.

[Feller, 1968] Feller, W. (1968). *An Introduction to Probability Theory and its Applications*, volume 1. Wiley, New York, 3rd ed edition.

[Frever et al., 2011] Frever, F., Aquino, K., Robinson, P. A., Ritter, P., and Breakspear, M. (2011). Bistability and non-Gaussian fluctuations in spontaneous corticol activity. *JNeurosci*, 29(26):8512–8524.

[Friedrich et al., 2011] Friedrich, R., Peinke, J., Sahimi, M., and Tabar, M. R. R. (2011). Approaching complexity by stochastic methods: From biological systems to turbulence. *Physics Reports*, 506:87–162.

[Frisch, 1995] Frisch, U. (1995). *Turbulence: the Legacy of A. N. Kolmogorov*. Cambridge University Press, Cambridge.

[Frisch et al., 1978] Frisch, U., Sulem, P., and Nelkin, M. (1978). A simple dynamical model of intermittent fully developed turbulence. *J. Fluid Mech.*, 87:719.

[Gardiner, 1985] Gardiner, G. W. (1985). *Handbook of Stochastic Methods*. Springer, 2 edition.

[Ghashghaie et al., 1996] Ghashghaie, S., Breymann, W., Peinke, J., Talkner, T., and Dodge, Y. (1996). Turbulent cascades in foreign exchange markets. *Nature*, 381:767–770.

[Gonzalez et al., 2007] Gonzalez, I. R. R., Lima, B. C., Pincheira, P. I. R., Brum, A. A., Macedo, A. M. S., Vasconcelos, G. L., Menezes, L. S., Raposo, E. P., Gomes, A. S. L., and Kashyap, R. (2007). Turbulence hierarchy in a random fibre laser. *Nat. Comm.*, 8:15731.

[Gradshteyn and Ryzhik, 1996] Gradshteyn, I. and Ryzhik, I. (1996). *Table of integrals, series, and products*. AP.

[Gurvich, 1960] Gurvich, A. S. (1960). Experimental research on frequency spectra of atmospheric turbulence. *Izv. Akad. Nauk SSSR*, vol. geo z. ser.:1042.

[Heston, 1993] Heston, S. (1993). A closed-form solution for options with stochastic volatility with applications to bond and currency options. *Rev. Finan. Stud.*, 6:327–343.

[Hull and White, 1987] Hull, J. and White, A. (1987). The pricing of options on assets with stochastic volatilities. *J. Finance*, 42:281–300.

[Johansson et al., 2013] Johansson, F. et al. (2013). *mpmath: a Python library for arbitrary-precision floating-point arithmetic (version 0.18). http://mpmath.org/*.

[Kholmyansky and Tsinober, 2008] Kholmyansky, M. and Tsinober, A. (2008). Kolmogorov 4/5 law, nonlocality, and sweeping decorrelation hypothesis. *Phys. Fluids*, 20(041704):1–4.

[Kilbas and Saigo, 2004] Kilbas, A. A. and Saigo, M. (2004). *H-transforms. Theory and applications*. CRC Press LLC.

[Kleinert and Chen., 2007] Kleinert, H. and Chen., X. (2007). Boltzmann distribution and market temperature. *Physica A*, 383:513–518.

[Kolmogorov, 1941a] Kolmogorov, A. N. (1941a). The local structure of turbulence in incompressible viscous fluid for very large Reynolds number. *Dokl. Akad. Nauk. SSSR*, 32:19.

[Kolmogorov, 1941b] Kolmogorov, A. N. (1941b). On degeneration (decay) of isotropic turbulence in an incom- pressible viscous liquid. *Dokl. Akad. Nauk. SSSR*, 30:299.

[Kolmogorov, 1962] Kolmogorov, A. N. (1962). A refinement of previous hypotheses concerning the local structure of turbulence in a viscous incompressible fluid at high Reynolds number. *J. Fluid Mech.*, 13:82.

[Landau and Lifshitz, 1987] Landau, L. D. and Lifshitz (1987). *Fluid Mechanics*. Oxford, 2 edition.

[Lawrence Livermore National Laboratory, 2018] Lawrence Livermore National Laboratory (2018). https://tasc.llnl.gov/galleries/image-gallery.

[Li et al., 2008] Li, Y., Perlman, E., Wan, M., Yang, Y., Meneveau, C., Burns, R., Chen, S., Szalay, A., and Eyink, G. (2008). A public turbulence database cluster and applications to study lagrangian evolution of velocity increments in turbulence. *J. Turb.*, 9:N31.

[Lux, 2001] Lux, T. (2001). Turbulence in financial markets:the surprising explanatory power of simple cascade models. *Quantitative Finance*, 1:632–640.

[Macêdo et al., 2017] Macêdo, A. M. S., Gonzalez, I. R. R., Salazar, D. S. P., and Vasconcelos, G. L. (2017). Universality classes of fluctuation dynamics in hierarchical complex systems. *Phys. Rev. E .*, 95:032315.

[Madan et al., 1998] Madan, D. B., Carr, P. P., and Chang, E. C. (1998). The variance gamma process and option pricing. *European Finance Review*, 2:79–105.

[Malevergne et al., 2005] Malevergne, Y., Pisarenko, V., and Sornette, D. (2005). Empirical distributions of stock returns: between the stretched exponential and the power law? *Quant. Finance*, 5:379–401.

[Malevergne and Sornette, 2006] Malevergne, Y. and Sornette, D. (2006). *Extreme Financial Risks: From Dependence to Risk Management*. Springer, Heidelberg.

[Mandelbrot, 1999] Mandelbrot, B. B. (1999). *Multifractals and 1/f Noise: Wild Self-Affinity in Physics (1963-1976), N14*. Springer-Verlag New York, 1 edition.

[Mantegna and Stanley, 2002] Mantegna, R. N. and Stanley, H. E. (2002). Scaling behavior in the dynamics of economic index. *Nature*, 376:46–49.

[Mantegna and Stanley, 2007] Mantegna, R. N. and Stanley, H. E. (2007). *An introduction to econophysics, correlations and complexity in finance*. Cambridge Univ. Press, Cambridge, UK.

[Masoliver and Perelló, 2006] Masoliver, J. and Perelló, J. (2006). Multiple time scales and the exponential ornstein-uhlenbeck stochastic volatility model. *Quantitative Finance*, 6(5):423–433.

[Matacz, 2000] Matacz, A. (2000). Financial modeling and option theory with the truncated Levy process. *Int. J. Theoretical Appl. Finance*, 3:143–160.

[Matia et al., 2004] Matia, K., Pal, M., Salunkay, H., and Stanley, H. E. (2004). Scale-dependent price fluctuations for the Indian stock market. *EPL (Europhysics Letters)*, 66:909–914.

[McCauley and Gunaratne, 2003] McCauley, J. L. and Gunaratne, G. H. (2003). An empirical model for volatility of returns and option pricing. *Physica A*, 329:213–221.

[McComb, 2014] McComb, W. D. (2014). *Homogeneous, Isotropic Turbulence: Phenomenology, Renormalization and Statistical Closures*. Oxford University Press, Oxford.

[Merton, 1973] Merton, R. (1973). Theory of rational option pricing. *Bell Journal of Economics and Management Science*, 4(1):141–183.

[Miranda and R.Riera, 2001] Miranda, L. C. and R.Riera (2001). Truncated lévy walks and an emerging market economic index. *Physica A*, 297:509–520.

[Mittal and Gupta, 1972] Mittal, P. K. and Gupta, K. C. (1972). An integral involving generalized function of two variables. *Proc. Indian Acad. Sci.*, 75(3):117–123.

[Müller et al., 1997] Müller, U. A., Dacorogna, M. M., é, R. D. D., Olsen, R. B., Pictet, O. V., and von Weizsäcker, J. E. (1997). Volatilities of different time resolutions - analyzing the dynamics of market components. *Journal of Empirical Finance*, 4:213–239.

[Muzy et al., 2000] Muzy, J., Delour, J., and Bacry, E. (2000). Modeling fluctuations of financial time series: from cascade process to stochastic volatility model. *The European Physical Journal B*, 17(3):537–548.

[Naert, 2005] Naert, A. (2005). *Progress in Turbulence*, volume 101 of *Proceedings in Physics*. Springer.

[Nakamura et al., 2016] Nakamura, T., Kiyono, K., Wendt, H., Abry, P., and Yamamoto, Y. (2016). Multiscale analysis of intensive longitudinal biomedical signals and its clinical applications. *Proceedings of the IEEE*, 104(2):242–261.

[Nelder and Mead, 1965] Nelder, J. A. and Mead, R. (1965). A simplex method for function minimization. *Comp. J.*, 7:308–313.

[Obukhov, 1941] Obukhov, A. M. (1941). Spectral energy distribution in a turbulent flow. *Izv. Akad. Nauk SSSR*, 5:453.

[Obukhov, 1962] Obukhov, A. M. (1962). Some specific features of atmospheric turbulence. *Journal of Geophysical Research*, 67(8):3011–3014.

[Parisi and Frisch, 1983] Parisi, G. and Frisch, U. (1983). On the singularity structure of fully developed turbulence, turbulence and predictability in geophysical fluid dynamics. *Proceed. Intern. School of Physics E. Fermi*, page 84.

[Pope, 2000] Pope, S. B. (2000). *Turbulent flows*. Cornell University.

[Press et al., 2007] Press, W. H., Teukolsky, S., Vetterling, W., and Flannery, B. (2007). *Numerical recipes: the art of scientific computing*. Cambridge Univ. Press, New York.

[Prudnikov et al., 1989] Prudnikov, A., Brychkov, Y., and Marichev, O. (1989). *Integrals and Series. Volume 3: More Special Functions*. Gordon and Breach (New York-London).

[Queirós, 2005] Queirós, S. M. D. (2005). On non-gaussianity and dependence in financial time series: a nonextensive approach. *Quant. Finance*, 5:475–487.

[Ramos et al., 2016] Ramos, A. M., Carvalho, J. A., and Vasconcelos, G. L. (2016). Exponential model for option prices: application to the Brazilian market. *Physica A*, 445:161–168.

[Richardson, 1922] Richardson, L. F. (1922). *Weather Prediction by Numerical Process*. Cambridge University Press, England.

[Rouse and Willitsch, 2017] Rouse, I. and Willitsch, S. (2017). Superstatistical energy distributions of an ion in an ultracold buffer gas. *Phys. Rev. Lett.*, 118(143401):1–6.

[Salazar, 2010] Salazar, D. (2010). *Modelo dinâmico hierárquico estochástico para intermitência em turbulência e em outros sistemas complexos*. Universidade Federal de Pernambuco.

[Salazar and Vasconcelos, 2010] Salazar, D. and Vasconcelos, G. L. (2010). Stochastic dynamical model of intermittency in fully developed turbulence. *Phys. Rev. E*, 82:047301.

[Salazar and Vasconcelos, 2012] Salazar, D. and Vasconcelos, G. L. (2012). Multicanonical distribution: Statistical equilibrium of multiscale systems. *Phys. Rev. E .*, 86:050103(R).

[Scott, 1987] Scott, L. O. (1987). Option pricing when the variance changes randomly: theory, estimation and an application. *The Journal of Financial and Quantitative Analysis*, 22(4):419–438.

[She and Lévêque, 1994] She, Z.-S. and Lévêque, E. (1994). Universal scaling laws in fully developed turbulence. *Phys. Rev. Lett.*, 72:336.

[Silva et al., 2004] Silva, A. C., Prange, R. E., and Yakovenko, V. M. (2004). Exponential distribution of financial returns at mesoscopic time lags: a new stylized fact. *Physica A*, 344:227–235.

[Sornette, 2001] Sornette, D. (2001). Fokker-planck equation of distributions of financial returns and power laws. *Physica A*, 290:211–217.

[Sornette, 2002] Sornette, D. (2002). Predictability of catastrophic events: Material rupture, earthquakes, turbulence, financial crashes, and human birth. *PNAS*, 99(1):2522–2529.

[S.P.Goyal and S.L.Mathur, 1976] S.P.Goyal and S.L.Mathur (1976). On integrals involving the H-function of two variables. *Indian J. Pure & Appl. Math*, 7:347–358.

[Tabak et al., 2009] Tabak, B., Takami, M., Cajueiro, D., and Petitinga, A. (2009). Quantifying price fluctuations in the brazilian stock market. *Physica A*, 388:59–62.

[Tsallis, 1988] Tsallis, C. (1988). Possible generalization of Boltzmann-Gibbs statistics. *J. Stat. Phys.*, 52:479–487.

[Tsallis, 2009] Tsallis, C. (2009). *Introduction to nonextensive statistical mechanics*. Springer, New York.

[Tsinober, 2009] Tsinober, A. (2009). *Fluid Mechanics and Its Aplications. An Informal Conceptual Introduction to Turbulence*, volume 92. Springer, Netherlands, second edition edition.

[Vasconcelos, 2004] Vasconcelos, G. L. (2004). A guided walk down wall street: an introduction to econophysics. *Braz. J. Phys*, 34:1039–1065.

[Vasconcelos et al., 2018] Vasconcelos, G. L., Salazar, D. S. P., and Macêdo, A. M. S. (2018). Maximum entropy approach to H-theory: Statistical mechanics of hierarchical systems. *Phys. Rev. E*, 97(022104):1–10.

[Vellekoop and Nieuwenhuis, 2007] Vellekoop, M. and Nieuwenhuis, H. (2007). On option pricing models in the presence of heavy tails. *Quantitative Finance*, 7.

[Vicente et al., 2006] Vicente, R., de Toledo, C. M., Leite, V. B., and Caticha, N. (2006). Underlying dynamics of typical fluctuations of an emerging market price index: The heston model from minutes to months. *Physica A: Statistical Mechanics and its Applications*, 361(1):272 – 288.

[Vulpiani and Livi, 2003] Vulpiani, A. and Livi, R. (2003). *The Kolmogorov legacy in physics: a century of turbulence and complexity*. Lecture notes in physics 636. Springe, Italy, 1 edition.

[Wilczek, 2016] Wilczek, M. (2016). Non-gaussianity and intermittency in an ensemble of gaussian fields. *New J. Phys.*, 18(125009).

[Xu et al., 2006] Xu, H., Ouellette, N., and Bodenschatz, E. (2006). Multifractal dimension of lagrangian turbulence. *Phys. Rev.Lett.*, (114503).

[Yaglom, 2001] Yaglom, A. (2001). *The century of turbulence theory: The main achievements and unsolved problems. In New trends in turbulence Turbulence: nouveaux aspects*. Springer.

Appendices

Appendix A - Itô Equation

Consider the stochastic differential equation for the generic process $x(t)$

$$dx(t) = a(x,t)dt + b(x,t)dW. \tag{A.1}$$

Let us now suppose that we have a new stochastic process z defined by

$$z(t) = F(x(t),t), \tag{A.2}$$

for which, we need to determine the local dynamics followed by the process $z(t)$, i.e., the SDE whose solution corresponds to the process $z(t)$. This can be released using the Itô formula, which we will review next.

Expanding the generalized function $F(x,t)$ in a Taylor series

$$\begin{aligned} dF(x(t)) &= F[x(t)+dx(t)] - F[x(t)] \\ &= \left(\frac{\partial F}{\partial t}\right)dt + \left(\frac{\partial F}{\partial x}\right)dx + \frac{1}{2}\left(\frac{\partial^2 F}{\partial t^2}\right)(dt)^2 + \frac{1}{2}\left(\frac{\partial^2 F}{\partial x^2}\right)(dx)^2 \\ &+ \frac{1}{2}\left(\frac{\partial^2 F}{\partial x \partial t}\right)dxdt + ... \end{aligned} \tag{A.3}$$

From (A.1) we have

$$(dx(t))^2 = a^2(dt)^2 + b^2(dW)^2 + 2ab\,dt\,dW. \tag{A.4}$$

As $W(t)$ is a Wiener process, we find terms $(dt)^2$ and $(dt)^{3/2}$ that can be vanished since these are smaller than dt, and the expression (A.4) becomes

$$(dx(t))^2 = b^2 dt. \tag{A.5}$$

Using the result above into (A.3) and retaining only terms up to first order, results

$$dF = \left(\frac{\partial F}{\partial t}\right)dt + \left(\frac{\partial F}{\partial x}\right)dx + \frac{1}{2}\left(\frac{\partial^2 F}{\partial t^2}\right)\left(b^2 dt + O((dt)^{3/2})\right). \tag{A.6}$$

Ordering terms, can be written

$$dF = \left(\frac{\partial F}{\partial t} + \frac{1}{2}b^2\frac{\partial^2 F}{\partial t^2}\right)dt + \frac{\partial F}{\partial x}dx. \tag{A.7}$$

Using again equation (A.1) in the second term, finally we obtain

$$dF = \left(\frac{\partial F}{\partial t} + a\frac{\partial F}{\partial x} + \frac{1}{2}b^2\frac{\partial^2 F}{\partial t^2}\right)dt + b\frac{\partial F}{\partial x}dW \tag{A.8}$$

Appendix B - Geometrical Brownian Motion (GBM)

The Geometrical Brownian Motion or Brownian motion with drift is defined as the solution for a stochastic process $S(t)$ obeying the SDE,

$$dS = \mu S dt + \sigma S dW \tag{B.1}$$

and subjects to the initial condition $S(t_0) = S_0$. The first term in the equation above is the deterministic part of the process and the second term is the unpredictable or probabilistic part. The constants μ and σ represent the mean drift velocity and the fluctuation amplitude of the Wiener process $W(t)$, respectively.

The process S can be replaced for an equivalent process $x = \ln S$, which considering the Itô equation (A.8) is described by the SDE

$$dx = \left(\mu - \frac{\sigma^2}{2}\right) dt + \sigma dW. \tag{B.2}$$

The exact stochastic integration for this process results

$$x(t) = x_0 + \left(\mu - \frac{\sigma^2}{2}\right)(t - t_0) + \sigma(W(t) - W(t_0)), \tag{B.3}$$

with the initial condition $x_0 = \ln S_0$. On the other hand, the solution for the initial process $S(t)$ with initial value $S(t_0) = S_0$, becomes

$$S(t) = S_0 e^{\left(\mu - \frac{\sigma^2}{2}\right)(t-t_0) + \sigma(W(t) - W(t_0))}. \tag{B.4}$$

The process described for (B.3) can also be written as

$$\ln \frac{S(t)}{S_0} = \left(\mu - \frac{\sigma^2}{2}\right)(t - t_0) + \sigma(W(t) - W(t_0)). \tag{B.5}$$

This process has associated a distribution $\mathcal{N}\left[\left(\mu - \frac{\sigma^2}{2}\right)\tau, \sigma\sqrt{\tau}\right]$ with $\tau = t - t_0$ [Vasconcelos, 2004]. Or in other words, we say that $S(t)$ follows a log-normal distribution:

$$f(S, t; S_0, t_0) = \frac{1}{\sqrt{2\sigma^2\tau}} \frac{1}{S} \exp\left(\frac{\left[ln\frac{S}{S_0} - \left(\mu - \frac{\sigma^2}{2}\right)\tau\right]^2}{2\sigma^2\tau}\right). \tag{B.6}$$

Appendix C - Fokker Plank Equation

In order to derive the Fokker-Planck equation, let us consider the generalized function $F[x(t)]$. By using the Itô equation (A.8), we can write

$$dF[x(t)] = \left(a[x(t),t]f'[x(t)] + \frac{1}{2}b[x(t),t]^2 f''[x(t)] \right) dt + b[x(t),t]f'[x(t)]dW(t) \tag{C.1}$$

or

$$\frac{dF[x(t)]}{dt} = a[x(t),t]f'[x(t)] + \frac{1}{2}b[x(t),t]^2 f''[x(t)] + b[x(t),t]f'[x(t)]\frac{dW(t)}{dt}. \tag{C.2}$$

Calculating the average of this stochastic process and remember that $W(t)$ is a Wiener process, results

$$\frac{d\langle f[x(t)]\rangle}{dt} = \langle a[x(t),t]f'[x(t)] + \frac{1}{2}b[x(t),t]^2 f''[x(t)]\rangle. \tag{C.3}$$

Now let us consider the variable $x(t)$ which follows a conditional probability density $p(x,t|x_0,t_0)$. The averages into (C.3) take the form

$$\begin{aligned} \frac{d\langle f[x(t)]\rangle}{dt} &= \int dx f(x)\partial_t p(x,t|x_0,t_0) \\ &= \int dx \left[a[x(t),t]\partial_x f + \frac{1}{2}b[x(t),t]^2\partial_x^2 f \right] p(x,t|x_0,t_0). \end{aligned} \tag{C.4}$$

Integrating by parts,

$$\begin{aligned} \int dx f(x)\partial_t p(x,t|x_0,t_0) = & \\ &= \int dx f(x) \left[-\partial_x a[x(t),t]p(x,t|x_0,t_0) + \frac{1}{2}\partial_x^2 b[x(t),t]^2 p(x,t|x_0,t_0) \right] \\ &+ \text{surface terms.} \end{aligned} \tag{C.5}$$

The surface terms vanish and as $f(x)$ is an arbitrary function, we have finally,

$$\partial_t p(x,t|x_0,t_0) = -\partial_x a(x,t)p(x,t|x_0,t_0) + \frac{1}{2}\partial_x^2 b(x,t)^2 p(x,t|x_0,t_0). \tag{C.6}$$

This relations is known as the Fokker-Plank equation (FPE).

Appendix D - Delta Hedging Strategy

Before to explain the delta hedge strategy, let us give the following definitions:

Portfolio: Is a set of different financial assets (investments) such as stocks, commodities, currency or derivatives. These investments generally have different financial risk and the overall risk of the portfolio is influenced by the value of individual assets. The type of portfolio depends principally on the risk which the holder is willing to assume or the investment objectives.

Short position : A Short position means that the investor lacks or sold a determined physic or financial asset.

Long position: A long position means that the investor bought a determined physic or financial asset.

Now let us review the delta hedging strategy by using a simple example. Consider and stock with a current price $S_0 = 57$, which at time t could have two prices, the upper price S_t^u or the lower price S_t^d, each one with probability $p = 1/2$. This is

$$S_t^u = 65 \quad \text{or} \quad S_t^d = \quad 53. \tag{D.1}$$

We can also consider a call option for this stock with an exercise price $K = 57$ and with maturity equal to t. Thus, at time t the payoff of the call option could have two prices with the same probability. According to the two possible stock prices, the two possibilities for the call price may be

$$\begin{aligned} C_t^u &= \max(65 - 57, 0) = 8\,, \quad \text{or} \\ C_t^d &= \max(53 - 57, 0) = 0. \end{aligned} \tag{D.2}$$

Furthermore, let us consider a portfolio made up of an option C and a short position on Δ stocks. Δ is an undetermined quantity of stocks which will be calculated from the delta-hedging argument. Thus, the value of the portfolio at time t, denoted as V_t, can be computed as

$$V_t = C_t - \Delta \cdot S_t. \tag{D.3}$$

where the signal $(-)$ is due to the assumption of a short position in stocks. So, at time $t = 0$ the value of the portfolio is given by

$$V_0 = C_0 - \Delta S_0 = C_0 - 57 \cdot \Delta. \tag{D.4}$$

On the other hand, at time equal t, the value of the portfolio could have one of the following

two values with a probability $p = 1/2$ each one. These are

$$\begin{aligned} V_t^u =& C_t^u - \Delta \cdot S_t^u = 8 - 65 \cdot \Delta \quad \text{or} \\ V_t^d =& C_t^d - \Delta \cdot S_t^d = -53 \cdot \Delta \end{aligned} \tag{D.5}$$

Thus, we want that the final value of the portfolio becomes the same in the two situations $V_t^u = V_t^d$. It leads us to find the value $\Delta = \frac{2}{3}$ for which the value of our portfolio will be protected.

Appendix E - Least Squares Method

Given a dataset of N points (x_i, y_i) (with i $= 1, 2, ..., N$) and a function model $f(x, \alpha)$, where α can be one or a set of constant parameters, the least squares method consists in to find the optimal values for the parameters into the model that provide the best fit of data. This is, we find the minimum of the sum of squared residuals SR which reads

$$SR = \sum_{i=1}^{N} \left[y_i - f(x_i, \alpha) \right]^2 . \tag{E.1}$$

The minimization is reached when the gradient of the sum of squared residuals related to the α_i parameters achieves zero value. That is

$$\frac{\partial [SR]}{\partial \alpha_i} = 0. \tag{E.2}$$

Depending on the number of parameters α there are different methods for the minimization of the residual function as those used during the development of this thesis, namely the Golden Search and Nelder-Mead methods.

The goodness of fit is determined by some criteria and parameters. Here, for example is used the coefficient of determination define as

$$R^2 = 1 - \frac{SR(\alpha_{min})}{SS_{total}} \tag{E.3}$$

where $SR(\alpha_{min})$ is the sum of squared residuals computed with the optimal parameters α_{min} which satisfy the relation (E.2). The quantity SS_{total} is the total sum of squared differences related to the arithmetic mean of dataset y_i, i.e.,

$$SS_{total} = \sum_{i=1}^{N} \left(y_i - \langle y \rangle \right)^2 \tag{E.4}$$

Appendix F - Hull-White and Heston model: Stationary Solution

Appendix F.1 - Hull-White

Consider the Hull-White stochastic process, which is given by

$$d\epsilon_1 = -\gamma_1(\epsilon_1 - \epsilon_0)dt + \kappa_1\epsilon_1 dW(t). \tag{F.1}$$

Using Appendix C, we can show that the process (F.1) has the associate Fokker-Planck equation in the form

$$\partial_t f_1 - \partial_{\epsilon_1}[\gamma_1(\epsilon_1 - \epsilon_0)f_1] - \frac{1}{2}\partial^2_{\epsilon_1}[\kappa_1^2\epsilon_1^2 f_1] = 0. \tag{F.2}$$

Considering long times, when the system achieves the statistical equilibrium, the probability distribution $f_1(\epsilon_1, t)$ satisfies

$$f_1(\epsilon_1) = \lim_{t\to\infty} f(\epsilon_1, t). \tag{F.3}$$

Using this condition in equation (F.2), the first term vanishes and the Fokker-Planck equation becomes

$$\partial_{\epsilon_1}[\gamma_1(\epsilon_1 - \epsilon_0)f_1] + \frac{1}{2}\partial^2_{\epsilon_1}[\kappa_1^2\epsilon_1^2 f_1] = 0. \tag{F.4}$$

Defining the parameter $\beta_1 = \frac{2\gamma_1}{\kappa_1^2}$, the equation above transforms as

$$\beta_1\partial_{\epsilon_1}[(\epsilon_1 - \epsilon_0)f_1] + \partial^2_{\epsilon_1}[\epsilon_1^2 f_1] = 0. \tag{F.5}$$

Integrating (F.5) once, we get

$$\beta_1(\epsilon_1 - \epsilon_0)f_1 + \partial_{\epsilon_1}[\epsilon_1^2 f_1] = 0. \tag{F.6}$$

Let us make the change of variable $\tilde{f}_1 = \epsilon_1^2 f_1$. In terms of this new variable we can write (F.6) as

$$\frac{\partial \tilde{f}_1}{\partial \epsilon_1} = -\frac{\beta_1(\epsilon_1 - \epsilon_0)}{\epsilon_1^2}\tilde{f}_1. \tag{F.7}$$

The equation above can be integrated, from which we obtain

$$\ln[\tilde{f}_1] = -\beta_1 \int \frac{(\epsilon_1 - \epsilon_0)}{\epsilon_1^2} d\epsilon_1 + \tilde{C} \tag{F.8}$$

or as a function of f_1 and applying the exponential

$$\epsilon_1^2 f_1(\epsilon_1) = C \exp\left[-\beta_1 \int \frac{(\epsilon_1 - \epsilon_0)}{\epsilon_1^2} d\epsilon_1\right]. \tag{F.9}$$

Therefore, we can write

$$\begin{aligned} f_1(\epsilon_1) &= \frac{C}{\epsilon_1^2}\exp\left[-\beta_1\ln(\epsilon_1) - \frac{\beta_1\epsilon_0}{\epsilon_1}\right] \\ f_1(\epsilon_1) &= \frac{C}{\epsilon_1^{\beta_1+2}}\exp\left[-\frac{\beta_1\epsilon_0}{\epsilon_1}\right]. \end{aligned} \tag{F.10}$$

In addition, we require a normalized PDF, such that

$$\int_0^\infty f_1(\epsilon_1)d\epsilon_1 = 1 \tag{F.11}$$

$$C\int_0^\infty \epsilon_1^{-\beta_1-2}\exp\left(-\frac{\beta_1\epsilon_0}{\epsilon_1}\right)d\epsilon_1 = 1. \tag{F.12}$$

Defining de variable $t = \frac{\beta_1\epsilon_0}{\epsilon_1}$, we can write (F.12) as

$$\frac{C}{(\beta_1\epsilon_0)^{\beta_1+1}}\int_0^\infty t^{\beta_1}e^{-t}dt = 1. \tag{F.13}$$

Using the definition of the gamma function

$$\Gamma(z) = \int_0^\infty t^{z-1}e^{-t}dt \tag{F.14}$$

in equation (F.13) and solving for C, we obtain

$$C = \frac{(\beta_1\epsilon_0)^{\beta_1+1}}{\Gamma(\beta_1+1)}. \tag{F.15}$$

So, the solution for the Fokker-Planck (F.4) is given by (F.10) with C given by (F.15). Therefore, we can finally write

$$f_1(\epsilon_1) = \frac{(\beta_1\epsilon_0)^{\beta_1+1}}{\Gamma(\beta_1+1)}\epsilon_1^{-\beta_1-2}e^{-\beta_1\epsilon_0/\epsilon_1}. \tag{F.16}$$

This function is called the inverse gamma PDF.

Appendix F.2 - Heston Model

In the Heston model the variable ϵ_1 follows the SDE

$$d\epsilon_1 = -\gamma_1(\epsilon_1 - \epsilon_0)dt + \kappa_1\sqrt{\epsilon_1\,\epsilon_0}\,dW(t). \tag{F.17}$$

The Fokker-Planck equation in the stationary regime for this stochastic process reads

$$\beta_1\partial_{\epsilon_1}[(\epsilon_1 - \epsilon_0)f_1] + \partial^2_{\epsilon_1}[\epsilon_1\epsilon_0 f_1] = 0, \tag{F.18}$$

where $\beta_1 = \frac{2\gamma_1}{\kappa_1^2}$. Integrating (F.18) once

$$\beta_1(\epsilon_1 - \epsilon_0)f_1 + \partial_{\epsilon_1}[\epsilon_1\epsilon_0 f_1] = 0. \tag{F.19}$$

Making the change of variable $\tilde{f}_1 = \epsilon_1\epsilon_0 f_1$, we can write (F.19) in the form

$$\frac{\partial \tilde{f}_1}{\partial \epsilon_1} = -\frac{\beta_1(\epsilon_1 - \epsilon_0)}{\epsilon_1\epsilon_0}\tilde{f}_1. \tag{F.20}$$

Integrating the equation above, results

$$\ln[\tilde{f}_1] = -\beta_1 \int \frac{(\epsilon_1 - \epsilon_0)}{\epsilon_1\epsilon_0} d\epsilon_1 + \tilde{C}. \tag{F.21}$$

This can be written in terms of the PDF $f_1(\epsilon_1)$ as

$$\epsilon_1\epsilon_0 f_1(\epsilon_1) = C \exp\left[-\beta_1 \int \frac{(\epsilon_1 - \epsilon_0)}{\epsilon_1\epsilon_0} d\epsilon_1\right] \tag{F.22}$$

$$\begin{aligned} f_1(\epsilon_1) &= \frac{C}{\epsilon_1\epsilon_0} \exp\left[\beta_1 \ln(\epsilon_1) - \frac{\beta_1\epsilon_1}{\epsilon_0}\right] \\ f_1(\epsilon_1) &= C\frac{\epsilon_1^{\beta_1 - 1}}{\epsilon_0} \exp\left[-\frac{\beta_1\epsilon_1}{\epsilon_0}\right]. \end{aligned} \tag{F.23}$$

Normalizing $f_1(\epsilon_1)$, we have

$$f_1(\epsilon_1) = \frac{(\beta_1/\epsilon_0)^{\beta_1}}{\Gamma(\beta_1)} \epsilon_1^{\beta_1 - 1} e^{-\beta_1\epsilon_1/\epsilon_0}. \tag{F.24}$$

This function is known as the gamma PDF.

Appendix G - Mellin Transform Application to Hierarchical Model for the Energy Flux

Appendix G.1 - Hierarchical Inverse Gamma Class Distribution

Now let us demonstrate how the Mellin transform can be used for the calculations of the integral

$$f_N(\epsilon_N) = \int_0^\infty d\epsilon_{N-1} \dots \int_0^\infty d\epsilon_1 \; f_N(\epsilon_N|\epsilon_{N-1}) \dots f_1(\epsilon_1|\epsilon_0), \tag{G.1}$$

where de conditional PDF $f(\epsilon_i|\epsilon_{i-1})$ for an inverse gamma PDF takes the form

$$f(\epsilon_i|\epsilon_{i-1}) = \frac{(\beta_i\epsilon_{i-1})^{\beta_i+1}}{\Gamma(\beta_i+1)}\epsilon_i^{-\beta_i-2}e^{-\beta_i\epsilon_{i-1}/\epsilon_i}. \tag{G.2}$$

The successive integration of (G.1) can be made in a general way as in [Macêdo et al., 2017] or using the definitions of the Mellin transform and the Meijer G-function as we show here. To describe de procedure, let us write the Mellin transform for the function $f(x)$ as

$$\mathcal{M}\{f(x)\}(s) = F(s) = \int_0^\infty x^{s-1}f(x)dx, \tag{G.3}$$

and some of its properties:

$$\begin{aligned} \mathcal{M}\{f(ax)\}(s) &= a^{-s}F(s) \\ \mathcal{M}\{f(a/x)\}(s) &= \mathcal{M}\{f(ax)\}(-s) = a^sF(-s) \\ \mathcal{M}\{x^bf(x)\}(s) &= F(s+b) \\ \mathcal{M}\{e^{-\alpha x}\}(s) &= \alpha^{-s}\Gamma(s). \end{aligned} \tag{G.4}$$

Also, let us introduce the Parseval's formula:

$$\int_0^\infty f(x)g(x)dx = \frac{1}{2\pi i}\int_{c-i\infty}^{c+i\infty} F(s)G(1-s)ds, \tag{G.5}$$

where $F(s)$ and $G(1-s)$ are the Mellin transformations of the functions $f(x)$ and $g(x)$ respectively.

As an example, we consider the marginal PDF for $f(\epsilon_2)$. This is defined as the integral with respect to $d\epsilon_1$ of the conditional probability $f(\epsilon_2|\epsilon_1)$, assuming that the stochastic variable ϵ_1 is distributed as $f(\epsilon_1|\epsilon_0)$. The result is proved to be written as a Meijer G-function. To do this, we use the Mellin transform to solve the integral

$$f_2(\epsilon_2) = \int_0^\infty f_2(\epsilon_2|\epsilon_1)f_1(\epsilon_1|\epsilon_0)d\epsilon_1. \tag{G.6}$$

Using (G.2), the integral above explicitly reads

$$f_2(\epsilon_2) = \frac{\beta_2^{\beta_2+1}\epsilon_2^{-\beta_2-2}}{\Gamma(\beta_2+1)}\frac{(\beta_1\epsilon_0)^{\beta_1+1}}{\Gamma(\beta_1+1)}\int_0^\infty \epsilon_1^{\beta_2+1}e^{-\beta_2\epsilon_1/\epsilon_2}\epsilon_1^{-\beta_1-2}e^{-\beta_1\epsilon_0/\epsilon_1}d\epsilon_1. \tag{G.7}$$

Defining the variable $\epsilon_1 \equiv x$, we can write the functions $g(x) = x^{\beta_2+1}e^{-\beta_2 x/\epsilon_2}$ and $f(x) = x^{-\beta_1-2}e^{-\beta_1\epsilon_0/x}$. Using the third property in (G.4), the Mellin transform for $g(x)$ looks like

$$\mathcal{M}\{g(x)\}(1-s) = \mathcal{M}\{x^{\beta_2+1}e^{-\beta_2 x/\epsilon_2}\}(1-s) = \mathcal{M}\{e^{-\beta_2 x/\epsilon_2}\}(2+\beta_2-s). \tag{G.8}$$

Now we can use the fourth line in equation (G.4) to obtain

$$\mathcal{M}\{g(x)\}(1-s) = \left(\frac{\beta_2}{\epsilon_2}\right)^{-(2+\beta_2-s)}\Gamma(2+\beta_2-s). \tag{G.9}$$

Similarly, for the Mellin transform of the function $f(x)$, we use the second line in (G.4), which reads

$$\mathcal{M}\{f(x)\}(s) = \mathcal{M}\{x^{-\beta_1-2}e^{-\beta_1\epsilon_0/x}\}(s) = \mathcal{M}\{x^{\beta_1+2}e^{-\beta_1\epsilon_0 x}\}(-s). \tag{G.10}$$

Now we can use the third and fourth line in (G.4) to obtain

$$\mathcal{M}\{f(x)\}(s) = \mathcal{M}\{e^{-\beta_1\epsilon_0 x}\}(2+\beta_1-s) = (\beta_1\epsilon_0)^{-(2+\beta_1-s)}\Gamma(2+\beta_1-s). \tag{G.11}$$

Replacing (G.9) and (G.11) into (G.5), the integral (G.6) can be written as

$$\begin{aligned}&\int_0^\infty f_2(\epsilon_2|\epsilon_1)f_1(\epsilon_1|\epsilon_0)d\epsilon_1\\ &= \frac{1}{\epsilon_0\beta_1\beta_2\Gamma(\beta_1+1)\Gamma(\beta_2+1)}\frac{1}{2\pi i}\int_{c-i\infty}^{c+i\infty}\left(\frac{\epsilon_2}{\beta_1\beta_2\epsilon_0}\right)^{-s}\Gamma(2+\beta_1-s)\Gamma(2+\beta_2-s)ds.\end{aligned} \tag{G.12}$$

Now, let us introduce the definition of the Meijer G-function

$$G_{p,q}^{m,n}\left(\left.\begin{matrix}\vec{a}_p\\ \vec{b}_q\end{matrix}\right|x\right) = \frac{1}{2\pi i}\int_{c-i\infty}^{c+i\infty}\frac{\prod_{j=1}^m\Gamma(b_j+s)\prod_{j=1}^n\Gamma(1-a_j-s)}{\prod_{j=n+1}^p\Gamma(a_j+s)\prod_{j=m+1}^q\Gamma(1-b_j-s)}x^{-s}ds, \tag{G.13}$$

where $\vec{a}_p = (a_1\ldots,a_p)$ and $\vec{a}_p = (b_1\ldots,b_q)$. Comparing this definition with (G.12) we can write

$$\begin{aligned}&\int_0^\infty f_2(\epsilon_2|\epsilon_1)f_1(\epsilon_1|\epsilon_0)d\epsilon_1\\ &\qquad= \frac{1}{\epsilon_0\beta_1\beta_2\Gamma(\beta_1+1)\Gamma(\beta_2+1)}G_{2,0}^{0,2}\left(\left.\begin{matrix}-\beta_1-1,-\beta_2-1\\ -\end{matrix}\right|\frac{\epsilon_2}{\beta_1\beta_2\epsilon_0}\right).\end{aligned} \tag{G.14}$$

The result above is the first integral in (G.1). Now consider the case with three scales. In this case, we need to solve the integral with respect to ϵ_2 in (G.2). Using the result (G.14) and the relation (G.2), the integral (G.1) for three scales becomes

$$f_3(\epsilon_3) = \frac{1}{\epsilon_0\beta_1\beta_2\Gamma(\beta_1+1)\Gamma(\beta_2+1)} \int_0^\infty \frac{(\beta_3\epsilon_2)^{\beta_3+1}\epsilon_3^{-\beta_3-2}e^{-\beta_3\epsilon_2/\epsilon_3}}{\Gamma(\beta_3+1)} G_{2,0}^{0,2}\left(\begin{matrix}-\beta_1-1,-\beta_2-1\\ -\end{matrix}\middle|\frac{\epsilon_2}{\beta_1\beta_2\epsilon_0}\right) d\epsilon_2. \tag{G.15}$$

This integral can be solved using the next properties of the Meijer G-function

$$x^\rho G_{p,q}^{m,n}\left(\begin{matrix}\vec{a}_p\\ \vec{b}_q\end{matrix}\middle| x\right) = G_{p,q}^{m,n}\left(\begin{matrix}\vec{a}_p+\rho\\ \vec{b}_q+\rho\end{matrix}\middle| x\right), \tag{G.16}$$

$$\int_0^\infty G_{p,q}^{m,n}\left(\begin{matrix}\vec{a}_p\\ \vec{b}_q\end{matrix}\middle|\eta x\right) G_{\sigma,\tau}^{\mu,\nu}\left(\begin{matrix}\vec{c}_\sigma\\ \vec{d}_\tau\end{matrix}\middle| wx\right) dx = \frac{1}{w} G_{p+\tau,q+\sigma}^{m+\nu,n+\mu}\left(\begin{matrix}\vec{a}_n,-\vec{d}_\tau,\vec{a}_p\\ \vec{b}_m,-\vec{c}_\sigma,\vec{b}_q\end{matrix}\middle|\frac{\eta}{w}\right), \tag{G.17}$$

and the representation of the exponential function as a Meijer G-function

$$e^{-x} = G_{0,1}^{1,0}\left(\begin{matrix}-\\ 0\end{matrix}\middle| x\right). \tag{G.18}$$

With the aid of the previous properties, the integral (G.15) reads

$$\begin{aligned} f_3(\epsilon_3) &= \frac{1}{\epsilon_0\epsilon_3\beta_1\beta_2\Gamma(\beta_1+1)\Gamma(\beta_2+1)\Gamma(\beta_3+1)} \\ &\quad\times \int_0^\infty \left(\frac{\beta_3\epsilon_2}{\epsilon_3}\right)^{\beta_3+1} G_{1,0}^{0,1}\left(\begin{matrix}-\\ 0\end{matrix}\middle|\frac{\beta_3\epsilon_2}{\epsilon_3}\right) G_{2,0}^{0,2}\left(\begin{matrix}-\beta_1-1,-\beta_2-1\\ -\end{matrix}\middle|\frac{\epsilon_2}{\beta_1\beta_2\epsilon_0}\right) d\epsilon_2 \\ &= \frac{1}{\epsilon_0\epsilon_3\beta_1\beta_2\Gamma(\beta_1+1)\Gamma(\beta_2+1)\Gamma(\beta_3+1)} \\ &\quad\times \int_0^\infty G_{2,0}^{0,2}\left(\begin{matrix}-\beta_1-1,-\beta_2-1\\ -\end{matrix}\middle|\frac{\epsilon_2}{\beta_1\beta_2\epsilon_0}\right) G_{1,0}^{0,1}\left(\begin{matrix}-\\ \beta_3+1\end{matrix}\middle|\frac{\beta_3\epsilon_2}{\epsilon_3}\right) d\epsilon_2. \end{aligned} \tag{G.19}$$

Using the so-called convolution property of the Meijer G-function (G.17), the stationary distribution of the variable ϵ_3 is given by

$$\begin{aligned} f_3(\epsilon_3) &= \frac{1}{\epsilon_0\beta_1\beta_2\beta_3\Gamma(\beta_1+1)\Gamma(\beta_2+1)\Gamma(\beta_3+1)} \\ &\quad\times G_{3,0}^{0,3}\left(\begin{matrix}-\beta_1-1,-\beta_2-1,-\beta_3-1\\ -\end{matrix}\middle|\frac{\epsilon_3}{\beta_1\beta_2\beta_3\epsilon_0}\right) \end{aligned} \tag{G.20}$$

It is easy to note that for the fourth scale we have the integral with respect to ϵ_3 of the product between the corresponding conditional distribution $f(\epsilon_4|\epsilon_3)$ (obtained by substituting

$i = 4$ into (G.2)) and the result (G.20). It leads to an integral of the product of two Meijer G-functions like in the case of $f_3(\epsilon_3)$. Solving the integral by using the properties of the Meijer G-function, we add the parameter $(-\beta_4 - 1)$ to the vector $\vec{a}_n$ in the Meijer function, the gamma function $\Gamma(\beta_4 + 1)$ in the product of gamma functions and β_4 in the product of βs. The integral corresponding to the fifth scale will follow a similar pattern, such that the PDF for an arbitrary scale N can be written in the form

$$f_N(\epsilon_N) = \frac{\Omega}{\epsilon_0\,\omega} G^{0,N}_{N,0}\left(\begin{matrix} -\boldsymbol{\beta_N} - \mathbf{1} \\ - \end{matrix}\middle|\, \frac{\epsilon_N}{\epsilon_0\,\omega}\right) \tag{G.21}$$

where $\boldsymbol{\beta_N} - \mathbf{1} = (\beta_1 - 1, \beta_2 - 1, \ldots, \beta_N - 1)$, $\Omega = \prod_{i=1}^{N} \frac{1}{\Gamma(\beta_i+1)}$ and $\omega = \prod_{i=1}^{N} \beta_i$.

Appendix G.2 - Hierarchical Gamma Class Distribution

Consider now the hierarchical Heston process with N scales (4.35). The marginal distribution $f_N(\epsilon_N)$ for a given scale N is given by the integral (G.1), but now de conditional PDF $f(\epsilon_i|\epsilon_{i-1})$ is given by the gamma distribution. Let us write the gamma distribution for ϵ_i conditioned to ϵ_{i-1} as

$$f(\epsilon_i|\epsilon_{i-1}) = \frac{(\beta_i/\epsilon_{i-1})^{\beta_i}}{\Gamma(\beta_i)} \epsilon_i^{\beta_i - 1} e^{-\beta_i \epsilon_i/\epsilon_{i-1}}. \tag{G.22}$$

The successive integration in the expression for $f_N(\epsilon_N)$ can be done using the Mellin transform and the Meijer G-function. For this, first we compute the marginal distribution $f(\epsilon_2)$ solving the integral for two scales

$$f(\epsilon_2) = \int_0^\infty f_2(\epsilon_2|\epsilon_1) f_1(\epsilon_1) d\epsilon_1 = \frac{\beta_2^{\beta_2}\epsilon_2^{\beta_2 - 1}}{\Gamma(\beta_2)} \frac{(\beta_1/\epsilon_0)^{\beta_1}}{\Gamma(\beta_1)} \int_0^\infty d\epsilon_1 \epsilon_1^{-\beta_2} e^{-\beta_2\epsilon_2/\epsilon_1} \epsilon_1^{\beta_1 - 1} e^{-\beta_1\epsilon_1/\epsilon_0}. \tag{G.23}$$

Using the change of variable $x = \epsilon_1$, we can write $g(x) = x^{-\beta_2} e^{-\beta_2\epsilon_2/x}$ and $f(x) = x^{\beta_1 - 1} e^{-\beta_1 x/\epsilon_0}$. Applying the second, third and fourth equations into (G.4), we can write the Mellin transform for $g(x)$ in the form

$$\begin{aligned} \mathcal{M}\{x^{-\beta_2} e^{-\beta_2\epsilon_2/x}\}(1 - s) &= \mathcal{M}\{x^{\beta_2} e^{-\beta_2\epsilon_2/x}\}(s - 1) = \mathcal{M}\{e^{-\beta_2\epsilon_2/x}\}(\beta_2 + s - 1) \\ &= (\beta_2\epsilon_2)^{-(\beta_2 - 1 + s)} \Gamma(\beta_2 - 1 + s). \end{aligned} \tag{G.24}$$

Similarly the corresponding Mellin transform for $f(x)$ is

$$\begin{aligned} \mathcal{M}\{x^{\beta_1 - 1} e^{-\beta_1 x/\epsilon_0}\}(s) &= \mathcal{M}\{e^{-\beta_1 x/\epsilon_0}\}(\beta_1 + s - 1) \\ &= \left(\frac{\beta_1}{\epsilon_0}\right)^{-(\beta_1 - 1 + s)} \Gamma(\beta_1 - 1 + s) \end{aligned} \tag{G.25}$$

Then we can use the Parseval formula (G.5) to write the integral (G.23) in the form

$$\int_0^\infty f_2(\epsilon_2|\epsilon_1) f_1(\epsilon_1) d\epsilon_1 = \frac{\beta_1\beta_2}{\epsilon_0\Gamma(\beta_1)\Gamma(\beta_2)} \frac{1}{2\pi i} \int_{c-i\infty}^{c+i\infty} \Gamma(\beta_1 - 1 + s)\Gamma(\beta_2 - 1 + s) \left(\frac{\beta_1\beta_2\epsilon_2}{\epsilon_0}\right)^{-s} ds. \tag{G.26}$$

Comparing this with the definition of the Meijer G-function (G.13), results

$$f_2(\epsilon_2) = \int_0^\infty f_2(\epsilon_2|\epsilon_1) f_1(\epsilon_1) d\epsilon_1 = \frac{\beta_1\beta_2}{\epsilon_0\Gamma(\beta_1)\Gamma(\beta_2)} G^{2,0}_{0,2}\left(\begin{matrix} - \\ \beta_1 - 1, \beta_2 - 1 \end{matrix}\middle| \frac{\beta_1\beta_2\epsilon_2}{\epsilon_0}\right). \tag{G.27}$$

The following integrals in equation (G.1) are solved using the properties of the Meijer G-function, such that for the case with N scales we obtain the solution

$$f_N(\epsilon_N) = \frac{\omega\,\Omega}{\epsilon_0} G^{N,0}_{0,N}\left(\begin{matrix} - \\ \boldsymbol{\beta} - \mathbf{1} \end{matrix}\middle| \frac{\omega\,\epsilon_N}{\epsilon_0}\right), \tag{G.28}$$

where $\omega = \prod_{j=1}^{N} \beta_j$, $\Omega = \prod_{j=1}^{N} 1/\Gamma(\beta_j)$ and $\boldsymbol{\beta} = (\beta_1 - 1, \ldots, \beta_N - 1)$

Appendix H - Properties of the Meijer G and Fox H functions

1. The Meijer G-function is defined as the Mellin-Barnes integral:

$$G_{p,q}^{m,n}\left(\left.\begin{matrix}\vec{a}_p\\ \vec{b}_q\end{matrix}\right|x\right)=\frac{1}{2\pi i}\int_{c-i\infty}^{c+i\infty}\frac{\prod_{j=1}^{m}\Gamma(b_j+s)\prod_{j=1}^{n}\Gamma(1-a_j-s)}{\prod_{j=n+1}^{p}\Gamma(a_j+s)\prod_{j=m+1}^{q}\Gamma(1-b_j-s)}x^{-s}ds. \tag{H.1}$$

2. The Fox H-function can be written in terms of the Meijer G-function in the form:

$$H_{p,q}^{m,n}\left[x\left|\begin{matrix}(a_1,C),\ldots,(a_p,C)\\ (b_1,C),\ldots,(b_q,C)\end{matrix}\right.\right]=\frac{1}{C}\,G_{p,q}^{m,n}\left(\left.\begin{matrix}(a_1,\ldots,a_p)\\ (b_1,\ldots,b_q)\end{matrix}\right|x^{1/C}\right) \tag{H.2}$$

3. Exponential as a Meijer G-function

$$e^{-x}=G_{0,1}^{1,0}\left(\left.\begin{matrix}-\\ 0\end{matrix}\right|x\right). \tag{H.3}$$

4. Error function as a Meijer G-function

$$\operatorname{erf}(x)=\frac{1}{\sqrt{\pi}}G_{1,2}^{1,1}\left(\left.\begin{matrix}1\\ \frac{1}{2},0\end{matrix}\right|x^2\right). \tag{H.4}$$

5. Power absorption

$$x^{\rho}G_{p,q}^{m,n}\left(\left.\begin{matrix}\vec{a}_p\\ \vec{b}_q\end{matrix}\right|x\right)=G_{p,q}^{m,n}\left(\left.\begin{matrix}\vec{a}_p+\rho\\ \vec{b}_q+\rho\end{matrix}\right|x\right). \tag{H.5}$$

6. Integral involving the product of two Meijer G-functions

$$\int_0^{\infty}G_{p,q}^{m,n}\left(\left.\begin{matrix}\vec{a}_p\\ \vec{b}_q\end{matrix}\right|\eta x\right)G_{\sigma,\tau}^{\mu,\nu}\left(\left.\begin{matrix}\vec{c}_\sigma\\ \vec{d}_\tau\end{matrix}\right|wx\right)dx=\frac{1}{w}G_{p+\tau,q+\sigma}^{m+\nu,n+\mu}\left(\left.\begin{matrix}\vec{a}_n,-\vec{d}_\tau,\vec{a}_p\\ \vec{b}_m,-\vec{c}_\sigma,\vec{b}_q\end{matrix}\right|\frac{\eta}{w}\right). \tag{H.6}$$

7. Argument inversion

$$G_{p,q}^{m,n}\left(\left.\begin{matrix}\vec{a}_p\\ \vec{b}_q\end{matrix}\right|x\right)=G_{q,p}^{n,m}\left(\left.\begin{matrix}1-\vec{b}_q\\ 1-\vec{a}_p\end{matrix}\right|\frac{1}{x}\right). \tag{H.7}$$

8. Bivariate Fox H-function and bivariate Meijer G-function:

The bivariate Fox H-function is defined as a double Mellin-Barnes integral, which can be found in references as [Mittal and Gupta, 1972,S.P.Goyal and S.L.Mathur, 1976]. In this representation the bivariate Fox H-function is given by

$$H[x,y] = \left(\frac{1}{2\pi i}\right)^2 \int_{L_1}\int_{L_2} \phi(s,t)\theta_1(s)\theta_2(t)x^s\, y^t ds\, dt. \tag{H.8}$$

where

$$\phi(s,t) = \frac{\prod_{j=1}^{n_1}\Gamma(1-a_j+\alpha_j\, s + A_j\, t)}{\prod_{j=n_1+1}^{p_1}\Gamma(a_j-\alpha_j\, s - A_j\, t)\prod_{j=1}^{q_1}\Gamma(1-b_j+\beta_j\, s + B_j\, t)}, \tag{H.9}$$

$$\theta_1(s) = \frac{\prod_{j=1}^{m_2}\Gamma(d_j-\delta_j\, s)\prod_{j=1}^{n_2}\Gamma(1-c_j+\gamma_j\, s)}{\prod_{j=m_2+1}^{q_2}\Gamma(1-d_j+\delta_j\, s)\prod_{j=n_2+1}^{p_2}\Gamma(c_j-\gamma_j\, s)}, \tag{H.10}$$

and

$$\theta_2(t) = \frac{\prod_{j=1}^{m_3}\Gamma(f_j-F_j\, t)\prod_{j=1}^{n_3}\Gamma(1-e_j+E_j\, t)}{\prod_{j=m_3+1}^{q_3}\Gamma(1-f_j+F_j\, t)\prod_{j=n_3+1}^{p_3}\Gamma(e_j-E_j\, t)}, \tag{H.11}$$

The Fox H-function $H[x,y]$ is denoted as

$$H(x,y) = H^{0,n_1:m_2,n_2:m_3,n_3}_{p_1,q_1:p_2,q_2:p_3,q_3}\left[\left.\begin{matrix}(a_{p_1};\alpha_{p_1},A_{p_1}):(c_{p_2},\gamma_{p_2}):(e_{p_3},E_{p_3})\\(b_{q_1};\beta_{q_1},B_{q_1}):(d_{q_2},\delta_{q_2}):(f_{q_3},F_{q_3})\end{matrix}\right| x,y\right], \tag{H.12}$$

or also in the form

$$H\left[x,y\right] = H\left[\left.\begin{matrix}\begin{pmatrix}0 & n_1\\ p_1 & q_1\end{pmatrix}\\ \begin{pmatrix}m_2 & n_2\\ p_2 & q_2\end{pmatrix}\\ \begin{pmatrix}m_3 & n_3\\ p_3 & q_3\end{pmatrix}\end{matrix}\right| \begin{matrix}(a_1;\alpha_1,A_1),\ldots,(a_{p_1};\alpha_{p_1},A_{p_1})\\(b_1;\beta_1,B_1),\ldots,(b_{q_1};\beta_{q_1},B_{q_1})\\(c_1,\gamma_1),\ldots,(c_{p_2},\gamma_{p_2})\\(d_1,\delta_1),\ldots,(d_{q_2},\delta_{q_2})\\(e_1,E_1),\ldots,(e_{p_3},E_{p_3})\\(f_1,F_1),...,(f_{q_3},F_{q_3})\end{matrix}\left|\begin{matrix}x\\ \\ y\end{matrix}\right.\right]. \tag{H.13}$$

The bivariate Meijer G-function is a particular case of the bivariate Fox H-function, where the elements $\alpha_j, \beta_j, A_j, B_j, \gamma_j, \delta_j, E_j, F_j$ are all equal to one. This is denoted as

$$G(x,y) = H^{0,n_1:m_2,n_2:m_3,n_3}_{p_1,q_1:p_2,q_2:p_3,q_3}\left(\left.\begin{matrix}(a_{p_1}):(c_{p_2}):(e_{p_3})\\(b_{q_1}):(d_{q_2}):(f_{q_3})\end{matrix}\right| x,y\right), \tag{H.14}$$

9. Integral involving the product of three Fox H-functions. Solution as a bivariate Fox H-function:

$$\int_0^\infty x^{\lambda-1} H_{p,q}^{m,0}\left[ax\middle|\begin{matrix}(a_p,\alpha_p)\\(b_q,\beta_q)\end{matrix}\right] H_{p_2,q_2}^{m_2,n_2}\left[\beta x^h\middle|\begin{matrix}(c_{p_2},\gamma_{p_2})\\(d_{p_2},\delta_{p_2})\end{matrix}\right] H_{p_3,q_3}^{m_3,n_3}\left[\delta x^k\middle|\begin{matrix}(e_{p_3},E_{p_3})\\(f_{p_3},F_{p_3})\end{matrix}\right] dx$$

$$= a^{-\lambda} H_{q,p:p_2,q_2:p_3,q_3}^{0,m:m_2,n_2:m_3,n_3}\left[\begin{matrix}(1-b_q-\lambda\beta_q;h\beta_q,\kappa\beta_q):(c_{p_2},\gamma_{p_2}):(e_{p_3},E_{p_3})\\(1-a_p-\lambda\alpha_p;h\alpha_p,\kappa\alpha_p):(d_{q_2},\delta_{q_2}):(f_{q_3},F_{q_3})\end{matrix}\middle|\frac{\beta}{a^h},\frac{\delta}{a^k}\right]. \tag{H.15}$$

10. Integral involving the product of three Fox H-functions. Solution as a series of univariate Fox H-function:

$$\int_0^\infty x^{\rho-1} H_{p,q}^{m,n}\left[ax^u\middle|\begin{matrix}(g_j,G_j)_{1,p_1}\\(h_j,H_j)_{1,q}\end{matrix}\right] H_{f,l}^{k,0}\left[bx\middle|\begin{matrix}(r_j,R_j)_{1,f}\\(u_j,U_j)_{1,l}\end{matrix}\right] H_{p_1,q_1}^{m_1,n_1}\left[yx^\lambda\middle|\begin{matrix}(a_j,\alpha_j)_{1,p_1}\\(b_j,\beta_j)_{1,q_1}\end{matrix}\right] dx$$

$$= \frac{1}{b^\rho}\sum_{h=1}^{m}\sum_{r=1}^{\infty}\frac{(-1)^r\prod_{j=1,j\neq h}^{m}\Gamma(h_j-H_j\rho_r)\prod_{j=1}^{n}\Gamma(1-g_j+G_j\rho_r)\,a^{\rho_r}}{r!\prod_{j=m+1}^{q}\Gamma(1-h_j+H_j\rho_r)\prod_{j=n+1}^{p}\Gamma(g_j-G_j\rho_r)\,b^{\rho u_r}H_h}$$

$$\times H_{p_1+l,q_1+f}^{m_1,n_1+k}\left[\frac{y}{b^\lambda}\middle|\begin{matrix}(a_j,\alpha_j)_{1,n_1},(1-u_j-(\rho+u\rho_r)U_j,\lambda U_j)_{1,l},(a_j,\alpha_j)_{n_1+1,p_1}\\(b_j,\beta_j)_{1,q_1},(1-r_j-(\rho+u\rho_r)R_j,\lambda R_j)_{1,f}\end{matrix}\right], \tag{H.16}$$

where $\rho_r=\frac{h_h+r}{H_h}$.

Appendix I - Hierarchical Hull-White Model for Option Pricing

The hierarchical Hull-White model for option pricing with N scales can be obtained resolving the integral (4.25). In other words, this is the average of the Black-Scholes formula computed over the distribution of the volatility $f_N(v_N)$ that in this case is a function like (G.21). So, the expression for the option price becomes

$$C(S,K,r,t,N) = \frac{\Omega}{v_0\,\omega}\int_0^\infty C(S,K,r,t|v_N)\,G^{0,N}_{N,0}\left(\begin{matrix}-\boldsymbol{\beta}-\mathbf{1}\\ -\end{matrix}\middle|\frac{v_N}{v_0\,\omega}\right)dv_N, \tag{I.1}$$

where $\Omega = 1/\prod_{i=1}^{N}\Gamma(\beta_i+1)$ and $\omega = \prod_{i=1}^{N}\beta_i$. The Black-Scholes price $C(S,K,r,t|v_N)$ is given by,

$$\begin{aligned} C(S,K,r,t|v_N) &= S\Phi(d_1) - Ke^{-r\tau}\Phi(d_2) \\ &= C_1(S,K,r,t|v_N) - C_2(S,K,r,t|v_N), \end{aligned} \tag{I.2}$$

where d_1 and d_2 are define as

$$\begin{aligned} d_1 &= \frac{ln\left(\frac{S}{K}\right) + (r+\sigma^2/2)\tau}{\sigma\sqrt{\tau}} \\ d_2 &= d_1 - \sigma\sqrt{\tau}. \end{aligned} \tag{I.3}$$

Choosing $v = \sigma^2$, like in the original work of Hull-White [Hull and White, 1987] and reordering terms, we have

$$\begin{aligned} d_1 &= \frac{ln\left(\frac{S}{K}\right) + r\tau}{\sqrt{v\,\tau}} + \frac{\sqrt{v\,\tau}}{2} \\ d_2 &= \frac{ln\left(\frac{S}{K}\right) + r\tau}{\sqrt{v\,\tau}} - \frac{\sqrt{v\,\tau}}{2}. \end{aligned} \tag{I.4}$$

Defining

$$\begin{aligned} a &= \ln\left(\frac{S}{K}\right) + r\tau \quad \text{and} \\ b &= \frac{1}{2}, \end{aligned} \tag{I.5}$$

we can write

$$\begin{aligned} d_1 &= \frac{a}{\sqrt{v\,\tau}} + b\sqrt{v\,\tau} \\ d_2 &= \frac{a}{\sqrt{v\,\tau}} - b\sqrt{v\,\tau}. \end{aligned} \tag{I.6}$$

In addition, we can write the first term in (I.2) as

$$\langle C_1(S,K,r,t|v_N)\rangle \equiv S\Psi_1(a,b). \tag{I.7}$$

So, with the changes made in (I.6), Ψ_1 can be written in the form

$$\Psi_1(a,b) = \frac{\Omega}{v_0\,\omega}\int_0^\infty \Phi\left(\frac{a}{\sqrt{v_N\tau}} + b\sqrt{v_N\tau}\right) G_{N,0}^{0,N}\left(\begin{matrix}-\boldsymbol{\beta}-\mathbf{1}\\ -\end{matrix}\middle|\frac{v_N}{v_0\,\omega}\right) dv_N. \tag{I.8}$$

This integral can be solved making the partial derivation respect to a. We then integrate the result with respect to v_N. Finally, we integrate again the last result with respect to a. Explicitly, this is written in the way

$$\begin{aligned}\Psi_1(a,b) &= \int_0^a \frac{\partial\Psi_1(a')}{\partial a'}\,da' + \Psi_1(a=0)\\ &= \Theta_1(a,b) + \Psi_1(a=0).\end{aligned} \tag{I.9}$$

So, following this procedure, the partial derivative of (I.8) with respect to a reads

$$\Psi_{1a} = \frac{\partial\Psi_1(a,b)}{\partial a} \tag{I.10}$$

$$\Psi_{1a} = \frac{e^{-ab}}{\sqrt{2\pi}}\frac{\Omega}{v_0\,\omega}\int_0^\infty \frac{1}{\sqrt{v_N\tau}} e^{-\frac{1}{2}\left(\frac{a^2}{v_N\tau}+b^2 v_N\tau\right)} G_{N,0}^{0,N}\left(\begin{matrix}-\boldsymbol{\beta}-\mathbf{1}\\ -\end{matrix}\middle|\frac{v_N}{v_0\,\omega}\right) dv_N. \tag{I.11}$$

Writing the exponential function as a Meijer G-function

$$e^{-x} = G_{0,1}^{1,0}\left(\begin{matrix}-\\ 0\end{matrix}\middle|x\right) \tag{I.12}$$

the integral (I.11) takes the form

$$\begin{aligned}\Psi_{1a} = \frac{e^{-ab}}{\sqrt{2\pi}}\frac{\Omega}{v_0\,\omega}\int_0^\infty \frac{1}{\sqrt{v_N\tau}} G_{0,1}^{1,0}\left(\begin{matrix}-\\ 0\end{matrix}\middle|\frac{a^2}{2v_N\tau}\right) G_{1,0}^{0,1}\left(\begin{matrix}1\\ -\end{matrix}\middle|\frac{2}{b^2 v_N\tau}\right)\\ \times G_{0,N}^{N,0}\left(\begin{matrix}-\\ \boldsymbol{\beta}+\mathbf{2}\end{matrix}\middle|\frac{v_0\,\omega}{v_N}\right) dv_N\end{aligned} \tag{I.13}$$

Using the change of variable $y_N = \frac{1}{v_N}$, the integral above can be written as

$$\begin{aligned}\Psi_{1a} = \frac{e^{-ab}}{\sqrt{2\pi}}\frac{\Omega}{v_0\,\omega\sqrt{\tau}}\int_0^\infty y_N^{-3/2} G_{0,1}^{1,0}\left(\begin{matrix}-\\ 0\end{matrix}\middle|\frac{a^2 y_N}{2\tau}\right) G_{1,0}^{0,1}\left(\begin{matrix}1\\ -\end{matrix}\middle|\frac{2y_N}{b^2\tau}\right)\\ \times G_{0,N}^{N,0}\left(\begin{matrix}-\\ \boldsymbol{\beta}+\mathbf{2}\end{matrix}\middle|v_0\,\omega\,y_N\right) dy_N.\end{aligned} \tag{I.14}$$

It is more convenient to write this expression as

$$\begin{aligned}\Psi_{1a} = \frac{\Omega e^{-ab}}{\sqrt{2\pi}}\left(\frac{v_0\,\omega}{\tau}\right)^{1/2}\int_0^\infty (v_0\,\omega y_N)^{-3/2} G_{0,1}^{1,0}\left(\begin{matrix}-\\ 0\end{matrix}\middle|\frac{a^2 y_N}{2\tau}\right) G_{1,0}^{0,1}\left(\begin{matrix}1\\ -\end{matrix}\middle|\frac{2y_N}{b^2\tau}\right)\\ \times G_{0,N}^{N,0}\left(\begin{matrix}-\\ \boldsymbol{\beta}+\mathbf{2}\end{matrix}\middle|v_0\,\omega\,y_N\right) dy_N.\end{aligned} \tag{I.15}$$

So, using property (H.5) of Meijer G-function, the factor $(v_0\,\omega\,y_N)^{-3/2}$ can be included into the last Meijer G-function. With this change we have

$$\Psi_{1a} = \frac{\Omega e^{-ab}}{\sqrt{2\pi}}\left(\frac{v_0\,\omega}{\tau}\right)^{1/2}\int_0^\infty G_{0,1}^{1,0}\left(\begin{matrix}-\\0\end{matrix}\middle|\frac{a^2 y_N}{2\tau}\right) G_{1,0}^{0,1}\left(\begin{matrix}1\\-\end{matrix}\middle|\frac{2y_N}{b^2\tau}\right) \times G_{0,N}^{N,0}\left(\begin{matrix}-\\\boldsymbol{\beta}+\mathbf{\frac{1}{2}}\end{matrix}\middle|v_0\,\omega\,y_N\right) dy_N. \tag{I.16}$$

This can be rewritten as

$$\Psi_{1a} = \frac{\Omega e^{-ab}}{\sqrt{2\pi}}\left(\frac{v_0\,\omega}{\tau}\right)^{1/2}\int_0^\infty G_{0,N}^{N,0}\left(\begin{matrix}-\\\boldsymbol{\beta}+\mathbf{\frac{1}{2}}\end{matrix}\middle|v_0\,\omega\,y_N\right) G_{1,0}^{0,1}\left(\begin{matrix}1\\-\end{matrix}\middle|\frac{2y_N}{b^2\tau}\right) \times G_{0,1}^{1,0}\left(\begin{matrix}-\\0\end{matrix}\middle|\frac{a^2 y_N}{2\tau}\right) dy_N \tag{I.17}$$

or using the Fox H-representation in (H.2)

$$\Psi_{1a} = \frac{\Omega e^{-ab}}{\sqrt{2\pi}}\left(\frac{v_0\,\omega}{\tau}\right)^{1/2}\int_0^\infty H_{0,N}^{N,0}\left(\begin{matrix}-\\\boldsymbol{\beta}+\mathbf{\frac{1}{2}},\mathbf{1}\end{matrix}\middle|v_0\,\omega\,y_N\right) H_{1,0}^{0,1}\left(\begin{matrix}1,1\\-\end{matrix}\middle|\frac{2y_N}{b^2\tau}\right) \times H_{0,1}^{1,0}\left(\begin{matrix}-\\0,1\end{matrix}\middle|\frac{a^2 y_N}{2\tau}\right) dy_N \tag{I.18}$$

The solution for the integral (I.18) can be obtained using the Fox H-function in two dimensions or its special case the bivariate Meijer G-functions defined in the properties (H.12) and (H.13). The general result was obtained by P. K. Mittal and K.C. Gupta in [Mittal and Gupta, 1972]. With this result the integral above becomes

$$\Psi_{1a} = \frac{\Omega e^{-ab}}{\sqrt{2\pi}}\frac{1}{\sqrt{v_0\,\omega\,\tau}}\mathbf{G_N}\left(\frac{2}{b^2\,\tau\,v_0\,\omega}, \frac{a^2}{2\tau\,v_0\,\omega}\right) \tag{I.19}$$

where

$$\mathbf{G_N}(x,y) = G_{N,0:1,0:0,1}^{0,N:0,1:1,0}\left(\begin{matrix}(-\boldsymbol{\beta}-\mathbf{\frac{1}{2}}) & : & (1) & : & (--)\\ (--) & : & (--) & : & (0)\end{matrix}\middle| x, y\right). \tag{I.20}$$

Thus, the first term in (I.9) is given by the integral with respect to a of the function (I.19) evaluated in the interval $[0, a]$. This integral cannot be computed analytically but an approximate result can be obtained by numerical integration. Therefore, we define the function $\Theta_1(a)$ which is given by

$$\Theta_1(a,b) = \frac{\Omega}{\sqrt{2\pi}}\frac{1}{\sqrt{v_0\,\omega\,\tau}}\int_0^a da' \quad e^{-a'b}\mathbf{G_N}\left(\frac{2}{b^2\tau v_0\,\omega}, \frac{a'^2}{2\tau v_0\,\omega}\right). \tag{I.21}$$

The result above can be simplified using the following change of variable

$$\begin{aligned} a &= ln\left(\frac{S}{K}\right) + r\tau \rightarrow \frac{1}{\sqrt{v_0\,\omega\,\tau}}\left[ln\left(\frac{S}{K}\right) + r\tau\right] \\ b &= \frac{1}{2} \rightarrow \frac{\sqrt{v_0\,\omega\,\tau}}{2} \end{aligned} \tag{I.22}$$

with which is possible to write $\mathbb{G}_{\boldsymbol{N}}\left(\frac{2}{b^2\tau v_0\,\omega}, \frac{a'^2}{2\tau v_0\,\omega}\right) \rightarrow \mathbb{G}_{\boldsymbol{N}}\left(\frac{2}{b^2}, \frac{a'^2}{2}\right)$ and the integral (I.21) becomes

$$\Theta_1(a,b) = \frac{\Omega}{\sqrt{2\pi}} \int_0^a da' e^{-a'b}\, \mathbb{G}_{\boldsymbol{N}}\left(\frac{2}{b^2}, \frac{a'^2}{2}\right). \tag{I.23}$$

The second average of the Black-Scholes price in (I.1) is given by the relation

$$\langle C_2(S,K,r,T|v_N)\rangle = Ke^{-r\tau}\Psi_2(a,b), \tag{I.24}$$

with

$$\Psi_2(a,b) = \frac{\Omega}{v_0\,\omega} \int_0^\infty \Phi\left(\frac{a}{\sqrt{v_N\tau}} - b\sqrt{v_N\tau}\right) G^{0,N}_{N,0}\left(\begin{matrix} -\boldsymbol{\beta} - \mathbf{1} \\ - \end{matrix}\middle| \frac{v_N}{v_0\,\omega}\right) dv_N. \tag{I.25}$$

The solution of (I.25) can be written as

$$\begin{aligned} \Psi_2(a,b) &= \int_0^a \frac{\partial\Psi_2(a')}{\partial a'}\, da' + \Psi_2(a=0) \\ &= \Theta_2(a,b) + \Psi_2(a=0), \end{aligned} \tag{I.26}$$

where the partial derivative respect to a of (I.25) is

$$\Psi_{2a} = \frac{\partial\Psi_2(a,b)}{\partial a}. \tag{I.27}$$

The solution for Θ_2 is obtained using a similar procedure to the one used in the case of Θ_1. So, the final result for the function Θ_2 becomes

$$\Theta_2(a,b) = \frac{\Omega}{\sqrt{2\pi}} \int_0^a da' e^{a'b} \mathbb{G}_{\boldsymbol{N}}\left(\frac{2}{b^2}, \frac{a'^2}{2}\right). \tag{I.28}$$

In view of the relations (I.9) and (I.26), the solution for our hierarchical Hull-White model (I.1) can be written as

$$C(S,K,r,t,N) = S\,\Theta_1(a,b) - K\,e^{-r\tau}\Theta_2(a,b) + S\,\Psi_1(a=0) - K\,e^{-r\tau}\Psi_2(a=0), \tag{I.29}$$

where functions $\Theta_1(a,b)$ and $\Theta_2(a,b)$ are given by the expressions (I.21) and (I.21), respectively.

The solution for $\Psi_1(a=0)$ is obtained from expression (I.7) and (I.8) solving the integral

$$\Psi_1(a=0) = \int_0^\infty \Phi\left(b\sqrt{v_N\tau}\right) f(v_N) dv_N. \tag{I.30}$$

Using the expression for $f_N(v_N)$, this integral reads

$$\Psi_1(a=0) = \frac{\Omega}{v_0\,\omega} \int_0^\infty \Phi\left(b\sqrt{v_N\tau}\right) G_{N,0}^{0,N}\left(\begin{matrix}-\boldsymbol{\beta}-\mathbf{1}\\ -\end{matrix}\middle|\frac{v_N}{\omega\,v_0}\right) dv_N. \tag{I.31}$$

The cumulative function $\Phi\left(b\sqrt{v_N\tau}\right)$ can be expressed in term of a Meijer G-function using the property (H.4). So the integral above looks in the form

$$\begin{aligned}\Psi_1(a=0) = \frac{\Omega}{v_0\,\omega} \int_0^\infty \frac{1}{2}\left[1 + \frac{1}{\sqrt{\pi}} G_{1,2}^{1,1}\left(\begin{matrix}1\\ \frac{1}{2};0\end{matrix}\middle|\frac{b^2 v_N\tau}{2}\right)\right] \\ \times G_{N,0}^{0,N}\left(\begin{matrix}-\boldsymbol{\beta}-\mathbf{1}\\ -\end{matrix}\middle|\frac{v_N}{v_0\,\omega}\right) dv_N.\end{aligned} \tag{I.32}$$

Using the properties of integration of the Meijer G-function, results

$$\Psi_1(a=0) = \frac{1}{2} + \frac{\Omega}{2\sqrt{\pi}}\frac{2}{b^2} G_{N+2,1}^{1,N+1}\left(\begin{matrix}-\boldsymbol{\beta}-\mathbf{1}, -\frac{1}{2}; 0\\ -1\end{matrix}\middle|\frac{2}{b^2}\right), \tag{I.33}$$

where now we have defined $b = \frac{\sqrt{v_0\omega\,\tau}}{2}$. The factor $2/b^2$ in the second term can be absorbed into the Meijer G - function using the property (H.5), with which we finally obtain

$$\Psi_1(a=0) = \frac{1}{2}\left[1 + \frac{\Omega}{\sqrt{\pi}} G_{N+2,1}^{1,N+1}\left(\begin{matrix}-\boldsymbol{\beta}, \frac{1}{2}; 1\\ 0\end{matrix}\middle|\frac{2}{b^2}\right)\right]. \tag{I.34}$$

Similarly $\Psi_2(a=0)$ in the the last term of (I.29) is

$$\Psi_2(a=0) = \frac{1}{2}\left[1 - \frac{\Omega}{\sqrt{\pi}} G_{N+2,1}^{1,N+1}\left(\begin{matrix}-\boldsymbol{\beta}, \frac{1}{2}; 1\\ 0\end{matrix}\middle|\frac{2}{b^2}\right)\right], \tag{I.35}$$

where we recall that $\omega = \prod_{j=1}^{N} \beta_j$, $\Omega = 1/\prod_{j=1}^{N} \Gamma(\beta_j + 1)$ and $\boldsymbol{\beta} = (\beta_1, \ldots, \beta_N)$.

Alternatively, the functions (I.9) and (I.26) can be expressed as a series of univariate Meijer G-functions. To obtain a solution in this representation, we can write the average of the Black-Scholes price as

$$C(S, K, r, t, N) = S\Psi_1(r, K, a) - Ke^{-r\tau}\Psi_2(r, K, a) \tag{I.36}$$

where $\Psi_1(r,K,a)$ and $\Psi_2(r,K,a)$ are the functions (I.9) and (I.26) respectively. Let us write $\Psi_1(r,K,a)=\Psi_1$ and $\Psi_2(r,K,a)=\Psi_2$ as

$$\begin{aligned}\Psi_1(a) &= \int_{-\infty}^{a} \frac{\partial \Psi_1(a')}{\partial a'}\, da' \\ \Psi_2(a) &= \int_{-\infty}^{a} \frac{\partial \Psi_2(a')}{\partial a'}\, da'.\end{aligned} \tag{I.37}$$

These integrals are easily calculated using the result in [S.P.Goyal and S.L.Mathur, 1976], which we have summarized in the property (H.16). The final result is

$$\begin{aligned}\Psi_1 = -\frac{\Omega}{\sqrt{2\pi}} \sum_{l=1}^{\infty} \frac{(-1)^l}{l!} \left(\frac{1}{2}\right)^l \frac{1}{b^{2l+1}} \Gamma(2l+1, ab) \\ \times G^{0,N+1}_{N+1,0}\left(\begin{matrix} 1, -\boldsymbol{l}-\boldsymbol{\beta}-\boldsymbol{\frac{1}{2}} \\ - \end{matrix} \middle| \frac{2}{b^2} \right)\end{aligned} \tag{I.38}$$

and

$$\begin{aligned}\Psi_2 = \frac{\Omega}{\sqrt{2\pi}} \sum_{l=1}^{\infty} \frac{(-1)^l}{l!} \left(\frac{1}{2}\right)^l \frac{1}{b^{2l+1}} \Gamma(2l+1, -ab) \\ \times G^{0,N+1}_{N+1,0}\left(\begin{matrix} 1, -\boldsymbol{l}-\boldsymbol{\beta}-\boldsymbol{\frac{1}{2}} \\ - \end{matrix} \middle| \frac{2}{b^2} \right),\end{aligned} \tag{I.39}$$

where $\Gamma(a,x) = \int_x^{\infty} t^{s-1}e^{-t}dt$ is the incomplete upper gamma function. Ω, a, b and $\boldsymbol{\beta}$ are defined in the same way as in the representation of bivariate Meijer G-functions.

Appendix J - Hierachical Heston Model for Option Pricing

Here we compute the average of the Black-Scholes price assuming the distribution of volatility to be a distribution of the gamma class (G.28). Now the first integral in the average of the call price (I.7), can be written as

$$\langle C_1(S,K,r,t|v_N)\rangle = S\,\Psi_1 = S\int_0^\infty \Phi\left(\frac{a}{\sqrt{v_N\tau}} + b\sqrt{v_N\tau}\right) f(v_N)dv_N, \tag{J.1}$$

where the statistical distribution of the stochastic volatility $f_N(v_N)$ is given by a gamma class distribution as equation (G.28). So, the integral (J.1) becomes

$$\Psi_1 = \frac{\omega\,\Omega}{v_0}\int_0^\infty \Phi\left(\frac{a}{\sqrt{v_N\tau}} + b\sqrt{v_N\tau}\right) G^{N,0}_{0,N}\left(\begin{matrix}-\\ \boldsymbol{\beta}-\mathbf{1}\end{matrix}\middle|\frac{\omega\,v_N}{v_0}\right) dv_N, \tag{J.2}$$

where $\omega = \prod_{j=1}^{N}\beta_j$, $\Omega = 1/\prod_{j=1}^{N}\Gamma(\beta_j)$ and $\boldsymbol{\beta} = (\beta_1,\ldots,\beta_N)$.

As in the case of the previous appendix, we can write Ψ_1 as

$$\begin{aligned}\Psi_1(a) &= \int_0^a \frac{\partial\Psi_1(a')}{\partial a'}\,da' + \Psi_1(a=0)\\ &= \int_0^a \Psi_{1a}\,da' + \Psi_1(a=0)\\ &= \Theta_1(a) + \Psi_1(a=0),\end{aligned} \tag{J.3}$$

where the partial derivative of (J.2) respect to a is

$$\Psi_{1a} = \frac{e^{-ab}}{\sqrt{2\pi}}\frac{\omega\,\Omega}{v_0}\int_0^\infty \frac{1}{\sqrt{v_N\tau}} e^{-\frac{1}{2}\left(\frac{a^2}{v_N\tau}+b^2v_N\tau\right)} G^{N,0}_{0,N}\left(\begin{matrix}-\\ \boldsymbol{\beta}-\mathbf{1}\end{matrix}\middle|\frac{\omega\,v_N}{v_0}\right) dv_N. \tag{J.4}$$

Writing the exponential functions as a Meijer G-functions (see eq (I.12)), the expression (J.4) becomes

$$\begin{aligned}\Psi_{1a} = \frac{e^{-ab}}{\sqrt{2\pi}}\frac{\omega\,\Omega}{v_0}\int_0^\infty \frac{1}{\sqrt{v_N\tau}} G^{1,0}_{0,1}\left(\begin{matrix}-\\ 0\end{matrix}\middle|\frac{a^2}{2v_N\tau}\right) G^{1,0}_{0,1}\left(\begin{matrix}-\\ 0\end{matrix}\middle|\frac{b^2v_N\tau}{2}\right)\\ \times G^{N,0}_{0,N}\left(\begin{matrix}-\\ \boldsymbol{\beta}-\mathbf{1}\end{matrix}\middle|\frac{\omega\,v_N}{v_0}\right) dv_N.\end{aligned} \tag{J.5}$$

Conveniently we write this equation in the form

$$\Psi_{1a} = \frac{e^{-ab}\Omega}{\sqrt{2\pi\tau}}\left(\frac{\omega}{v_0}\right)^{\frac{3}{2}}\int_0^\infty \left(\frac{\omega\, v_N}{v_0}\right)^{-\frac{1}{2}} G_{0,1}^{1,0}\left(\begin{matrix}-\\0\end{matrix}\middle|\frac{a^2}{2v_N\tau}\right) G_{0,1}^{1,0}\left(\begin{matrix}-\\0\end{matrix}\middle|\frac{b^2 v_N\tau}{2}\right) \times G_{0,N}^{N,0}\left(\begin{matrix}-\\\boldsymbol{\beta}-\mathbf{1}\end{matrix}\middle|\frac{\omega\, v_N}{v_0}\right) dv_N. \tag{J.6}$$

The factor $\left(\frac{\omega\, v_N}{v_0}\right)^{-\frac{1}{2}}$ can be included into the third G-function by using the property (H.5). In addition, the argument in the first G-function can be inverted by using property (H.7). With this changes and ordering the G-functions, the expression above finally reads

$$\Psi_{1a} = \frac{e^{-ab}\Omega}{\sqrt{2\pi\tau}}\left(\frac{\omega}{v_0}\right)^{\frac{3}{2}}\int_0^\infty G_{0,N}^{N,0}\left(\begin{matrix}-\\\boldsymbol{\beta}-\frac{\mathbf{3}}{\mathbf{2}}\end{matrix}\middle|\frac{\omega\, v_N}{v_0}\right) G_{0,1}^{1,0}\left(\begin{matrix}-\\0\end{matrix}\middle|\frac{b^2 v_N\tau}{2}\right) \times G_{1,0}^{0,1}\left(\begin{matrix}1\\-\end{matrix}\middle|\frac{2v_N\tau}{a^2}\right) dv_N, \tag{J.7}$$

or in the H-Fox representation (see equation (H.2))

$$\Psi_{1a} = \frac{e^{-ab}\Omega}{\sqrt{2\pi\tau}}\left(\frac{\omega}{v_0}\right)^{\frac{3}{2}}\int_0^\infty H_{0,N}^{N,0}\left[\frac{\omega\, v_N}{v_0}\middle|\begin{matrix}-\\(\boldsymbol{\beta}-\frac{\mathbf{3}}{\mathbf{2}},\mathbf{1})\end{matrix}\right] H_{0,1}^{1,0}\left[\frac{b^2 v_N\tau}{2}\middle|\begin{matrix}-\\(0,1)\end{matrix}\right] \times H_{1,0}^{0,1}\left[\frac{2v_N\tau}{a^2}\middle|\begin{matrix}(1,1)\\-\end{matrix}\right] dv_N. \tag{J.8}$$

The integral above can be solved using the property (H.15) and the equivalence between the Fox-H function and the Meijer G-function. So we can write

$$\Psi_{1a} = \frac{e^{-ab}\Omega}{\sqrt{2\pi\tau}}\left(\frac{\omega}{v_0}\right)^{\frac{1}{2}} \boldsymbol{\mathbb{G}_N}\left(\frac{2\tau v_0}{a^2\,\omega}, \frac{b^2\tau v_0}{2\,\omega}\right), \tag{J.9}$$

where $\boldsymbol{\mathbb{G}_N}(x,y)$ is used to denote the bivariate Meijer G-function

$$\boldsymbol{\mathbb{G}_N}(x,y) = G_{N,0:1,0:0,1}^{0,N:0,1:1,0}\left(\begin{matrix}(-\boldsymbol{\beta}+\frac{\mathbf{3}}{\mathbf{2}}) & : & (1) & : & (--)\\ (--) & : & (--) & : & (0)\end{matrix}\middle| x, y\right). \tag{J.10}$$

Therefore, the first term in (J.3) is given by the integral with respect to a of the result (J.9). This is

$$\Theta_1 = \frac{\Omega}{\sqrt{2\pi\tau}}\left(\frac{\omega}{v_0}\right)^{\frac{1}{2}}\int_0^a da' \quad e^{-a'b}\boldsymbol{\mathbb{G}_N}\left(\frac{2\tau v_0}{a'^2\,\omega}, \frac{b^2\tau v_0}{2\omega}\right). \tag{J.11}$$

It can be simplified by the change of variable,

$$a = ln\left(\frac{S}{K}\right) + r\tau \rightarrow \sqrt{\frac{\omega}{v_0\tau}}\left[ln\left(\frac{S}{K}\right) + r\tau\right]$$
$$b = \frac{1}{2} \rightarrow \frac{1}{2}\sqrt{\frac{v_0\tau}{\omega}}. \tag{J.12}$$

So, the integral (J.11) becomes

$$\Theta_1(a,b) = \frac{\Omega}{\sqrt{2\pi}}\int_0^a da' e^{-a'b}\mathbb{G}_{\boldsymbol{N}}\left(\frac{2}{a'^2}, \frac{b^2}{2}\right). \tag{J.13}$$

The second average of the Black-Scholes price is given by the relation

$$\langle C_2(S,K,r,t|v_N)\rangle = Ke^{-r\tau}\Psi_2(a). \tag{J.14}$$

Applying an analogous procedure to that of the case to compute Θ_1, we have

$$\Theta_2(a,b) = \frac{\Omega}{\sqrt{2\pi\tau}}\left(\frac{\omega}{v_0}\right)^{\frac{1}{2}}\int_0^a da'\, e^{a'b}\,\mathbb{G}_{\boldsymbol{N}}\left(\frac{2}{a'^2}, \frac{b^2}{2}\right). \tag{J.15}$$

Here $\mathbb{G}_{\boldsymbol{N}}(x,y)$ is given by the expression (J.10). So, the solution for the hierarchical Heston model for option pricing results,

$$C(r,K,S,N) = S\Theta_1(a,b) - Ke^{-r\tau}\Theta_2(a,b) + S\Psi_1(a=0) - Ke^{-r\tau}\Psi_2(a=0). \tag{J.16}$$

Now for the calculation of $\Psi_1(a=0)$, we write the expression (J.1) as

$$\Psi_1(a=0) = \int_0^\infty \Phi\left(b\sqrt{v_N\tau}\right) f_N(v_N)dv_N. \tag{J.17}$$

Replacing $f_N(v_N)$ by the distribution of the gamma class (G.28),

$$\Psi_1(a=0) = \frac{\omega\,\Omega}{v_0}\int_0^\infty \Phi\left(b\sqrt{v_N\tau}\right) G_{0,N}^{N,0}\left(\begin{matrix} - \\ \boldsymbol{\beta} - \mathbf{1}\end{matrix}\middle| \frac{\omega\, v_N}{v_0}\right) dv_N. \tag{J.18}$$

The cumulative function $\Phi(x)$ can be expressed as Meijer G-function by using the property (H.4). So, the integral (J.18) reads

$$\Psi_1(a=0) = \frac{\omega\,\Omega}{v_0}\int_0^\infty \frac{1}{2}\left[1 + \frac{1}{\sqrt{\pi}}G_{1,2}^{1,1}\left(\begin{matrix} 1 \\ \frac{1}{2}; 0\end{matrix}\middle| \frac{b^2 v_N\tau}{2}\right)\right]$$
$$\times G_{0,N}^{N,0}\left(\begin{matrix} - \\ \boldsymbol{\beta} - \mathbf{1}\end{matrix}\middle| \frac{\omega\, v_N}{v_0}\right) dv_N. \tag{J.19}$$

Using the convolution property (H.6) of the Meijer G-function, we finally obtain the solution

$$\Psi_1(a=0) = \frac{1}{2}\left[1 + \frac{\Omega}{\sqrt{\pi}} G^{N+1,1}_{2,N+1}\left(\begin{matrix}\frac{1}{2}; 1 \\ \boldsymbol{\beta}, 0\end{matrix}\middle| \frac{2}{b^2}\right)\right], \tag{J.20}$$

where we have defined $b = \frac{1}{2}\sqrt{\frac{v_0\tau}{w}}$ in the equation above. Similarly for $\Psi_2(a=0)$ in the last term of (J.16), we obtain

$$\Psi_2(a=0) = \frac{1}{2}\left[1 - \frac{\Omega}{\sqrt{\pi}} G^{N+1,1}_{2,N+1}\left(\begin{matrix}\frac{1}{2}; 1 \\ \boldsymbol{\beta}, 0\end{matrix}\middle| \frac{2}{b^2}\right)\right], \tag{J.21}$$

Therefore, the solution for te call option price calculated as the average of the Black-Scholes formula under the assumption that the volatility follows a hierarchical Heston process can be computed by using (J.16) together with (J.13), (J.15), (J.20) and (J.21).

Appendix K - Asymptotic Behavior of the Hierarchical Distributions

Appendix K.1 - Symmetric Power Law Class or Symmetric Inverse Gamma Class Distribution of Velocity Increments

In this section we analyze the asymptotic behaviour of the symmetric power-law class distribution shown in section 5.7.1. For this, let us write the Meijer G-function for small argument as

$$G_{p,q}^{m,n}\left(\left.\begin{matrix}\vec{a}_p\\ \vec{b}_q\end{matrix}\right|x\right) \sim \sum_{k=1}^{m} C_k x^{b_k}, \quad \text{for } x \to 0. \tag{K.1}$$

Using (H.7) to invert the argument of the Meijer G-function into (G.21) and considering $\epsilon_N \to \infty$, we can write

$$G_{N,0}^{0,N}\left(\left.\begin{matrix}-\boldsymbol{\beta}-\mathbf{1}\\ -\end{matrix}\right|\frac{\epsilon_N}{\epsilon_0 w}\right) = G_{0,N}^{N,0}\left(\left.\begin{matrix}-\\ \boldsymbol{\beta}+\mathbf{2}\end{matrix}\right|\frac{\epsilon_0 w}{\epsilon_N}\right) \sim \sum_{k=1}^{m} C_k \left(\frac{\epsilon_N}{\epsilon_0 w}\right)^{-b_k}, \tag{K.2}$$

with $b_k = \beta_k + 2$. Thus, replacing into (5.57), it is possible to write

$$P_N(\delta v) \sim \sum_{k=1}^{m} C_k \int_0^\infty \epsilon_N^{-1/2} \exp\left(-\frac{\delta v^2}{2\epsilon_N}\right)\left(\frac{\epsilon_N}{\epsilon_0 w}\right)^{-b_k} d\epsilon_N. \tag{K.3}$$

Using the change of variable $u = \frac{\delta v^2}{2\epsilon_N}$, we can write the expression above in the form

$$P_N(\delta v) \sim \sum_{k=1}^{m} C_k (\delta v^2)^{1/2-b_k} \int_0^\infty u^{b_k - 3/2} e^{-u} du. \tag{K.4}$$

The integral in (K.4) gives the gamma function $\Gamma(b_k - 1/2)$ that does not depend on δv, i.e. the result is a constant. Therefore, using this fact and substituting b_k, we finally have

$$P_N(\delta v) \sim \sum_{k=1}^{m} C_k (\delta v^2)^{1/2-\beta_k-2} = \sum_{k=1}^{m} C_k |\delta v|^{-2\beta_k-3} \tag{K.5}$$

Therefore, this model exhibits power-law tails that decay as $\frac{1}{|\delta v|^{2\beta+3}}$.

Appendix K.2 - Asymmetric Distribution of Velocity Increments. Inverse Gamma Class

This is the asymmetric version of the case in previous section. In this case, we substitute (K.2) into (6.6). Using the change of variable $y = \delta v + \mu\epsilon$, this reads

$$P_N(y) \sim \sum_{k=1}^{m} C_k e^{\mu y} \int_0^\infty \epsilon_N^{-1/2} \exp\left(-\frac{y^2}{2\epsilon_N} - \frac{\mu^2 \epsilon_N}{2}\right)\left(\frac{\epsilon_N}{\epsilon_0 w}\right)^{-b_k} d\epsilon_N. \tag{K.6}$$

Writing $\epsilon_N u = |y|$ and making the algebraic operations we have

$$P_N(y) \sim \sum_{k=1}^{m} C_k \, e^{\mu y} \, |y|^{-1/2-b_k} \int_0^{\infty} u^{b_k-3/2} \exp\left[-\left(\frac{u}{2} + \frac{\mu^2}{2} u^{-1} \right) |y| \right] du \tag{K.7}$$

The asymptotic behavior of the integral above can be obtained using the saddle point method. To do this, we need to define the functions:

$$\begin{aligned} A =& |y| \\ f(u) =& u^{b_k-3/2} \\ g(u) =& \frac{u}{2} + \frac{\mu^2}{2} u^{-1} \\ g'(u) =& \frac{1}{2} - \frac{\mu^2}{2} u^{-2} \\ g''(u) =& \mu^2 \, u^{-3}. \end{aligned} \tag{K.8}$$

The function $g(u)$ has a maximum in u_0 for which we must do $g'(u_0) = 0$. So, we find $u_0 = |\mu|$. With this results and using the approximation of the saddle point method for the integral in the expression (K.7), we can write

$$P_N(y) \sim \sum_{k=1}^{m} C_k \, e^{\mu y} \, |y|^{-1/2-b_k} f(u_0) e^{-A\, g(u_0)} \sqrt{\frac{2\pi}{A\, g''(u_0)}}. \tag{K.9}$$

Using the definitions in (K.8) into expression (K.9), we can write

$$P_N(y) \sim \sum_{k=1}^{m} C_k \, |y|^{-b_k} e^{\mu y} \, e^{-|\mu||y|}. \tag{K.10}$$

Therefore, the asymptotic behavior of the asymmetric model obtained of using the inverse gamma class distribution for the energy dissipation rate ϵ can displays different tails on each side of the distribution. Depending on the value of μ, we have the two cases:
i) Considering $\mu > 0$ we have

$$P_N(y) \sim \left(\sum_{k=1}^{N} \frac{C_k}{|y|^{\beta_k+2}} \right) \times \begin{cases} 1 & , \quad \text{for} \quad y \to \infty, \\ e^{-2\mu|y|} & , \quad \text{for} \quad y \to -\infty. \end{cases} \tag{K.11}$$

ii) For $\mu < 0$, as is the case for turbulent flows, we obtain

$$P_N(y) \sim \left(\sum_{k=1}^{N} \frac{C_k}{|y|^{\beta_k+2}} \right) \times \begin{cases} 1 & , \quad \text{for} \quad y \to -\infty, \\ e^{-2|\mu|y} & , \quad \text{for} \quad y \to \infty. \end{cases} \tag{K.12}$$

Appendix K.3 - Symmetric Stretched Exponential Class or Symmetric Gamma Class Distribution of Velocity Increments

Let us start from the relation (5.63) and then we use the expansion of the Meijer G-function when $\epsilon_N \to \infty$ [Kilbas and Saigo, 2004]

$$G_{0,N}^{N,0}\left(\begin{matrix} - \\ \boldsymbol{\beta_N - 1} \end{matrix}\middle| \frac{w\epsilon_N}{\epsilon_0}\right) \sim (\alpha\,\epsilon_N)^{\bar{\beta}-\frac{3}{2}+\frac{M}{2}}\,\exp\left(-\frac{1}{M}(\alpha\,\epsilon_N)^M\right). \tag{K.13}$$

With $M = \frac{1}{N}$, $\bar{\beta} = \frac{1}{N}\sum_{k=1}^{N}\beta_k$ and $\alpha = \frac{w}{\epsilon_0}$. Replacing the result above into (5.63), results

$$P_N(\delta v) \sim \int_0^\infty \epsilon_N^{\bar{\beta}-2+\frac{M}{2}}\exp\left(-\frac{\delta v^2}{2\epsilon_N} - \frac{1}{M}(\alpha\epsilon_N)^M\right) d\epsilon_N. \tag{K.14}$$

Defining the variable $u\epsilon_N = \delta v^{\frac{2}{M+1}}$, the integral above becomes

$$P_N(\delta v) \sim y^{\frac{2}{M+1}(\beta-1+M/2)}\int_0^\infty u^{-\bar{\beta}-\frac{M}{2}}\exp\left[\left(-\frac{u}{2} - \frac{1}{M}\alpha^M u^{-M}\right)\delta v^{\frac{2M}{M+1}}\right] du. \tag{K.15}$$

So, with $|\delta v| >> 1$ we can use the saddle point method to approximate the integral. For this end, we define the functions

$$\begin{aligned}
A =& \delta v^{\frac{2M}{M+1}}\\
f(u) =& u^{-\bar{\beta}-\frac{M}{2}}\\
g(u) =& \frac{u}{2} + \frac{1}{M}\alpha^M u^{-M}\\
g'(u) =& \frac{1}{2} - \alpha^M u^{-M-1}\\
g''(u) =& (M+1)\alpha^M u^{-M-2}\\
u_0 =& \left(2\alpha^M\right)^{\frac{1}{M+1}}\\
f(u_0) =& constant\\
g(u_0) =& \frac{M+1}{M}\left(\frac{\alpha}{2}\right)^{\frac{M}{M+1}}\\
g''(u_0) =& constant
\end{aligned} \tag{K.16}$$

Using the results (K.16), we can approximate the integral (K.15) as

$$\begin{aligned}
P_N(\delta v) \sim& \delta v^{\frac{2}{M+1}(\bar{\beta}-1+M/2)} f(u_0) e^{-A\,g(u_0)}\sqrt{\frac{2\pi}{A\,g''(u_0)}}\\
=& \delta v^{\frac{2N}{N+1}(\bar{\beta}-1)}\exp\left[-(N+1)\left(\frac{w\,\delta v^2}{2\epsilon_0}\right)^{\frac{1}{N+1}}\right].
\end{aligned} \tag{K.17}$$

This is a stretched exponential type function.

Appendix K.4 - Asymmetric Distribution of Velocity Increments. Gamma Class

In this case, we study the asymptotic behavior of the integral (6.6). Thus, using (K.13) as asymptotic approximation for $f(\epsilon_N)$, this integral becomes

$$P_N(y) \sim e^{\mu y} \int_0^\infty \epsilon^{\bar{\beta}-2+\frac{M}{2}} \exp\left(-\frac{y^2}{2\epsilon} - \frac{\mu^2\epsilon}{2} - \frac{1}{M}(\alpha\epsilon)^M\right) d\epsilon, \tag{K.18}$$

where $M = \frac{1}{N}$, $\bar{\beta} = \frac{1}{N}\sum_{k=1}^{N}\beta_k$, $\alpha = \frac{w}{\epsilon_0}$ and $y = \delta\tilde{v} + \mu\epsilon$. Defining the variable $\epsilon_N = |y|\,t$, with $|y| >> 1$, we obtain

$$P_N(y) \sim e^{\mu y}|y|^{\bar{\beta}-1+\frac{M}{2}} \int_0^\infty t^{\bar{\beta}-2+\frac{M}{2}} \exp\left(-\frac{|y|}{2t} - \frac{\mu^2\,|y|\,t}{2} - \frac{1}{M}(\alpha\,|y|\,t)^M\right) dt. \tag{K.19}$$

To apply the asymptotic approximation for the integral (K.19), we define the functions

$$\begin{aligned} f(t) =& t^{\bar{\beta}-2+\frac{M}{2}}. \\ g(t) =& \frac{|y|}{2t} + \frac{\mu^2\,|y|\,t}{2} + \frac{1}{M}(\alpha\,|y|\,t)^M \quad \text{and its derivatives,} \\ g'(t) =& -\frac{|y|}{2t^2} + \frac{\mu^2\,|y|}{2} + (\alpha\,|y|)^M\,t^{M-1}, \\ g''(t) =& \frac{|y|}{t^3} + (M-1)(\alpha\,|y|)^M\,t^{M-2}. \end{aligned} \tag{K.20}$$

We require that $g'(t_0) = 0$, so we can write

$$0 = -\frac{|y|}{2t_0^2} + \frac{\mu^2\,|y|}{2} + \frac{1}{M}(\alpha\,|y|)^M\,t_0^{M-1}, \tag{K.21}$$

solving to t_0 in this expression, we obtain

$$t_0 = \frac{1}{|\mu|}\left[1 + \frac{2\,\alpha^M}{\mu^2}\,(|y|\,t_0)^{M-1}\right]^{-1/2}. \tag{K.22}$$

Since $\frac{1}{N} < 1$ and $|y| >> 1$, it is possible to approximate the transcendental function t_0 as

$$\begin{aligned} t_0 \sim& \frac{1}{|\mu|}\left[1 - \frac{\alpha^M\,|y|^{M-1}}{|\mu|^{M+1}}\right], \\ t_0^{-1} \sim& |\mu|\left[1 + \frac{\alpha^M\,|y|^{M-1}}{|\mu|^{M+1}}\right] \quad \text{and} \\ t_0^M \sim& \frac{1}{|\mu|^M}\left[1 - M\frac{\alpha^M\,|y|^{M-1}}{|\mu|^{M+1}}\right]. \end{aligned} \tag{K.23}$$

With this result, when the functions $g'(t)$ and $g''(t)$ defined in (K.20) are evaluated in $t = t_0$ become

$$\begin{aligned} g(t_0) =& |\mu||y| + \frac{1}{M}\left(\frac{\alpha\,|y|}{|\mu|}\right)^M \\ g''(t_0) \sim& |\mu|^{-3/2}|y|^{-1/2} \end{aligned} \tag{K.24}$$

Using the expressions in (K.24) and the first equation in (K.20), the integral (K.19) can be written approximately as

$$P_N(y) \sim e^{\mu y}|y|^{\bar{\beta}-1+\frac{M}{2}} f(t_0)e^{-g(t_0)}\,|g''(t_0)|^{-1/2} \tag{K.25}$$

$$P_N(y) \sim e^{\mu y}\,|y|^{\bar{\beta}-\frac{3}{2}+\frac{M}{2}} \exp\left(-|\mu||y| - \frac{1}{M}\left(\frac{\alpha\,|y|}{|\mu|}\right)^M\right). \tag{K.26}$$

Therefore, the asymptotic analysis shows that our asymmetric model based on the gamma class distribution for ϵ has different tails on each side of the distribution, as in the case shown in Appendix K. Let us see this as follows:

i) For $\mu > 0$ it results:

$$P_N(\delta v) \sim |y|^{\bar{\beta}-\frac{3}{2}+\frac{M}{2}} \times \begin{cases} \exp\left(-2|\mu||y| - \frac{1}{M}\left(\frac{\alpha\,|y|}{|\mu|}\right)^M\right) & , \quad \text{for} \quad y \to -\infty, \\ \exp\left(-\frac{1}{M}\left(\frac{\alpha\,|y|}{|\mu|}\right)^M\right) & , \quad \text{for} \quad y \to \infty, \end{cases} \tag{K.27}$$

ii) For $\mu < 0$ we obtain

$$P_N(\delta v) \sim |y|^{\bar{\beta}-\frac{3}{2}+\frac{M}{2}} \times \begin{cases} \exp\left(-\frac{1}{M}\left(\frac{\alpha\,|y|}{|\mu|}\right)^M\right) & , \quad \text{for} \quad y \to -\infty, \\ \exp\left(-2|\mu||y| - \frac{1}{M}\left(\frac{\alpha\,|y|}{|\mu|}\right)^M\right) & , \quad \text{for} \quad y \to \infty. \end{cases} \tag{K.28}$$

Appendix L - Asymmetric Distributions: Square-Root Model

In chapter 6 we found an asymmetric model for the distribution of velocity increments in turbulence. This distribution is written in terms of a bivariate function namely the Meijer G-function. There, we assumed the conditional PDF of velocity increments to be a Gaussian distribution with conditional average proportional to ϵ, this is $\langle \delta v|\epsilon\rangle \sim \epsilon$ and with conditional variance $\sigma^2_{\delta v|\epsilon} \sim \epsilon$. An alternative model is found if we consider for example that the conditional average of the velocity increments is proportional to the square root of ϵ, that is $\langle \delta v|\epsilon\rangle \sim \sqrt{\epsilon}$, and variance $\sigma^2_{\delta v|\epsilon} \sim \epsilon$. Like in the models of chapter 6, the particular case with a scale $N = 1$ can be written using a known function, at less for the case in which we use an inverse gamma class for the distribution of ϵ. To show this, let us write the marginal distribution of velocity increments $P(\delta v_r)$ as

$$P(\delta v_r) = \int_0^\infty \frac{1}{\sqrt{2\pi\epsilon_r}} \exp\left[-\frac{\left(\delta v_r - \mu(\sqrt{\epsilon_r} - \langle\sqrt{\epsilon_r}\rangle)\right)^2}{2\epsilon_r}\right] f(\epsilon_r)d\epsilon_r. \tag{L.1}$$

Replacing the distribution $f(\epsilon_r)$ by an inverse gamma function like (5.51), the integral above can be written as

$$P(\delta v_r) = \frac{e^{-\mu^2/2}}{\sqrt{2\pi}} \frac{(\epsilon_0\beta)^{\beta+1}}{\Gamma(\beta+1)} \int_0^\infty \epsilon_r^{-\beta-5/2} \exp\left[-\frac{\left((\delta v_r + \mu\langle\sqrt{\epsilon_r}\rangle)^2 + 2\beta\epsilon_0\right)}{2\epsilon_r}\right] \exp\left[\frac{\mu(\delta v_r + \mu\langle\sqrt{\epsilon_r}\rangle)}{\sqrt{\epsilon_r}}\right] d\epsilon_r. \tag{L.2}$$

This integral can be solved by using the following property:

$$\int_0^\infty x^{\nu-1} e^{\beta x^2} e^{-\gamma x} dx = (2\beta)^{-\nu/2}\Gamma(\nu) e^{\frac{\gamma^2}{8\beta}} D_{-\nu}\left(\frac{\gamma}{\sqrt{2\beta}}\right), \tag{L.3}$$

where D_ν is the parabolic cylinder function , and the constants β and ν must satisfy the conditions $Re(\beta) > 0$ and $Re(\nu > 0)$, respectively [Gradshteyn and Ryzhik, 1996]. Thus, defining the variables $x = 1/\epsilon_r$ and $y = \delta v_r + \mu\langle\sqrt{\epsilon_r}\rangle$, and using property (L.3), the solution for (L.2) becomes

$$P(y) = \sqrt{\frac{2}{\pi}}\, e^{-\mu^2/2} \frac{\Gamma(2\beta+3)(\epsilon_0\beta)^{\beta+1}}{\Gamma(\beta+1)} \left(y^2 + 2\beta\epsilon_0\right)^{-\frac{(2\beta+3)}{2}} e^{\frac{\mu^2 y^2}{4(y^2+2\beta\epsilon_0)}} D_{-(2\beta+3)}\left(\frac{-\mu y}{\sqrt{2(y^2+2\beta\epsilon_0)}}\right). \tag{L.4}$$

Therefore, under the assumptions considered above we obtain a new PDF for the velocity increments given by (L.4). The integral (L.1) for the general case with N scales can be written again in terms of a bivariate Fox H-function as shown in the next section.

Appendix L.1 - General Case with N Scales

Gamma inverse class

Replacing the distribution $f(\epsilon_r)$ by the inverse gamma class distribution with N scales (5.51) in the integral (L.1), we can write this as an integral involving the product of three Fox H-functions. Using the properties in Appendix H we can write (L.1) in the form

$$P_N(y) = \frac{\Omega\, e^{-\frac{\mu^2}{2}}}{\sqrt{2\,\pi\epsilon_0\,\omega}} \int_0^\infty H_{0,N}^{N,0}\left[\frac{\epsilon_0\,\omega}{\epsilon_N}\middle|\begin{matrix}(-,-)\\ (\boldsymbol{\beta}+\frac{\mathbf{5}}{\mathbf{2}},\mathbf{1})\end{matrix}\right] H_{0,1}^{1,0}\left[\frac{y^2}{2\,\epsilon_N}\middle|\begin{matrix}(-,-)\\ (0,1)\end{matrix}\right] H_{0,1}^{1,0}\left[-\mu\sqrt{\frac{y^2}{\epsilon_N}}\middle|\begin{matrix}(-,-)\\ (0,1)\end{matrix}\right] d\epsilon_N. \tag{L.5}$$

where $\Omega = \prod_{i=1}^N \frac{1}{\Gamma(\beta_i+1)}$, $w = \prod_{i=1}^N \beta_i$ and $\boldsymbol{\beta} = (\beta_1,\ldots,\beta_N)$. Applying the property (H.15), the distribution $P_N(y)$ can be written in terms of a bivariate Fox H-function as

$$P_N(y) = \frac{\Omega\, e^{-\frac{\mu^2}{2}}}{\sqrt{2\,\pi\epsilon_0\,\omega}}\, \mathbb{H}_{\boldsymbol{N}}\left(\frac{y^2}{2\,\epsilon_0\,\omega}, -\mu\sqrt{\frac{y^2}{\epsilon_0\,\omega}}\right), \tag{L.6}$$

where we have used the notation $\mathbb{H}_{\boldsymbol{N}}(x,y)$ to represent the bivariate Fox H-function:

$$\mathbb{H}_{\boldsymbol{N}}(x,y) = H_{N,0:0,1:0,1}^{0,N:1,0:1,0}\left[\begin{matrix}(-\boldsymbol{\beta}-\frac{\mathbf{1}}{\mathbf{2}};\mathbf{1},\frac{\mathbf{1}}{\mathbf{2}}) & : & (-,-) & : & (-,-)\\ (-;-) & : & (0,1) & : & (0,1)\end{matrix}\middle| x,y\right]. \tag{L.7}$$

Gamma class

Like in the previous case, if we substitute the distribution $f(\epsilon_r)$ in (L.1) by a generalized gamma distribution in the (5.54), we can write again this as a product of three H-functions. After using some properties of the fox H-function and simple calculations, we get the integral

$$P_N(y) = \frac{\Omega\, e^{-\frac{\mu^2}{2}}}{\sqrt{2\,\pi}}\left(\frac{\omega}{\epsilon_0}\right)^{\frac{3}{2}} \int_0^\infty H_{0,N}^{N,0}\left[\frac{\omega\,\epsilon_N}{\epsilon_0}\middle|\begin{matrix}(-,-)\\ (\boldsymbol{\beta}-\frac{\mathbf{3}}{\mathbf{2}},\mathbf{1})\end{matrix}\right] H_{1,0}^{0,1}\left[\frac{2\,\epsilon_N}{y^2}\middle|\begin{matrix}(1,1)\\ (-,-)\end{matrix}\right] H_{1,0}^{0,1}\left[-\frac{1}{\mu}\sqrt{\frac{\epsilon_N}{y^2}}\middle|\begin{matrix}(1,1)\\ (-,-)\end{matrix}\right] d\epsilon_N. \tag{L.8}$$

where $w = \prod_{j=1}^N \beta_j$, $\Omega = 1/\prod_{j=1}^N \Gamma(\beta_j)$ and $\boldsymbol{\beta} = (\beta_1,\ldots,\beta_N)$. Using the property (H.15), integral above gives

$$P_N(y) = \frac{\Omega\, e^{-\frac{\mu^2}{2}}}{\sqrt{2\,\pi}}\sqrt{\frac{\omega}{\epsilon_0}}\, \mathbb{H}_{\boldsymbol{N}}\left(\frac{2\,\epsilon_0}{y^2\,\omega}, -\frac{1}{\mu}\sqrt{\frac{\epsilon_0}{y^2\,\omega}}\right), \tag{L.9}$$

where now $\mathbb{H}_{\boldsymbol{N}}(x,y)$ denotes the Fox H-function

$$\mathbb{H}_{\boldsymbol{N}}(x,y) = H_{N,0:1,0:1,0}^{0,N:0,1:0,1}\left[\begin{matrix}(-\boldsymbol{\beta}+\frac{\mathbf{3}}{\mathbf{2}};\mathbf{1},\frac{\mathbf{1}}{\mathbf{2}}) & : & (1,1) & : & (1,1)\\ (-;-) & : & (-,-) & : & (-,-)\end{matrix}\middle| x,y\right]. \tag{L.10}$$